論文 / 著書情報
Article / Book Information

題目(和文)	不規則な境界を有する堆積層内における地震波の伝播に関する研究
Title(English)	Study on seismic wave propagation in sedimentary layers with irregular interfaces
著者(和文)	山中浩明
Author(English)	HIROAKI YAMANAKA
出典(和文)	学位:工学博士, 学位授与機関:東京工業大学, 報告番号:甲第2086号, 授与年月日:1989年3月26日, 学位の種別:課程博士, 審査員:
Citation(English)	Degree:Doctor of Engineering, Conferring organization: , Report number:甲第2086号, Conferred date:1989/3/26, Degree Type:Course doctor, Examiner:
学位種別(和文)	博士論文
Type(English)	Doctoral Thesis

STUDY ON SEISMIC WAVE PROPAGATION IN SEDIMENTARY LAYERS WITH IRREGULAR INTERFACES

Hiroaki YAMANAKA

Tokyo Institute of Technology

January, 1989

ABSTRACT

In this work we investigate the propagation of seismic waves within the deep sedimentary layers of southwestern Kanto district, Japan.

The underground structure down to the top layer of the earth's crust is made clear three-dimensionally by employing seismic refraction techniques using explosions. The obtained P-wave velocities of the two sedimentary layers are 1.8 and 2.8 km/sec, respectively. Two kinds of basements with P-wave velocities of 4.8 and 5.5 km/sec are found. Although the layer with P-wave velocity of 5.5 km/sec exists all over the area, the layer with P-wave velocity of 4.8 km/sec can not be located in the northeastern half of the area. The obtained underground structure is in good agreement with results of the other geoscientific investigations.

The observed distinct later phases in the seismograms from explosions and shallow earthquakes are explained by two-dimensional multiple reflection of body wave within sedimentary layers. It is pointed out from a simple forward modeling based on ray theory that the incident angle from the basement into sedimentary layers and the dip angle of the interface between sedimentary layers and the basement play important roles in amplifying the multiple-reflected waves.

Furthermore, the behavior of seismic waves in underground structure with a step-like topography of basement is discussed. Later phases affected by the step-like topography are detected in seismograms observed from explosions and earthquakes at the sites where the step-like topography is postulated. They are interpreted to be caused by the focusing of direct and diffracted waves at the edge of the step.

The propagation of surface waves is also investigated. Distinct dispersive later phases observed during the Western Nagano earthquake of 1984 are interpreted as Love-wave modulated by the deep sedimentary layers. Good fitting of synthetic seismograms by finite difference modelings with the observed ones is accomplished. It is pointed out through

numerical modelings for various subsurface structural models that the configuration of the sedimentary layers is important for the amplification of surface waves.

It is concluded from this study that earthquake ground motions are affected not only by irregularities of underground structure near observational site, but also by those in a whole of propagation path.

Acknowledgements

The author is grateful to Professor Kazuoh Seo for his helpful advice, support and encouragement throughout this work and for careful reviewing the manuscript. The instructive suggestion and comment from Emeritus Professor Hiroyoshi Kobayashi and Professor Tatsuo Ohmachi are acknowledged. The author express also his sincere thank to Professor Saburoh Midorikawa and Mr. Takanori Samano for kind support and useful discussion. The author would like to acknowledge Emeritus Professor Etsuzo Shima and Mr. Masumi Yamagisawa, Earthquake Research Institute, University of Tokyo for informative suggestion and support during seismic experiments. The author would like to thank Dr. G-Akis Tselentis, Earthquake Research Institute, University of Tokyo for kind review of this manuscript.

The author deeply indebted to members of Research Group for the Basement Structure of Tokyo Metropolitan Area, to public officials at Tokyo Metropolis, Kanagawa Prefecture and Kawasaki City, to Mr. Kenji Itoh, National Research Center for Disaster Prevention, for providing explosion data. He also thanks to Japan Meteorological Agency for making earthquake records at Tokyo and Yokohama during the Western Nagano earthquake available.

Some parts of this work were carried out during a stay of the author at Institute of Geophysics, Swiss Federal Institute of Technology, Zurich, as an exchange student with a support of the exchange student program between Swiss Federal Institute of Technology and Tokyo Institute of Technology. The author wishes to thank to members at the institute of Geophysics, specially, to Dr. Dieter Mayer-Rosa, for kind support.

The author indebted to graduate students in Seo and Kobayashi Laboratories at Tokyo Institute of Technology for their help of observation of earthquakes and explosions. Encouragement through the work by secretary Ms. Yohko Hata is acknowledged.

Data processings and numerical modelings were carried out on DEC VAX8600, Sun-4 and HITAC M180 at Tokyo Institute of Technology, Nagatsuta, and on DEC VAX8650 at Swiss Federal Institute of Technology, Zurich. The author thanks to members concerned.

CONTENTS

CHAPTER 1. INTRODUCTION

1.1 The Importance of Knowing Deep Underground Structure in Earthquake Engineering

The evaluation of effects of soft sedimentary layers on earthquake ground motions has been still one of the most important subjects in earthquake engineering. At the first stage, the primary interest of engineers was concentrated on ground motions less than 1 sec, because their objectives were to reduce seismic damage of low-rise buildings and wooden houses which are characterized by short natural periods. Recent construction of a number of large-scale structures, such as high-rise buildings, large oil storage tanks, long-spanned bridges, etc, with a natural period range between two and 20 sec requires the precise evaluation and prediction of longer period ground motions.

Intensive work in this subject was carried out in the last two decades. The first systematic investigations were conducted to elucidate the nature of a 2.5 sec long period component in a strong ground motion observed at Hachinohe during the Tokachi-Oki earthquake of 1968(Osawa, 1972). After this worthy work, many investigations related with long period ground motions were performed dealing with various aspects of engineering. Review of these work will be described in the next section. Through these investigations, it was recognized that deep underground structures with low S-wave velocities (around 1 km/sec) have significant influences on longer period earthquake ground motions. Actually, longer period ground motions are often observed at the stations where deep sedimentary layers overly basement with S-wave velocity more than 3 km/s (e.g., Hanks, 1975; Seo, 1980).

Despite of a large number of contributions, the characteristics of longer period ground motions are still a matter of debate. One of the difficulties is due to low quality of observational data of ground motions and the uncomplete knowledge of deep underground structures.

Detailed knowledge of the deep underground structure is also needed, when we define a seismic bedrock for seismic microzoning. Seismic waves travel from a source to the

seismic bedrock with similar characteristics. Then, the variation of ground motions on the free surface at every site is mainly due to the effects of the sedimentary layers over the seismic bedrock. Using this concept, we can distinguish between source and site effects. Therefore, the seismic bedrock is required to exist all over the considered area with the same physical characteristics. Moreover, the variations of the physical characteristics below the seismic bedrock should be small as compared with those over the seismic bedrock. It was proposed that the layer with an S-wave velocity of 3 km/sec is suitable for the seismic bedrock in the Kanto district (Seo, 1981).

1.2 Review of Previous Studies

It was often pointed out in many studies that earthquake ground motions observed on the free surface are significantly affected by deep underground structures corresponding to propagation paths. Here, the previous work on (a) surveys of deep underground structure, (b) effects of deep sedimentary layers on seismic wave propagation evaluated from earthquake observations and (c) numerical forward modelings of seismic wave propagation are reviewed.

(a) Previous studies on surveys of deep sedimentary layers

The assessment of the velocity distribution in depth has been one of the most important issues in seismology, specially, in explosion seismology. A large number of seismological work was devoted to this objective by means of various methods, such as travel time analyses of seismic waves from explosions and earthquakes, dispersion analysis of surface waves, analyses of gravity data (e.g., Mikumo, 1966; Yoshii, 1979). Although underground structures in many regions have been assessed in seismology, this is not enough for engineering purposes. Due to the fact that crustal and mantle structures are the main interest of most of seismologists, the sedimentary layers are considerably simplified and are inadequate for engineering use.

The first seismic refraction survey of deep sedimentary layers' structure for engineering purpose at Hachinohe was carried out in 1970, where strong motion records were obtained during the Tokachi-Oki earthquake of 1968. As a result of this, the sedimentary layers were found to have P-wave velocities of around 2 km/sec down to a basement of a P-wave velocity of 5 km/s (Okada, 1971). After this experiment, seismic refraction surveys of sedimentary layers were carried out in several areas, such as the Kyoto basin (Kitsunezaki et al., 1971), the Kanto district (Shima et al., 1976a), the Nagoya district (Masaki, 1985). Recently, Toriumi et al (1988) conducted a refraction experiment in Osaka plain. Sedimentary layers' structures down to the top layer of the earth's crust with P-wave velocities more than 5 km/sec were more or less known from these investigations.

Amaike et al. (1982) performed a seismic reflection experiment in the Kyoto basin and found reflectors up to several hundred meters in depth. However, seismic reflection surveys of deep sedimentary layers is not often adopted for the purpose of earthquake engineering, because it is not easy to deduce P- or S-waves velocities of strata and to acquire considerably dense data for identification of reflected phases on land.

Another kind of seismic surveys for estimating structure of deep sedimentary layers were carried out by means of a down-hole method by Ohta et al.(1977, 1978a) and Yamamizu et al.(1981). Although the resultant underground structures were significantly accurate, they provided only information for the vicinity of each site. These results become important reference points during interpretations of refraction data.

In the above-described studies, the elastic properties of sedimentary layers were directly measured. Such direct measurements require a large effort in data acquisition and interpretation. Hence, attempts to estimate the underground structure indirectly with smaller efforts by measurements of longer period microtremors were tried by some researchers in Japan (e.g., Ohta et al., 1978b). Although the clear understanding of longer period microtremors is still pending, their applicability to earthquake engineering has been demonstrated. For example, Kagami et al.(1986) estimated spatial distribution of site

amplification effects by spectral ratios of microtremors at sediments to that at firm rock, and Horike (1985) determined S-wave velocities of sedimentary layers by an inversion of phase velocities derived from an array observation of microtremors.

(b) Previous studies on the effects of deep sedimentary layers on seismic wave propagation from earthquake observation

Local site effects on earthquake ground motions have been successfully discussed by 1-dimensional multiple reflections of S-waves in a shallow subsurface structure with a depth of several ten meters as well-described by Kanai (1982). In the early 70's, when high-rise buildings began to be built in Japan, it was pointed out from the investigation of the strong ground motions observed at Hachinohe in Aomori prefecture during the Tokachi-Oki earthquake of 1968 that the contribution of S-waves, were not sufficient to explain the observed longer period ground motion and the effect of surface waves was not negligible (e.g., Shima, 1970). Kamiyama (1979) suggested that longer period components in this strong ground motion at Hachinohe is a surface wave generated in the vicinity where the subsurface structure drastically varies. Also, the appearance of surface waves in strong motion records during the San Fernando earthquake of 1971 was pointed out (Hanks, 1975, 1976). Tanaka et al. (1979) investigated the characteristics of longer period ground motions in many old strong motion records at Hongo, Tokyo, and pointed out that ground motions with a period of 8 sec are predominant in Tokyo. The paper-recorded strong motion data from JMA seismographs were also used for engineering purposes (e.g., Katayama and Shino, 1984), because these seismographs are distributed all over Japan and earthquake records have been considerably accumulated.

In order to understand seismic wave propagation rationally, records obtained at a site are not sufficient and array analyses of earthquake ground motions are required. Seo (1978) pointed out from comparative observations that longer period ground motions observed in the Kanto plain are Love waves amplified within sedimentary layers. Kudo et

al. (1984) made array observation and concluded that the variation of predominant period in longer period range is due to the difference of the thickness of deep sedimentary layers. Lui and Heaton (1984) carried out an array analysis of a number of strong ground motions observed during the San Fernando earthquake of 1976, California, and concluded that longer period ground motions observed on sedimentary layers are due to the excitation of surface waves within sedimentary layers. Such surface waves which are generated in the margin of a basin and propagate horizontally are often called local surface waves. The appearance of local surface waves were also suggested by Toriumi (1975), Toriumi et al. (1982), Horike (1988) and Hoshiba et al. (1988). They also concluded that this kind of the surface waves can not be explained by simple 1-dimensional considerations.

Body wave propagation in deep sedimentary layers with several kilometers in depth has not been discussed fully. Seo and Kobayashi (1982) and Kinoshita (1985) pointed out the existence of multiple reflections within deep sedimentary layers and they applied the proposed propagation mechanism to evaluate surface wave amplification. Irikura and Kasuga(1980) observed earthquake ground motions in the vicinity where a step-like topography of a basement are speculated and concluded that 1-D multiple reflections of S-waves are not sufficient to explain the observation.

(c) Previous work on numerical forward modelings of seismic wave propagation

Computational modeling is one of the effective ways for evaluating the response of irregular subsurface ground structures where no analytical solutions can be derived. In the following, we review the computational investigations of seismic wave propagation in inhomogeneous media.

A fundamental inhomogeneous underground structural model is a model which allows vertical inhomogeneities. Matrix methods, such as the Haskell's method (Haskell, 1953), is a typical one. Harkrider proposed a method for computations of surface wave excitation in multilayered media with a fault mechanism by considering only normal mode contribution

(1964, 1970). For instance, Kudo (1978) and Swanger and Boore (1978) used this method and achieved good agreements of synthetic seismograms with earthquake ground motions observed on sedimentary layers. Moreover, Kudo (1980) improved the normal mode summation method by a combination of the Alsop's method (1966) where transmission and reflection coefficients of surface waves are introduced between two underground structural models. Inoue et al (1982) also used the normal mode summation method and compared the synthetic results with design spectra for civil engineering structure.

The reflectivity method which is often used for interpretations of explosion data is also a method for modeling in vertically inhomogeneous media (Fuchs and Mueller, 1971). Recently, a 2-D reflectivity method was developed by Kohketsu (1987a) and he concluded that irregularities larger than one-tenth of the considered wavelength can not be ignored through modelings for various underground structural models (Kohketsu, 1987b).

Aki and Larner (1971) devised a method to compute SH-wave field due to plane wave incidence in a surface layer overlying a half-space with a irregular interface. Bard and Bouchon (1980a, 1980b, 1985) carried out systematic computational investigations of time domain response of a basin using the Aki and Larner technique and pointed out the existence of local surface waves and 2-D resonance pattern. Kasuga and Irikura (1982) applied this method to simulate wave propagation in a subsurface structure with a step-like topography of a basement and compared with observed spectra. The extension of the Aki-Larner method to multi-layered media with irregular interfaces was proposed by Horike (1987). This extended technique was applied to simulate earthquake ground motions in the Kyoto basin (Hoshiba et al., 1988).

Methods with approximations of discretization, such as finite element method and finite difference method, are more general and flexible than the above synthetic methods, in spite of requirement for large computational capacities. A finite element method is popular in the field of structure dynamics and is also applied to wave propagation problems (e.g., Lysmer and Drake, 1972; Smith, 1975). Zama (1981b) explained the distribution of the

damage during the Nankaido earthquake of 1944 using a finite element modeling. He also apllied the method to simulate surface wave propagation in realistic underground structural models of the Kanto plain and pointed out the importance of the effects of the irregularities of the subsurface ground structures (1981c). A finite difference method is also often used, specially in the field of seismology and geophysical exploration (e.g., Boore, 1972 ; Kelly et al., 1976). Vidale and Helmberger (1988) investigated seismic wave propagation in a sedimentary basin by a finite difference modeling with source descriptions and obtained good fittings with strong motion records observed during the San Fernando earthquake of 1971. Ohtsuki et al. (1983, 1984a) combined a finite element method with a method similar to a finite difference method, and discussed SV and Rayleigh waves propagation. Moreover, they (1984b) compared the observed seismic responses of shallow sedimentary layers with a thickness of about 20 meters with synthetic ones.

Ray theoretical synthetic methods are different procedures from the above-mentioned methods. The seismic response of a dipping layer overlying a basement due to a plane wave incidence was discussed by Ishii and Ellis (1970) and Sanchez-Sesma and Velazquz (1987). Irikura (1976) investigated the response of two surface layers over a basement in a similar way. In these simple geometrical models with planar interfaces, the effect of geometrical spreading do not have to be included. Hong and Helmberger (1978) developed a geometrical optics method to allow computation of wave propagation in a media with nonplanar interface. For computations of wave propagation in general inhomogeneous media, asymptotic ray theory is often used, specially in explosion seismology (e.g., Cerveny, 1985). Recently, a ray method based on a parabolic approximation, the Gaussian beam method, has been applied (Cerveny, 1982; Nowack and Aki, 1984), in which reliable synthetic seismograms can be obtained even in shadow zones and caustics. Although these ray methods in inhomogeneous media require small computational efforts and the contribution of each ray is easily identified, they are approximated methods in high frequency and the synthetic results are not accurate in a period range longer than the scale of irregularities of under-

ground structural models as examined by Maczo et al. (1987).

Although 3-dimensional computations began to be attempted with simple models (Horike, 1988; Sanchez-Sesma, 1988; Cherveny et al., 1982; Reshef et al., 1988), simulation for realistic structural models is still a difficult problem.

Considering the three kinds of investigations mentioned above, it is concluded that the basic dta are too few to evaluate earthquake ground motions with enough accuracy for engineering purpose. In particular, structures of deep sedimentary layers covering large area are unknown. Consequently, proper and realistic underground structural models could not fully be used in many investigations on modelings of seismic wave propagation. A detailed knowledge of the deep sedimentary layers' structure can allow us to understand the characteristics of earthquake ground motions and to accomplish numerical modelings with practical engineering meaning.

1.3 Objectives and Approach

An earthquake ground motion consists of many phases which arrive at a station one after another. These later phases make ground motion complex, because of their constructive and destructive interferences. Usually, it is very difficult to understand all the features of ground motions.

The identification the origins of these phases and the assessment of the underground structures from these later phases is one of most important targets in seismological research. On the other hand, this kind of investigation has not been often performed in the field of earthquake engineering, because much of interest of engineers is concentrated on the character of the whole of earthquake ground motions (e.g. peak amplitude, duration, envelope form etc.), and not the characteristics of each phase. However, the sequence of later phases determines the general character of ground motions. Hence, proper understanding of later

phases can facilitate the understanding the characteristics of ground motions. The fundamental object of this study is to understand the nature of distinct later phases seen in observed seismograms.

Generally, factors which determine the characteristics of earthquake ground motions are considered to be effects from source, path and local sites. Although these three effects should be combined in predicting earthquake ground motions, only site effects are investigated in the present study; site effects can arise strong differences of ground motions at each site. In particular, the effects of deep sedimentary layers, on which large cities are generally located, are investigated in the respect to seismic wave propagation.

In order to accomplish the objective, it is needed to know underground structure in the area considered. In this study, the southwestern part of the Kanto district, Japan, was chosen as the field. At first, seismic refraction surveys using explosions were performed to make clear the underground structure down to the upper layer of the earth's crust in the area. The underground structure is important for assessing the expected longer period ground motions in the Tokyo Metropolitan area during large earthquakes which might occur along the Sagami and the Suruga troughs, because the underground structure corresponds to the propagation path of seismic waves to the whole of the Metropolitan area. It is also valuable to clarify the underground structure in the area, because a few surveys were carried out before and it becomes one of the objectives of this study, too.

The explosion seismograms obtained during the seismic surveys were used not only for making clear the underground structure, but also for understanding propagation mechanism of seismic waves in the sediments. Because of well-defined source parameters, such as location and origin time, and their impulsive wave forms, this kind of investigation is useful for understanding wave propagation phenomena.

Next, some propagation characteristics of distinct later phases in earthquake ground motions observed in seismic arrays were interpreted using the assessed structure of the deep sedimentary layers. Furthermore, numerical modeling was carried out to confirm the

proposed propagation mechanisms of body and surface waves in various underground structural models.

CHAPTER 2. SEISMIC SURVEYS OF DEEP UNDERGROUND STRUCTURE IN THE SOUTHWESTERN KANTO DISTRICT, JAPAN

2.1 Review of Previous Studies on Underground Structure in the Southwestern Kanto District, Japan

In the Kanto district, Japan, knowledge of the deep sedimentary layers had been very few: geological investigation (e.g., Kakimi, 1973) and geophysical research (Ishii, 1962, Hatayama, 1964). In particular, the underground structure in the southwestern Kanto district which is the field of this study was unknown. In 1975, the first refraction survey was carried out in the Tokyo Metropolitan area by the Research Group for Basement Structure of Tokyo Metropolitan Area and it was revealed that the thicknesses of surface layers having P-wave velocities of 1.8 and 2.8 km/sec are 1.3 and 1.0 km, respectively, that the P-wave velocity of the basement in Tokyo is 5.5 km/sec (Shima et al., 1976a). Shima et al. (1976b) observed the reverse shot at Yoshikawa and refined the underground structure model. The explosions at Yumenoshima have been still continued twice a year since 1975, because another objective is to detect the P-wave variation for the purpose of earthquake prediction. Therefore, a large number of explosion data are being acquired. In the following, 'basement' means a firm rock with a P-wave velocity around and more than 5 km/sec.

In the southwestern part, the underground structure from Yumenoshima to Takao was made clear (Shima et al., 1978). Shima et al. (1976c) observed explosions at Ohgishima and concluded that the thickness of the sedimentary layers at Ohgishima is almost the same as that at Yumenoshima. Kasahara et al.(1976a, 1976b) made a refraction survey from Yokohama in Kanagawa prefecture to Han'noh in Saitama prefecture and obtained underground structure where two kinds of basements with a velocities of 4.8 and 5.5 km/sec exist and the thickness of the sedimentary layers becomes larger toward Yokohama. Seo and Kobayashi (1980) observed the Yumenoshima explosion on a profile from Yumenoshima to Enoshima and suggested the possibility of a basement velocity of 5.1 km/sec. Attempts to assess the underground structure three-dimensionally were also carried out (Shima, 1980;

Seo et al., 1982). Since there were no reversed shots except for the explosion at Yoshikawa and most of the available data were derived from the explosions at Yumenoshima, some ambiguities still remain.

More detailed knowledge on underground structure was derived from marine seismic reflection surveys in the Tokyo Bay area (Kato, 1984). A down-hole measurement of P- and S-waves was performed at the Fuchu deep borehole by Yamamizu et al. (1978). They concluded that the depth to a layer with a P-wave velocity of 4.8 km/sec is about 2 km at the borehole site. Moreover, they compared the profiles with geological data.

As it has been discussed above, the velocity profiles at a few sites in the southwestern Kanto district were already well-known. However, the underground structure of a whole of the area is not still clarified. Therefore, engineering requirement where underground structural models at arbitrary sites are needed can not be satisfied.

2.2 Seismic Refraction Surveys

2.2.1 Outline of seismic refraction surveys

The field of the investigation is depicted in Fig. 2-1: the southwestern Kanto district, Japan. The Kanto plain forms a tectonic basin and there is the Kanto Mountains at the western side of the area. An outcrop of a basement rock having a P-wave velocity of about 5 km/s can be found at the foot of Mt. Takao.

The location of the temporary stations and the explosion sites are depicted in Fig. 2.1. It should be noted that all the explosions were not detonated at the same time, but we observed a few explosions at stations on some surveying lines. The origin times and the locations of the explosions are listed in Table 2-1. The explosions with 100 to 500 kg dynamite were fired in boreholes approximately 100 meters in depth during midnights for achieving better S/N ratios. The observation was carried out by the Research Group for Basement Structure of Tokyo Metropolitan Area, in which the author is involved, and

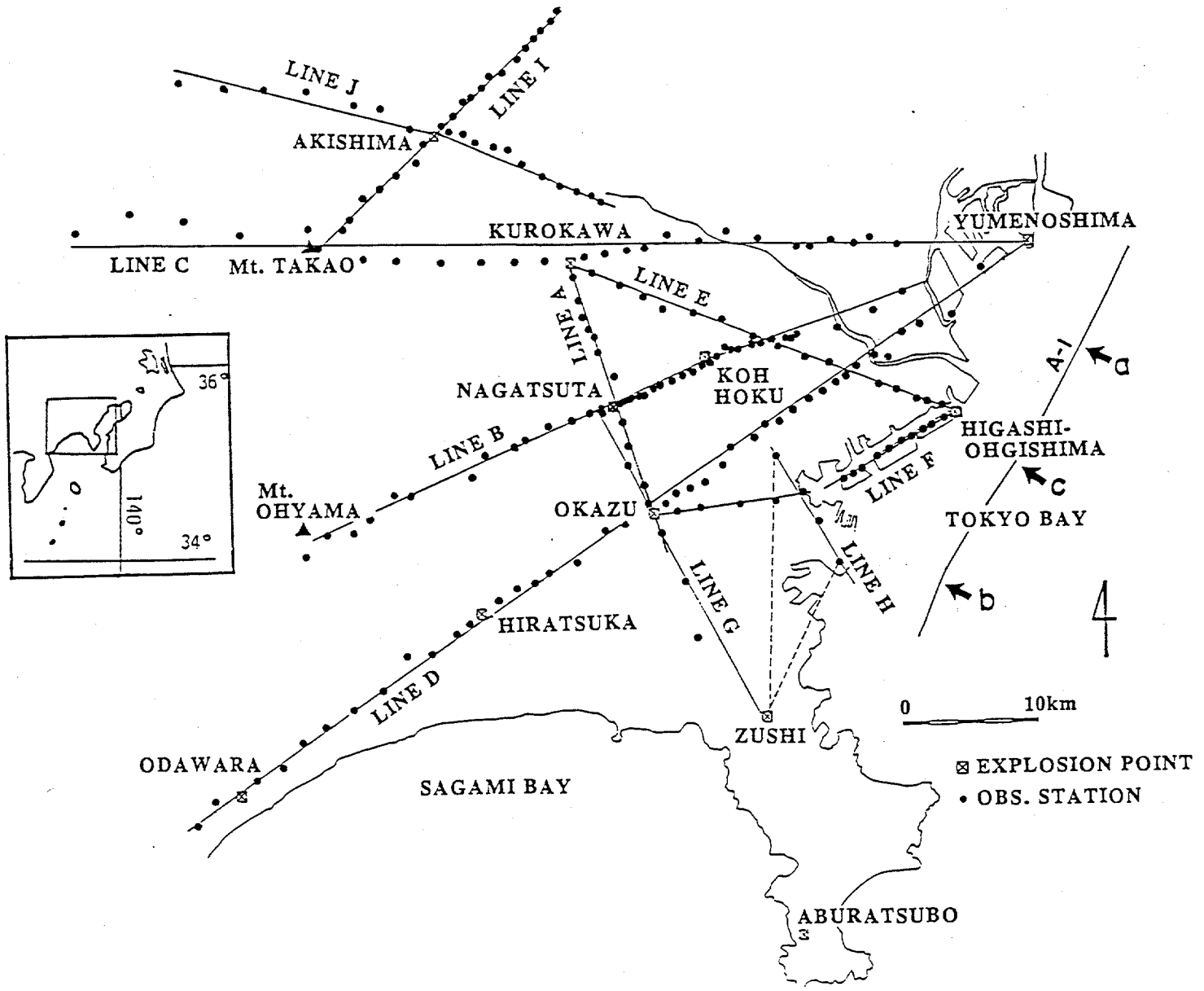

Fig. 2-1. Map of the studied field, the south-western Kanto District, Japan. Solid circles and solid lines show temporary observation stations and surveying lines, respectively. Explosion points are indicated by squares.

Table 2-1. Origins of explosions for seismic surveys

No	LOCATION	ORIGIN TIME	LAT.	LONG.	CHARGE(kg)
1	HIGASHI OHGISHIMA	'83 03/13 01:52:00.217	35 30 06.9	139 46 28.3	300
2	YUMENOSHIMA (17TH)	'83 03/13 02:02:01.14	35 36 54.7	139 50 14.4	500
3	OKAZU	'83 03/13 02:12:00.412	35 26 33.2	139 31 08.8	300
4	HIRATSUKA	'83 03/13 02:21:59.167	35 22 52.0	139 22 38.8	300
5	KUROKAWA	'83 10/16 01:52:00.132	35 36 20.5	139 27 27.7	300
6	YUMENOSHIMA (18TH)	'83 10/16 02:01:59.05	35 36 44.7	139 50 17.4	500
7	NAGATSUTA	'83 11/18 02:03:00.15	35 30 50.0	139 29 20.6	100
8	YUMENOSHIMA (19TH)	'84 03/11 02:02:00.23	35 36 45.3	139 50 17.5	500
9	AKISHIMA	'84 03/11 02:12:00.411	35 41 33.0	139 21 07.5	100
10	ODAWARA	'84 03/11 02:22:00.092	35 15 55.6	139 10 28.7	300
11	YUMENOSHIMA (20TH)	'84 11/11 02:01:59.474	35 36 43.5	139 50 18.8	500
12	KOHHOKU (YOKOHAMA)	'84 11/25 02:02:00.166	35 32 23.1	139 34 14.4	450
13	ZUSHI	'84 11/25 02:12:00.537	35 18 30.6	139 36 23.6	300
14	ABURATSUBO	'84 11/23 02:22:00.337	35 09 57.6	139 37 54.8	450

additionally by Tokyo Metropolis, Kanagawa Prefecture and Kawasaki City. Most of the seismometers used for the observation were electromagnetic seismometer with a natural period of 0.22 sec. The surveying lines are;

Kurokawa-Okazu line (Line A): Between Kurokawa (Kawasaki) and Okazu (Yokohama)

Yumenoshima-Ohyama line (Line B): From Yumenoshima to Ohyama

Yumenoshima-Takao line (Line C): From Yumenoshima (Tokyo) towards the west via Kurokawa (Kawasaki) and Takao

Yumenoshima-Odawara line (Line D): From Yumenoshima to Odawara via Okazu (Yokohama) and Hiratsuka

Kurokawa-Higashiohgishima line (Line E): From Kurokawa to Higashiohgishima (Kawasaki)

Okazu-Higashiohgishima line (Line F): From Okazu to Higashiohgishima

Zushi-Nagatsuta line (Line G): From Zushi to Nagatsuta (Yokohama)

Yokohama line (Line H): Around Yokohama

Tokorozawa-Takao line (Line I): From Tokorozawa (Saitama) to Takao via Akishima explosion site

Fuchu-Itsukaichi line (Line J): From Fuchu to Itsukaichi (Tokyo) via Akishima explosion site

The travel time analyses by means of refraction method were carried out to obtain P-wave velocity profiles of the underground structure for each surveying line in Fig. 2-1, so that the disagreement at the crossed points between surveying lines becomes as small as possible.

2.2.2 Underground structure along the Kurokawa-Okazu line

16 temporary stations are installed along a line from Kurokawa to Okazu. The seismograms observed at stations in the Kurokawa-Okazu line from the Kurokawa and the Okazu explosions are displayed in Figs. 2-2 and 2-3. The amplitude scale of explosion

seismograms is arbitrary (also in the following). Since the surveying line is relatively short, clear onsets could be obtained from the both explosions. Although no initial phases can be seen in Fig. 2-3, the arrivals of the onsets were detected from the records with higher amplification factors. The obtained arrival times of the initial phases are shown in Table 2-2. Three layered structure can be deduced from the travel time curve in Fig. 2-4. The P-wave velocities are 2.0, 2.9 and 4.8 km/sec, up to down, respectively. In the following travel time analysis, a velocity means a P-wave one. Because of the short length of the surveying line, the layer with a velocity of 5.3-5.6 km/sec which was usually found in the seismic surveys in the Kanto district could not be found in this line.

The explosion at Yumenoshima was also observed at the stations along this surveying line. The source-sites geometry is like a fan shooting. The travel times of the onsets for the Yumenoshima explosion are shown in Table 2-2, too. Because of the longer epicentral distances, these initial phases can be interpreted as the phases propagating in the layer with a velocity of 5.3-5.6 km/sec. In order to determine this refractor velocity, we compared the distribution of two kinds of time-terms; the time-terms corresponding to thicknesses of layers overlying the layers with a velocity of 4.8 km/sec and of 5.3-5.6 km/sec. The comparison is shown in Fig. 2-5. The former time-terms (dotted line) are derived from the Kurokawa and the Okazu explosions. The latter time-terms (solid line) are obtained from the Yumenoshima explosion by assuming that the refractor velocities are 5.3 to 5.6 km/sec and the time-term at Yumenoshima is 1.03 sec. The time-term at Yumenoshima was obtained by Shima et al. (1976a). The refractor's velocity can not be determined only from this figure. It is considered, however, that this velocity is 5.5 km/sec from similar consideration for Yumenoshima-Ohyama line discussed later.

Using the travel time data from the Kurokawa and the Okazu explosions and the time-terms derived from the Yumenoshima explosion, the P-wave velocity profile between Kurokawa and Okazu was obtained as depicted in Fig. 2-6. The depth to the layer with a velocity of 4.8 km/sec becomes slightly shallower towards Okazu, while that to the layer

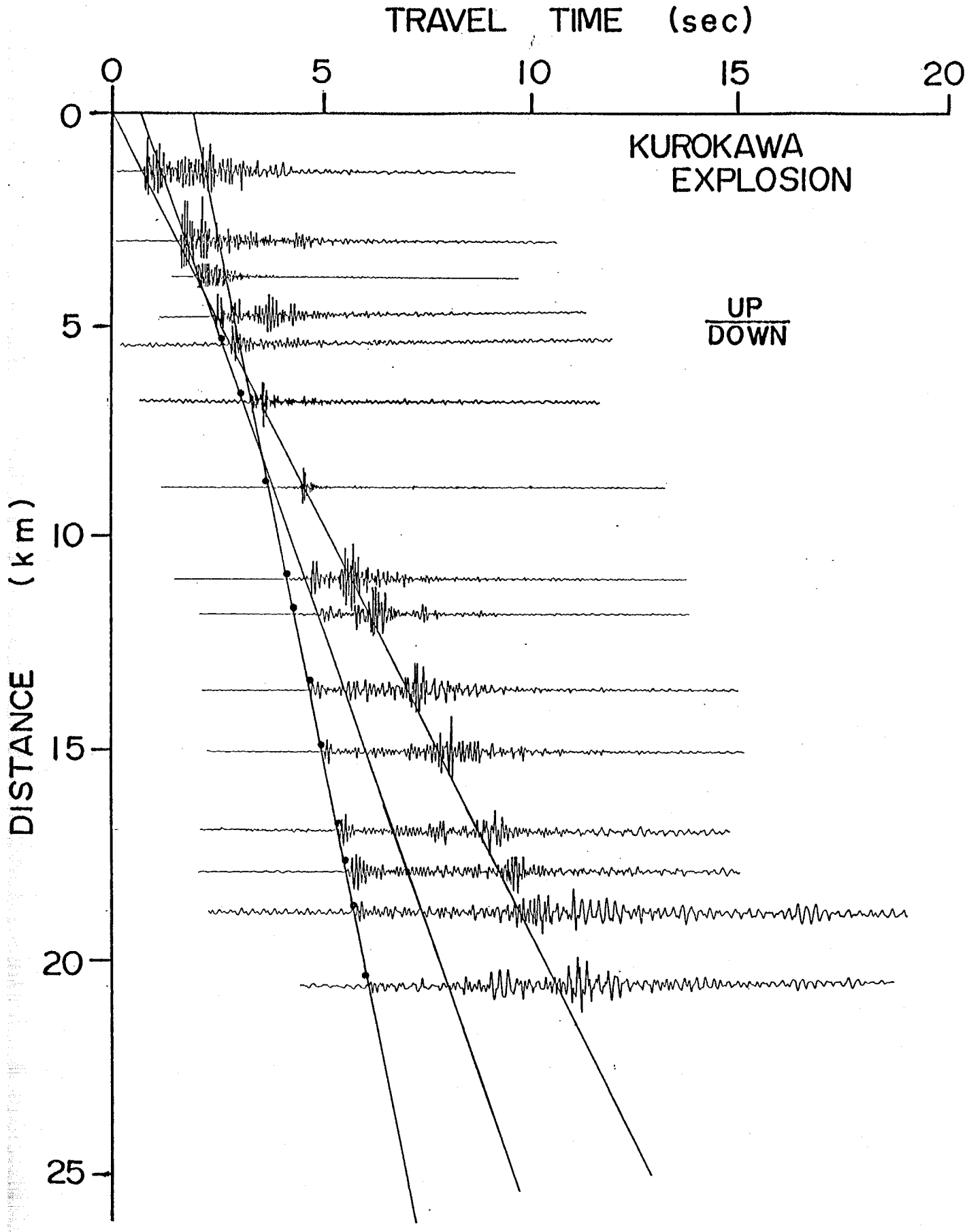

Fig. 2-2. Observed seismograms at the stations along the Kurokawa-Okazu line (Line A in Fig. 2-1) during the Kurokawa explosion. Each trace indicates vertical ground velocity and is normalized to its maximum amplitude. Each solid circle shows onset of initial phase.

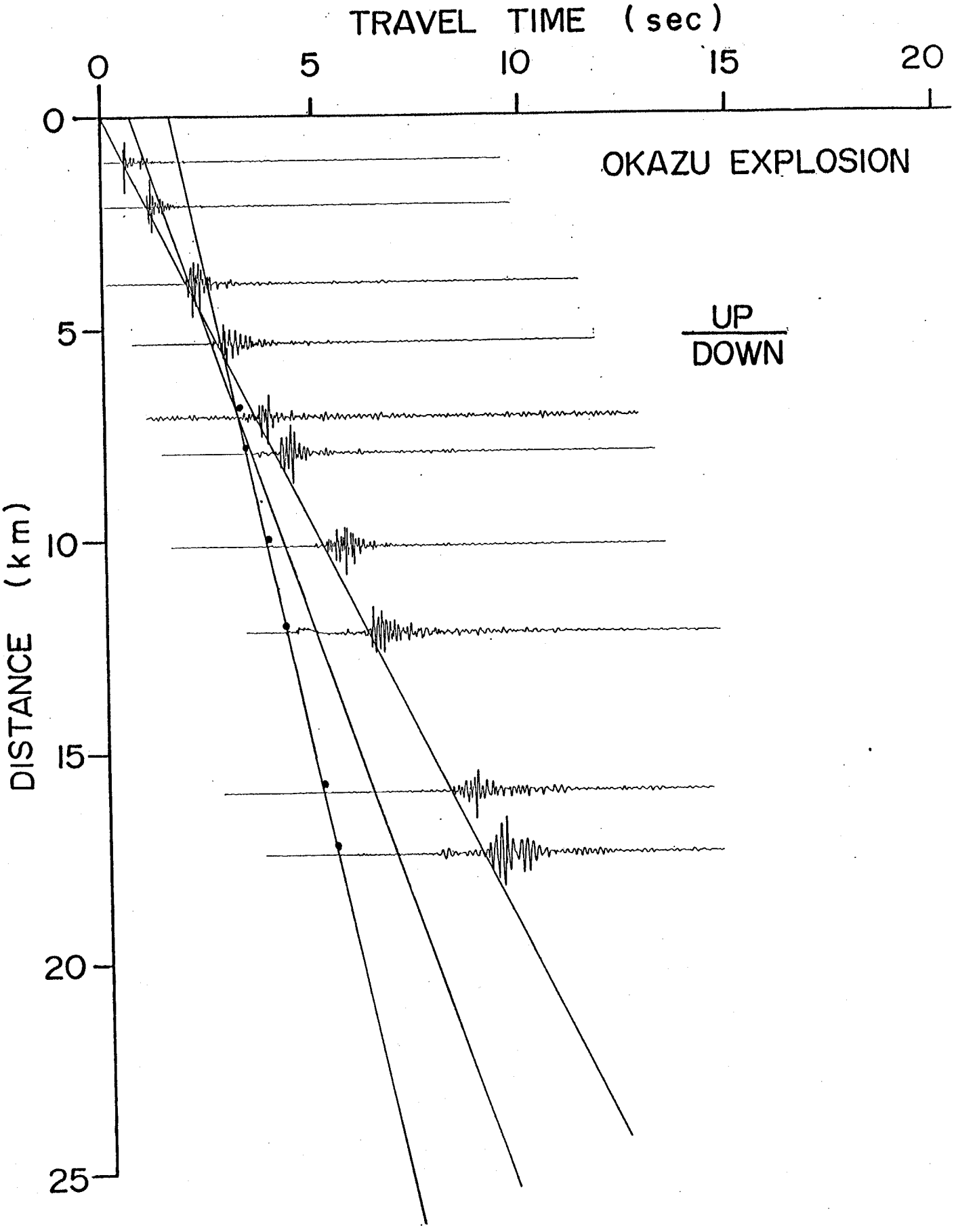

Fig. 2-3. Observed seismograms at the stations along the Kurokawa-Okazu line (Line A in Fig.1) during the Kurokawa explosion. Each trace indicates vertical ground velocity and is normalized to its maximum amplitude. Each solid circle shows onset of initial phase.

Table 2-2. Travel times of initial phases obtained
from Kurokawa, Okazu and Yumenoshima explosions

No	STATION	LOCATION		OKAZU		KUROKAWA		YUMENOSHIMA	
		LAT.	LONG.	D(km)	T(s)	D(km)	T(s)	D(km)	T(s)
0	KUROKAWA	35 36 20.5	139 27 27.7					34.48	8.43
1	WAKO	35 35 37.9	139 27 42.9	17.45	5.37	01.37	0.69	34.15	8.43
2	KANAI KITA	35 34 44.7	139 27 51.2	15.95	5.13	03.01	1.54	34.08	8.52
3	KANAI	35 34 21.0	139 28 10.6			03.84	1.96	33.69	8.52
4	TAMAGAWA UNIV	35 33 49.6	139 28 17.1			04.81	2.40	33.67	8.57
5	NARUSEDAI 1	35 33 31.8	139 28 34.9			05.47	2.63	33.32	8.51
6	NARUSEDAI 2	35 32 51.0	139 28 51.6	12.15	4.21	06.79	3.09	33.16	8.54
7	NAGATSUTA	35 31 52.7	139 29 30.4	10.16	3.77	08.81	3.69	32.66	8.50
8	T.I.T NGT	35 30 34.1	139 29 16.9	07.94	3.38	11.02	4.13	33.73	8.63
9	WAKABADAI	35 30 13.4	139 29 46.3	07.10	3.15	11.84	4.31	33.26	8.55
10	HODOGAYA C.C.	35 29 16.9	139 30 02.5	05.31	2.50	13.62	4.70	33.56	8.60
11	SEYA	35 28 29.5	139 30 08.1	03.90	2.00	15.07	4.91	34.07	8.66
12	KIBOUGAOKA 1	35 27 39.8	139 30 52.3	02.10	1.15	16.85	5.33	33.81	8.61
13	KIBOUGAOKA 2	35 27 04.5	139 30 58.9	01.01	0.58	17.94	5.53	34.22	8.67
14	OKAZU S.P.	35 26 36.8	139 31 07.4			18.82	5.66	34.50	8.69
15	OKAZU	35 25 44.8	139 31 38.7			20.59	6.00	34.75	8.97

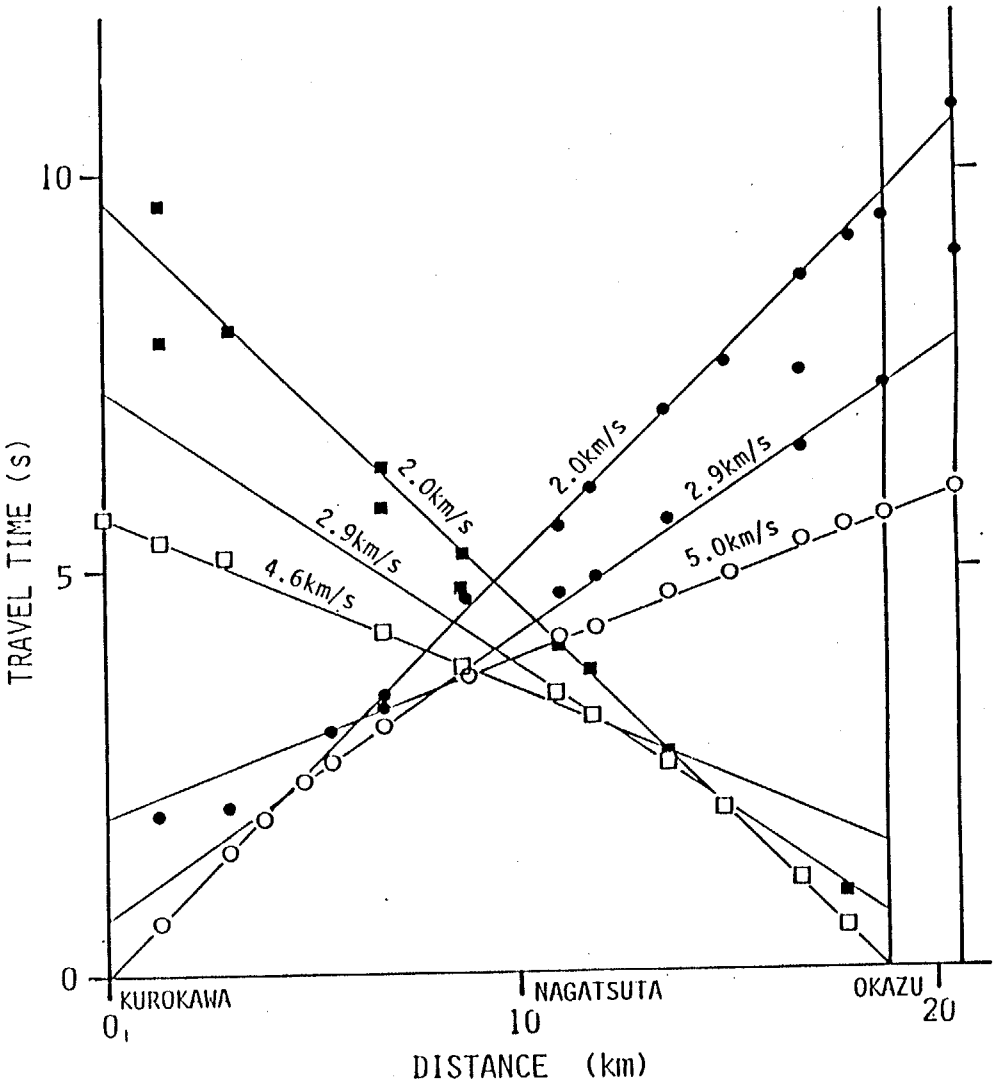

Fig. 2-4. Travel time diagram for the Kurokawa-Okazu line (Line A).

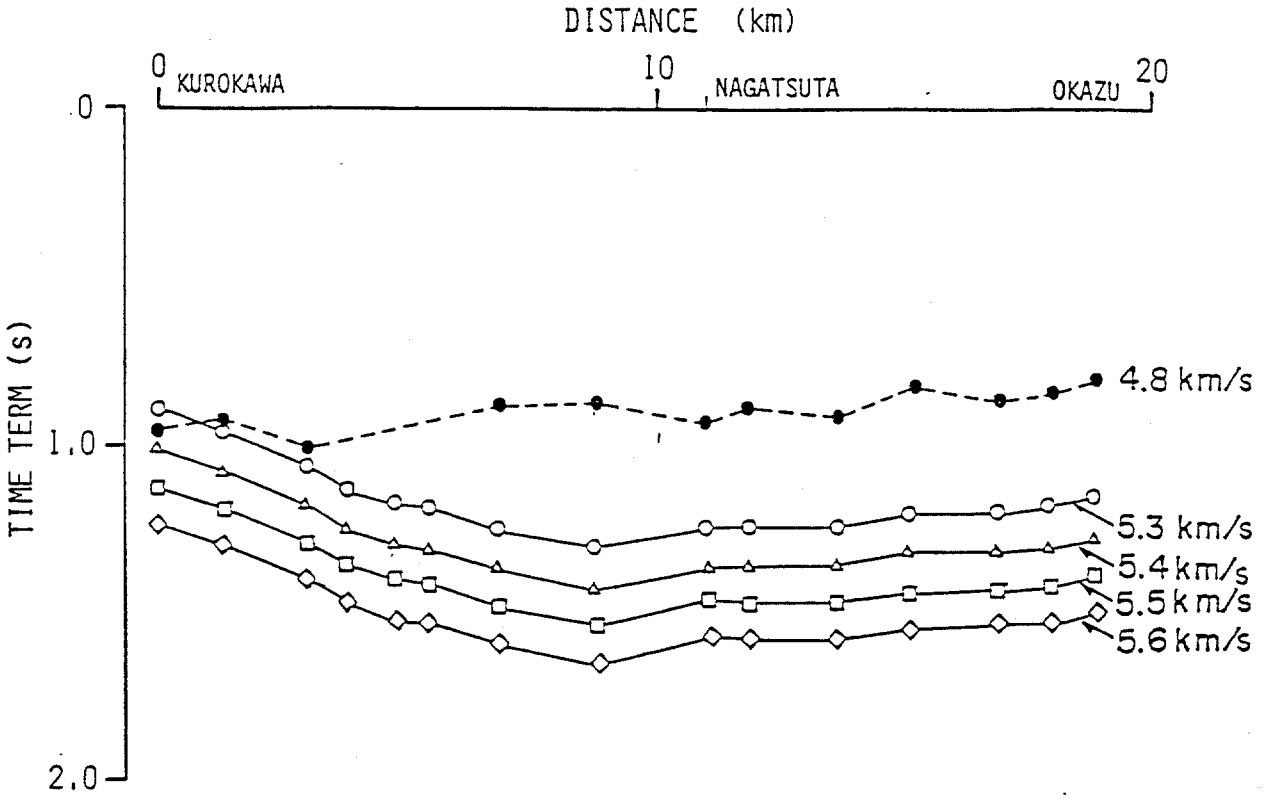

Fig. 2-5. Distribution of time-terms between Kurokawa and Okazu. Broken line shows time-terms to a layer with a P-wave velocity of 4.8 km/sec. Solid lines show time-terms of a layer beneath the layer with a velocity of 4.8 km/sec, when the refractor velocity is assumed 5.3, 5.4, 5.5 and 5.6 km/sec.

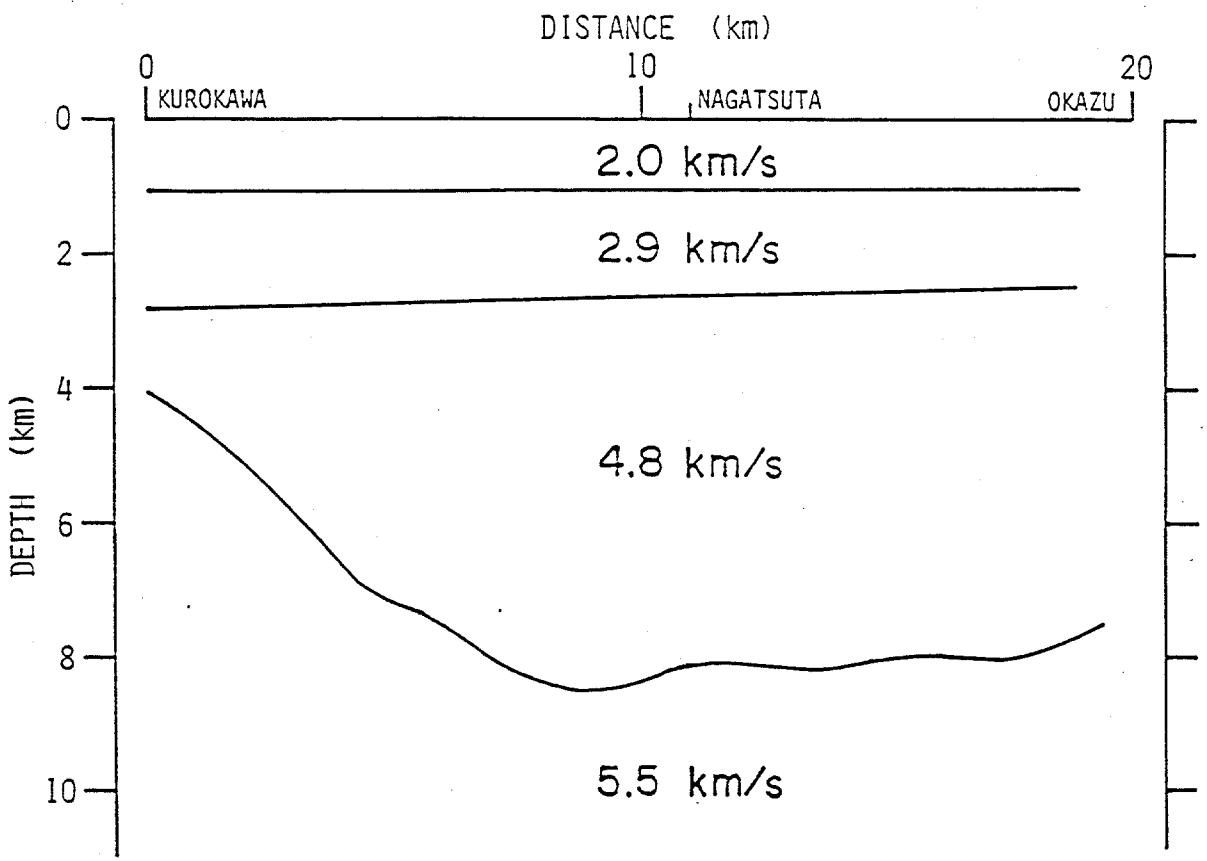

Fig. 2-6. Underground structure between Kurokawa and Okazu.

having a velocity of 5.5 km/sec becomes drastically deeper from Kurokawa to Okazu.

2.2.3 Underground structure along the Yumenoshima-Ohyama line

The Nagatsuta explosion site is located in the middle of the Kurokawa-Okazu line and the two surveying lines were spread in the east and the west directions from the Nagatsuta explosion site. This explosion corresponds to a reverse shot for the explosion at Yumenoshima. The explosion at Yumenoshima was also observed along the line by Seo (1981). This data was included in the interpretation, too.

The seismograms observed from the Nagatsuta explosion along the lines to the east and the west are displayed in Figs. 2-7 and 2-8, respectively. Each trace in the figures indicate vertical velocity with an arbitrary amplitude scale. Since the observation was carried out in a densely populated area and the charge size of dynamite was not large, S/N ratios at the stations with long distances were not high, specially, in the eastern side. Later phase with a low velocity seen in the seismograms at W1 to W4 is considered to be surface wave or direct SV-wave.

The travel times of the initial phases are shown in Table 2-3. Fig. 2-9 shows the travel time diagram for the Nagatsuta explosion. The travel time curve of onsets of the Yumenoshima explosion obtained by Seo (1981) is also shown in the same figure. The results of the travel time analysis along the Kurokawa-Okazu line discussed earlier indicate clearly that the underground structure consists of four layers whose P velocities are 2.0, 2.9, 4.8 and 5.3-5.6 km/sec. The velocity of the bottom layer is not clear. The same velocity profile can be expected at the Nagatsuta explosion site which is located between Okazu and Kurokawa. Since the intercept times of the travel time curves having apparent velocities of 6.8 and 4.4 km/sec are equal to two times of the time-term to the layer with a velocity of 4.8 km/sec derived at Nagatsuta from the Kurokawa-Okazu line, it is considered that the apparent velocities of 4.4 and 6.8 km/sec is due to a dipping of the layer with a velocity of 4.8 km/sec and the depth to this layer becomes drastically shallower towards the west. The apparent velocity of 5.2 km/sec as can be seen from the Yumenoshima explosion is due to

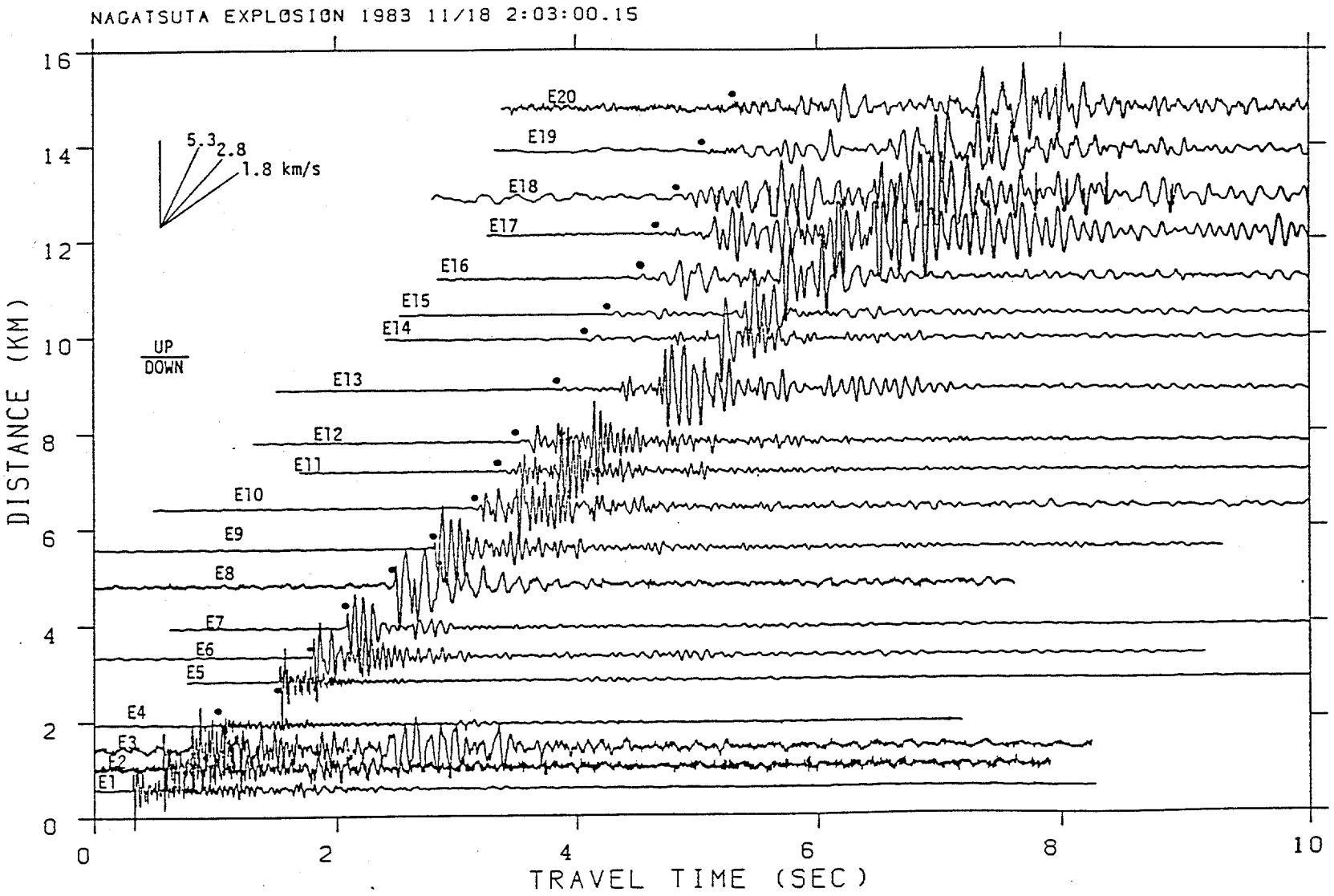

Fig. 2-7. Observed seismograms at the stations in the east from Nagatsuta along the Yumenoshima-Ohyama line (line B in Fig. 2-1). Each trace indicates vertical ground velocity and is normalized to its maximum amplitude. Each solid circle shows onset of initial phase.

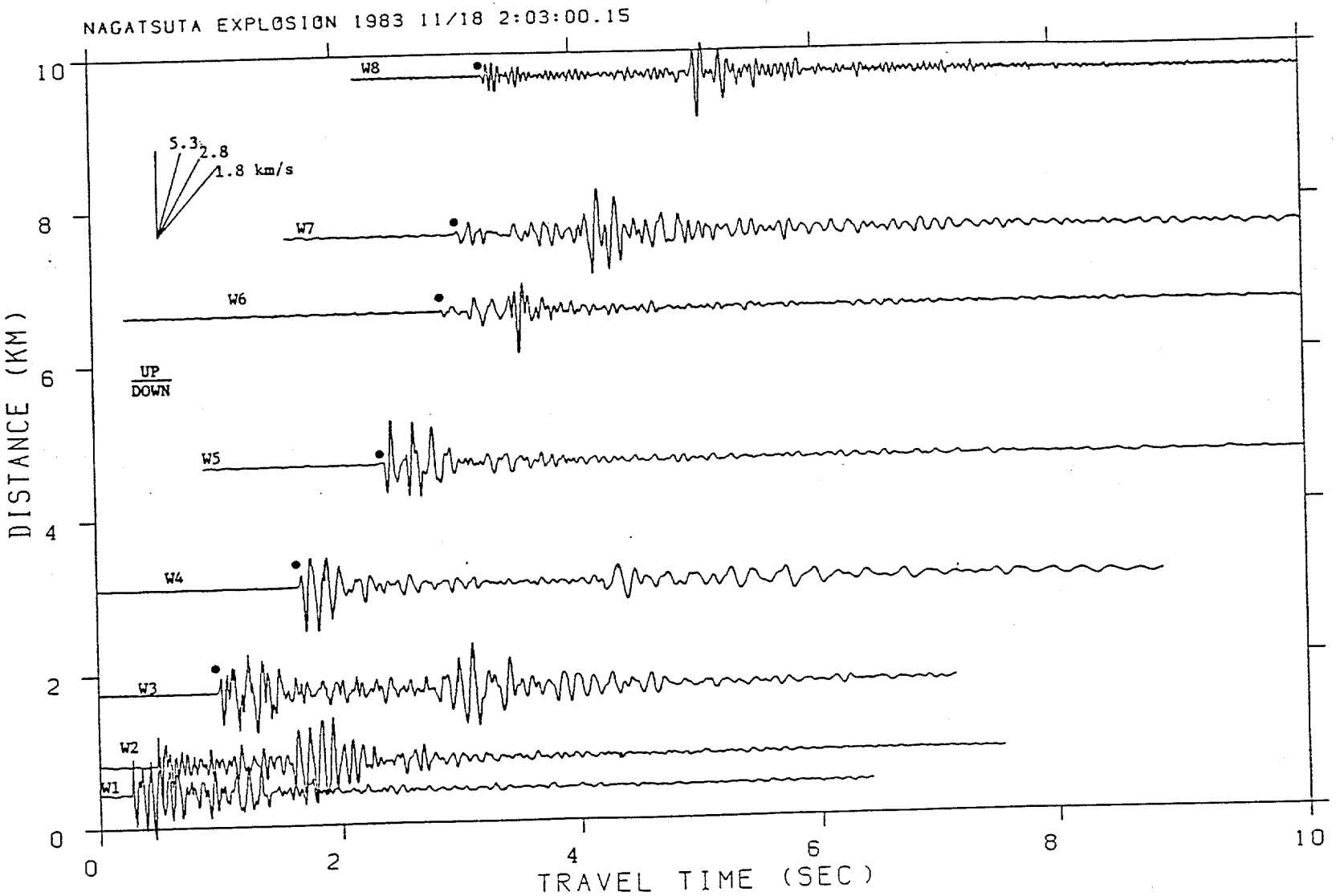

Fig. 2-8. Observed seismograms at the stations in the west from Nagatsuta along the Yumenoshima-Ohyama line (line B in Fig. 2-1). Each trace indicates vertical ground velocity and is normalized to its maximum amplitude. Each solid circle shows onset of initial phase.

Table 2-3. Travel times of initial phases obtained from Nagatsuta explosion

No	STATION	LOCATION		NAGATSUTA	
		LAT.	LONG.	D(km)	T(s)
E01	NAKAMURA	35 30 55.5	139 29 42.4	00.58	0.31
E02	NAGATSUTA 1	35 31 03.2	139 29 57.6	01.02	0.56
E03	NAGATSUTA 2	35 31 04.9	139 30 13.7	01.42	0.79
E04	SHOWA UNIV.	35 31 05.8	139 30 34.8	01.93	1.03
E05	TOHKAICHIBA	35 31 14.8	139 31 08.9	02.83	1.52
E06	HOUAI	35 31 19.0	139 31 28.4	03.34	1.80
E07	MIYAMAE	35 31 30.2	139 31 49.0	03.94	2.08
E08	NISHI HASSAKU	35 31 44.2	139 32 20.1	04.83	2.48
E09	KAWAWA 1	35 31 49.6	139 32 49.6	05.58	2.75
E10	KAWAWA 2	35 21 05.1	139 33 18.6	06.43	3.07
E11	KOUHOKU 1	35 32 11.2	139 33 47.8	07.18	3.27
E12	KOUHOKU 2	35 32 19.1	139 34 10.0	07.79	3.42
E13	CHIGASAKI	35 32 30.5	139 34 51.0	08.88	3.76
E14	NAKAGAWA 1	35 32 48.6	139 35 26.6	09.93	4.08
E15	NAKAGAWA 2	35 32 53.5	139 35 46.8	10.45	4.26
E16	MINAMI YAMADA	35 32 54.8	139 36 18.0	11.20	4.51
E17	HIGASHI YAMADA	35 33 03.7	139 36 52.6	21.11	4.66
E18	TAKADA	35 33 11.0	139 37 22.3	12.89	4.88
E19	SHIMODA	35 33 15.9	139 38 01.2	13.87	5.07
E20	IDA	35 33 22.2	139 38 36.2	14.76	5.34
W01	SUZUKAKEDAI	35 30 34.1	139 29 04.2	00.44	0.26
W02	MINAMI TUKUSINO	35 30 39.0	139 28 50.5	00.83	0.49
W03	TSURUMA	35 30 28.2	139 28 16.3	01.75	0.98
W04	TSUKIMINO	35 30 12.9	139 27 26.2	03.10	1.65
W05	MIDORINO	35 29 58.2	139 26 26.5	04.67	2.34
W06	KURIHARA	35 29 34.3	139 25 14.0	06.64	2.88
W07	ZAMA	35 29 21.3	139 24 37.4	07.64	3.01
W08	NISHI ZAMA	35 28 54.9	139 23 22.1	09.70	3.25

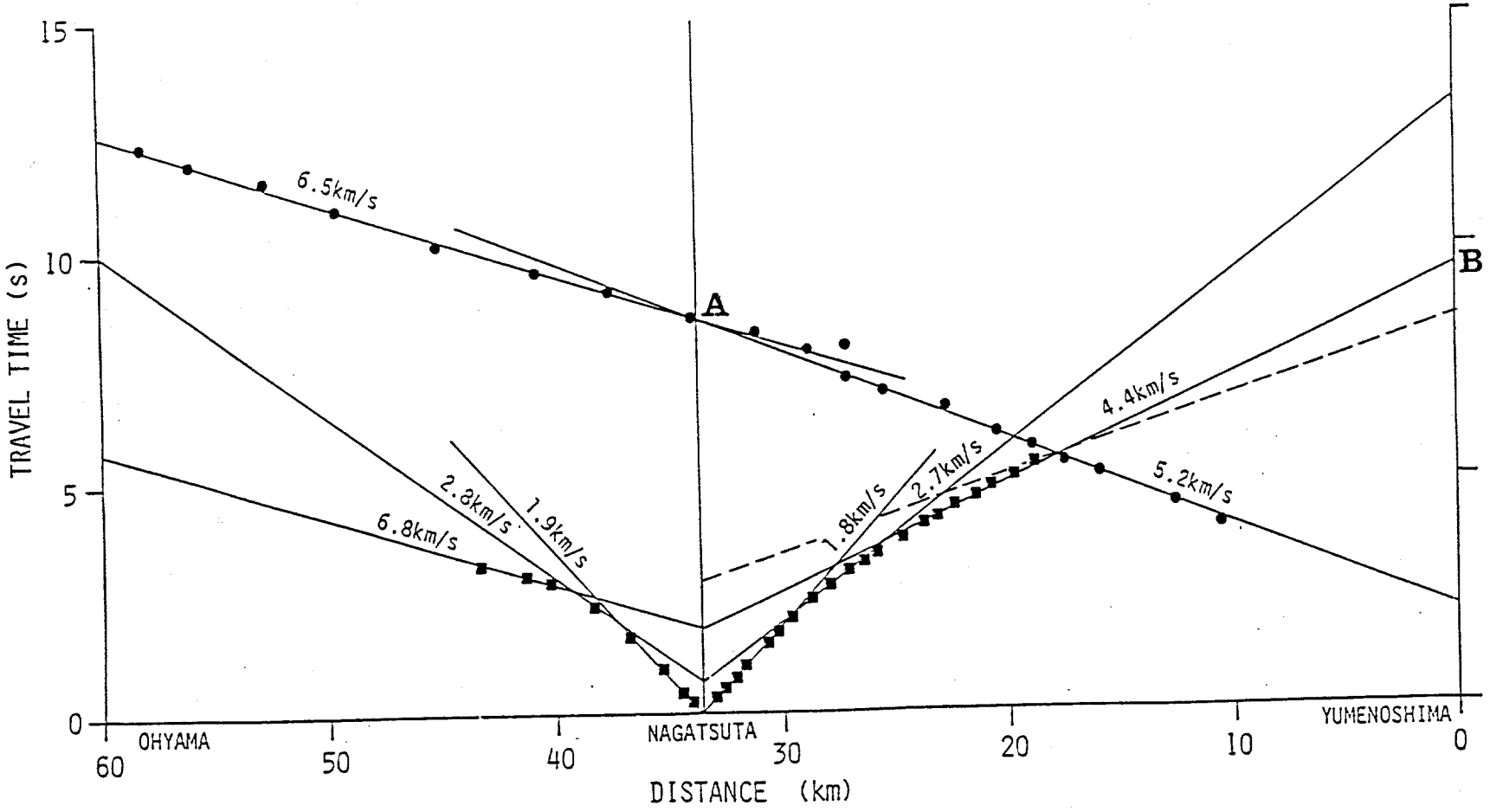

Fig. 2-9. Travel time diagram for the Nagatsuta-Ohyama line (Line B). Travel time data by Seo (1981) were also used. A broken line shows an assumed travel time curve for refracted wave in a layer with a velocity of 5.5 km/sec.

the phase propagating in the layer with a velocity of 5.3-5.6 km/sec beneath the layer with a velocity of 4.8 km/sec, because of inconsistence of A and B in the travel time diagram in Fig. 2-9.

In order to see the details of the travel time diagram, the reduced travel time diagram for the eastern profile was drawn with a reduction velocity of 4.8 km/sec (Fig. 2-10). There are two breaks in the travel time curve of the initial phases at distances from 5 to 10 km. This travel time curve suggests either step-like topography of the layer with a velocity of 2.8 km/sec or a velocity of 4.8 km/sec. The wave forms of the initial phases observed in the east direction were compared to know which possibility is plausible. Fig. 2-11 shows the close-up of the initial phases at distances of 5 to 14 km. The dots in the figure indicate the arrivals of the initial motions. The wave forms of the initial motions differ at the station before and after E13; the periods of the initial phases at the stations far from E14 become longer than those at the stations before E13. Therefore, we assumed that the initial motions at the stations from E9 to E14 propagate in the same layer having a velocity of 2.8 km/sec.

The true velocity of the layer with an apparent velocity of 5.2 km/sec from the Yumenoshima explosion was determined by comparing the distribution of the different kinds of time-terms as discussed before. The distributions of the time-terms from the Nagatsuta and the Yumenoshima explosions are shown in Fig. 2-12. The broken line indicates the time-terms derived by assuming that the refractor velocity is 4.8 km/s and the time-term at the explosion site, Nagatsuta, is 0.93 sec. These time-terms correspond to the thicknesses of the layers overlying the layer with a P-wave velocity of 4.8 km/sec. The solid lines show the time-terms down to the layer beneath the layer with a velocity of 4.8 km/sec, when the refractor velocities are assumed as 5.3 to 5.6 km/sec and the time-term at the explosion site, Yumenoshima, is 1.03 sec. The time-terms indicated by the broken line should be smaller than those by the solid lines. Therefore, the refractor must have a velocity more than 5.5 km/sec. This can also be seen from the travel time diagram in Fig. 2-9. The broken line in the travel time diagram is a travel time curve so that it keeps the recipro-

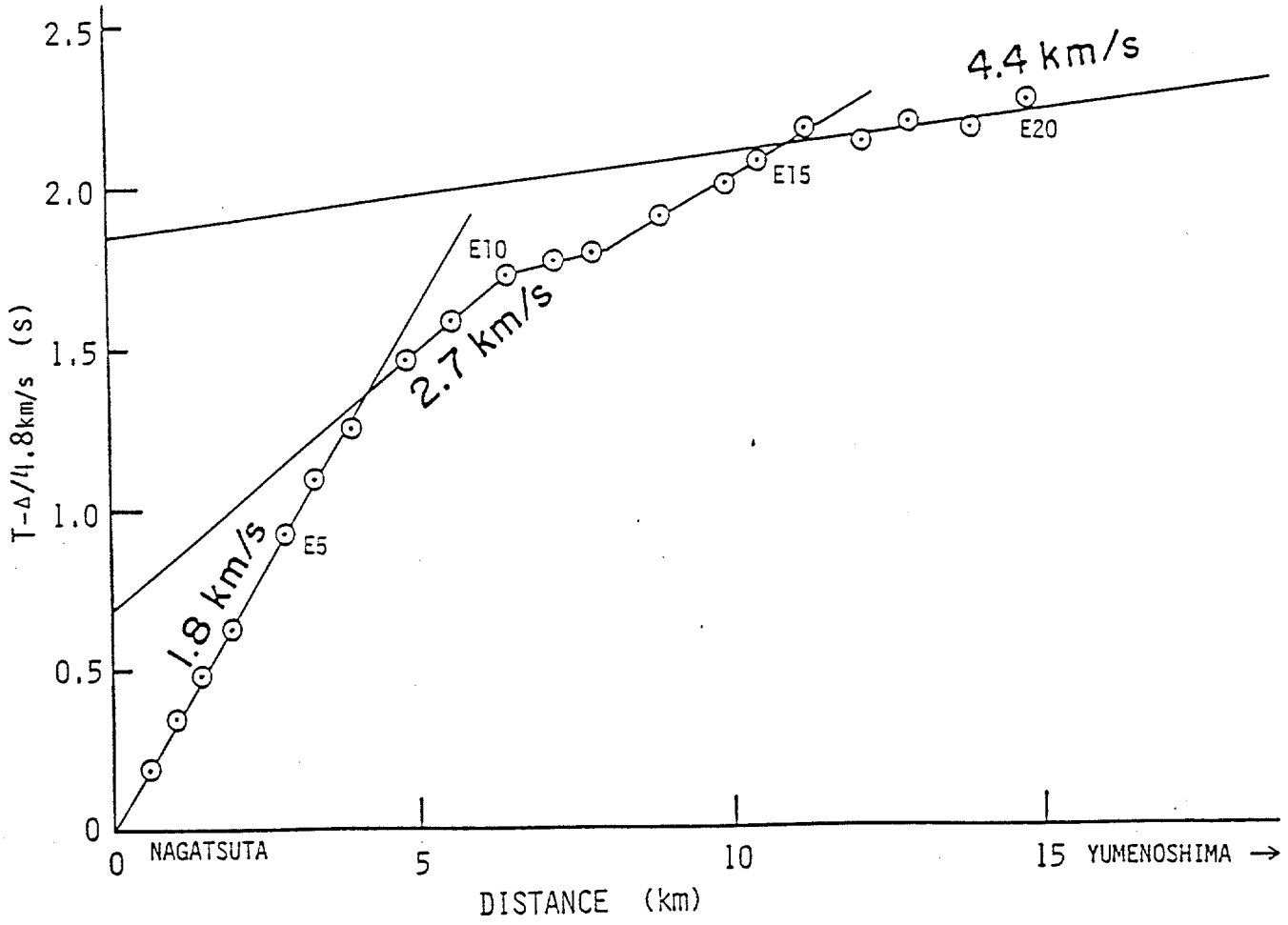

Fig. 2-10. Reduced travel time diagram for Nagatsuta explosion in the eastern direction.

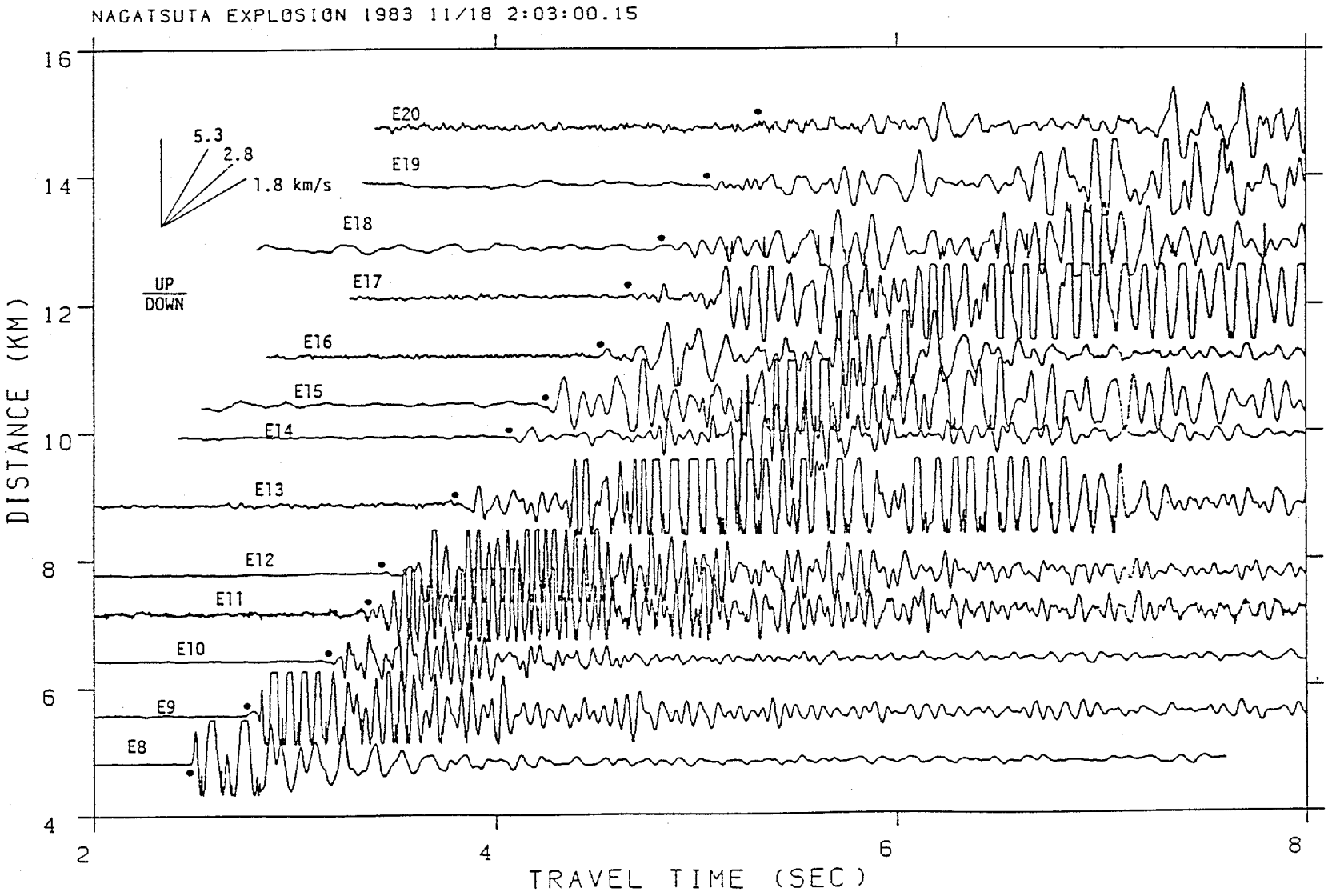

Fig. 2-11. Close up of initial motions of the seismograms in Fig. 2-7.

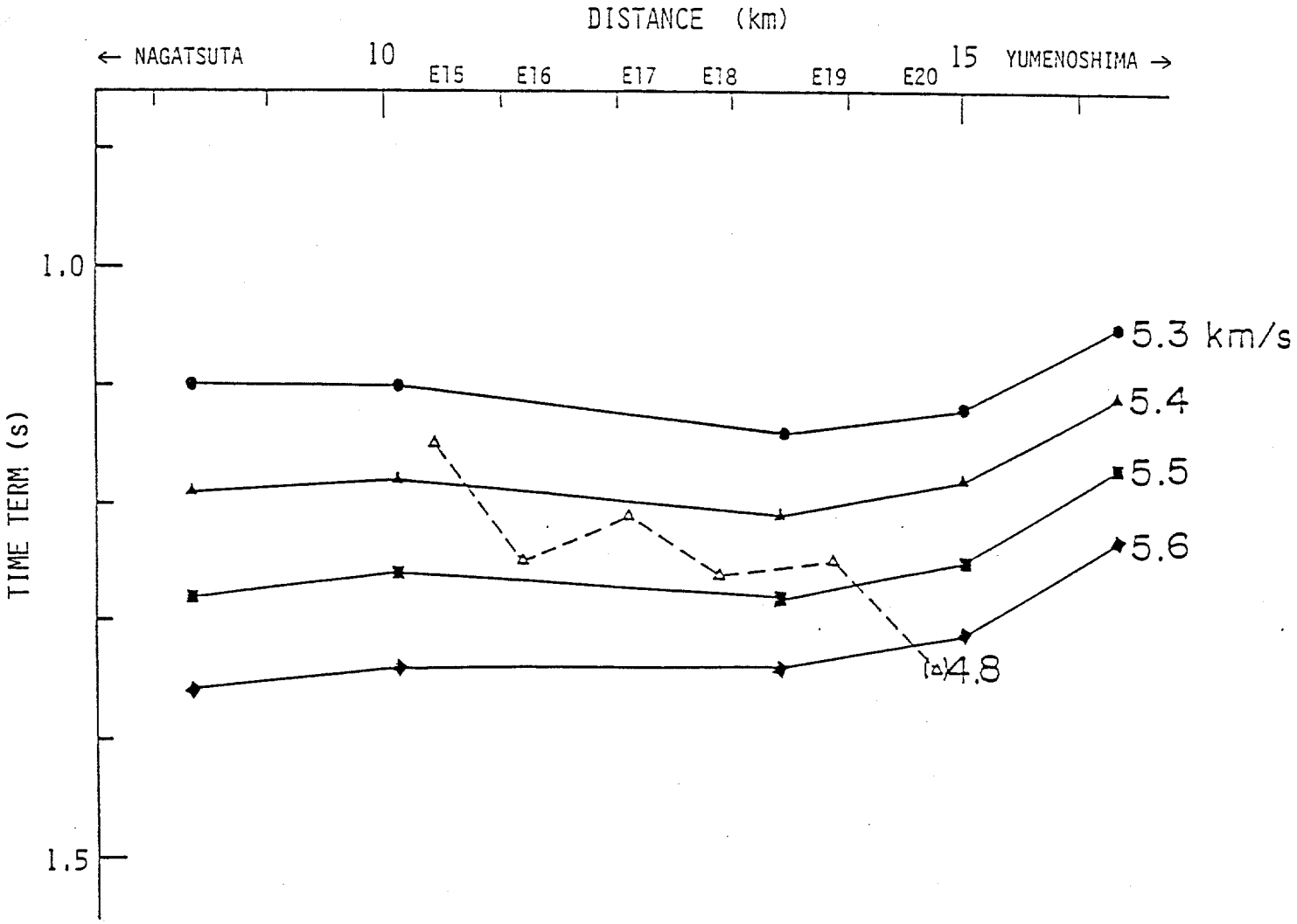

Fig. 2-12. Distribution of time-terms between Nagatsuta and Yumenoshima. Broken line shows time-terms to a layer with a P-wave velocity of 4.8 km/sec. Solid lines show time-terms of a layer beneath the layer with a velocity of 4.8 km/sec, when the refractor velocity is assumed 5.3, 5.4, 5.5 and 5.6 km/sec.

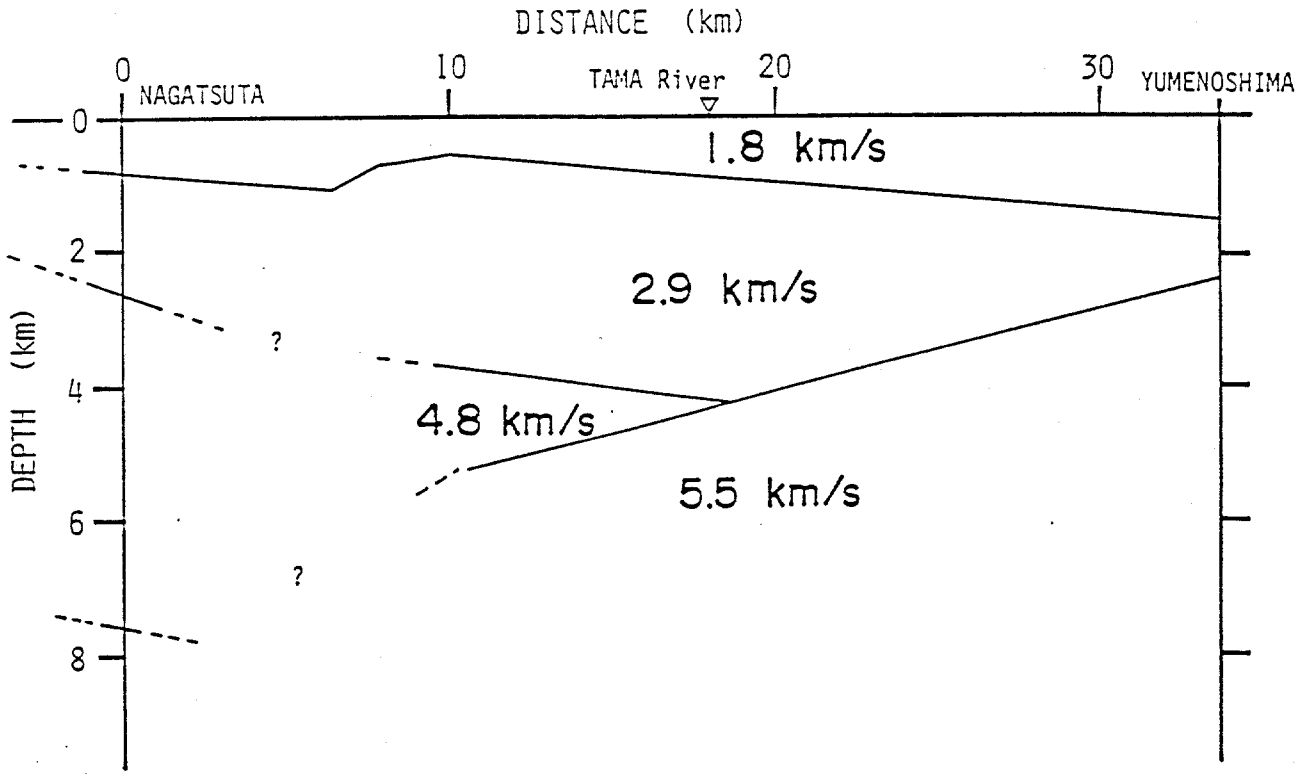

Fig. 2-13. Underground structure between Yumenoshima and Nagatsuta.

cal time at the Yumenoshima explosion site and it does not arrive before the arrivals of the refracted phases propagating in the layer with a velocity of 4.8 km/sec from the Nagatsuta explosion. The true velocity of 5.5 km/sec can be derived from this assumed travel time curve and that of the Yumenoshima explosion.

On the basis of the above interpretation, the underground structure between Yumenoshima and Nagatsuta was constructed as shown in Fig. 2-13. The step like structure exists at a distance of about 7 km from Nagatsuta. The thickness of the layer with a velocity of 4.8 km/sec becomes smaller towards Yumenoshima. The depth to the layer with a velocity of 5.5 km/sec was determined from the apparent velocity of 5.2 km/sec. Although the Nagatsuta explosion was conducted as a reverse shot of the Yumenoshima explosion, the seismic waves from the Nagatsuta explosion could not reach the layer with a velocity of 5.5 km/sec. Hence, the step-like topography of the layer with a velocity of 5.5 km/sec, which was suggested by Seo (1981), could not be confirmed from this experiment.

2.2.4 Underground structure along the Yumenoshima-Takao line

The P-wave profile along the Yumenoshima-Takao line was already carried out by Shima et al. (1978a). Since the Kurokawa explosion which corresponds to a reverse shot for the Yumenoshima explosion was newly observed, the re-interpretation of underground structure for this line was performed.

Fig. 2-14 shows the observed vertical velocities of the Yumenoshima explosion along the Yumenoshima-Takao line by way of Kurokawa. Impulsive noises seen in some traces at the stations with distances more than 50 km were due to leaking of clock signals. This, however, makes no trouble to determine the arrival times of the onsets. Later phases, two seconds after the onsets of the initial phases, can be seen in the traces at around 20 km distances from Yumenoshima. This is probably due to a multiple reflection within the sedimentary layers as suggested by Shima et al. (1978a). The propagation mechanism of these later phases will be discussed in the chapter 3. Figs. 2-15a and 2-15b show the seismograms obtained from the Kurokawa explosion along the surveying lines toward the east, for

Yumenoshima, and toward the west, for Takao, respectively. In the seismograms at distances more than 45 km from Yumenoshima, direct waves can not be seen. This suggests that the thickness of the top sedimentary layer becomes very thin or it does not exist in the west from there.

The arrival times of the onsets of the Yumenoshima and the Kurokawa explosions are shown in Table 2-4. The travel time diagram is depicted in Fig. 2-16. The travel time data from explosions at Yumenoshima by Shima et al. (1978a) were also included in the analysis. The P-wave velocity of the last layer is 5.4 km/sec between Yumenoshima and Kurokawa and its depth is almost constant. A high apparent velocity of 7.7 km/sec was derived towards the west from Kurokawa. Kaneda et al. (1979) proposed a crustal structure in the west of Takao, in which a layer having a velocity of 6.2 km/sec exists at a depth of approximately 10 km. According to this result, we have a possibility of a refracted wave propagating in this layer for the origin of the branch of the travel time curve with the high apparent velocity. However, the intercept time of this branch at the Kurokawa explosion site is the same as that of the travel time curve due to the onsets of the initial phases propagating in the layer with a velocity of 5.4 km/sec from the Kurokawa explosion. Therefore, it is quite natural to consider that the high apparent velocity is caused by a dipping of the layer with a velocity of 5.4 km/sec. The apparent velocity of the onsets from both the explosions becomes again as low as 5.5 km/sec in the west of Takao. Since it was confirmed from geological investigations that a firm rock is exposed in the west of Takao, the apparent velocity is considered to correspond to the true velocity of the basement.

Fig. 2-17 shows the underground structure between Yumenoshima and Takao derived from the travel time analysis. Although the underground structure, as a whole, is similar to that of Shima et al. (1978a), the higher validity could be derived by the observation of the reverse shot; specially the true velocity of the last layer. The P-wave profile at Kurokawa from this result slightly differs from that obtained from the result of the Kurokawa-Okazu line discussed earlier. The layer with a velocity of 4.8 km/sec exists in the Kurokawa-Okazu

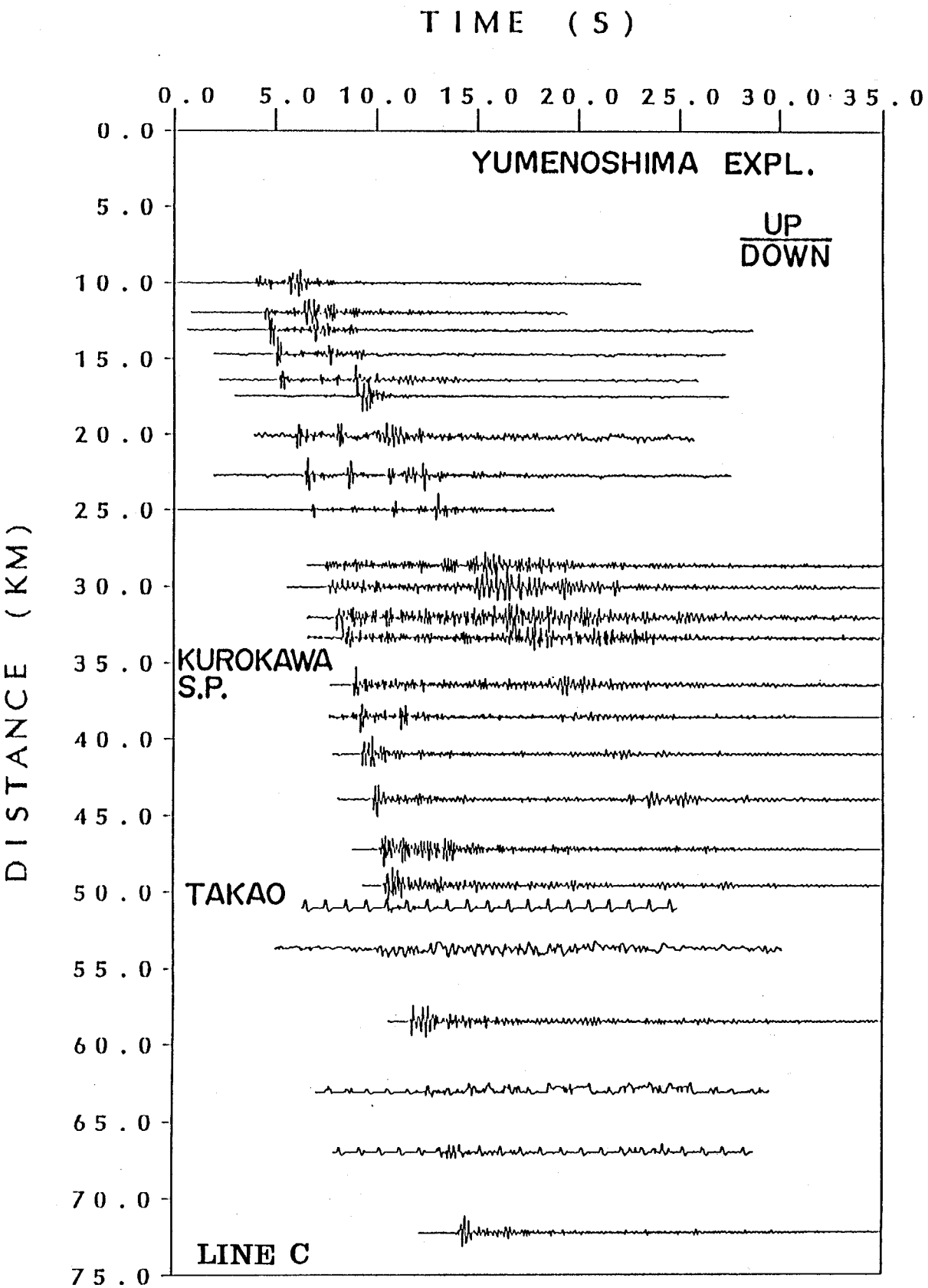

Fig. 2-14. Observed seismograms at the stations along the Yumenoshima-Takao line (Line C in Fig. 2-1) during the Yumenoshima explosion. Each trace indicates vertical ground velocity and is normalized to its maximum amplitude.

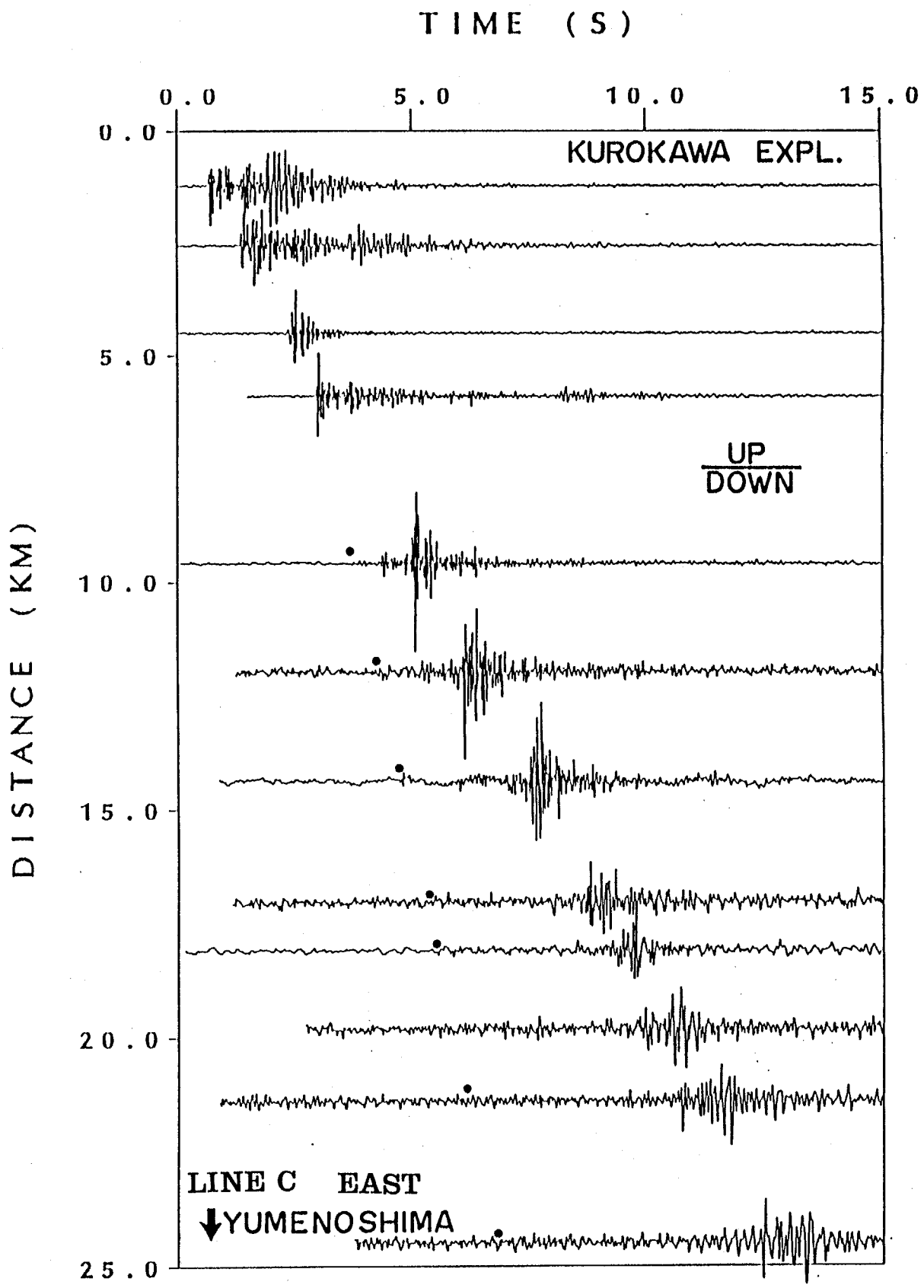

Fig. 2-15a. Observed seismograms at the stations along the eastern part of the Yumenoshima-Takao line (Line C) during the Kurokawa explosion. Each trace indicates vertical ground velocity and is normalized to its maximum amplitude. Each solid circle shows onset of initial phase.

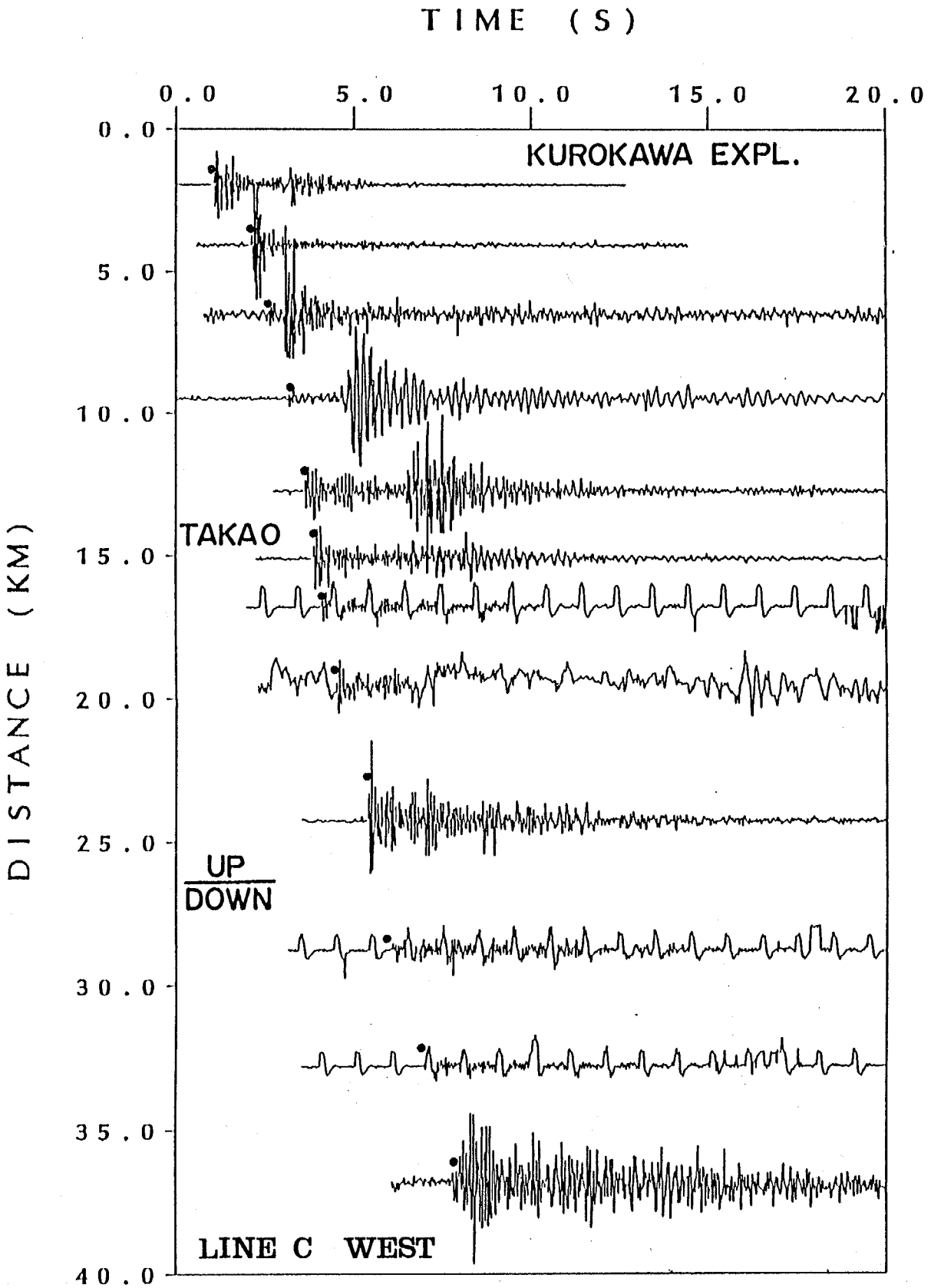

Fig. 2-15b. Observed seismograms at the stations along the western part of the Yumenoshima-Takao line (Line C) during the Kurokawa explosion. Each trace indicates vertical ground velocity and is normalized to its maximum amplitude. Each solid circle shows onset of initial phase.

Table 2-4. Travel times of initial phases obtained from Yumenoshima(18th) and Kurokawa explosions

No	STATION	LOCATION		YUMENOSHIMA		KUROKAWA	
		LAT.	LONG.	D(km)	T(s)	D(km)	T(s)
01	YOSHIMIZU SHO	35 36 56.5	139 43 39.8	10.01	03.97	24.49	(6.81)
02	OYAMADAI SHO	35 37 10.2	139 42 23.1	11.96	04.38	22.58	(6.40)
03	ISIBUMI SHO	35 36 57.1	139 41 37.0	13.10	04.55	21.40	(6.14)
04	TORITU DAI	35 37 03.4	139 40 33.8	14.70	04.92	19.83	
05	TODOROKI SHO	35 36 48.0	139 38 43.6	17.46	05.26	18.10	(5.37)
06	NAKAMACHI SHO	35 36 48.0	139 38 43.6	17.46	05.41	17.03	(5.16)
07	KINUTA MINAMI SHO	35 37 10.3	139 36 56.5	20.17	05.94	14.40	4.65
08	KOMAE 3 SHO	35 37 29.6	139 35 15.8	22.73	06.39	11.97	4.17
09	NOBORITO SHO	35 37 09.0	139 33 44.6	24.99	06.72	09.60	3.65
10	HIGASISUGE SHO	35 37 23.9	139 32 24.1	27.03	07.13	07.70	3.28
11	HOSOYAMA	35 36 51.9	139 31 18.8	28.65	07.42	05.90	2.93
12	CHIYOGAOKA SHO	35 36 49.5	139 30 22.8	30.06	07.61	04.50	2.34
13	INAGI 2 SHO	35 36 45.4	139 29 04.4	32.04	07.96	02.55	1.31
14	KUROKAWA	35 36 36.5	139 28 11.9	33.36	08.33	01.22	0.63
15	KUROKAWA S.P.	35 36 20.5	139 27 27.7	34.42	08.43		
16	MINAMI TOYOGAOKA	35 36 30.4	139 26 10.4	36.42	08.80	01.97	1.05
17	NAGASAKA	35 36 28.4	139 24 46.0	38.54	09.16	04.08	2.10
18	MINAMI OHSAWA	35 36 24.4	139 23 09.0	40.98	09.25	06.51	2.57
19	TAMABI DAI	35 36 30.0	139 21 11.4	43.94	09.79	09.48	3.15
20	SOUBU GOLF	35 36 37.4	139 19 01.8	47.20	10.15	12.74	3.63
21	TAKAO 1	35 36 44.1	139 17 27.6	49.57	10.35	15.12	3.87
22	TAKAO 2	35 37 58.4	139 16 31.9	51.01	10.51	16.77	4.10
23	TAKAO TUNNEL	35 38 00.0	139 14 44.3	53.72		19.45	4.51
24	SOKOSAWA	35 37 57.8	139 11 30.9	58.58	11.70	24.26	5.39
25	HASIZUME	35 38 22.4	139 08 36.3	63.00	12.40	28.71	6.15
26	OGURA	35 38 39.1	139 05 57.8	67.00	13.21	32.74	6.98
27	OKUYAMA	35 38 02.8	139 03 08.0	71.23	13.99	36.87	7.84

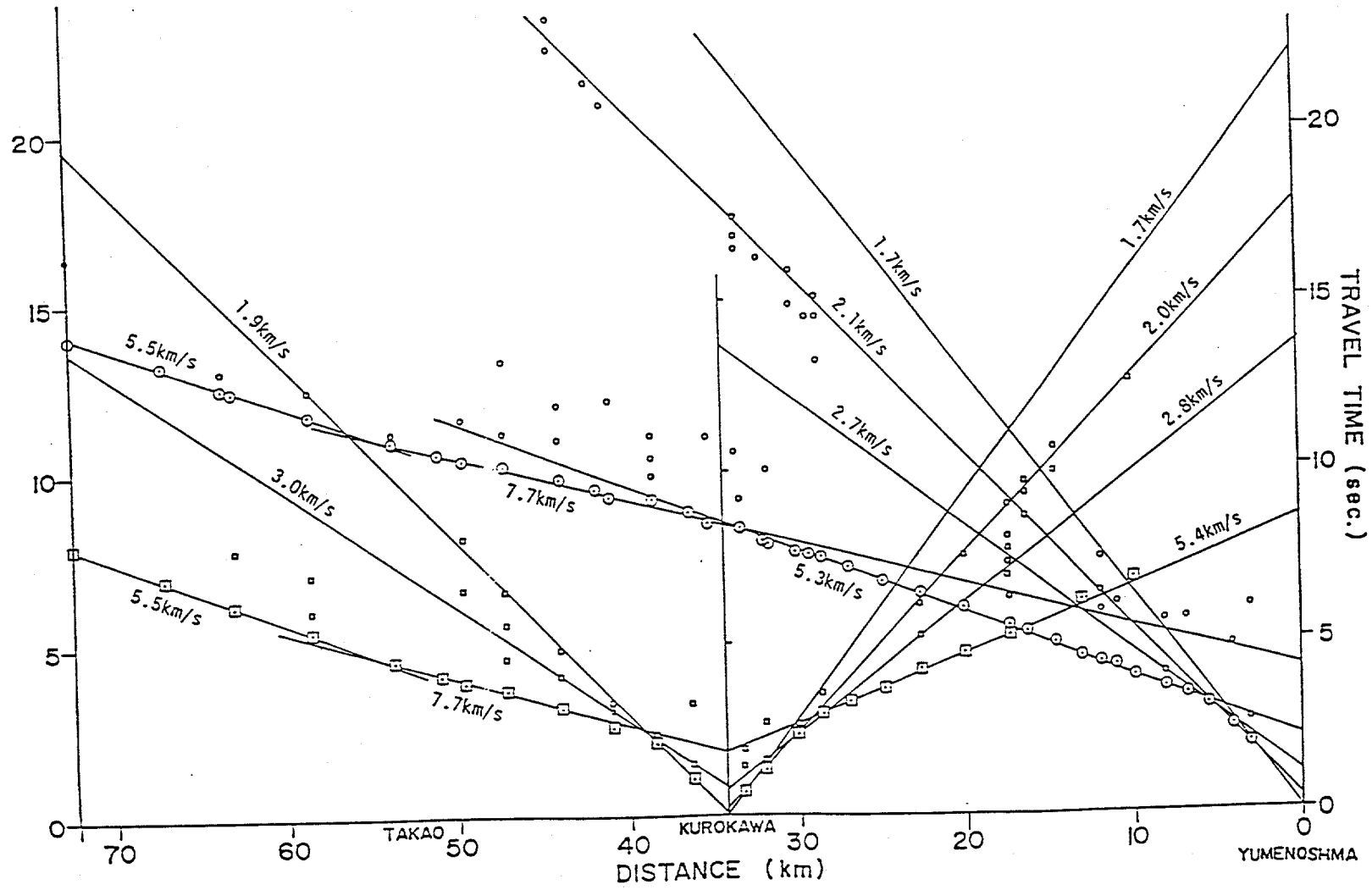

Fig. 2-16. Travel time diagram for the Yumenoshima-Takao line (Line C). Travel time data by Shima et al.(1978) are also used.

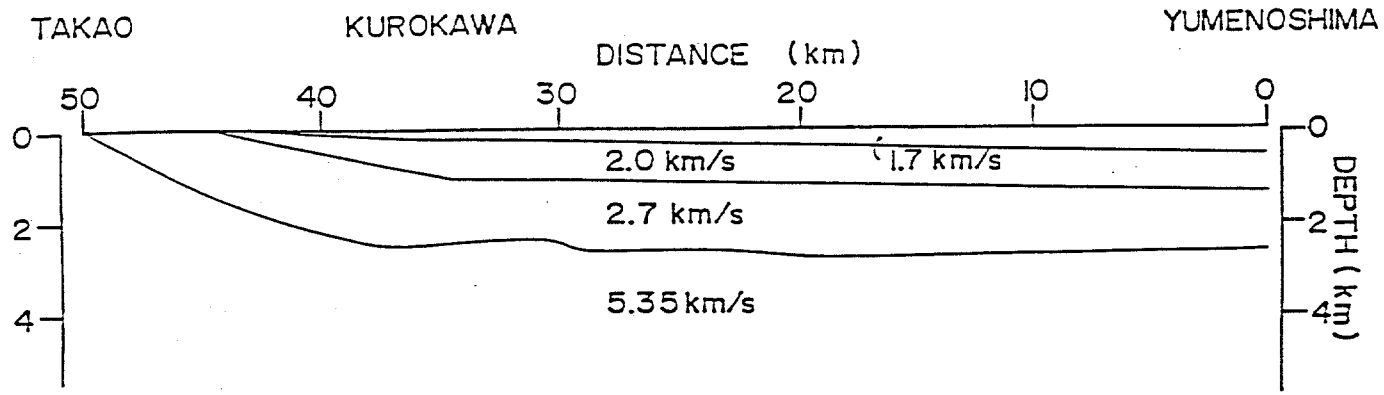

Fig. 2-17. Underground structure between Yumenoshima and Takao. The layer with a P-wave velocity of 5.35km/s is exposured in the western side of Takao.

profile. Since the thickness of the layer with a velocity of 4.8 km/sec is very thin in the vicinity of the Kurokawa explosion point as shown in Fig. 2-6, the layer becomes a blind layer, sometimes called a hidden layer, in some directions. This thickness becomes larger toward the south, therefore, the layer with a velocity of 4.8 km/sec was detected in the Kurokawa-Okazu line.

2.2.5 Underground structure along the Yumenoshima-Odawara line

This is a long profile which has four explosions at Yumenoshima, Okazu, Hiratsuka and Odawara. The observation was carried out mainly by Kanagawa Prefecture. The arrival times of the initial phases were estimated in this study as shown in Table 2-5a and 2-5b. Since the seismograms observed between Hiratsuka and Odawara were very noisy, this part of the profile was excluded from the interpretation. The travel time diagram is depicted in Fig. 2-18. The travel time curves were determined so that the intercept times at Okazu explosion site do not differ from those for the Kurokawa-Okazu line. Apparent velocities of 4.3 km/sec for Yumenoshima and 5.0 km/sec for Hiratsuka from the Okazu explosion can be seen in the branch of the travel time curves. Its intercept time is equal to that at Okazu explosion site in the Kurokawa-Okazu line. Therefore, these branches are considered to be caused by a refracted wave propagating in the layer with a velocity of 4.8 km/sec. Branches with an apparent velocities of 5.7 km/sec seen in the travel time curves of the Okazu and the Hiratsuka explosions are reversed by that with an apparent velocity of 5.25 km/sec in the travel time curve of the Yumenoshima explosion. The ture velocity can be determined as 5.5 km/sec for the bottom layer; this is coincident with the results of the Yumenoshima-Ohyama line. Since a travel time branch for the layer with a velocity of 4.8 km/sec can not be obtained from the Yumenoshima explosion, the layer becomes a blind layer near Yumenoshima. The apparent velocity of the initial phases from the Yumenoshima explosion becomes as high as 5.8 km/sec. According to the interpretation of the travel time curve for the Yumenoshima-Kurokawa line, it is considered that the higher apparent velocity is also due to a dipping of the bottom layer having a P-wave velocity of

Table 2-5a. Travel times of initial phases obtained from Higashiohgishima, Yumenoshima(17th), Okazu and Hiratsuka explosions

No	STATION	LOCATION LAT.	LOCATION LONG.	H. OHGISHIMA D(km)	H. OHGISHIMA T(s)	YMS(17) D(km)	YMS(17) T(s)	OKAZU D(km)	OKAZU T(s)	HIRATSUKA D(km)	HIRATSUKA T(s)
0	YUMENOSHIMA S.P	35 36 54.7	139 50 14.4	13.79	4.65	0.00		34.63		49.14	(11.18)
1	BOUHAYEI	35 35 47.8	139 47 53.8	10.72		4.10	2.27	30.54		45.04	
2	KEIHIN JIMA	35 34 06.1	139 46 25.1	7.46	3.33	7.71	3.54	27.02	(14.67)	41.57	(12.11)
3	KEIHIN OHHASI	35 34 06.1	139 45 42.8			8.58	3.67	26.07	(13.98)	40.60	
4	OHMORI 4 SHO	35 33 43.6	139 44 45.2	7.16	3.31	10.16	3.88	24.48	(8.91)	39.00	
5	TOUKAMA CHU	35 33 28.0	139 43 56.4	7.28	3.59	11.45	4.37	23.19	(7.81)	37.70	
6	MINAMI ROKUGOU	35 32 32.7	139 43 09.9	6.72	3.33	13.39	4.59	21.28		35.83	
7	TAKAHATA SHO	35 32 31.2	139 42 33.4	7.40	3.49	14.16	4.80	20.48	6.19	35.01	8.85
8	SAIWAI CHO	35 32 05.7	139 41 51.1	7.89	(4.78)	15.49	5.03	19.16	6.02	33.69	8.59
9	HIE JINJA	35 31 47.8	139 41 07.9	8.65		16.69		17.94		32.47	
10	YAKOU	35 31 28.4	139 40 33.4	9.29		17.75	5.48	16.89	5.54	31.42	(7.74)
11	SUEYOSHI CHU	35 31 12.2	139 40 33.4	9.17		18.66	5.74	15.98	(5.66)	30.51	
12	SISIGAYA SHO	35 30 49.2	139 39 17.3	10.94		20.02	5.90	14.62	5.08	29.16	7.73
13	UENOMIYA CHU	35 30 33.9	139 38 31.6	12.04		21.23	6.16	13.40	4.89	27.93	7.44
14	SHINOHARA SHO	35 29 59.0	139 37 48.8	13.09		22.73	6.44	11.91	4.54	26.45	7.16
15	SHINOHARA NISHI	35 29 54.7	139 37 03.8	14.23		23.75	6.64	10.89	4.21	25.41	6.85
16	KATAKURA	35 29 29.6	139 36 24.2	15.27		25.00	6.80	9.63	3.92	24.16	6.65
17	HAZAWA SHO	35 29 06.8	139 35 25.4	16.81		26.63	7.36	8.02	3.58	22.52	6.28
18	KAMIHOSHIKAWA	35 28 21.8	139 34 52.5	17.83	5.95	28.09	7.74	6.56	3.03	21.11	(6.09)
19	HODOGAYA SHO	35 27 44.7	139 33 56.2	19.46	6.17	29.09	7.94	4.76	2.37	19.32	5.76
20	SAKONYAMA 1 SHO	35 27 30.9	139 33 13.5	20.60	6.39	31.03	8.14	3.61	1.89	18.17	5.47
21	MINAMI HONJYUKU	35 27 18.0	139 32 30.6	21.75	6.58	32.15	8.34	2.48	1.34	17.03	5.18
22	KASIWA YOUCHIEN	35 27 01.0	139 31 49.9	22.87	6.76	33.30	8.55	1.34	0.75	15.88	5.00
23	OKAZU S.P.	35 26 33.2	139 31 08.8	24.10	(6.99)	34.63	8.74	0.00		14.56	4.67
24	SYOYOU KOH	35 26 04.4	139 29 52.1	26.20	(7.53)	36.73	9.12	2.13	1.26	12.44	4.23
25	SIMOWADA SHO	35 25 40.3	139 28 32.9	28.33		38.83		4.26	1.99	10.33	3.72
26	RENKOH JI	35 24 37.7	139 27 16.1	30.77		41.49		6.86	3.07	7.72	3.03
27	OIJI TAISYA	35 24 16.7	139 26 01.2	32.77	(8.58)	43.43		8.83	3.73	5.57	2.40
28	GOSYOMI SHO	35 23 59.0	139 25 11.8	34.13		44.77		10.18	3.89	4.38	1.95
29	KISIBO JIN	35 23 45.7	139 24 26.6	35.34	(8.80)	45.96		11.38	4.07	3.18	1.40
30	ASAHI SHO	35 23 14.8	139 23 18.7	37.27		47.92		13.34	4.36	1.23	0.62
31	HIRATSUKA S.P.	35 22 52.0	139 22 38.8	38.46		49.14	11.25	14.56	4.65	0.00	
32	KANDA SHO	35 22 23.5	139 22 00.0	39.69		50.44		15.84	4.84	1.32	0.70
33	YOKOUCHI SHO	35 22 05.7	139 21 20.9	40.81		51.57		16.97	5.18	2.43	1.08
34	TOYOTA SHO	35 21 19.5	139 20 02.2	43.18	10.72	54.01	12.02	19.40	5.62	4.87	1.86
35	NOUGYO SOUKEN	35 21 16.7	139 18 52.8	44.84	10.90	55.54	12.28	20.98	(5.95)	6.42	2.15
36	HAKKEN JINJYA	35 19 54.3	139 17 39.7	47.52	11.21	58.45	12.91	23.83	(6.31)	9.33	2.79
37	SUGAWARA JINJYA	35 19 08.0	139 16 11.9	50.12	11.72	61.09	13.28	26.47	7.08	11.96	3.38
38	ISSIKI SHO	35 18 28.3	139 14 41.1	52.71	(11.96)	63.68	13.71	29.06	7.57	14.54	3.91
39	SIMONAKA SHO	35 17 55.7	139 13 39.9	54.54	(12.11)	65.52	14.12	30.91	(7.92)	16.39	4.42
40	TAKARA KONGOUJI	35 16 55.6	139 12 39.6	56.70	(13.34)	67.81	(14.77)	33.18		18.70	(5.26)
41	SIMOFUCHU SHO	35 16 32.5	139 11 25.3	58.70		69.77		35.15	(9.23)	20.64	(5.75)
42	ODAWARA S.P.	35 15 52.0	139 10 31.5	60.47	(13.82)	71.59	15.42	36.69	(9.86)	22.47	6.30
43	ODAWARA CITY OF	35 15 41.4	139 09 20.2	62.23		73.28	15.51	38.66		24.14	(6.75)
44	OHTUBO JI	35 14 49.3	139 08 27.0	64.15		75.23		40.65		26.16	

Table 2-5b. Travel times of initial phases obtained from Yumenoshima(19th) and Odawara explosions

No	STATION	LOCATION		YMS(19)		ODAWARA	
		LAT.	LONG.	D(km)	T(s)	D(km)	T(s)
1	OKAZU	35 26 35.2	139 31 07.7	34.53	8.76	36.96	9.58
2	SYOYOU KOH	35 26 03.3	139 29 43.5	36.84	9.11	34.64	9.08
3	SIMOWADA SHO	35 25 37.2	139 28 35.8	38.72	9.36	32.77	8.69
4	RENKOH JI	35 24 39.5	139 26 59.5	41.34	10.07	30.15	8.08
5	OHJI TAISYA	35 24 16.6	139 26 00.8	43.35	10.44	28.14	7.88
6	GOSYOMI SHO	35 23.56.2	139 25 10.7	44.75		26.74	7.47
7	KISIBO JIN	35 23 49.3	139 24 26.0	45.82	10.60	25.69	7.06
8	ASAHI SHO	35 23 12.3	139 23 19.5	47.85	10.92	23.66	6.63
9	HIRATSUKA S.P.	35 22 49.9	139 22 39.8	49.06	11.24	22.44	6.33
10	KANDA SHO	35 22 25.2	139 22 01.9	50.29		21.21	5.94
11	YOKOUCHI SHO	35 22 06.2	139 21 17.4	51.54	11.65	19.97	5.71
12	TOYOTA SHO	35 21 19.5	139 20 01.4	53.93	12.24	17.57	5.09
13	JINJYA	35 20 36.0	139 18 59.3	55.97	(12.60)	15.52	
14	HAKKEN JINJYA	35 19 53.8	139 17 40.9	58.33	12.98	13.16	4.16
15	SUGAWARA JINJYA	35 18 59.2	139 16 15.9	61.05	13.36	10.44	3.12
16	ISSIKI SHO	35 18 27.0	139 14 36.9	63.69		7.82	
17	SIMONAKA SHO	35 17 54.2	139 13 39.0	65.47	14.49	6.04	2.14
18	BEMTENYAMA 1	35 17 31.1	139 13 13.3	66.30	14.65	5.20	1.97
19	BENTENYAMA 2	35 17 16.1	139 12 38.1	67.40	15.09	4.10	1.73
20	NAEKAWA	35 16 51.5	139 11 56.9	68.68	(15.27)	2.82	1.30
21	SIMOFUCHU SHO	35 16 32.9	139 11 29.0	69.58	15.39	1.91	0.87
22	KAMONOMIYA EKI	35 16 14.7	139 10 58.9	70.53	15.57	0.96	0.46
23	ODAWARA S.P.	35 15 55.6	139 10 28.7	71.45		0.00	

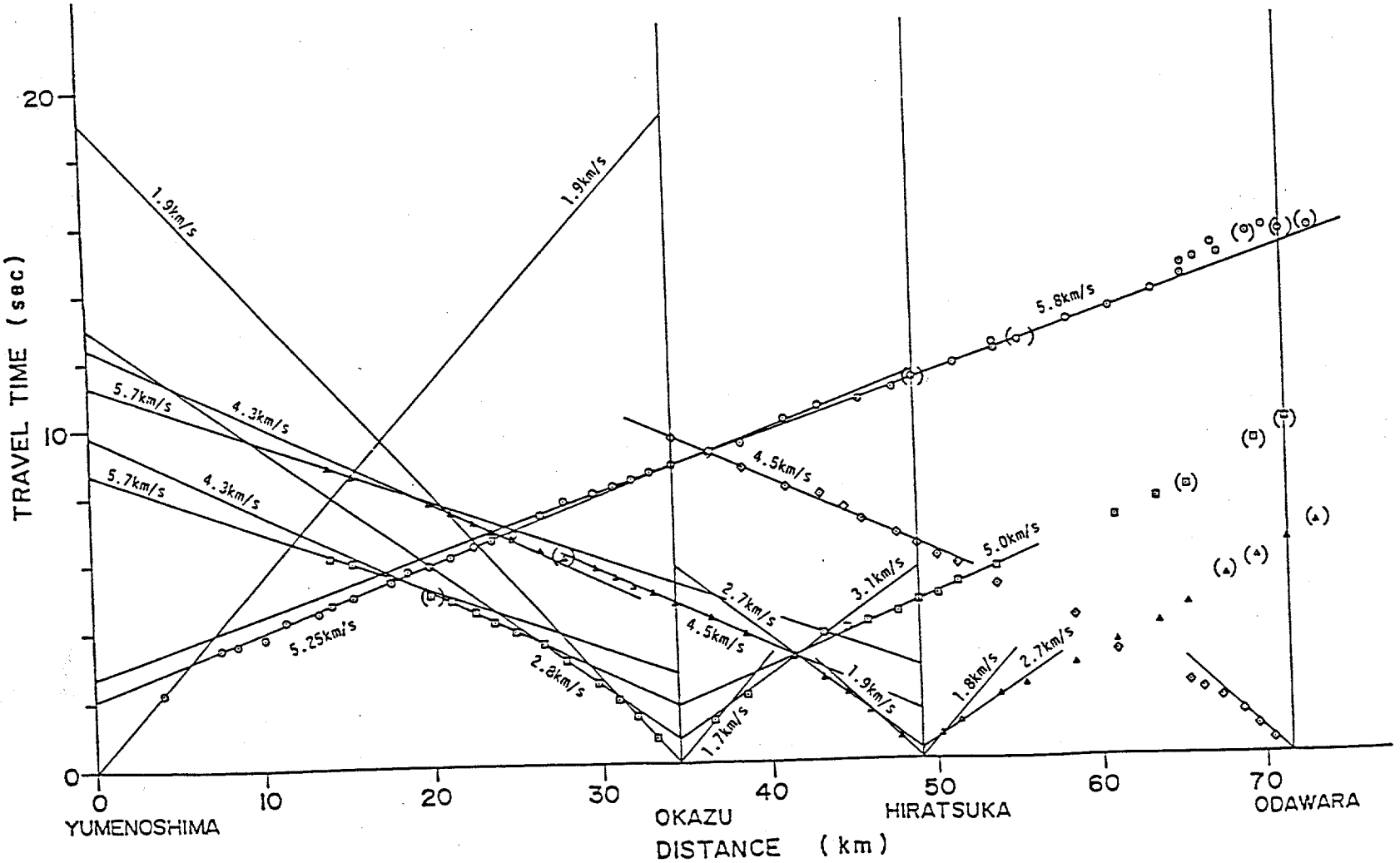

Fig. 2-18. Travel time diagram for the Yumenoshima-Odawara line (Line D in Fig. 2-1).

5.5 km/sec.

Fig. 2-19 shows the P-wave velocity profile between Yumenoshima and Hiratsuka derived from the above interpretation. The underground structure consists of four layers whose velocities are 1.8, 2.8, 4.8 and 5.5 km/sec. The depth to the layer with a velocity of 4.8 km/sec at distances less than 20 km from Yumenoshima was assumed from the extrapolation of the travel time curve as indicated by the broken line. A step-like topography of the layer with a velocity of 5.5 km/sec, exists at 25 km distance from Yumenoshima. In the western side of the fault, the thickness of the layer with a velocity of 4.8 km/sec is approximately 4 km. In the figure, the depth to the bottom layer is indicated by a broken line around Hiratsuka, because of the noisy onsets. The thickness of the top layer is deduced to become shallower from Yumenoshima to Hiratsuka.

2.2.6 Underground structure along the Kurokawa-Higashiohgishima line

The observation of the Kurokawa and the Higashiohgishima explosions along the Kurokawa-Higashiohgishima line was carried out by Kawasaki City. The arrival times of the initial phases were estimated in this study as shown in Table 2-6. Since the S/N ratios of the records from the Kurokawa explosion near the Higashiohgishima explosion site were low, the arrival times of the initial phases could not be determined.

The travel time diagram is shown in Fig. 2-20. The intercept times of the layers with velocities of 2.8 and 4.7 km/sec at the Kurokawa explosion site were determined so as to fit with those derived from the Kurokawa-Okazu line. The travel time branches with apparent velocities of 4.8 and 5.6 km/sec can be seen in the travel time curve of the onsets from the Higashiohgishima explosion. These branches indicate the existence of two layers with velocities of 4.7 and 5.5 km/sec as can be seen in the profile between Yumenoshima and Hiratsuka. The underground structure deduced is shown in Fig. 2-21. The surface layers with velocities of 1.7 to 2.2 km/sec are determined in detail. However, it makes no significant differences, when we consider these layers as a single layer with a velocity of 2 km/sec. The depth to the layer with a velocity of 5.5 km/sec around Higashiohgishima could not be

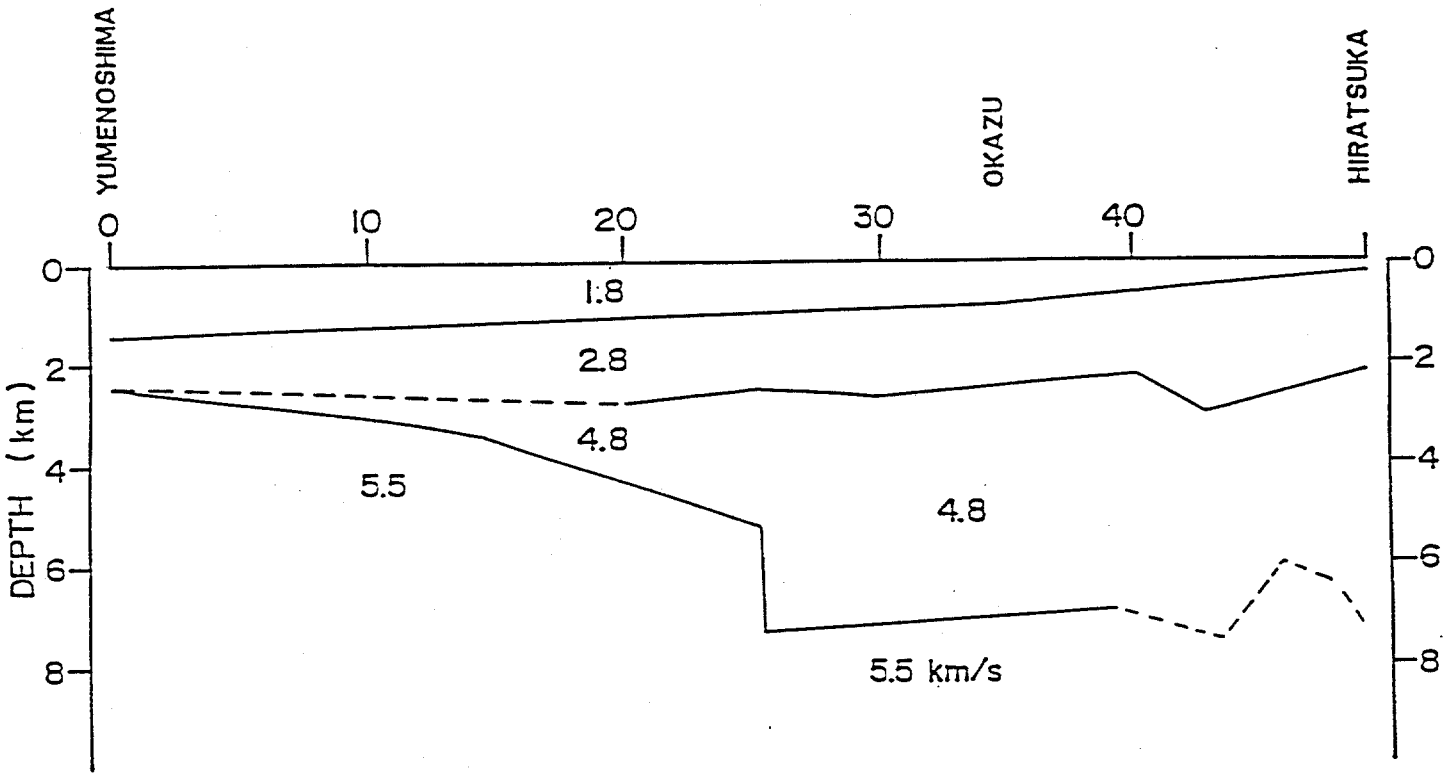

Fig. 2-19. Underground structure for the Yumenoshima-Odawara line (line D). Underground structure between Hiratsuka and Odawara is not estimated because of uncertainty of the travel time data.

Table 2-6. Travel times of initial phases obtained from
Kurokawa, Higashiohgishima and Yumenoshima(17th and 18th) explosions

No	STATION	LOCATION		KUROKAWA		H. OHGISHIMA		YMS(17)		YMS(18)	
		LAT.	LONG.	D(km)	T(s)	D(km)	T(s)	D(km)	T(s)	D(km)	T(s)
0	KUROKAWA S.P	35 36 20.5	139 27 27.7	0.00						34.48	8.43
1	MITUBISI FACT.	35 36 21.3	139 27 30.0			30.90	8.03	34.35	(8.53)		
2	SHINKOU JI	35 36 11.7	139 28 00.2	0.86	0.44					33.67	8.31
3	TOYKOU GAKUEN	35 35 59.0	139 28 32.6	1.76	0.92	29.19	7.67	32.81	8.09	32.87	8.08
4	SHIRATORI JINJA	35 35 58.0	139 29 15.4	2.80	1.50						
5	ZENSHO JI	35 35 34.8	139 29 40.4	3.62	1.87	27.33	7.29	31.16	7.82	31.21	7.83
6	MIYAMADAI KOEN	35 35 16.4	139 30 28.4	4.94	2.44					30.05	7.66
7	SHIROYAMA SHO	35 35 18.7	139 30 56.0	5.58	2.77	25.37	7.03	29.31	7.51	29.35	7.45
8	SUSUKINO SHO	35 34 35.3	139 32 01.7	7.62	3.50	23.33	6.82	27.84	7.29	27.87	7.30
9	YAMAUCHI CHU	35 34 25.6	139 33 19.2	9.53	3.88	21.42	6.35	25.97	7.07	25.99	7.03
10	ARIMA CHU	35 34 04.3	139 34 49.7	11.89	4.38	19.06	(6.03)			23.87	6.71
11	YAMANA SHO	35 33 24.1	139 36 23.9	14.55	4.98	16.40	(5.47)	21.89	6.35	21.88	6.40
12	TAKADA H. SHO	35 32 56.3	139 37 40.5	16.66	5.40	14.29	5.02	20.35	6.03	20.32	6.02
13	NICHIDAI CHU	35 32 29.3	139 39 00.0	18.83	5.90	12.12	4.51	18.84	5.68	18.78	5.78
14	OGURA SHO	35 32 18.0	139 40 07.0	20.53	(6.25)	10.42	4.11	17.51	5.47	17.43	5.42
15	MINAMIKAWARA S	35 32 03.1	139 41 39.7			8.11	3.68	15.77	5.12	15.66	5.04
16	FUJIMI CHU	35 31 28.9	139 42 41.6			6.24	3.18	15.19	5.00	15.05	4.92
17	SAKURAMOTO SHO	35 31 02.0	139 43 28.8			4.83	2.57	14.91	(4.94)		
18	IRIEZAKI GESUI	35 30 51.1	139 44 30.0			3.28	1.87	14.17	(4.68)		
19	MITUI SEITOH	35 30 40.5	139 44 57.0			2.52	1.47	14.03	(4.54)		
20	FUTOH OFFICE	35 30 00.7	139 45 48.2			1.03	0.78	14.40	4.69		
21	H. OHGISHIMA	35 30 06.7	139 46 28.3	30.95	(8.27)	0.00		13.79	4.60	13.55	4.54

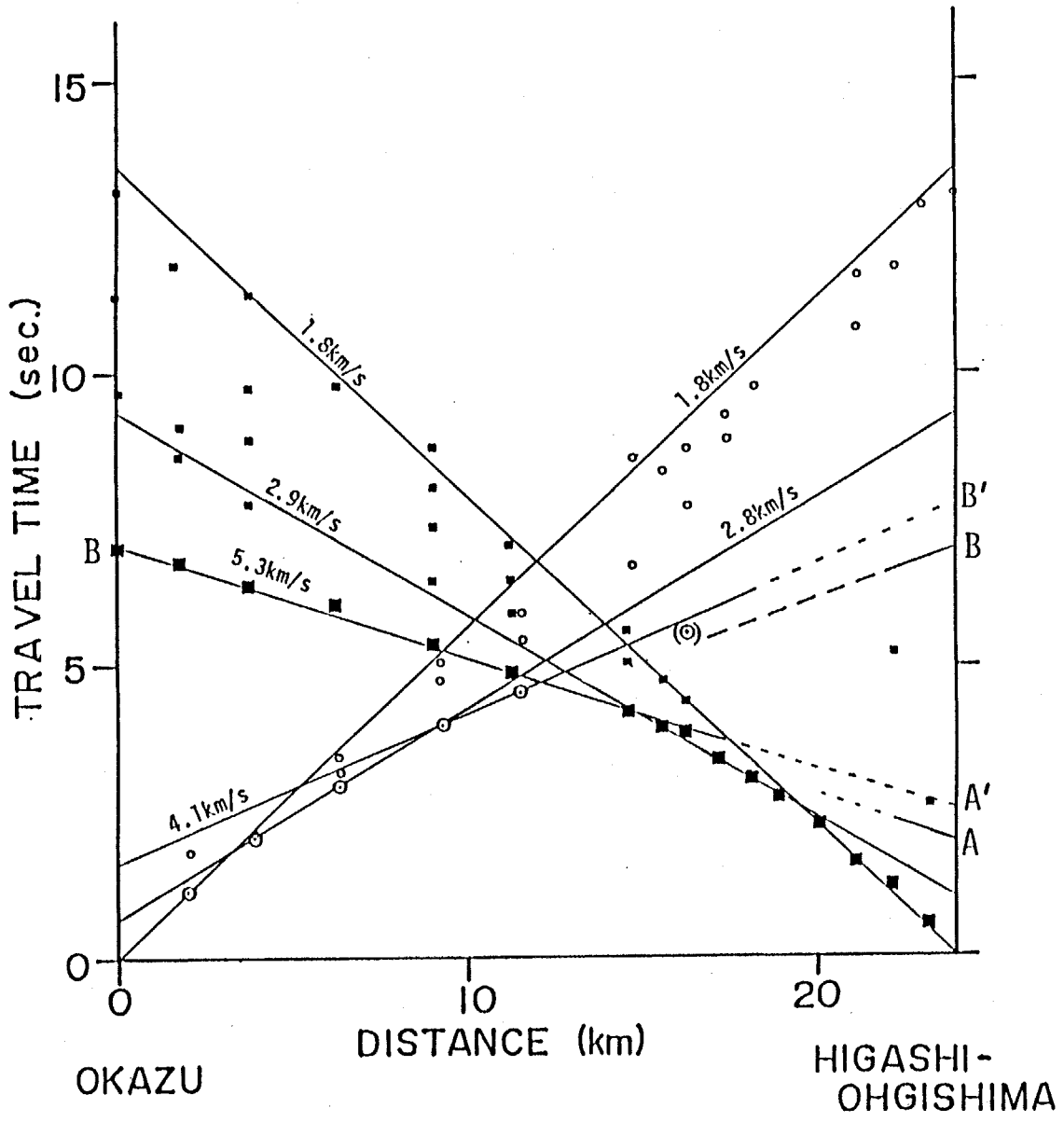

Fig. 2-20. Travel time diagram for the Higashiohgishima-Kurokawa line (Line E in Fig. 2-1).

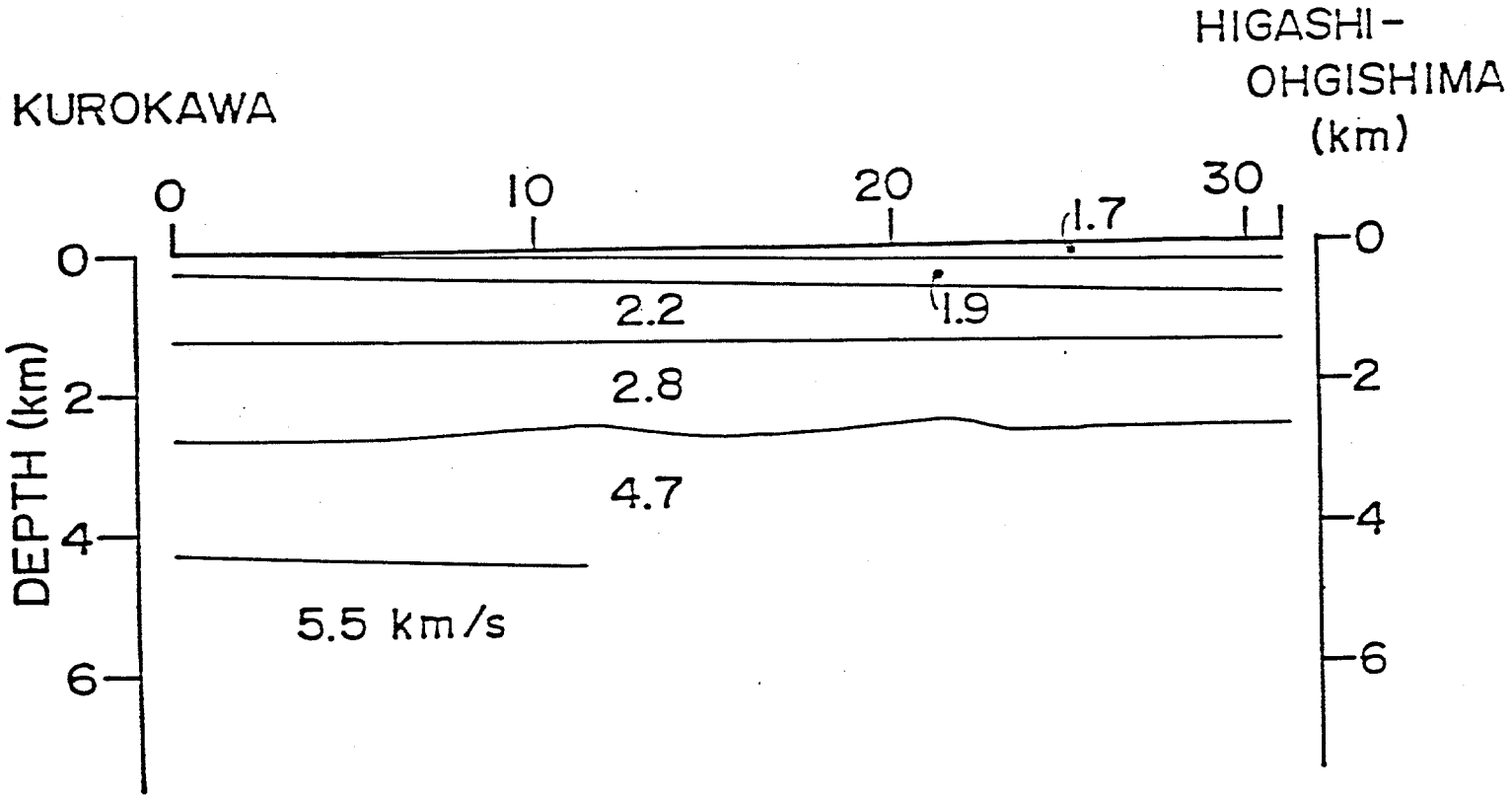

Fig. 2-21. Underground structure between Higashiohgishima and Kurokawa.

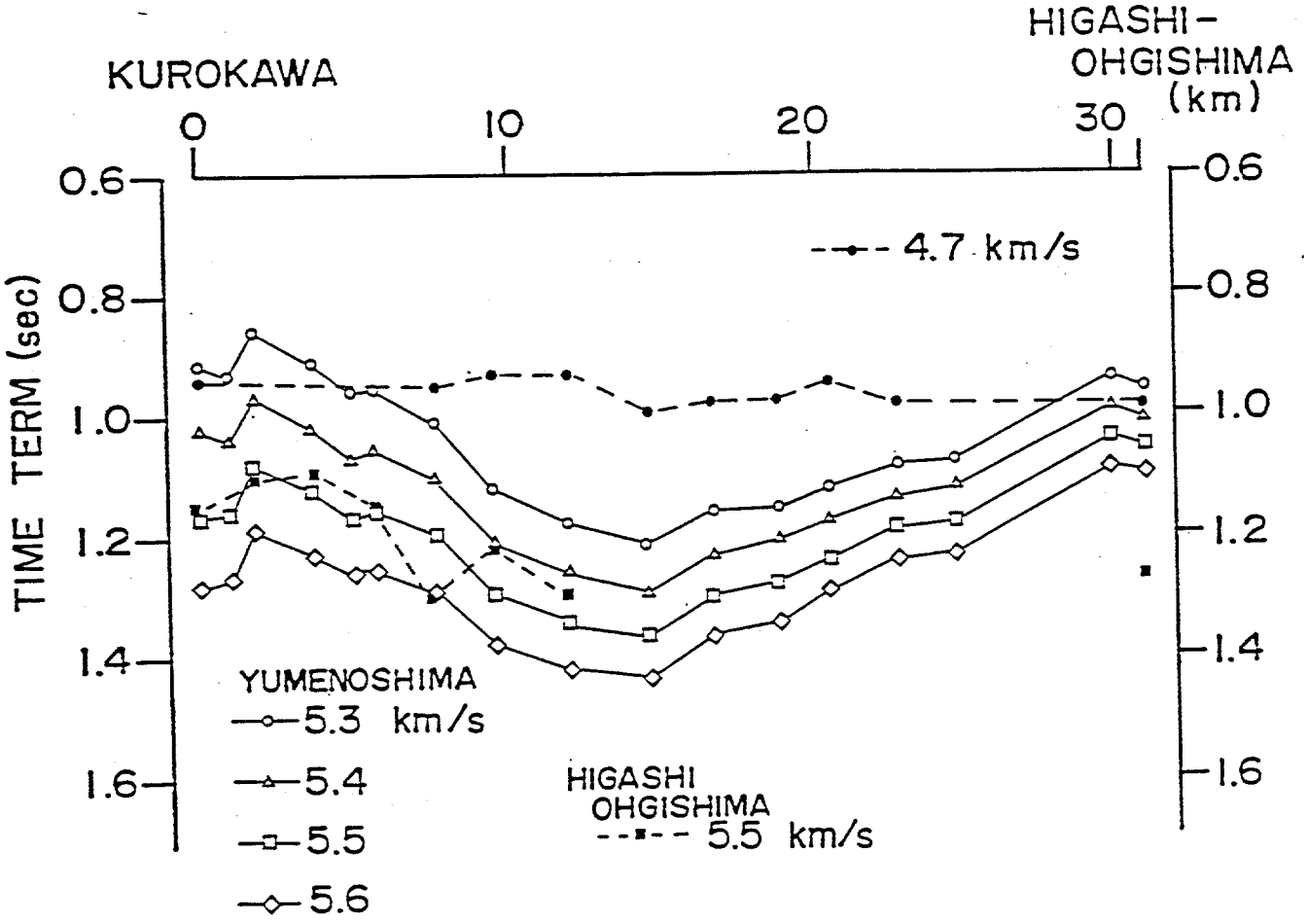

Fig. 2-22. Comparison of time-terms derived from the Higashiohgishima and Kurokawa explosions and those from the Yumenoshima explosion. The disagreement of both time-terms is found around Kurokawa when refractor velocity is 5.5km/s. The contradiction, however, arises around Higashiohgishima.

determined, because of the low S/N ratios of the seismograms.

The explosions at Yumenoshima were also observed along this line. The travel times of the onsets are shown in Table 2-6. According to the results of the Yumenoshima-Odawara and the Yumenoshima-Takao lines, it is considered that the initial phases propagate in the layer with a velocity of 5.5 km/sec. Similarly to the analysis for the Kurokawa-Okazu line, the distributions of the time-terms are compared. The solid lines in Fig. 2-22 indicate the time-terms from the Yumenoshima explosion by assuming that the time-term at Yumenoshima is 1.03 sec and the refractors' velocities are 5.3 to 5.6 km/sec. The broken line with squares denotes the distribution of the time-terms to the layer with a velocity of 5.5 km/sec as derived from the Higashiohgishima explosion. The time-terms to the layer with a velocity of 4.7 km/sec were also derived from the Kurokawa and the Higashiohgishima explosions as indicated by a broken line with circles. The two distributions of the time-terms for the layer with a velocity of 5.5 km/sec are almost similar around the Kurokawa explosion site. The time-term for the layer with a velocity of 5.5 km/sec at the Higashiohgishima explosion is equal to a half of the intercept time there (Th in Fig. 2-20). It, however, is inconsistent with the distribution of the time-terms from the Yumenoshima explosion as indicated by the solid lines in Fig. 2-22. Because the intercept time is derived from the extrapolation of the travel time curve, it is considered that the real depth to this layer is similar to the distribution of the time-terms from the Yumenoshima and the intercept time can not give the proper time-term at Higashiohgishima. Then, it is expected that the layer with a velocity of 4.8 km/sec would become thick in the middle between Kurokawa and Higashiohgishima, where the Yumenoshima-Ohyama line crosses with this line. This tendency, however, is not in a agreement with the results of the Yumenoshima-Ohyama line.

2.2.7 Underground structure along the Okazu-Higashiohgishima line

The Okazu and the Higashiohgishima explosions were also observed along a line from Okazu to Higashiohgishima. The ground velocities observed from the Okazu and the

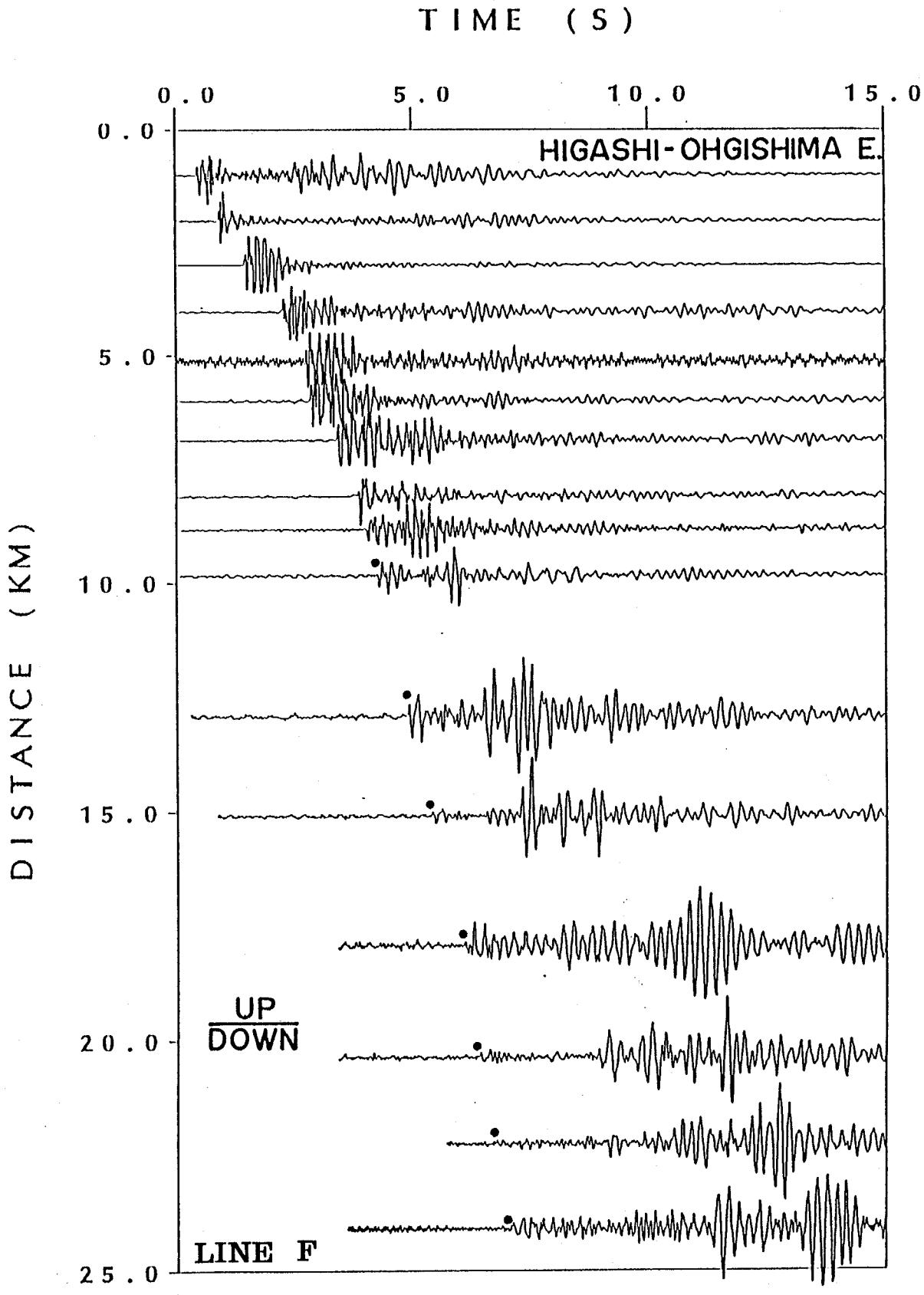

Fig. 2-23a. Observed seismograms at the stations along the Higashiohgishima-Okazu line (Line F in Fig. 2-1) during the Higashiohgishima explosion. Each trace indicates vertical ground velocity and is normalized to its maximum amplitude. Each solid circle shows onset of initial phase.

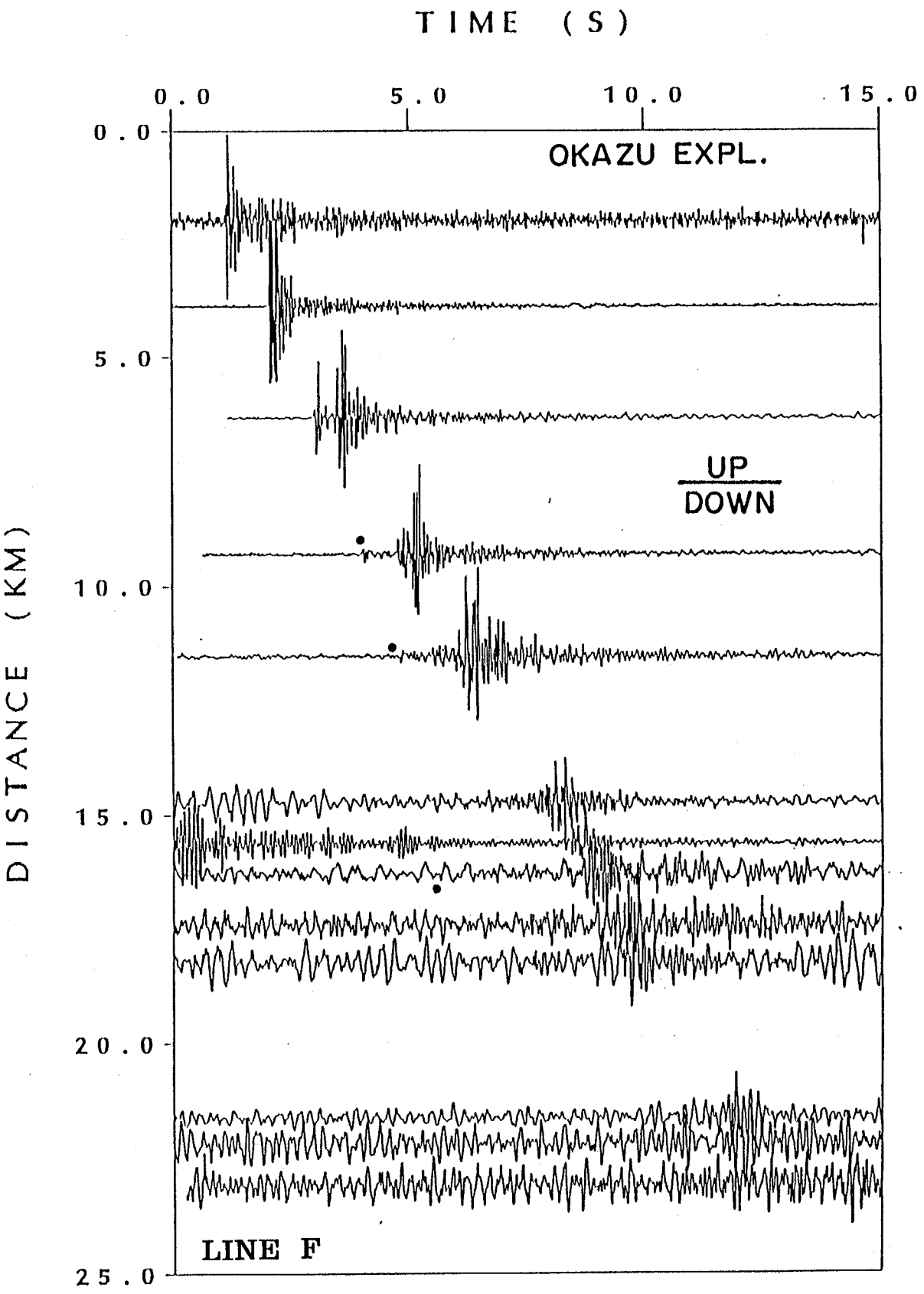

Fig. 2-23b. Observed seismograms at the stations on the Higashiohgihshima-Okazu line (Line F) during the Okazu explosion. Each trace indicates vertical ground velocity and is normalized to its maximum amplitude. Each solid circle shows onset of initial phase.

Table 2-7. Travel times of initial phases obtained from Okazu, Higashiohgishima and Yumenoshima explosions

No	STATION	LOCATION		OKAZU		KUROKAWA		YUMENOSHIMA	
		LAT.	LONG.	D(km)	T(s)	D(km)	T(s)	D(km)	T(s)
1	HIGASHI OHGISHIMA S.P.	35 30 06.9	139 46 28.3	0.00		24.10		13.79	4.60
2	HIGASHI OHGISHIMA 1	35 29 49.6	139 45 52.7	1.00	0.59	23.09		14.66	4.81
3	HIGASHI OHGISHIMA 2	35 29 36.7	139 45 17.0	2.02	1.22	22.12		15.43	5.02
4	HIGASHI OHGISHIMA 3	35 29 22.1	139 44 42.5	3.00	1.62	21.16		16.26	
5	OHGISHIMA 1	35 29 08.0	139 44 05.0	4.04	2.26	20.14		17.13	5.55
6	OHGISHIMA 2	35 28 52.1	139 43 26.2	5.14	2.73	19.08		18.08	
7	OHGISHIMA 3	35 28 35.2	139.42 58.0	6.01	3.08	18.27		18.91	5.76
8	OHGISHIMA 4	35 28 22.1	139 42 27.5	6.88	3.36	17.44		19.69	5.96
9	DAIKOKU FUTOH 1	35 27 59.6	139 41 46.8	8.11	3.82	16.31	(5.57)	20.87	6.25
10	DAIKOKU FUTOH 2	35 27 46.0	139 41 22.6	8.85	3.91	15.64		21.57	6.37
11	DAIKOKU FUTOH 3	35 27 26.9	139 40 49.6	9.86	4.19	14.74		22.55	6.62
12	SHINKOH FUTOH	35 27 10.6	139 38 43.9	12.91	4.86	11.53	4.55	25.03	7.10
13	NISHI CHU	35 26 56.5	139 37 16.9	15.09	5.35	9.31	4.01	26.90	7.50
14	IWASAKI	35 26 46.8	139 35 19.8	17.95	6.04	6.34	2.93	29.31	8.02
15	IMAI	35 26 36.1	139 33 42.5	20.37	6.37	3.88	2.03	31.43	8.25
16	TOTUKA C.C.	35 26 25.4	139 32 28.0	22.26	6.79	2.01	1.12	33.13	8.60
17	OKAZU S.P.	35 26 33.2	139 31 08.8	24.10	6.99	0.00		34.64	8.74

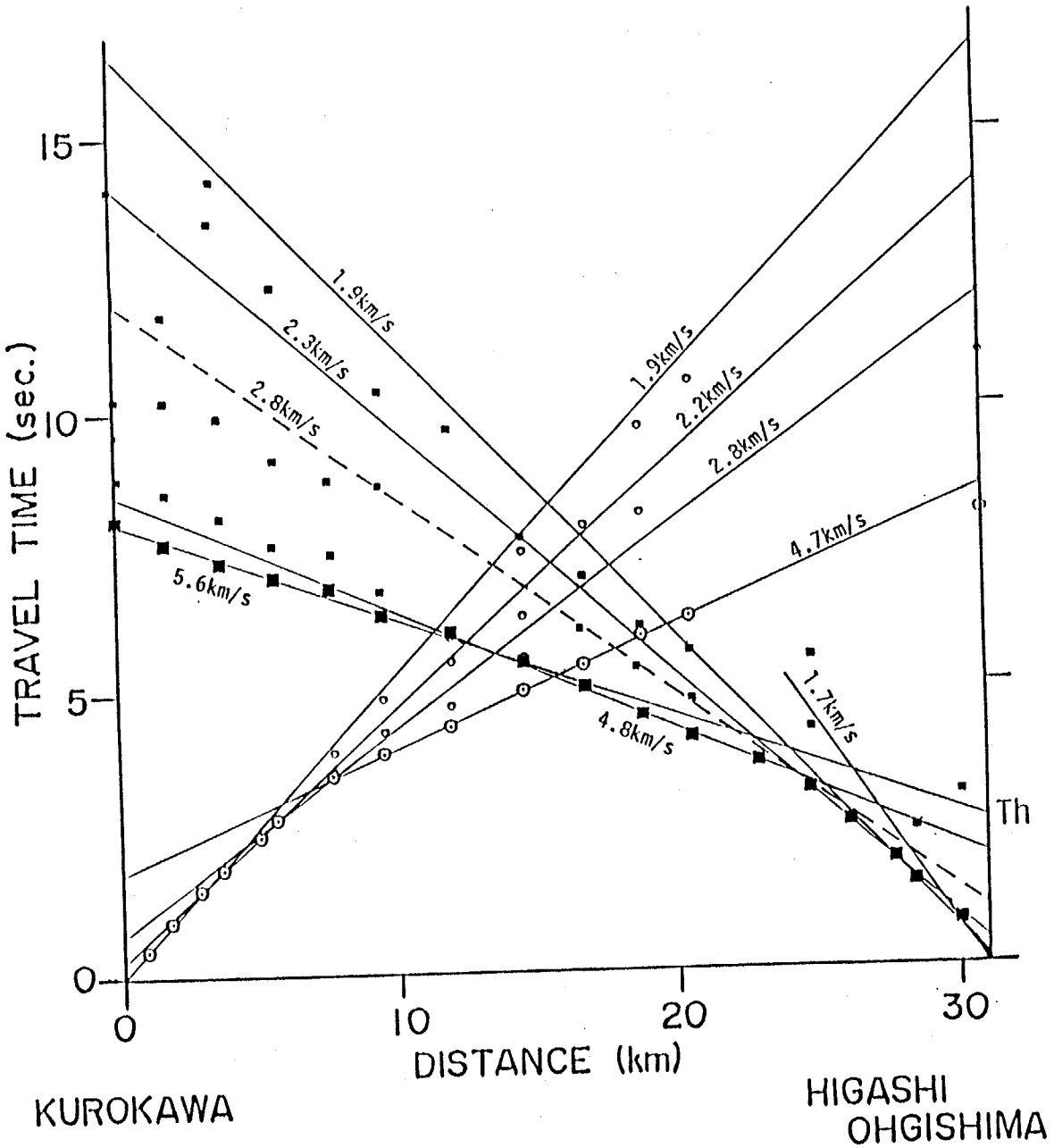

Fig. 2-24. Travel time diagram for the Higashiohgihshima-Okazu line (Line F).

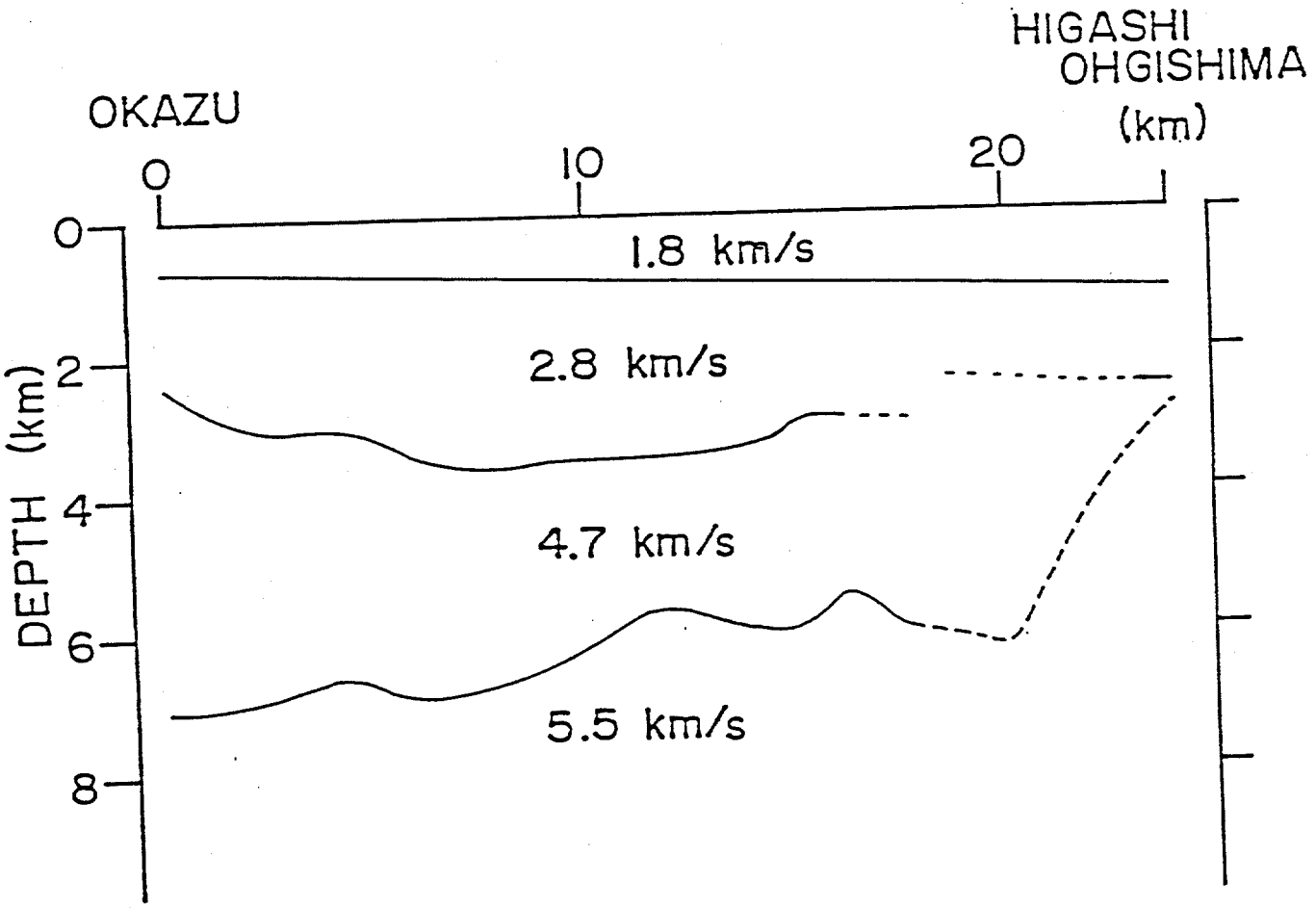

Fig. 2-25. Underground structure between Higashiohgishima and Okazu. Travel time data from the Yumenoshima explosion are also used to estimate the structure assuming the refractor velocity is 5.5km/s.

Higashiohgishima explosions are displayed in Figs. 2-23a and 2-23b, respectively. Since the stations near the Higashiohgishima explosion site were installed near the coast of the Tokyo bay, the S/N ratios of the records due to the Okazu explosion were low and the initial phase arrivals could not be detected.

The travel times of the initial phases are shown in Table 2-7. The travel time diagram is depicted in Fig. 2-24. The velocities of the sedimentary layers are 1.8 and 2.8 km/sec as well as the other profile. An apparent velocity of 5.3 km/sec can be seen in the travel time diagram of the Higashiohgishima explosion, while it becomes 4.1 km/sec from the Okazu explosion. The travel time curve of the third layer from the Okazu explosion was determined by considering the intercept time at Okazu in the results of the Kurokawa-Okazu line. The resultant true velocity for the third layer was deduced as 4.7 km/sec. However, the intercept time for the travel time curve of this layer at the Higashiohgishima shot point (A in Fig. 2-24) differs from that derived from the Kurokawa-Higashiohgishima line (A'). Furthermore, the extended travel time with an apparent velocity of 4.1 km/sec from the Okazu explosion (B') differs from the reciprocal travel time from the Higashiohgishima explosion (B). It can be interpreted that the depth to the third layer varies drastically at around 10 km distance form the Higashiohgishima explosion site. On the basis of this interpretation, the underground structural model is constructed as shown in Fig. 2-25. The explosion at Yumenoshima was also observed along this line. As it is deduced from the results of the Yumenoshima-Odawara line, the initial phases propagate in the layer with a velocity of 5.5 km/sec. Using this travel time data like a fan shooting, the depth to the layer was also determined. The layer with a velocity of 4.7 km/sec has the maximum depth in the middle of the two explosion sites. The thickness of the layer with a velocity of 4.8 km/sec is not so large near Higashiohgishima, but, it becomes larger towards Okazu. Some ambiguities still remain as indicated by broken lines.

2.2.8 Underground structure along the Ohfuna and the Yokohama lines

The explosions were detonated at Kouhoku, Zushi and Aburatsubo by the National Research Center for Disaster Prevention. These explosions were observed in three surveying lines. The Kouhoku line was conducted to investigate the subsurface step-like topography seen in the Yumenoshima-Ohyama line suggested by Seo (1981). Temporary stations were set in the eastern and western direction from the Kouhoku explosion (Kouhoku line). The second surveying is from the Zushi explosion site to Nagatsuta (Ohfuna line). The last one consists of four stations around Yokohama (Yokohama line).

The velocities observed in the eastern and the western of the Kouhoku line from the Kouhoku explosion are displayed in Figs. 2-26a and 2-26b, respectively. Since the seismograms at the stations with epicentral distances more than 10 km have low S/N ratios, it is difficult to detect the onsets. Moreover, no distinct phases including later arrivals can be seen in the seismograms obtained at the stations of 15 km away from the Kouhoku explosion site. The obtained arrival times are shown in Table 2-8. The travel time diagram is depicted in Fig. 2-27. Although the thickness of the top layer could be deduced as seen in Fig. 2-27, the depth to the lower interface could not be known. No distinct phases could be seen in the records along this line from the other explosions .

The records with higher S/N ratios could be obtained at the stations along the Ohfuna line. Figs. 2-28a, b and c show the seismograms observed along the Ohfuna line from the Kouhoku, the Zushi and the Aburatsubo explosions, respectively. Although the direct wave propagating in the top layer can be seen in the seismograms from the Kouhoku and the Zushi explosions, we can find no later phases in the seismograms from the Aburatsubo explosion, except for the initial phases with an apparent velocity of 4.7 km/sec. This means that the surface layer with a velocity of about 2 km/sec does not exist or is very thin in the vicinity of the Aburatsubo explosion site. In fact, outcrop of a formation of the Miura group which is considered to correspond to the layer with a velocity of 2.8 km/sec was confirmed from geological investigations. The travel times of the initial phases are shown in Table 2-8. The travel time diagram is shown in Fig. 2-29. Apparent velocities of 4.7

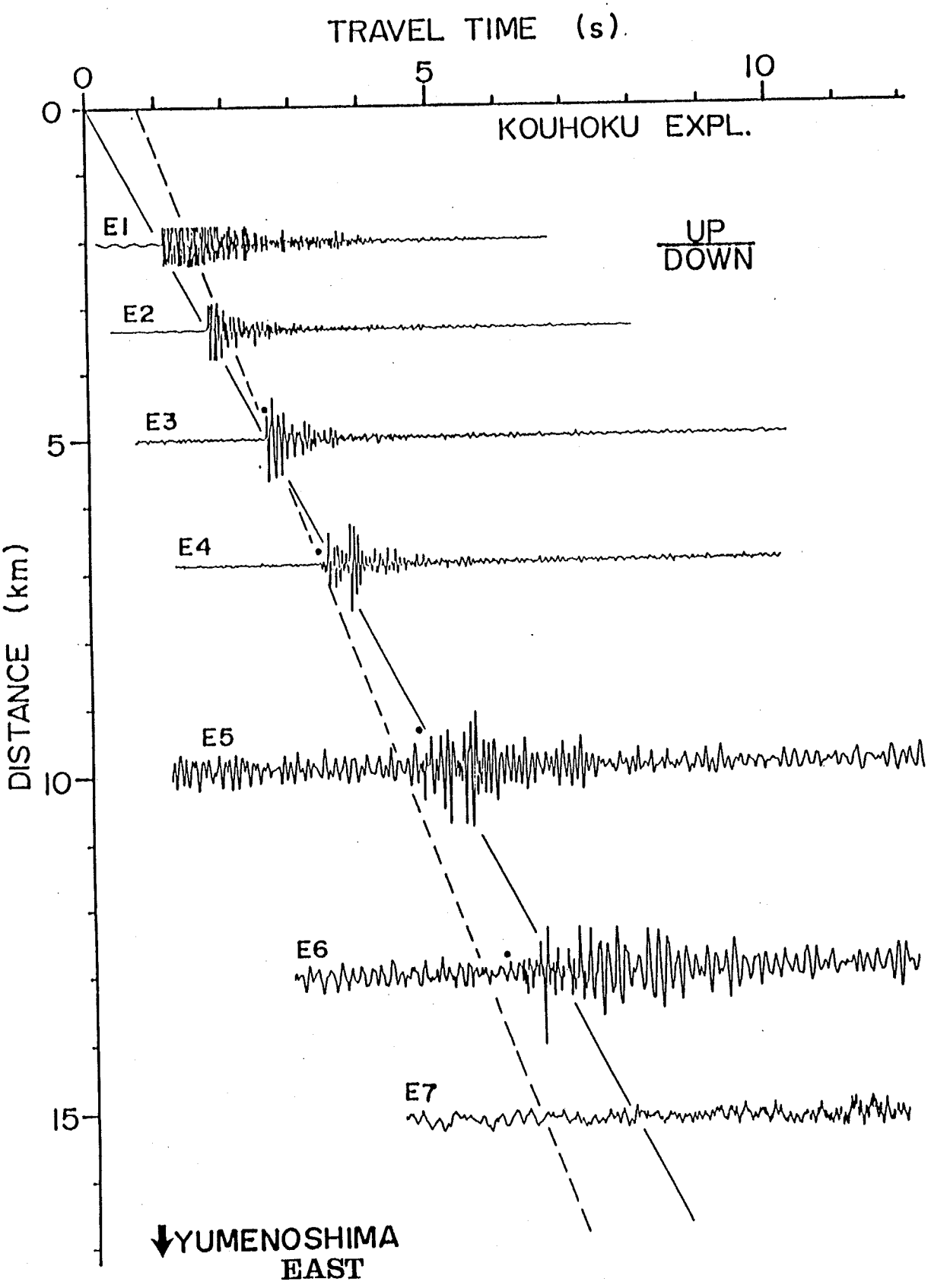

Fig. 2-26a. Observed seismograms at the stations along the eastern part of the Kouhoku line during the Kouhoku explosion. Each trace indicates vertical ground velocity and is normalized to its maximum amplitude. Each solid circle shows onset of initial phase.

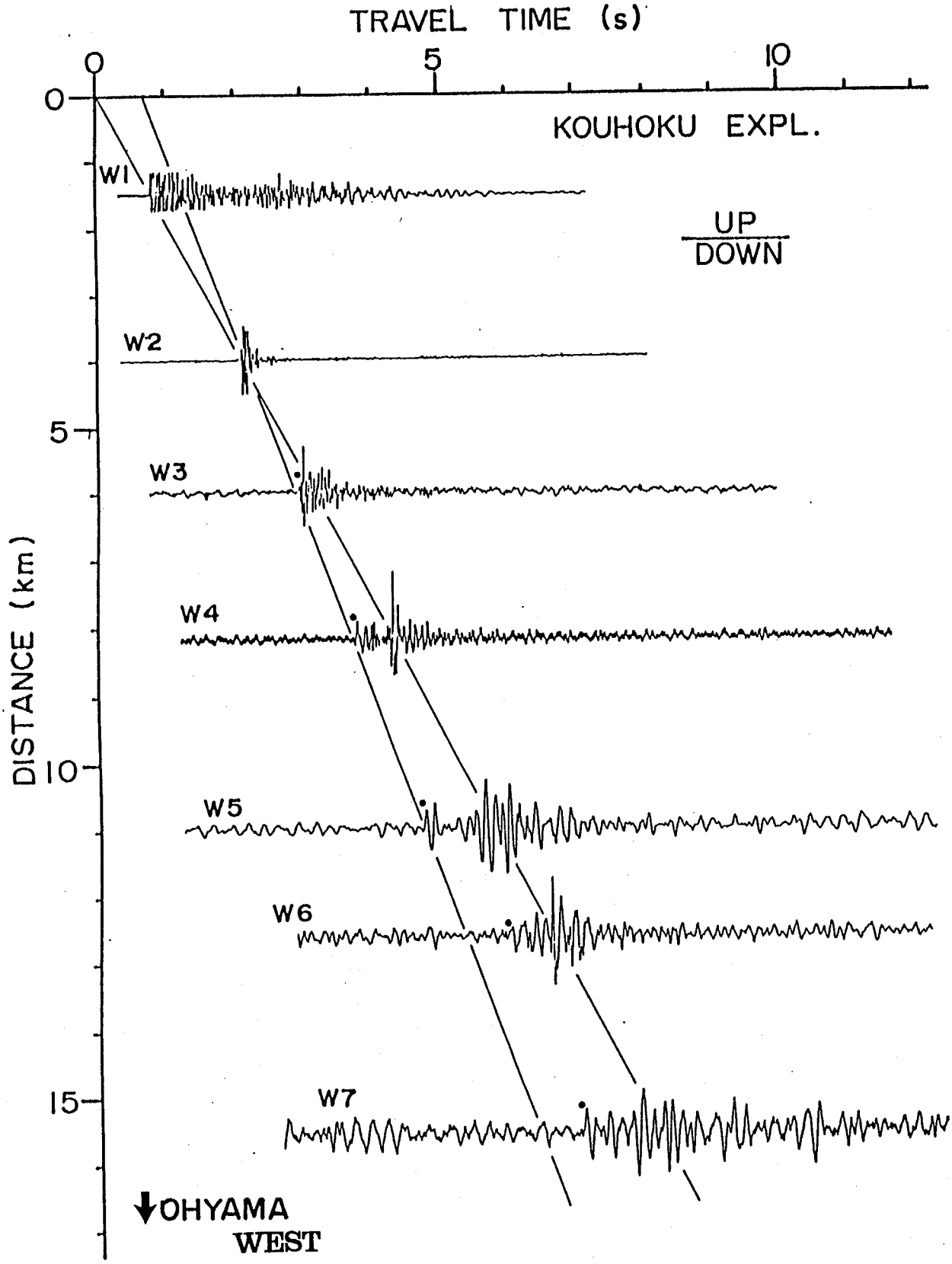

Fig. 2-26b. Observed seismograms at the stations along the western part of the Kouhoku line during the Kouhoku explosion. Each trace indicates vertical ground velocity and is normalized to its maximum amplitude. Each solid circle shows onset of initial phase.

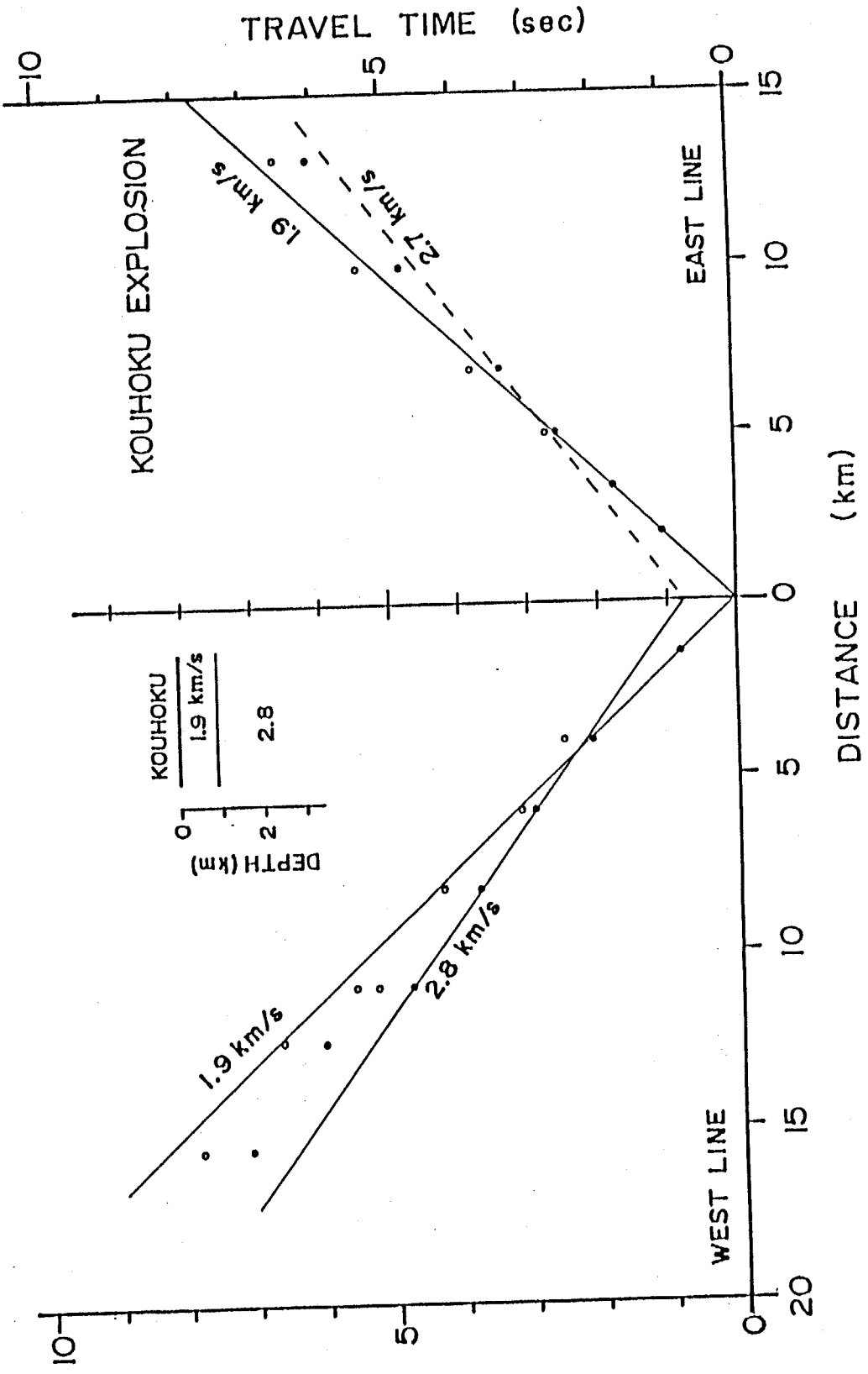

Fig. 2-27. Travel time diagram for the the Kouhoku line. The deduced underground structure at the Kouhoku explosion point are also depicted.

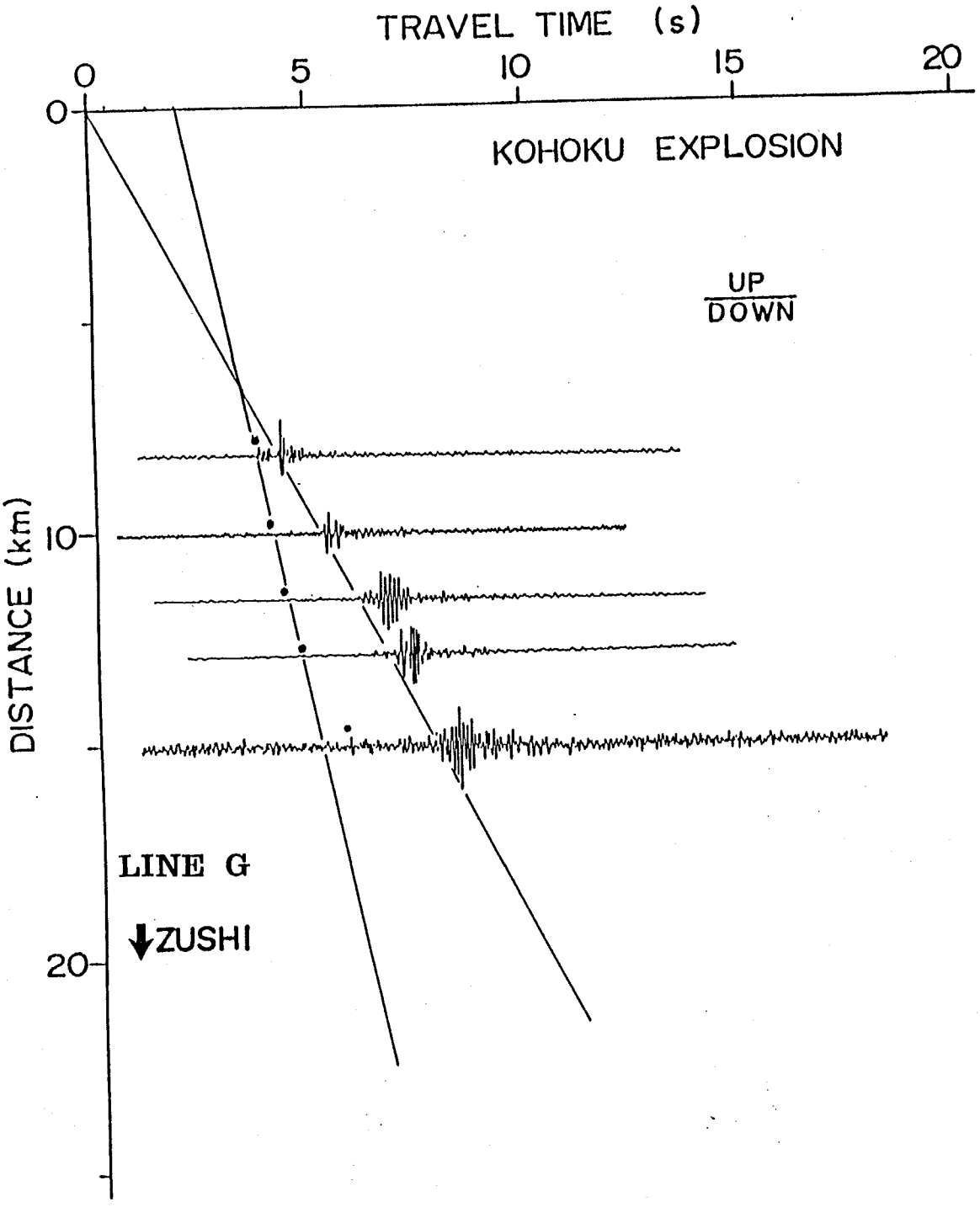

Fig. 2-28a. Observed seismograms at the stations along the Ohfuna line (Line G in Fig. 2-1) during the Kouhoku explosion. Each trace indicates vertical ground velocity and is normalized to its maximum amplitude. Each solid circle shows onset of initial phase.

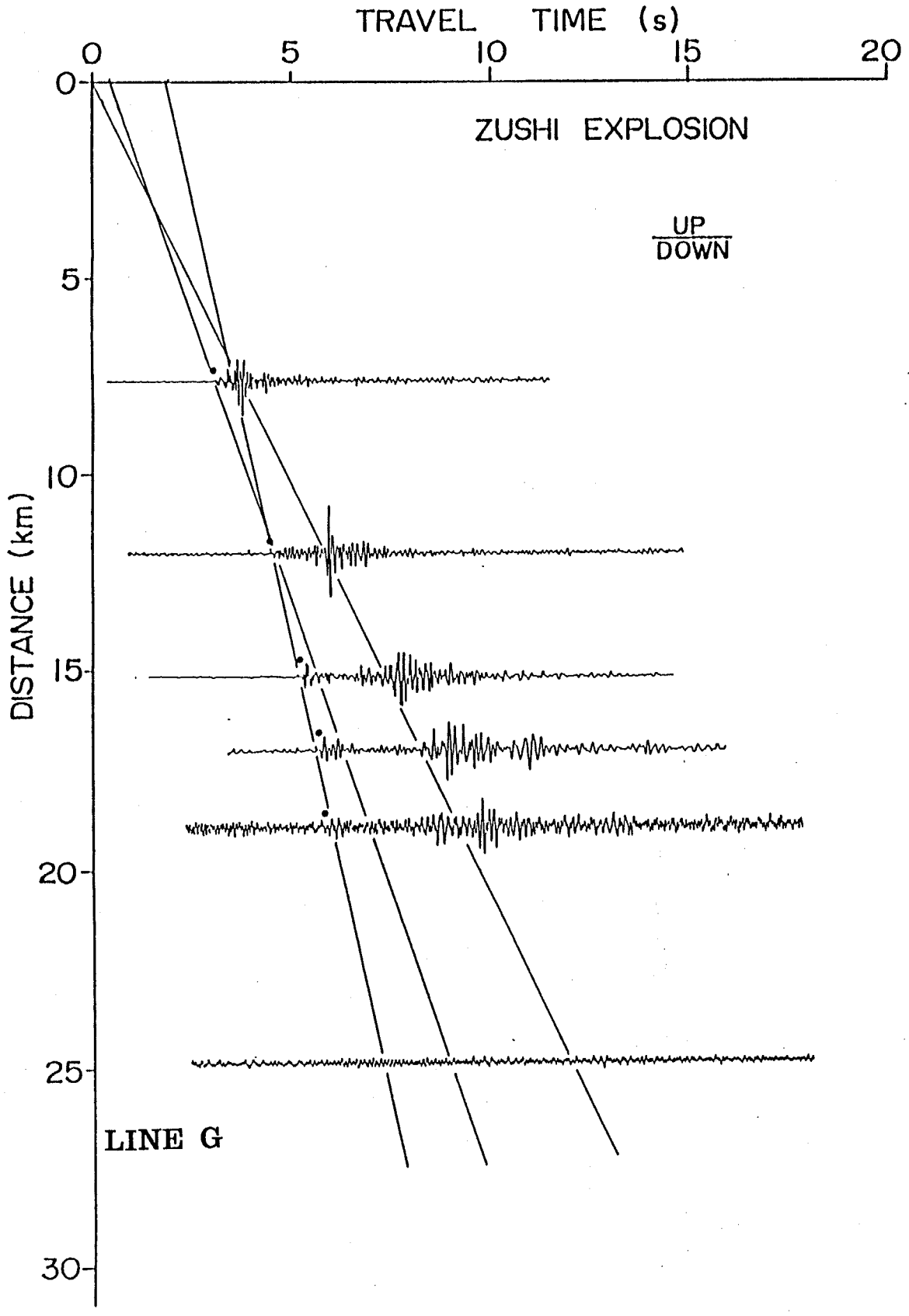

Fig. 2-28b. Observed seismograms at the stations along the Ohfuna line (Line G) during the Zushi explosion. Each trace indicates vertical ground velocity and is normalized to its maximum amplitude. Each solid circle shows onset of initial phase.

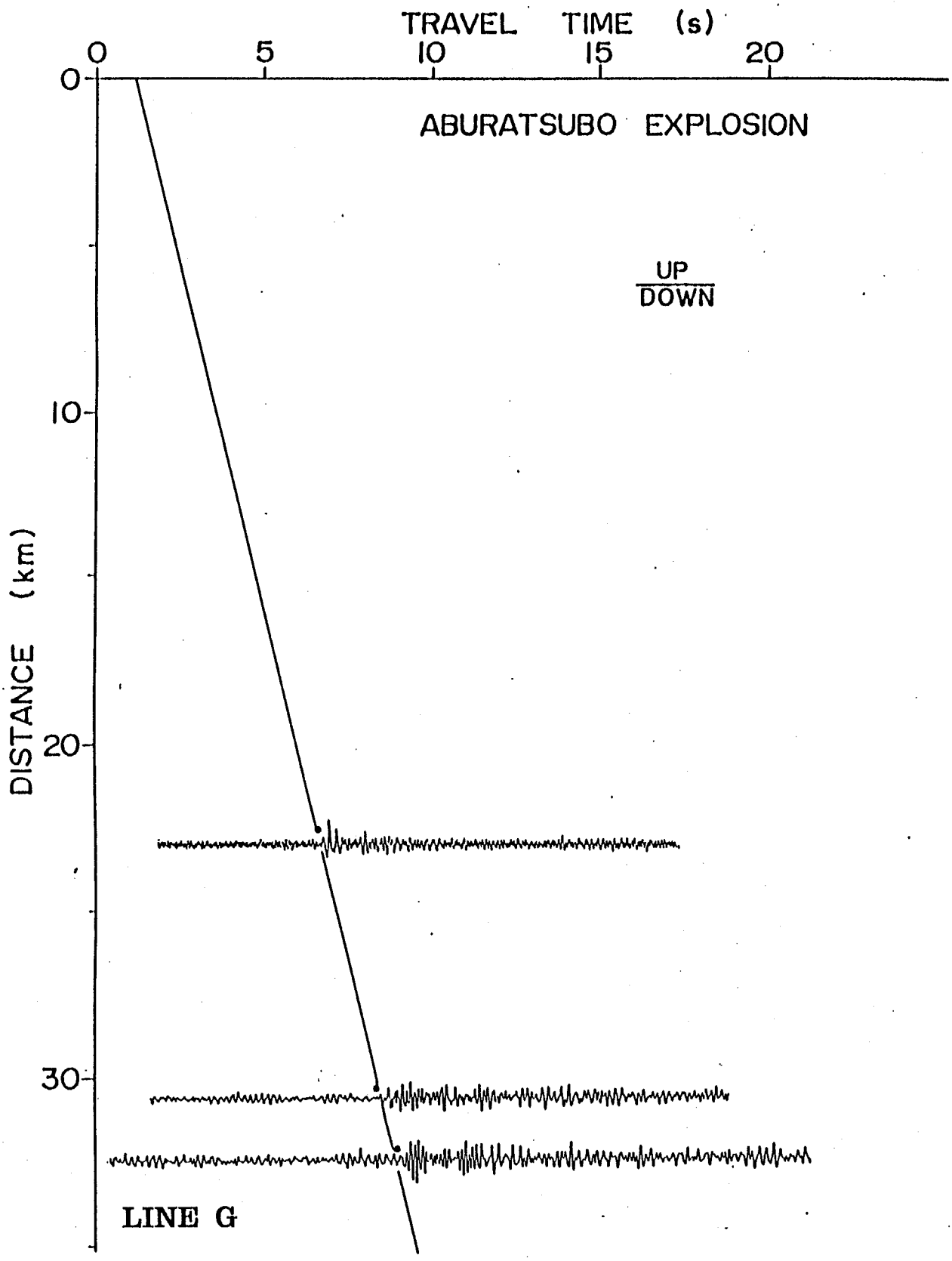

Fig. 2-28c. Observed seismograms at the stations along the Ohfuna line (Line G) during the Aburatsubo explosion. Each trace indicates vertical ground velocity and is normalized to its maximum amplitude. Each solid circle shows onset of initial phase.

Table 2-8. Travel times of initial phases obtained from Kouhokum Zushi and Aburatsubo explosions

No	STATION	LOCATION		KOUHOKU		ZUSHI		ABURATSUBO	
		LAT.	LONG.	D(km)	T(s)	D(km)	T(s)	D(km)	T(s)
E1	KAWAWA	35 32 04.1	139 33 18.8	1.48	0.81	25.48		41.47	
E2	NAKAGAWA	35 32 49.5	139 35 27.3	2.04	1.09	26.49		42.44	
E3	SHIN YOSHIDA	35 32 57.6	139 36 18.8	3.34	1.75	26.70		42.59	
E4	TAKADA	35 33 09.1	139 37 22.7	4.98	2.59	27.10		42.88	
E5	IDA	35 33 25.0	139 38 35.5	6.88	3.35	27.75		43.37	
E6	TAMAGAWA	35 33 38.3	139 40 35.1	9.90	4.77	28.67		43.96	
E7	IKEGAMI	35 34 23.2	139 42 32.0	13.10	6.07	30.78		45.69	
E8	IRIARAI	35 34 50.2	139 43 49.8	15.22		32.21		46.85	
W1	SUGIYAMA JINJYA	35 31 29.7	139 31 49.2	3.98	2.09	24.97		40.87	9.32
W2	SHOWA UNIV.	35 31 05.9	139 30 34.9	5.98	2.94	24.87	8.72	40.63	
W3	T.I.T NAGASTUTA	35 30 34.1	139 29 16.5	8.19	3.76	24.75		40.30	
W4	YAMATO	35 30 14.1	139 27 27.7	10.96	4.72	25.53	9.03	40.70	
W5	MIDORINO	35 29 57.8	139 26 26.1	12.59	5.99	25.98	8.77	40.88	
W6	ZAMA	35 29 21.4	139 24 36.6	15.56	7.08	26.83		41.15	
W7	ICHI MINAMI	35 28 09.4	139 22 25.2	19.47		27.66		41.04	
W8	SUWA JINJYA	35 27 28.2	139 18 50.9	24.95		31.30		43.41	10.20
W9	HINATA YAKUSHI	35 26 11.0	139 16 41.1	28.88		33.03	8.40	44.01	9.92
S1	HIGASHI KIBOUGAOKA	35 27 39.6	139 30 52.0	10.09	4.02	18.86	5.90	34.43	
S2	OKAZU SHOT POINT	35 26 36.9	139 31 06.6	11.65	4.30	16.97	5.64	32.48	8.92
S3	OKAZU	35 25 41.9	139 31 38.8	12.95	4.67	15.09	5.19	30.62	8.40
S4	MOTOMACHI	35 24 17.4	139 32 44.7	15.12	(5.79)	12.07	4.48	27.63	
S5	HONGODAI	35 21 45.1	139 33 16.3	19.70		7.62	3.07	22.92	6.77
Y1	NAKAMARU	35 28 44.1	139 37 23.2	8.27	4.08	18.95	6.06	34.72	
Y2	SHINKOU FUTOU	35 27 12.6	139 38 44.6	11.75		16.46	5.60	31.91	
Y3	YOKOHAMA JMA	35 26 13.6	139 39 19.8	13.75	(6.98)	14.93	5.42	30.14	
Y4	SANKEIEN	35 24 50.0	139 39 52.5	16.36	8.41	12.81	5.00	27.65	

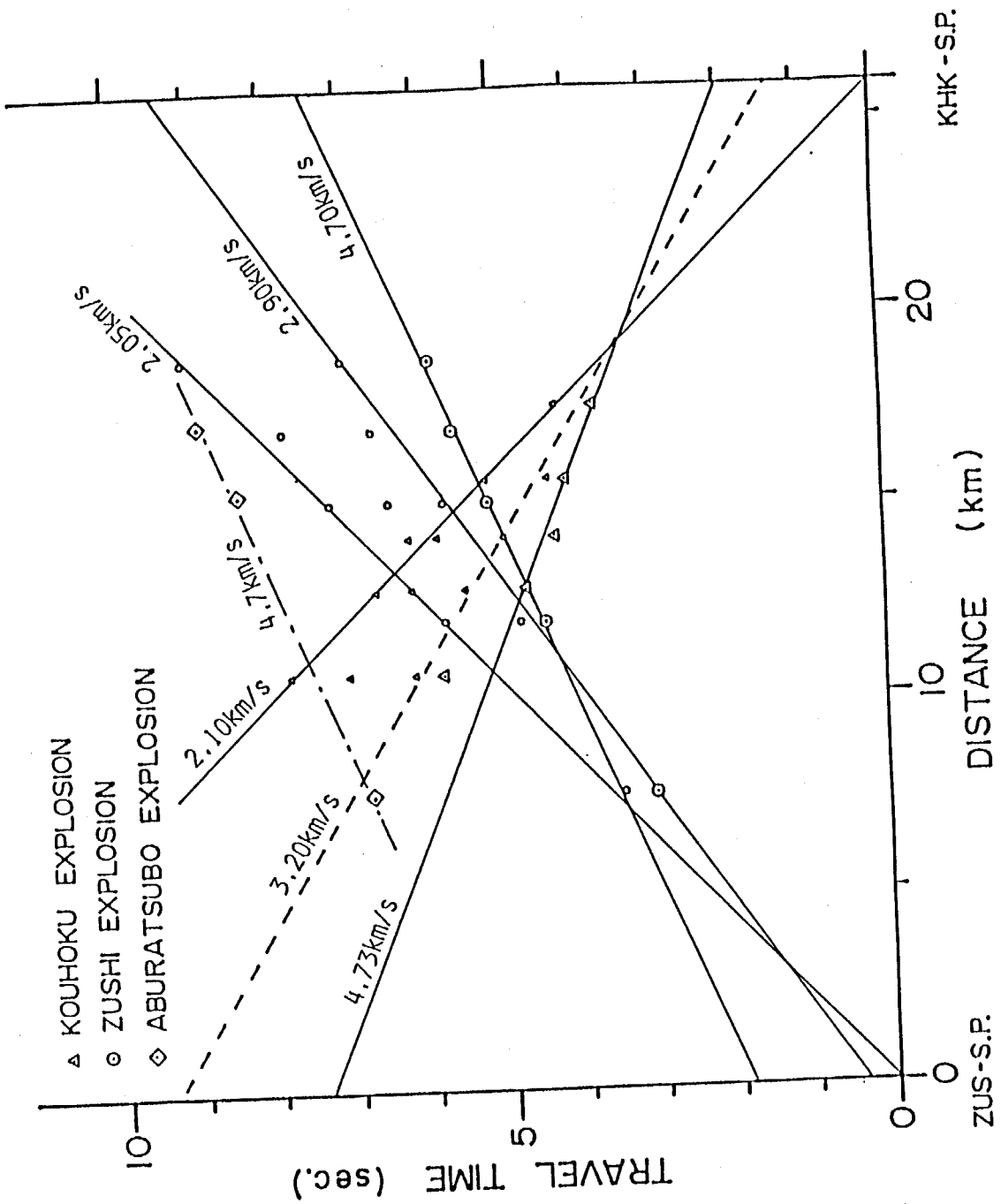

Fig. 2-29. Travel time diagram for the Ohfuna line (Line G).

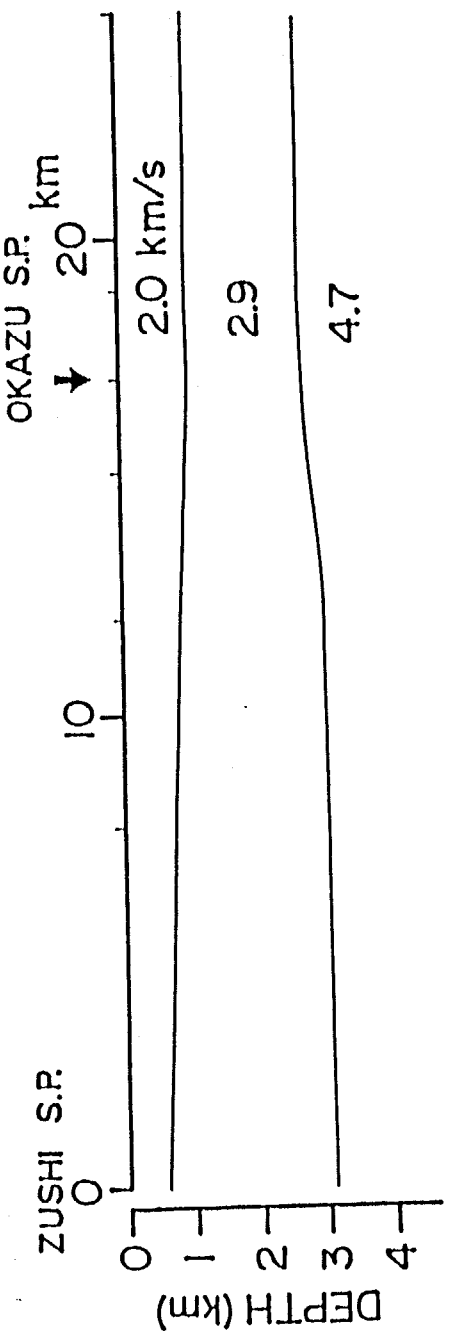

Fig. 2-30. Underground structure for the Ohfuna line (line G).

km/sec can be seen in the branches of travel time curves of all the explosions. As we set no observation stations near the Zushi explosion site, a detailed structure of the surface layers could not be obtained. Then, using the travel times of the later arrivals and the results of the Kurokawa-Okazu line, we determined the underground structure as depicted in Fig. 2-30. The top layer with a velocity of 1.8 km/sec becomes thinner towards the Zushi explosion site. However, the depth to the layer having a velocity of 4.7 km/sec does not so vary along the line.

The explosion at Zushi was also observed along the Yokohama line as shown in Fig. 2-31. No arrivals could be detected from the other explosions. The Okazu-Higashiohgishima line crosses with this line at a distance of approximately 16 km from the Zushi explosion site (cf, arrow in Fig. 2-31). We assumed, here, that the initial phases propagate in the layer with a velocity of 4.7 km/sec as it was discussed for the Ohfuna line. Then, we deduced an underground structure, such that it does not differ from the underground structure of the Okazu-Higashiohgishima line. The resultant underground structure is shown in Fig. 2-32. The depth to the layer with a velocity of 4.8 km/sec at Yokohama is greater than 4 km.

2.2.9 Underground structure around Akishima

The four surveying lines were spread with a center at the Akishima explosion site in four directions: for Fuchu, Tokorozawa, Itsukaichi and Takao. Tachikawa active fault is located between the explosion site and Tokorozawa. To know the structure of the fault was one of the targets of the survey.

The seismograms observed along the four lines are shown in Fig. 2-33a to Fig. 2-33d. No later phases propagating in the surface layer directly can be seen in the seismograms observed around Itsukaichi and Takao. The travel times of the onsets are shown in Table 2.9 and the travel time diagrams are depicted in Figs. 2-34a and 2-34b. The upper two layers have P-wave velocities of 1.8 and 2.3 km/sec and the top layer becomes quite thin in the west of the Akishima explosion site. Since there are no reverse explosions, the true

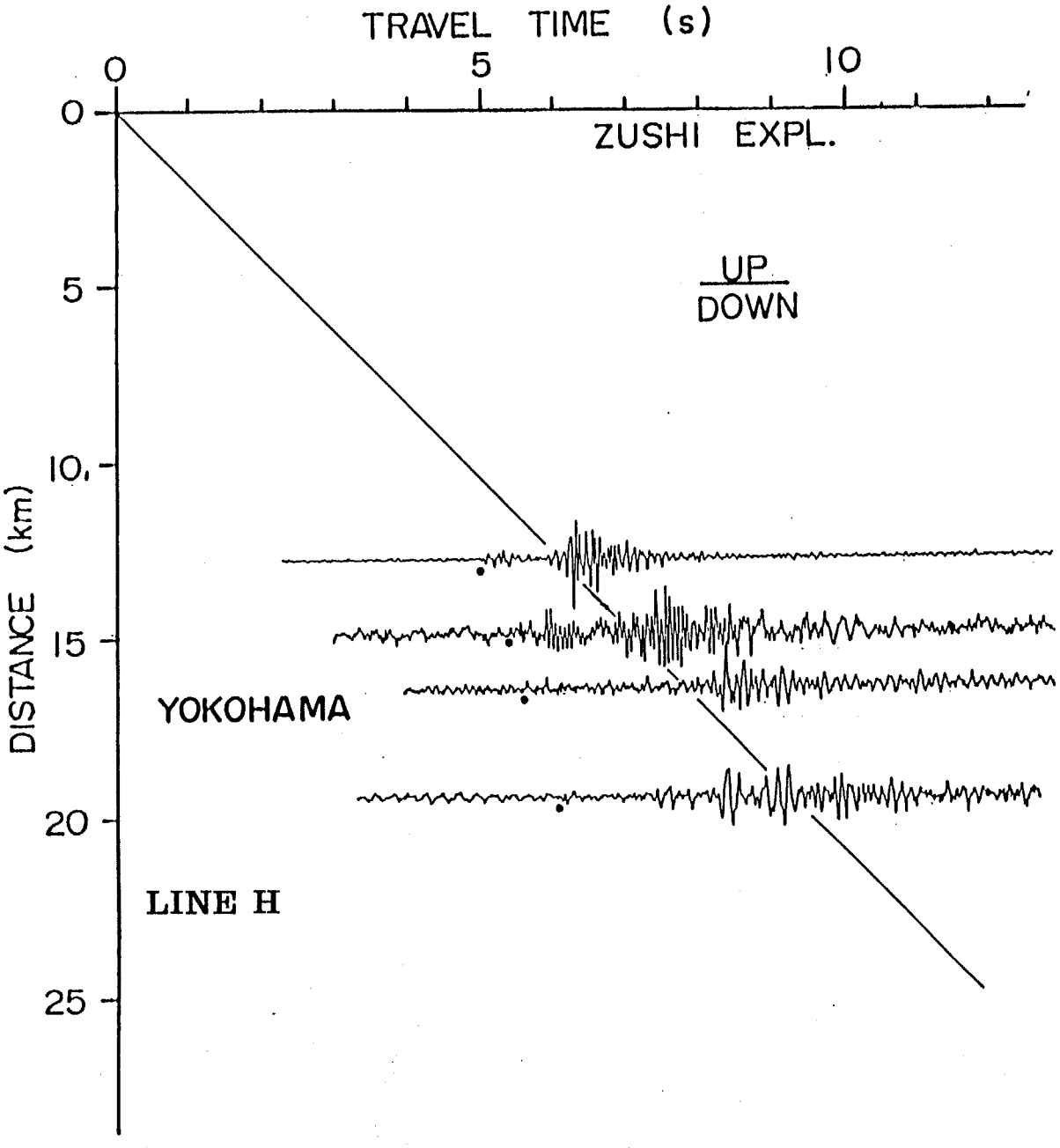

Fig. 2-31. Observed seismograms at the stations along the Yokohama line (Line H in Fig. 2-1) during the Zushi explosions. Each trace indicates vertical ground velocity and is normalized to its maximum amplitude. Each solid circle shows onset of initial phase.

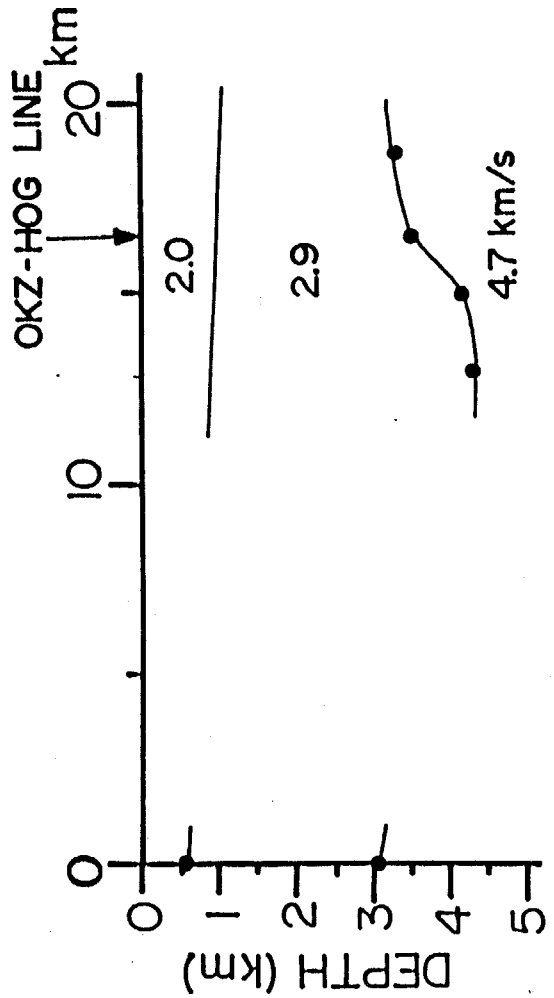

Fig. 2-32. Underground structure for the Yokohama line (line H).

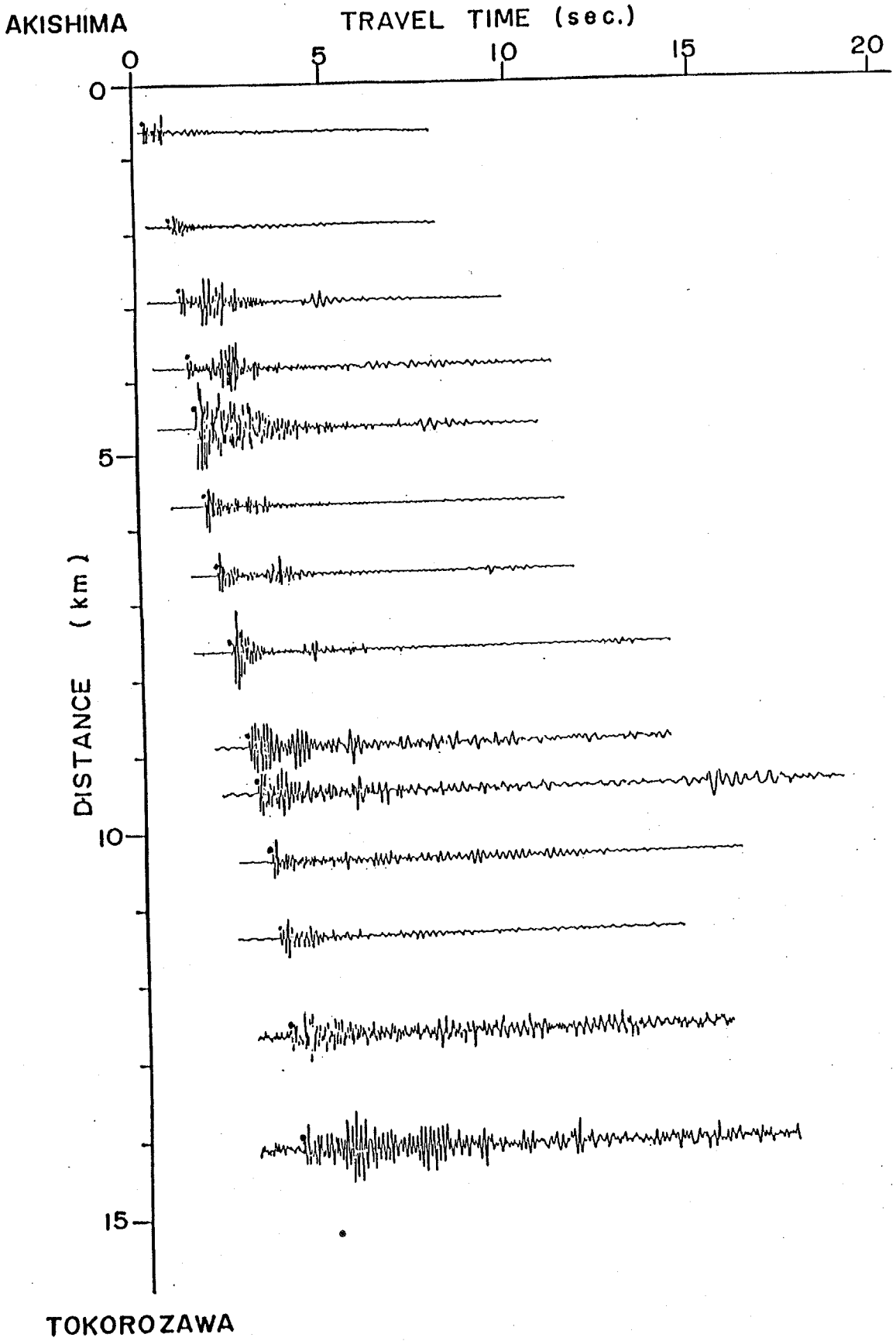

Fig. 2-33a. Observed seismograms at the stations for Tokorozawa along the Tokorozawa-Takao line (Line I in Fig. 2-1) during the Akishima explosions. Each trace indicates vertical ground velocity and is normalized to its maximum amplitude. Each solid circle shows onset of initial phase.

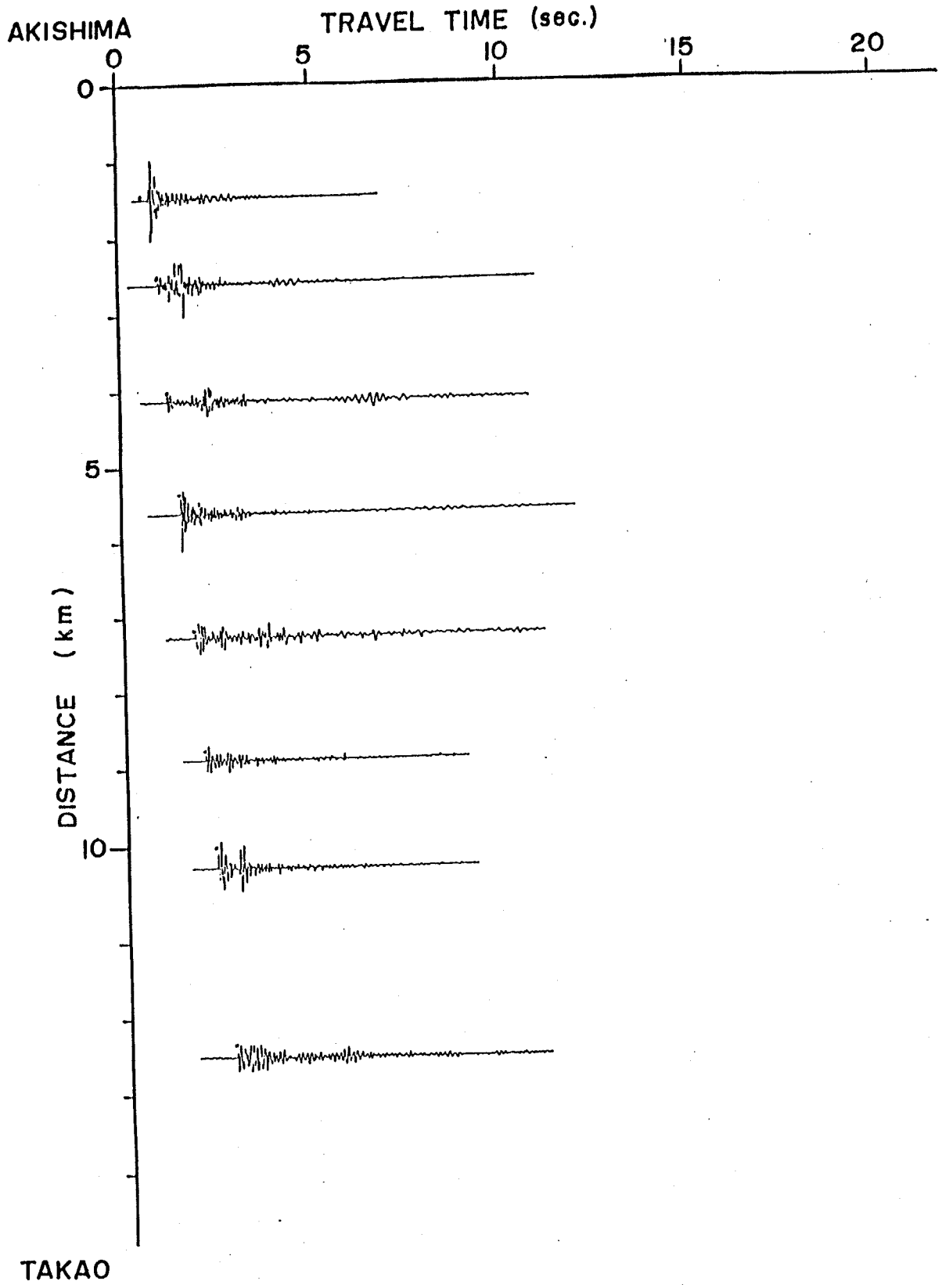

Fig. 2-33b. Observed seismograms at the stations for Takao along the Tokorozawa-Takao line (Line I in Fig. 2-1) during the Akishima explosions. Each trace indicates vertical ground velocity and is normalized to its maximum amplitude. Each solid circle shows onset of initial phase.

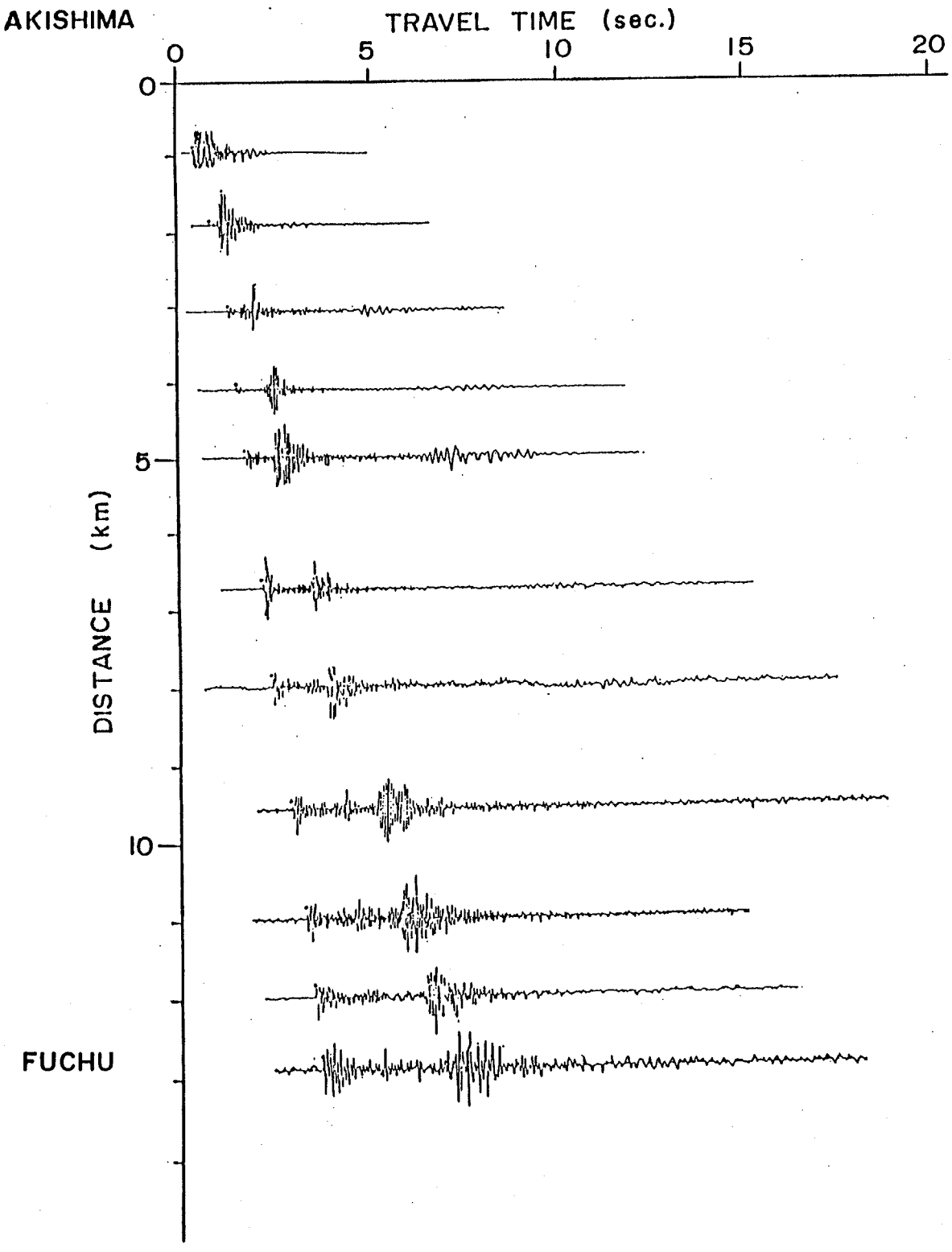

Fig. 2-33c. Observed seismograms at the stations for Fuchu along the Fuchu-Itsukaichi line (Line J in Fig. 2-1) during the Akishima explosions. Each trace indicates vertical ground velocity and is normalized to its maximum amplitude. Each solid circle shows onset of initial phase.

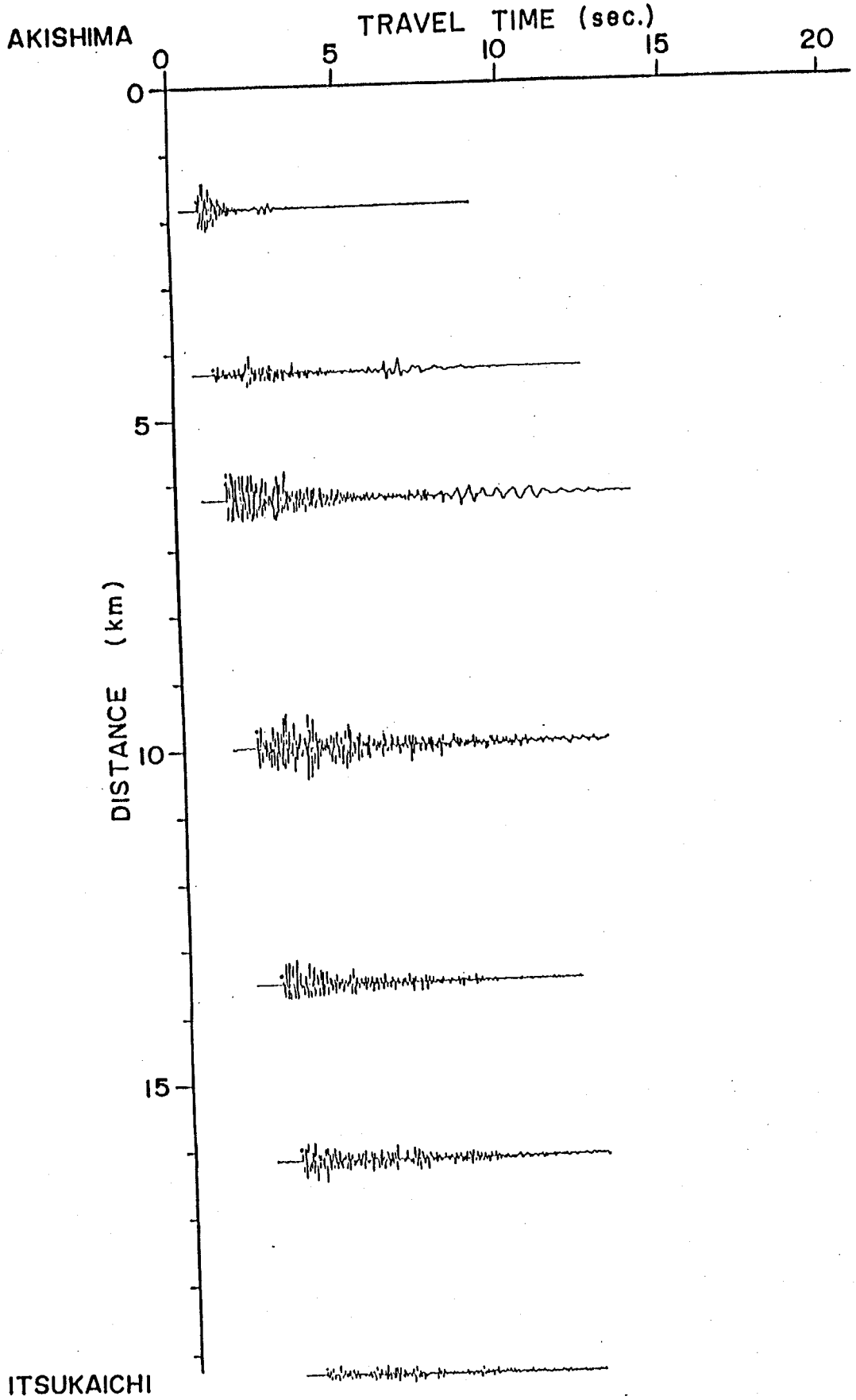

Fig. 2-33d. Observed seismograms at the stations for Itsukaichi along the Fuchu-Itsukaichi line (Line J in Fig. 2-1) during the Akishima explosions. Each trace indicates vertical ground velocity and is normalized to its maximum amplitude. Each solid circle shows onset of initial phase.

Table 2-9. Travel times of initial phases obtained from Akishima explosion

No	STATION		LOCATION LAT.	LOCATION LONG.	AKISHIMA EXP. D(km)	AKISHIMA EXP. T(s)
0	AKISHIMA S.P.		35 41 33.0	139 21 07.5	0.00	0.00
1	TANAKA SHO	(TKR1)	35 41 50.5	139 21 22.6	0.66	0.29
2	SEISEN CHU	(TKR2)	35 42 12.3	139 22 05.4	1.89	0.92
3	ZUIUN CHU	(TKR3)	35 42 44.1	139 22 25.1	2.93	1.18
4	MUSASINO SHO	(TKR4)	35 42 58.8	139 22 58.0	3.84	1.36
5	TACHIKAWA 5 CHU	(TKR5)	35 43 15.0	139 23 23.6	4.65	1.56
6	KAMISUNAKAWA SHO	(TKR6)	35 43 45.2	139 23 46.7	5.71	1.79
7	MIDORI YOUCHIEN	(TKR7)	35 43 55.3	139 24 25.0	6.62	2.05
8	HIGASHIYAMATO 10 SHO	(TKR8)	35 44 20.0	139 24 54.9	7.69	2.33
9	HIGASHIYAMATO 9 SHO	(TKR9)	35 44 54.5	139 25 21.8	8.91	2.74
10	UNSEIJI	(TKR10)	35 45 05.3	139 25 40.7	9.49	2.95
11	TAMA-KO	(TKR11)	35 45 24.3	139 26 09.4	10.41	3.32
12	HIKAWA JINJYA	(TKR12)	35 45 24.6	139 26 42.1	11.40	3.50
13	ARAHATA SHO	(TKR13)	35 46 21.1	139 27 08.4	12.69	3.71
14	TOKOROZAWA KOH	(TKR14)	35 46 54.3	139 27 49.1	14.14	3.99
15	TAIRA CHO	(FCH1)	35 41 18.4	139 21 41.0	0.96	0.43
16	KOMIYA CHO	(FCH2)	35 41 05.3	139 22 15.0	1.90	0.83
17	SAKAE CHO	(FCH3)	35 40 52.7	139 22 59.0	3.07	1.29
18	HINO JINJYA	(FCH4)	35 40 53.9	139 23 43.0	4.09	1.54
19	HINO 1 CHU	(FCH5)	35 40 38.0	139 24 14.3	4.99	1.75
20	HACHIMAN JINJYA	(FCH6)	35 40 02.4	139 25 10.5	6.72	2.19
21	HINO JINJYA	(FCH7)	35 39 11.7	139 25 32.9	7.97	2.38
22	YOTUYA SHO	(FCH8)	35 39 22.7	139 26 53.0	9.57	2.86
23	SUMIYOSI SHO	(FCH9)	35 39 09.1	139 27 46.3	10.97	3.21
24	DOUSAI CENTER	(FCH10)	35 39 02.3	139 28 28.4	12.02	3.41
25	MINAMITAMA GESUIJYO	(FCH11)	35 38 42.9	139 28 55.7	12.89	3.57
26	TENSO JINJYA	(TKO1)	35 41 03.9	139 20 20.2	1.49	0.61
27	KUMANO JINJYA	(TKO2)	35 40 33.3	139 19 54.0	2.61	1.03
28	HACHIOHJI 2 CHU	(TKO3)	35 40 02.6	139 19 06.2	4.13	1.24
29	KISSYO IN	(TKO4)	35 39 27.7	139 18 23.9	5.64	1.55
30	TOUSYO JI	(TKO5)	35 38 57.2	139 17 28.6	7.30	1.85
31	ASAKAWA CHU	(TKO6)	35 38 06.8	139 16 59.6	8.90	2.08
32	CABLE CAR STATION	(TKO7)	35 37 41.3	139 16 13.0	10.29	2.32
33	MINAMI ASAKAWA	(TKO8)	35 36 50.7	139 15 09.4	12.52	2.73
34	TAKI	(ITK1)	35 42 02.0	139 20 03.0	1.85	0.84
35	CHILIN UNIV	(ITK2)	35 42 26.9	139 18 28.5	4.33	1.25
36	SUMMER LAND	(ITK3)	35 42 40.8	139 17 13.0	6.25	1.55
37	INA	(ITK4)	35 43 20.8	139 14 50.5	10.04	2.22
38	KUBOKAWARA	(ITK5)	35 43 05.3	139 12 21.5	13.52	2.78
39	HONJYUKU	(ITK6)	35 43 39.5	139 08 34.9	16.18	3.20
40	AOKI DAIRA	(ITK7)	35 43 17.0	139 10 36.7	19.31	3.72

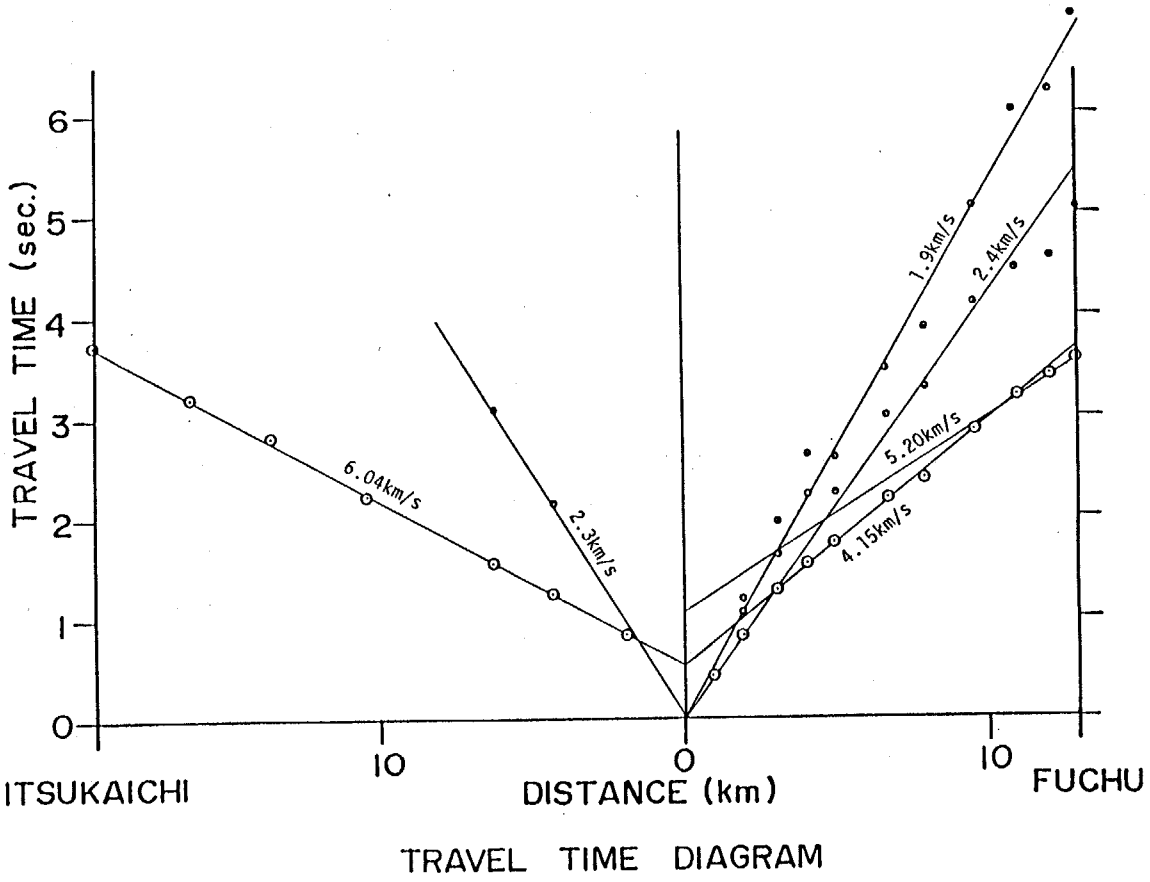

Fig. 2-34b. Travel time diagram for the Fuchu-Itsukaichi line (Line J).

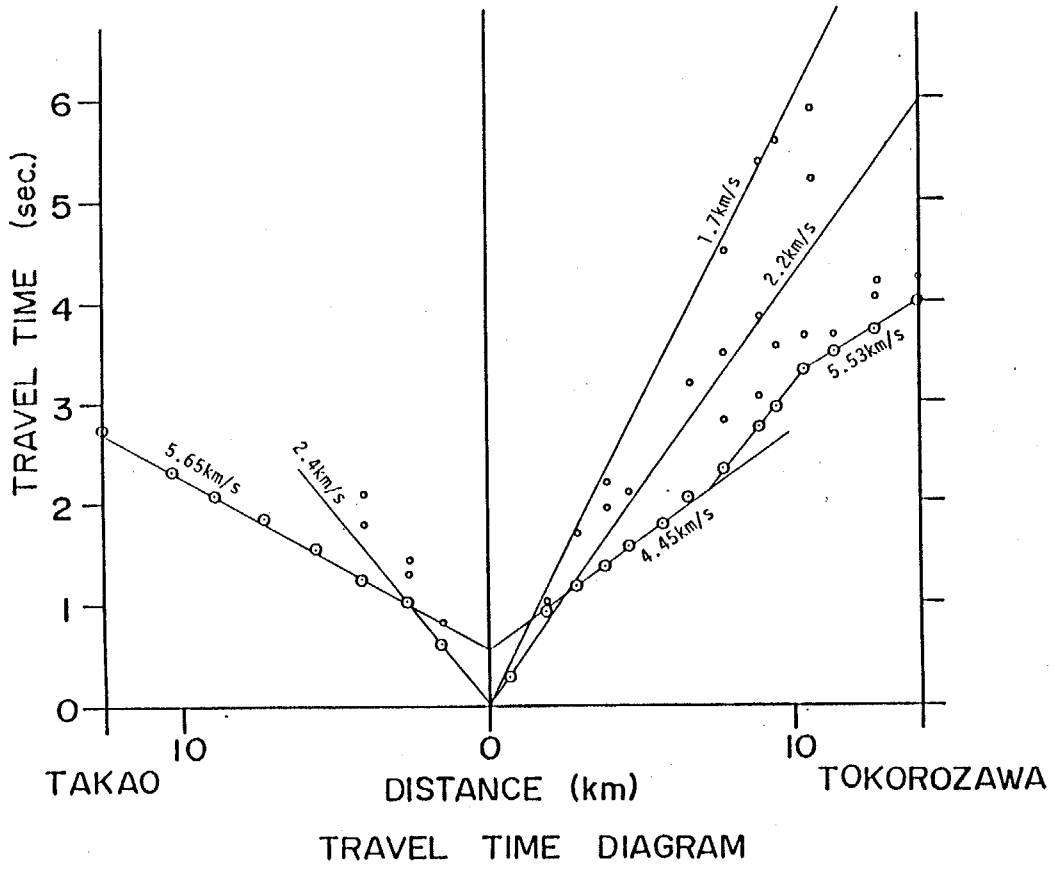

Fig. 2-34a. Travel time diagram for the Tokorozawa-Takao line (Line I).

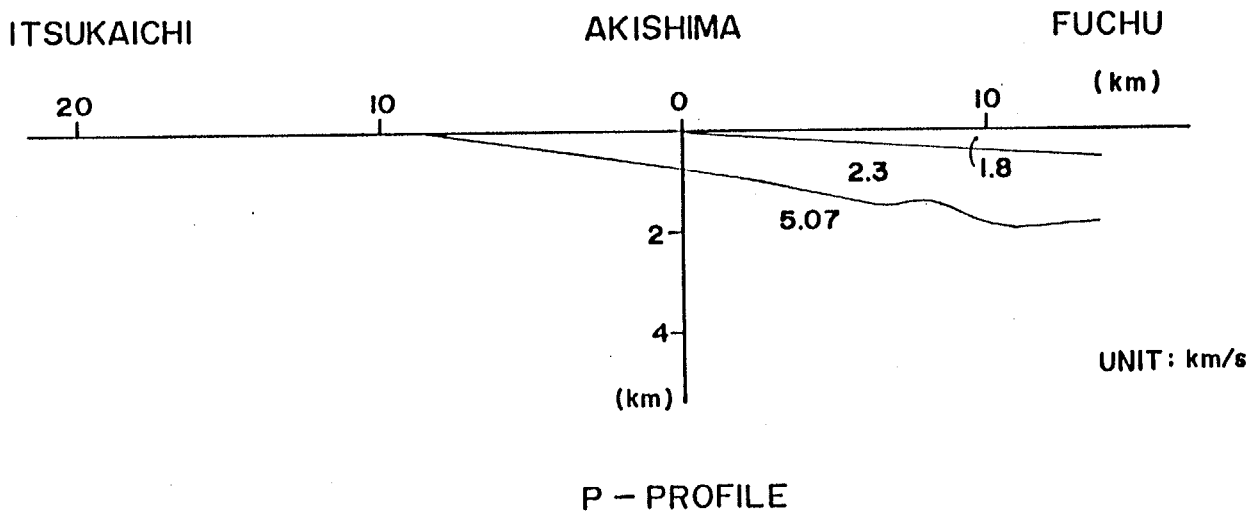

Fig. 2-35b. Underground structure for the Fuchu-Itsukaichi line (line J).

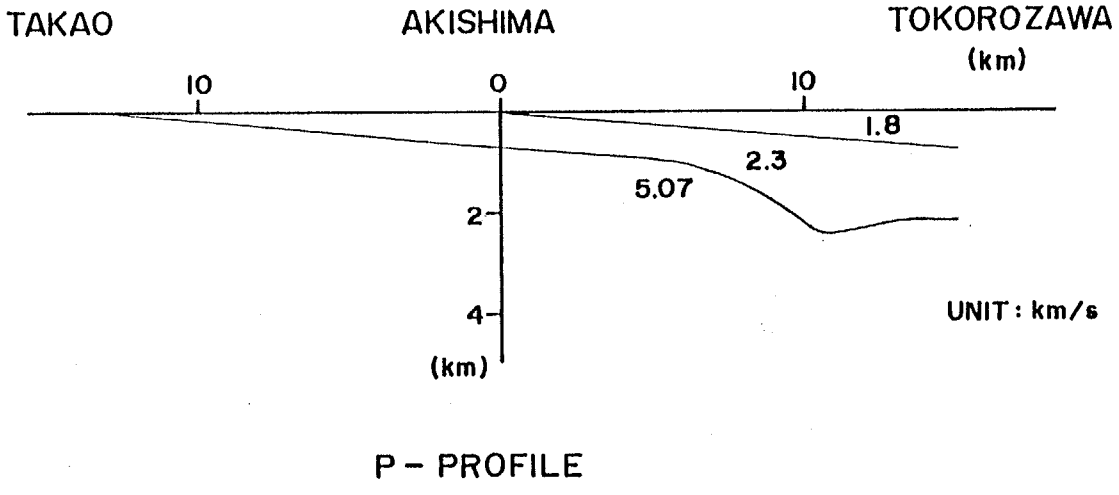

Fig. 2-35a. Underground structure for the Tokorozawa-Takao line (line I).

velocity of the bottom layer can not be determined. We assumed, here, that the average of the apparent velocities of 5.07 km/sec is the true velocity of the bottom layer. Then, the depth to the bottom layer becomes smaller towards Takao and Itsukaichi, as deduced from higher apparent velocities. The travel time delay can be seen at a distance of around 7 km from the explosion site toward Tokorozawa.

The underground structure obtained along the Tokorozawa-Takao and the Fuchu-Itsukaichi lines are depicted in Figs. 2-35a and 2-35b. The bottom layer with a velocity of 5.07 km/sec is exposed around Takao and Itsukaichi. The depth to the bottom layer is 0.7 km at the explosion site, Akishima, and 2 km at Fuchu. This suggests that the bottom layer is the same as the bottom layer having a velocity of 4.8 km/sec at the Fuchu deep borehole. The analysis of the seismogram observed at the bottom of the Fuchu deep borehole from the Akishima explosion discussed later supports this interpretation.

A fault downed to the northeast could be found at the stations with epicentral distances 7 to 10 km where the Tachikawa active fault exists. It was deduced from geological work that the Tachikawa active fault is down-faulted to the southwest and the maximum dislocation is 70 m in the Kazusa formation (The Research Group for Active Fault, 1980). The layer with a velocity of 1.8 km/sec belongs to the Kazusa formation. That is, the down-faulted side near the free surface differs from that in the bottom layers. The northeast down-faulted topography of the basement layer was also confirmed by the gravity anomalous data (Tada, 1983). He also suggested that the recent fault process differs from old one. The results which support the Tada's speculation were obtained from this seismic surveys.

2.3 Three-dimensional Features of Underground Structure

It is important for a rational prediction of earthquake ground motions to understand underground structure three-dimensionally and to make underground structural models at various sites available. In particular, variation of sedimentary layers from a source to sites

becomes one of the significant factors to determine surface wave amplification.

In order to understand the general features of the sedimentary layers in the southwestern Kanto district, the P-wave velocity profiles derived at every explosion site are compared (Fig. 2-36). The velocity profiles obtained at the Fuchu deep bore-hole are also displayed in this figure (Yamamizu et al., 1981). Several features can be pointed out as follows;

1) The bottom layer with a P-wave velocity of 5.5 km/sec can be found in the most of the area. It can be regarded as the so-called "seismic bedrock" in the area, because the seismic bedrock is required to exist beneath all the sites of consideration.

2) The layer with a P-wave velocity of 4.8 km/sec does not exist or is very thin in the northeastern half of the area, such as Kurokawa and Yumenoshima (around Tokyo), while it becomes considerably thick (4 km) in the southwestern half of the area, such as Nagatsuta and Okazu (around Yokohama).

3) The thickness of the top sedimentary layer with a P-wave velocity of 1.8 km/sec is smaller than that of the second one with a velocity of 2.8 km/sec in the southwestern part; however the tendency is opposite in the northeastern part.

In the Kanto plain, Shima (1980) and Seo et al. (1982) already reported three-dimensional features of the underground structures. They, however, used the distribution of the time-terms only from the explosions at Yumenoshima to express the 3-dimensional underground structures. The time-term method, often called as the delay-time method, is very simple and has been successfully used in interpretations of refraction data (e.g., Scheidegger and Willmore, 1957; Yoshii and Asano, 1972). It, however, is difficult to obtain configurations of sedimentary layers from time-terms at arbitrary sites. Kohler and Fuis (1986) obtained the basement depth maps using a linear relation between a time-term and a basement depth in the Imperial valley region where the velocities of sedimentary layers vary linearly with increasing depth. There are, however, some discontinuities within the sedimentary layers in the Kanto district and a simple linear relation between time-terms

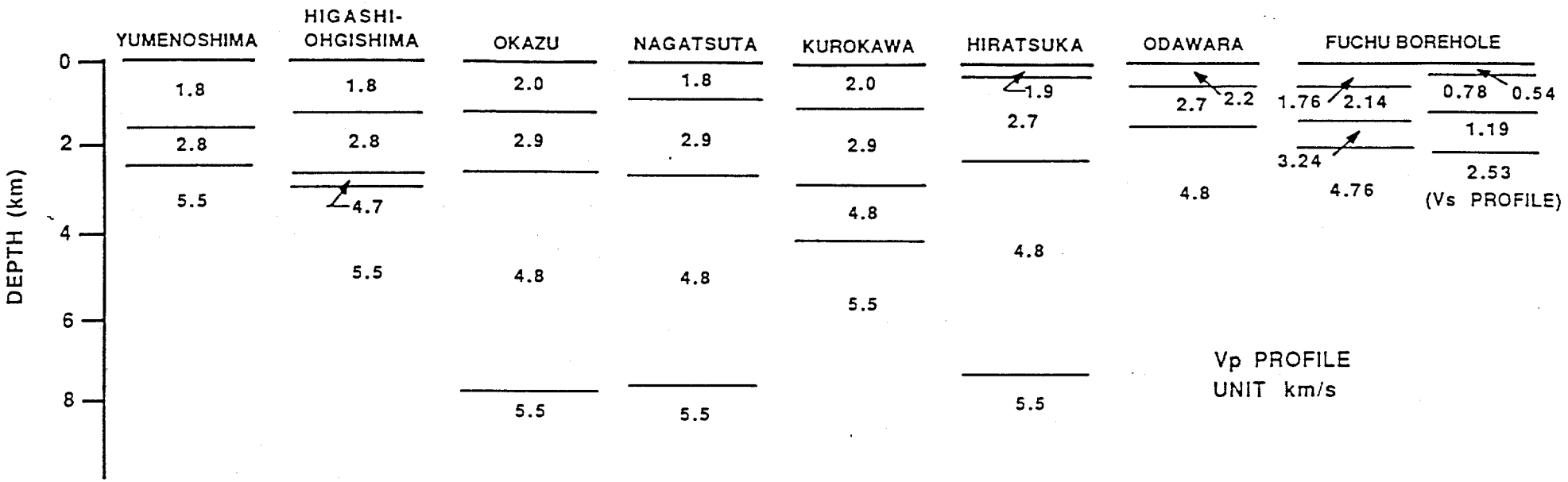

Fig. 2-36. Underground structure at explosion sites. The underground structure at the Fuchu deep borehole is also depicted (after Yamamizu et al., 1978).

and basement depth can not be expected. Here, we attempted to express underground structure three-dimensionally using the knowledge obtained before, in spite of the remaining ambiguities.

The contour map for the depth to the layer with a P-wave velocity of 4.8 km/sec is shown in Fig. 2-37. As the depth to this layer is still questionable in some places, the depths were interpolated by using the time-terms. Around Yumenoshima, this layer does not exist or is very thin. In the northern part from the Nagatsuta explosion site, the depth is 2.5-3.0 km. In the west of Nagatsuta, the depth becomes shallower. A maximum depth of more than 4 km can be seen near the Yokohama harbor. As discussed before, we have discrepancy of underground structural models near the cross point between the Yumenoshima-Ohyama and the Higashiohgishima-Kurokawa lines and it is still pending.

The 5.5 km/sec contour is depicted in Fig. 2-38. The depth does not vary as around 2.5 km between Yumenoshima and Kurokawa. It becomes drastically shallower towards the west from Kurokawa and appears at the free surface around Mt. Takao. A step-like topography can be found on this basement layer. In the western side beyond the step-like structure, the depth to the layer with a velocity of 5.5 km/s becomes more than 6 km and becomes shallower towards the west. Near the Higashiohgishima explosion site, the step-like structure approaches a gentler decline. It should be noted that the Tachikawa active fault is located on the northwestern extension of the step-like topography of the basement. A discussion in this respect will be made in the next section. Since the layer on this interface has a high velocity of 4.8 km/sec, a small error of the travel times can result in large variations of the depth. It should be noted that this contour map would be improved by future work.

From the engineering point of views, the low-velocity sedimentary layers overlying the layer with a P-wave velocity of 4.8 km/sec are important. In particular, the depth to the interface between P-wave velocities of 1.8 and 2.8 km/sec is considered to have considerable effects to ground motions as well as the depth to the layer with a P-wave velocity of 4.8

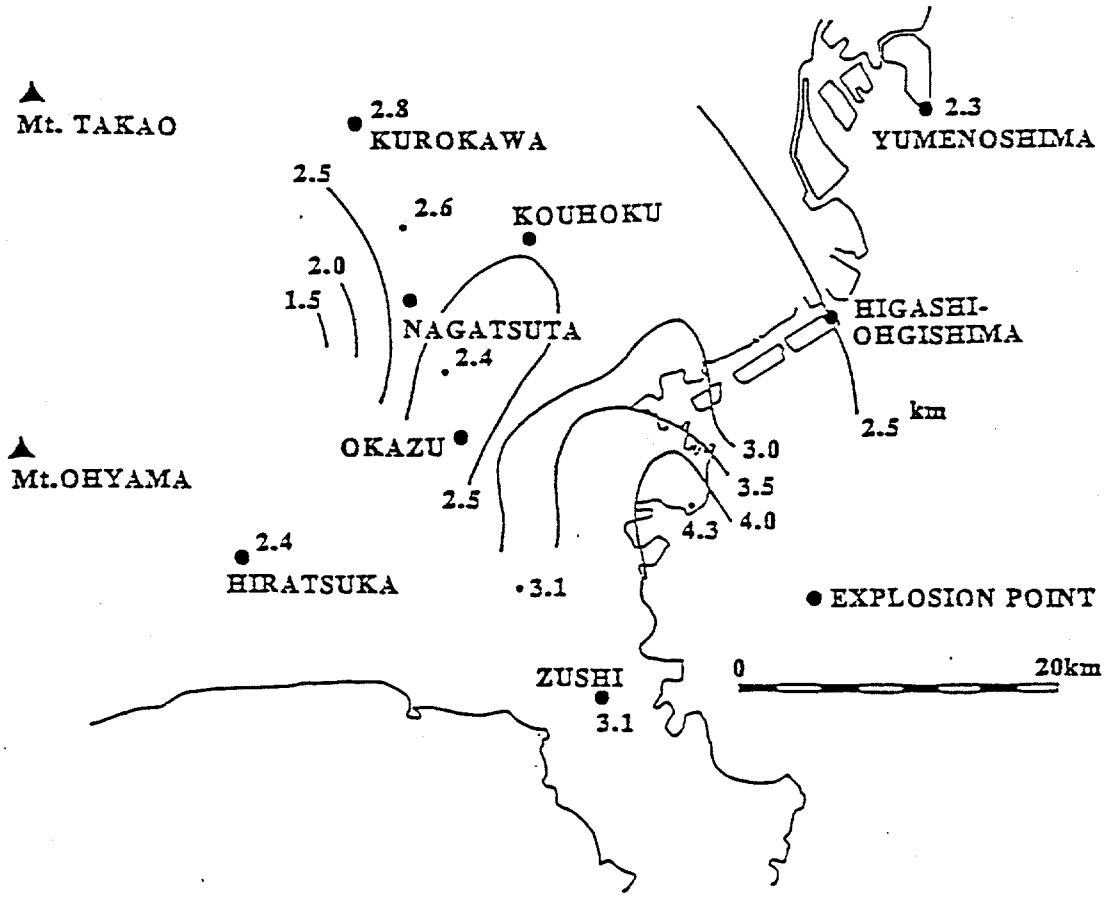

Fig. 2-37. Contours of depth of the layer with a P-wave velocity of 4.8 km/s in the south western Kanto district. Numbers in the figure indicate the depth in kilometer.

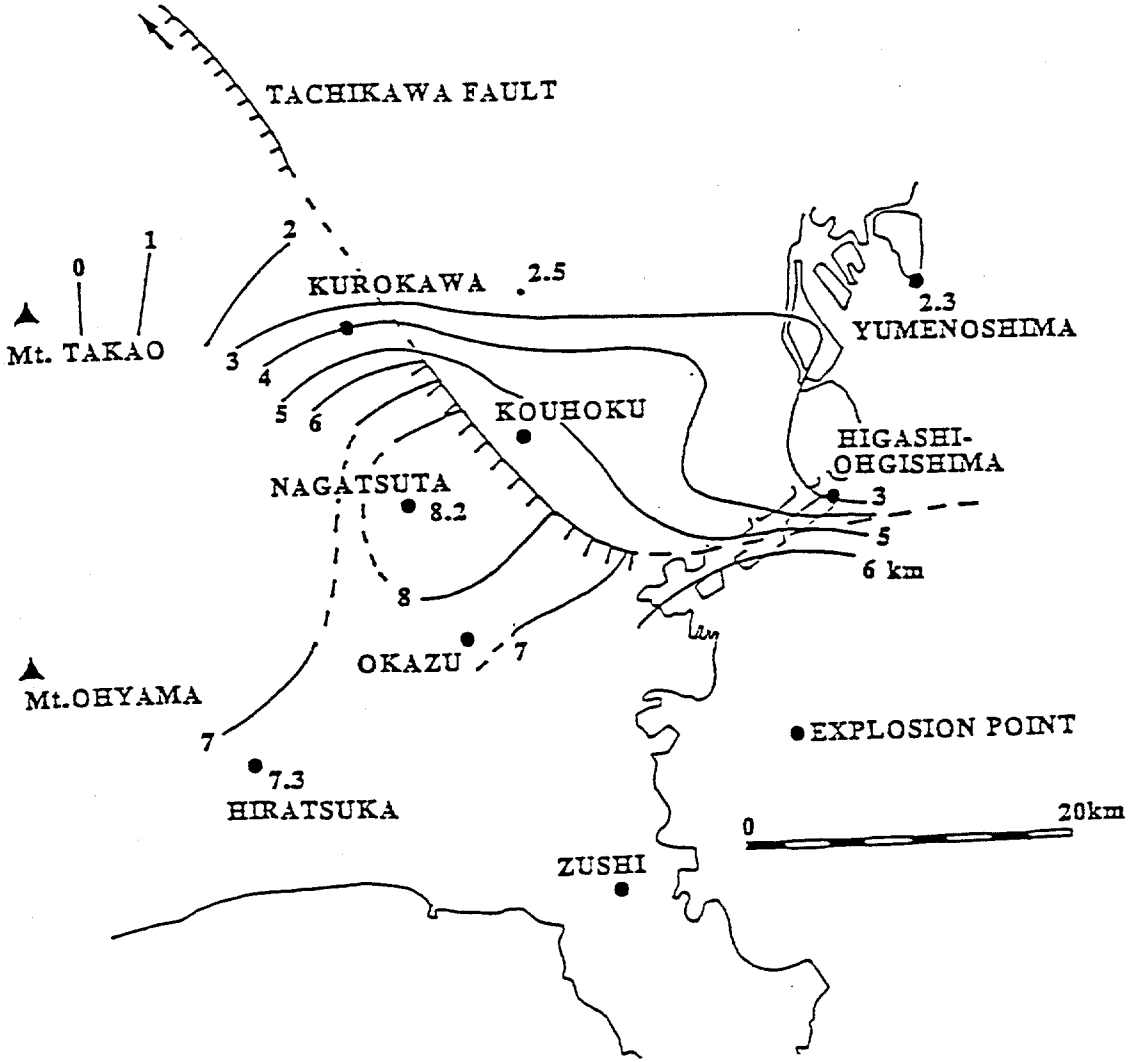

Fig. 2-38. Contours of depth of the layer with a P-wave velocity of 5.5 km/s in the south western Kanto district. Numbers in the figure indicate the depth in kilometer.

km/sec. The discussion in this respect will be done in the chapter 5. The refraction method used in this study is not suitable for the surveys of the upper interface of the sedimentary layers; a few phases propagating along the top of the layer with a velocity of 2.8 km/sec were observed as initial phases and later arrivals of these phases can not be well identified, because of disturbance of former arrivals. In spite of small amount of data, we attempted to express the distribution of the depth to this interface under some assumption,

As the interface is relative young from geological sense and is not significantly affected by metamorphism after sedimentation of the top part of the layer with a velocity of 2.8 km/sec, the thickness of the first layer would not vary so drastically. Moreover, the results of the seismic surveys in the Tokyo bay area (Kato, 1984) show that the interface has no drastic variation with depth. Accordingly, we approximate the distribution of the depth to this interface by a simple function using the available data: travel times of the initial phases propagating in the layer with a velocity of 2.8 km/sec and underground structure at the explosion sites. The following function of a plane was employed to express the depth Z in kilometers;

$$Z(x,y) = ax+by+c \qquad (2\text{-}1)$$

where x,y are distances in the EW and NS directions from an origin of 35 ° 40'N, 140 ° E in kilometers and a,b and c are constants. Fig. 2-39 shows the result of the regression analysis from data at 38 sites. The constants a,b,c were determined as -0.01325, -0.01497, 1.6051, respectively. Although the accuracy is not so good, the general up-dipping trend of the interface towards the southwest can be derived. This trend is in agreement with the results of the seismic reflection survey in the Tokyo bay area (Kato, 1984). In the area, the step-like topography of the basement can be found. Even if a step exists on this interface, its influences would be included in an error of this rough estimation. In future work, it will be required to survey this interface at many sites and to combine such knowledge with that of the deeper structure.

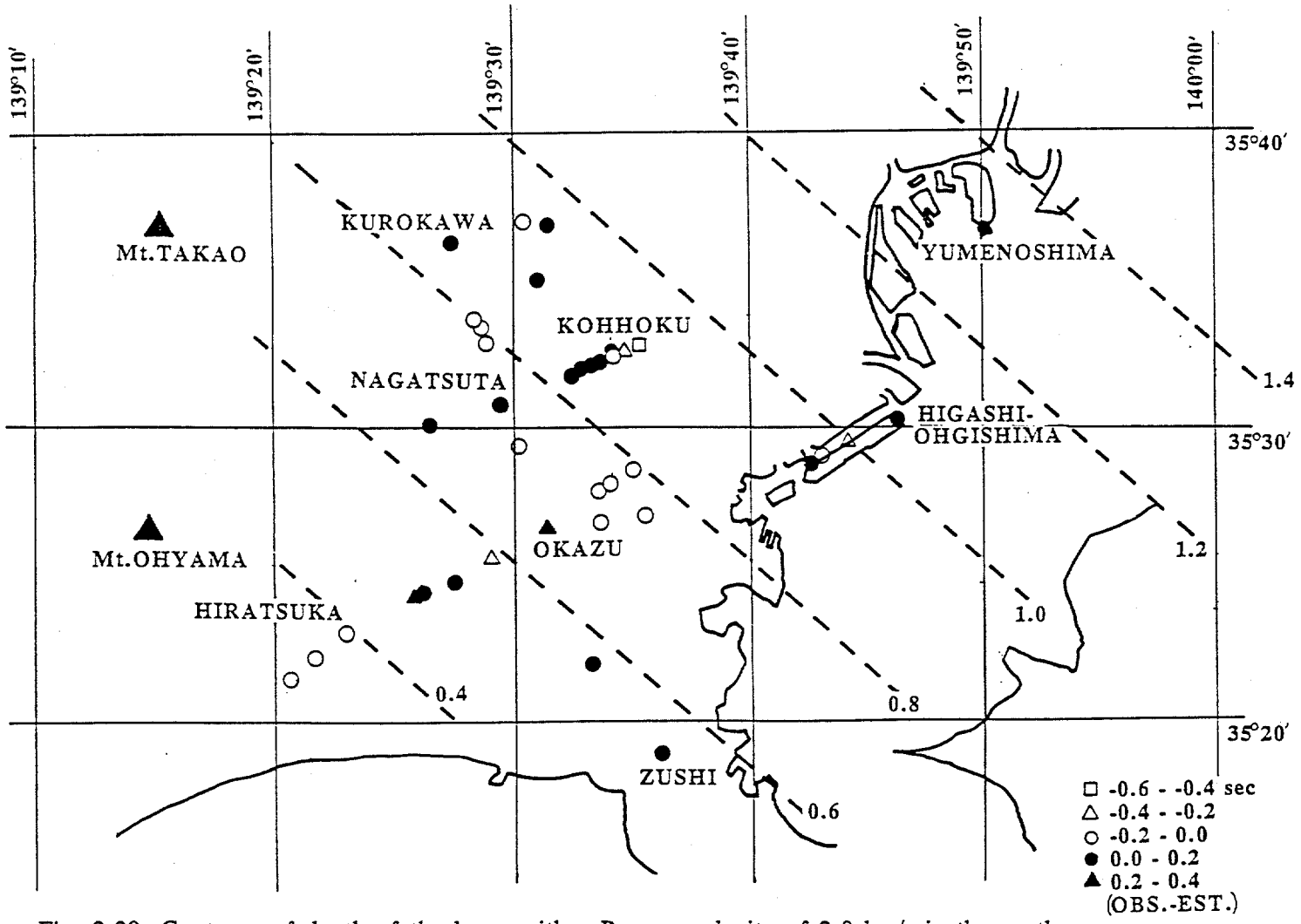

Fig. 2-39. Contours of depth of the layer with a P-wave velocity of 2.8 km/s in the south western Kanto district. Numbers in the figure indicate the depth in kilometer. The depth map was approximated by a regression of a plane using available travel time data and structures at explosion sites. The circles, triangles and squares denote regression errors at points where data are available.

2.4 Comparison with Results Obtained from Other Investigations

In this section, we will compare the underground structures obtained in this study with results from other investigations. The comparison is important and useful, because we can check the validity of the results and extrapolate them to the other area where the underground structures are still unknown.

2.4.1 Seismic surveys

According to the systematic work by Shima et al. (e.g., 1978a), it was revealed that the underground structure consists of three layers whose P-wave velocities are 1.8, 2.8, 5.6 km/sec in the center of Tokyo. Although these three layers also exist in our profile, the layer having a velocity of 4.8 km/sec can be found with significant thickness. Kasahara et al. (1976a,b) made a seismic refraction survey from Yokohama to Han'noh and proposed the underground structural model as shown in Fig. 2-40, in which the layers with P-wave velocities of 4.8 and 5.5 km/sec exist. The thickness of the layer with a velocity of 4.8 km/sec is determined about 0.5 km in the northern part from Fuchu and it becomes drastically larger in the south from the middle between Yokohama and Fuchu. This feature is evidently in agreement with our results as seen in the profile from Okazu to Kurokawa in Fig. 2-6. The explosion site at Yokohama (C) in their experiment is located approximately 10 km away from the Nagatsuta explosion site toward Yumenoshima and the thickness of the layer with a velocity of 4.8 km/sec is about 3 km; this is also consistent.

Seo et al. (1982) suggested that the existence of the layers with velocities of 4.7 and 5.3 km/sec and the 4.7km/sec-layer reaches near the free surface near Enoshima. Around the Zushi explosion site in this study, it was known that the depth to the layer with a velocity of 4.8km/sec is about 3 km. This comparison leads us to the possibility of the drastic depth variation near Enoshima. On the other hand, Yamamizu (1983) compiled explosion data, deep borehole data and gravity data, and proposed a model of subsurface structure from Enoshima to Tsukuba, which has sedimentary layers with thickness of 2 km overlying the layer with a velocity of 4.8 km/sec at Enoshima. We could not determine the

subsurface structure near Enoshima. It remains still an open problem.

Seismic reflection surveys along several surveying lines were carried out in the Tokyo Bay by Hydrographic Department, Maritime Safety Agency. The underground structure beneath one of the lines from off Futtu (Chiba) toward the northeast (A-1 in Fig. 2-1) was interpreted as shown in Fig. 2-41 (Kato, 1984). The underground structure consists of 6 layers named as TA to TF in the figure. As compared with our results, agreement can be pointed out as follows;

1) The depth to the top of the TD layer becomes larger towards the northeast and it is determined as 1.3 km off Yumenoshima and 0.5 km off Yokohama, approximately. The interval P-wave velocities for the layers overlying the TD layer are estimated as 1.5-2.2 km/sec by a velocity analysis. Therefore, they correspond well to the first layer in our results.

2) The interval P-wave velocity for the TD layer is obtained as 2.1-3.3 km/sec and its thickness distributes from 1.0 to 1.6 km. This layer is considered to correspond to the second one in our results.

3) The TE layer begins to appear at the area off Haneda (a in Fig. 2-41). The thickness becomes larger towards the south off Yokohama (b in Fig. 2-41). This distribution pattern is similar to that of the 4.8 km/sec layer in this study. The interval velocity for the TE layer, however, is estimated as 3.1-4.1 km/sec and the thickness is also smaller (1.3 km) around off Yokohama than that obtained in this study. Since the interval velocity of the TE layer is determined smaller than that of our study, such difference of thickness can arise in converting from the time section to the depth section. In general, the velocity of a layer can be determined better by the refraction method than by the reflection method. If a higher interval velocity is estimated, the thickness of the TE layer would be larger.

4) The depth to the TF layer is 2.3 km at off Yumenoshima. This layer corresponds to the layer with a P-wave velocity of 5.5 km/sec in our study. The interval velocity of the

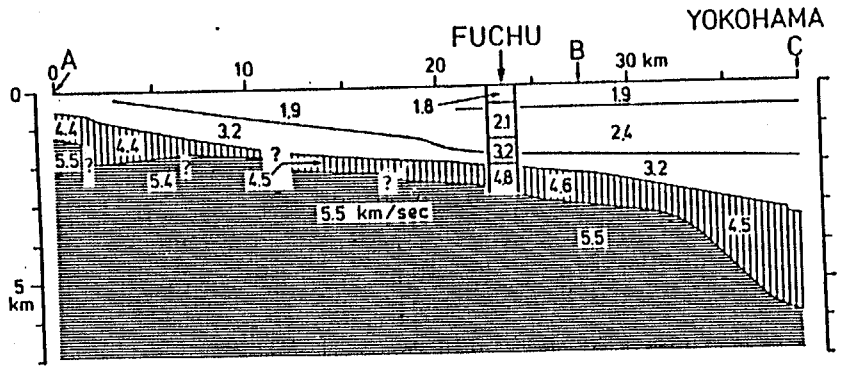

Fig. 2-40. Underground structure along a line between Han'noh and Yokohama (after Kasahara et al., 1976a,b).

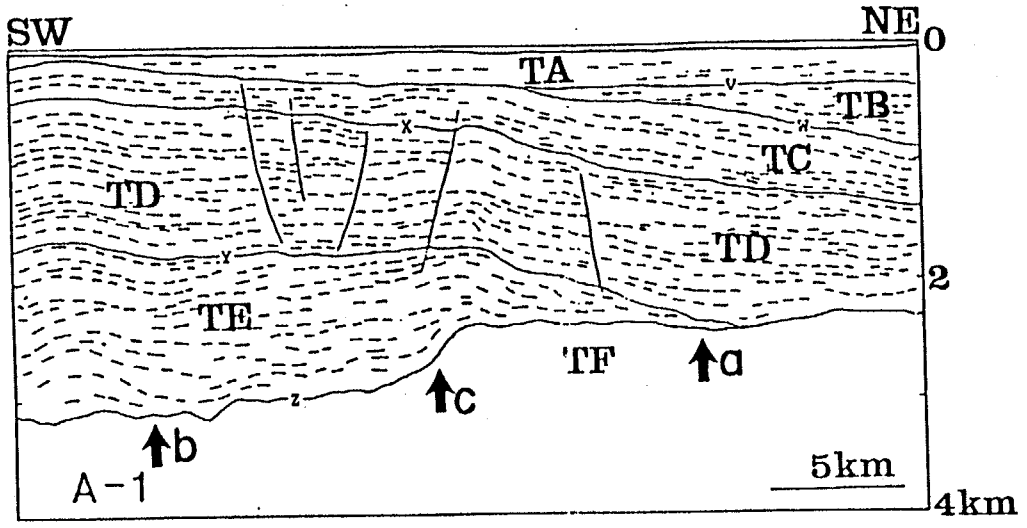

Fig. 2-41. Depth section of one of the seismic reflection profiles (A-1 in Fig. 2-1) carried out in Tokyo Bay after Kato(1984).

TF layer is not determined, because there are no reflectors beneath this layer.

5) At off Ohgishima (c in Fig. 2-41), the depth to the TF layer becomes drastically larger toward the south. This structural feature corresponds well with the step-like structure topography of the layer with a velocity of 5.5 km/sec found in this study. The step-like topography can not be seen in the upper layer overlying the TF layer.

These comparisons show that the underground structure derived in this study is proper, although the slight differences which can be seen between the TF layer and the layer with a velocity of 5.5 km/sec. Such a difference, however, is not particularly important in terms of geophysical prospecting; each survey method has its advantages and disadvantages and the resultant subsurface profiles at a site, more or less, depend on the method applied. It should be noted that it becomes important in future work to combine these available data and to construct a rational underground structural model so as to make the discrepancy as small as possible.

Seo et al. (1982) and Tada (1982) suggested the step-like topography of the basement in the extension of the Tachikawa active fault. In this study, it could be confirmed except for the profile from Yumenoshima to Takao. Moreover, it is considered that this feature continues toward the Tokyo bay area, according to the results of the reflection surveys discussed above. As discussed by Tada (1983), the step-like topography might be related with the nature of the Tachikawa active fault. Hence, the existence of such a structure can not be negligible in considering seismic hazard reduction in the Tokyo Metropolitan area. More investigations from various fields will be required to know if the step-like structure is active fault or not.

2.4.2 Borehole data

In the area, a deep borehole down to the layer with a P-wave velocity of 4.8 km/s is made to observe the activity of the crust by the Research Center for Disaster Prevention. The P- and S-waves velocity profiles have been clarified by the down hole measurements;

the bottom layer of the borehole with a P-wave velocity of 4.8 km/s is located at a depth of about 2 km (Yamamizu et al., 1981). In our results, the layer can be found 2.8 km in depth at the Kurokawa explosion site. The both profiles are displayed in Fig. 2-36. The configuration of the sedimentary layers are similar. As the Kurokawa explosion site is located 5 km apart to the south from the borehole, the difference of the depth to the layer with a velocity of 4.8 km/sec is not so odd.

The other deep borehole data were obtained at Kawasaki, Hodogaya and Isogo. Although no velocity measurements were carried out at these boreholes, the depth to the discontinuity between formations of the Kazusa and the Miura groups were estimated; this corresponds to the interface between the first and the second layers in our results. The depths to the interface are 0.7 km at Kawasaki (Fukuda et al., 1976), 1.0 km at Hodogaya and 1.1 km at Isogo (Kikuchi, 1962), respectively. Considering the accuracy of the distribution of the depth to this interface proposed in the previous section, it seems to be harmonic with these borehole data.

2.4.3 Gravity anomaly

Gravity anomaly is often used to understand 3-dimensional features of underground structures in geophysics and geophysical prospecting. Gravity data in the southern Kanto district are compiled by the Hydrographic Department, Maritime Safety Agency (1987). Fig. 2-42. shows the distribution of free-air gravity anomaly. Free air anomaly indicates deviation of measured gravity from a standard gravity (Tsuboi, 1979). Therefore, it becomes negative, if materials of the earth are low density. Most of the Kanto plain belong to the area with negative anomaly. Tada (1976) concluded that this negative anomaly is mainly caused by the sedimentary layers. The greatest negative value of the gravity anomaly can be seen in the northern part of Yokohama. The depth to the layer with a velocity of 4.8 km/sec in Fig. 2-37 becomes larger toward the Yokohama harbor. This implies that the negative free air anomaly in the area can not be explained only by the sedimentary layers. On the other hand, the depth map to the layer with a velocity of 5.5 km/sec in Fig.

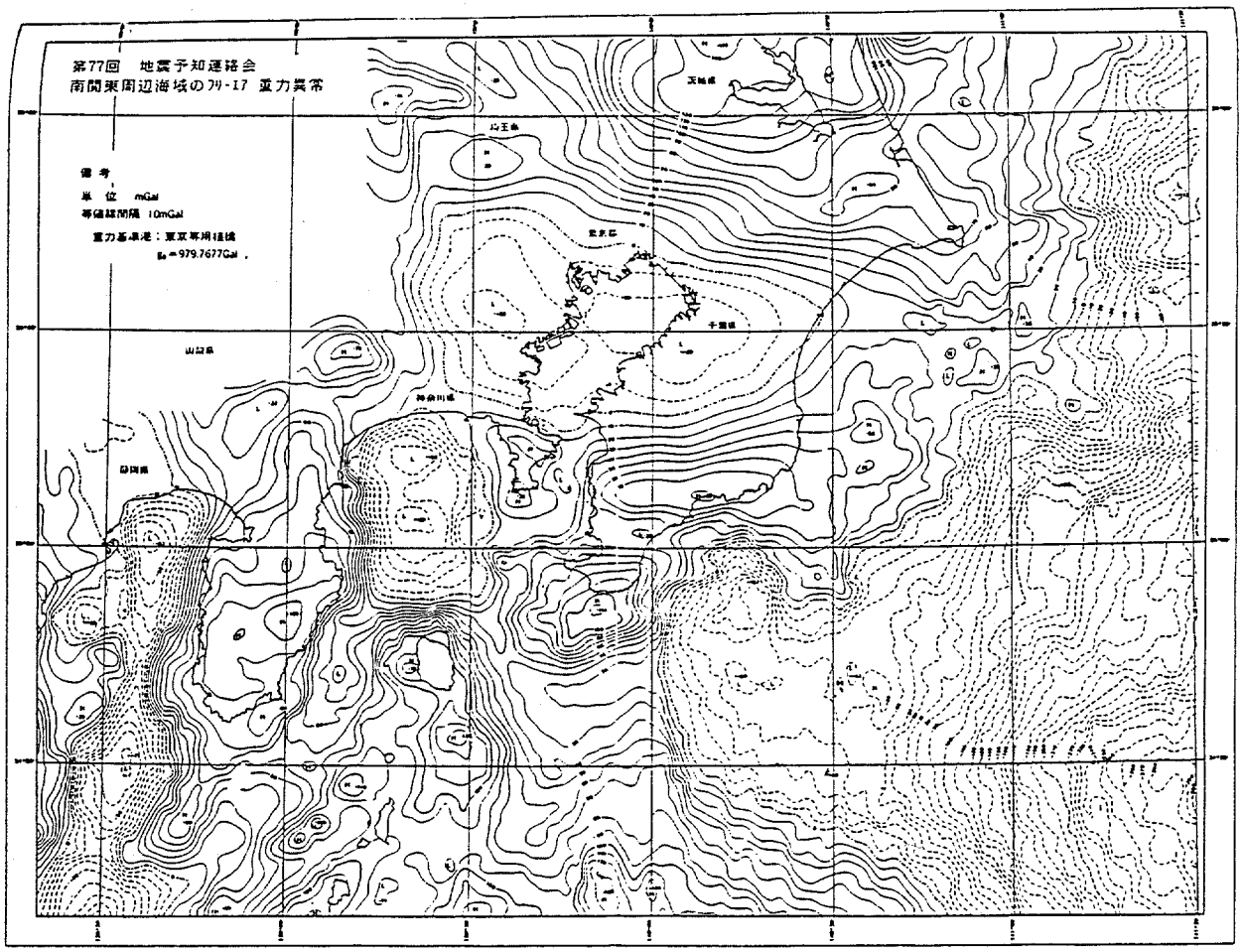

Fig. 2-42. Free gravity anomalies in the vicinity of the southern Kanto district (Hydrographic department, Maritime Safety Agency, 1987).

2-38 shows a similar tendency to the negative free air anomaly.

2.4.4 Geological data

As compared with geological classification, the top two layers belong to the Pleistocene (Kazusa group) and the Miocene (Miura group), respectively.

Yajama (1981) proposed a geological structure of the pre-Tertiary basement under the Kanto plain from a petrological investigation. According to his results, the pre-Tertiary basement of the Kanto plain is deduced as shown in Fig. 2-43. The basement rocks are classified as Sambagawa metamorphic belt, Chichibu Paleozoic belt, Shimanto northern belt, Shimanto southern belt from north to south. The geological age becomes younger from north to south. In our results, the layer with a velocity of 4.8 km/sec becomes thin around Kurokawa and Yumenoshima. As compared with Fig. 2-43, the layer could be interpreted as the Shimanto northern belt and the lower layer with a velocity of 5.5 km/sec could belong to the Chichibu Paleozoic belt or the Sambagawa metamorphic belt. This hypothesis suggests a possibility to exist a basement layer with a less velocity than 4.8 km/sec near Enoshima, which corresponds to the Shimanto southern belt.

On the other hand, Mikami (personal communication) suggested another geological interpretation of the layer with a velocity of 4.8 km/sec. Accordingly, this layer would be green tuff, because the thickness of the layer is significantly large and green tuff has also large thickness in the Tanzawa Mountains in the west side of the area considered.

Although it is clear that the third and bottom layers belong to Pre-Neogene, more detailed classification is difficult only from the results of this surveys. In the future, more discussions will be needed to compare with geology in details.

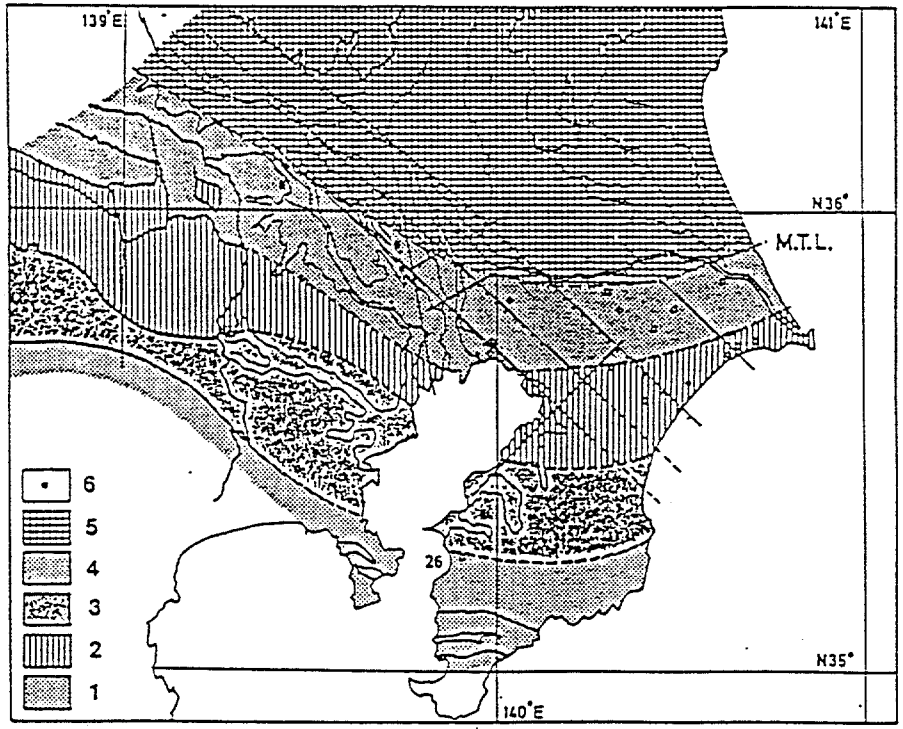

Fig. 2-43. Geological map of the basement in the Kanto plain (Yajima, 1981).
1: Sanbagawa metamorphic belt.
2: Chichibu Paleozoic belt.
3: Shimanto northern belt.
4: Shimanto southern belt.
5: Inner zone.
6: Yoshimi metamorphic belt.

CHAPTER 3. TWO-DIMENSIONAL MULTIPLE REFLECTION OF SEISMIC WAVES WITHIN SEDIMENTARY LAYERS

In this chapter, we interpret the later phases in seismograms obtained from explosions and earthquakes in the southwestern Kanto plain considering the propagation mechanism of body waves and two-dimensional multiple reflection. Next, the characteristics of two-dimensional multiple reflection are discussed by a simple modeling.

3.1 Multiple-reflected Phases in Explosion Seismograms at the Fuchu Deep Borehole

3.1.1 Later phases in seismograms observed from an explosion at Yumenoshima

There is a deep borehole in the southwestern part of the Kanto plain as shown in Fig. 3-1: the Fuchu borehole crustal activity observatory (Fuchu deep borehole, in the following). The corresponding velocity profiles can be seen in Fig. 2-36 (Yamamizu et al., 1981). The borehole reaches a firm rock with an S-wave velocity of 2.5 km/sec at a depth of 2750 m. The earthquake recordings have been carried out at the bottom of the borehole by the National Research Center for Disaster Prevention.

Most of seismic waves from the explosions in the seismic surveys discussed in the previous chapter were observed at the bottom of the borehole. When they are compared with earthquake ground motions, explosion seismograms give a key to the understanding of propagation mechanisms of seismic waves, because of impulsive wave forms and the well-defined source parameters, such as origin time and location.

The observation of the explosion at Yumenoshima was also done at the free surface of the borehole. Fig. 3-2 shows the velocity seismograms obtained at the bottom and the free surface of the borehole from the Yumenoshima explosion. The lower and upper traces indicate the radial component at the bottom and the vertical one at the free surface, respectively. An explosion effectively generates a dilatational phase. Moreover, the propagation direc-

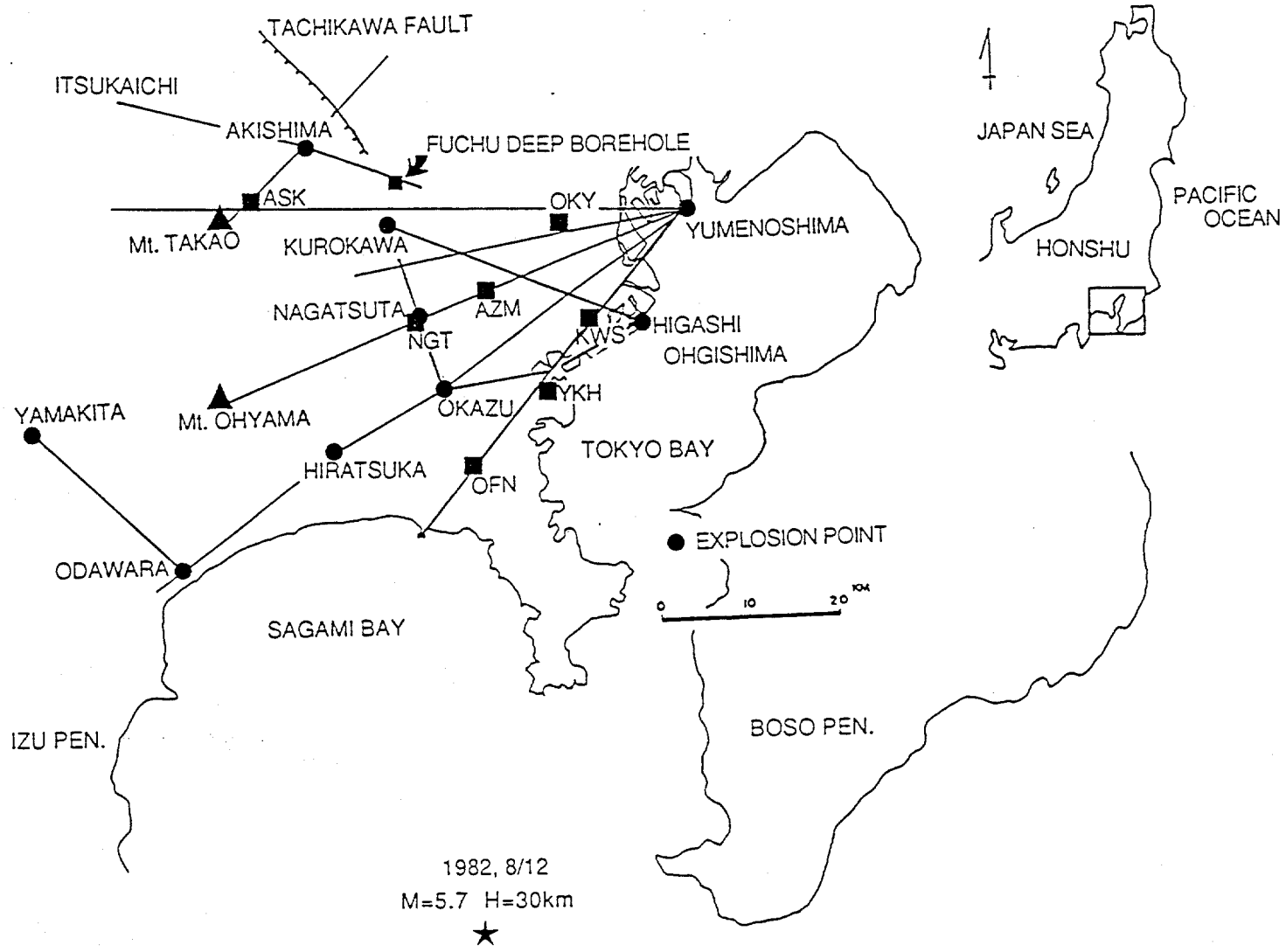

Fig. 3-1. Location of the Fuchu deep borehole, explosion sites, surveying lines and earthquake observation points in the southwestern Kanto district, Japan.

tion from the refractor into the bottom layer of the borehole is slightly oblique and it becomes almost vertical near the free surface, because of low-velocity layers. Therefore, these two components are used for the comparison in Fig. 3-2. The particle motions in the plane of the vertical and horizontal components at the bottom of the borehole are also depicted in Fig. 3-2. The particle motion of the initial P-wave arrival at the bottom is polarized in an oblique direction. This means that the initial phase is the refracted phase which propagates in the layer with a P-wave velocity of about 5.5 km/s beneath the bottom layer of the borehole, where the seismometers are installed, and comes upward around the borehole. The arrival time difference of the initial phases observed at the free surface and the bottom, 0.9 sec, is in good agreement with the calculated one, 0.85 sec. As for the distinct later phases in the bottom trace, the first part of the particle motion (A) shows a downward oblique direction. The second part (B), however, indicates an upward direction. All distinct later phases in the surface trace arrive between those in the surface trace. Consequently, the distinct later phases should be interpreted as multiple-reflected phases between the free surface and the top of the refractor with a P-wave velocity of 5.5 km/sec; almost in the sedimentary layers.

The schematic diagram of the propagation mechanism is illustrated in Fig. 3-3. The multiple reflections in the figure occur in the receiver region and they might also occur in the source region; the wave from the explosion reflected multiply near the source, then travels in the refractor and comes up to the receiver. In this case, the multiple-reflected phases have the same propagation direction as that of the initial phase. However, the observed particle motions of the later phases are different from that of the initial phase. Therefore, it is reasonable to assume that the observed distinct later phases are generated by multiple reflections near the receiver region.

As seen in the velocity profile for the borehole, some interfaces above the layer with a P-wave velocity of 4.8km/s have also high impedance ratios. Assuming the flat layering of the underground structure at the borehole, the reflection coefficients of a P-wave due to a

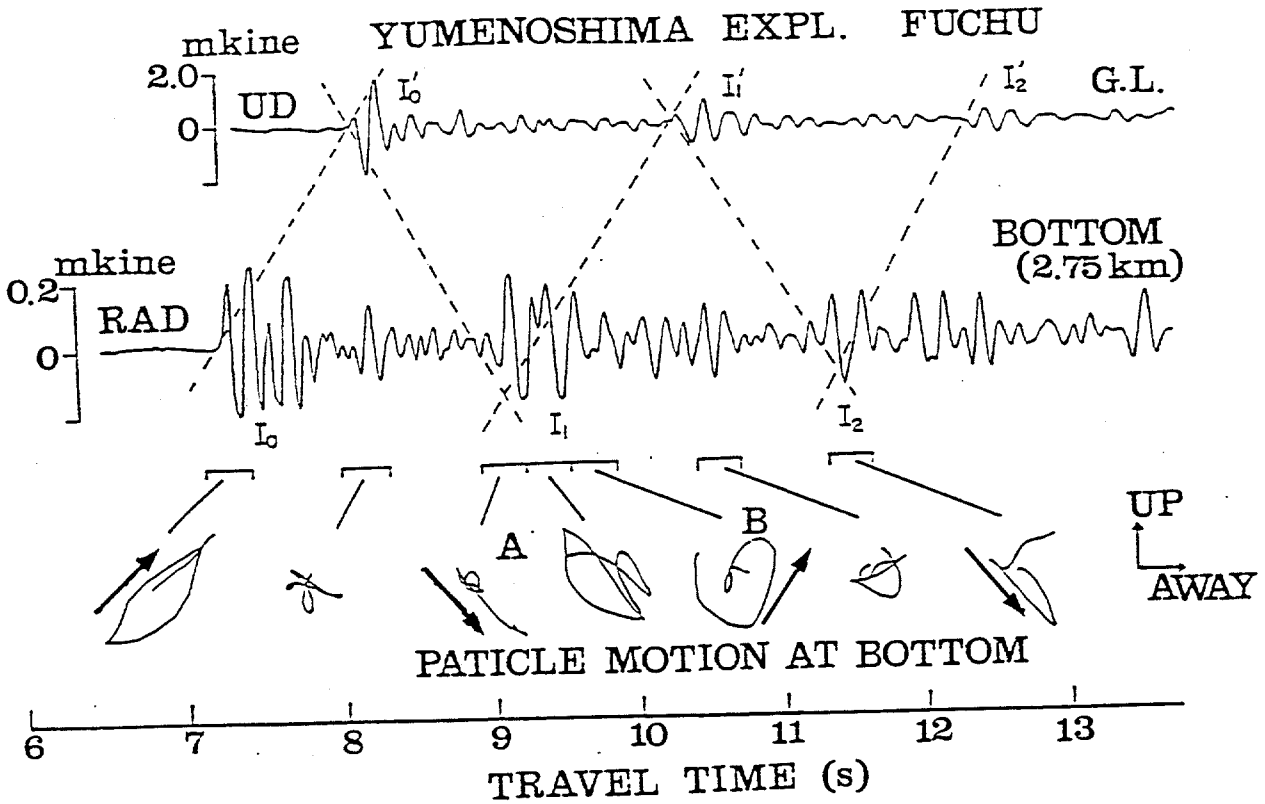

Fig. 3-2. Seismograms observed during the Yumenoshima explosion at the free surface (upper trace) and the bottom (lower trace) of the Fuchu deep borehole. Particle motions in the radial-vertical plane at the bottom are also depicted.

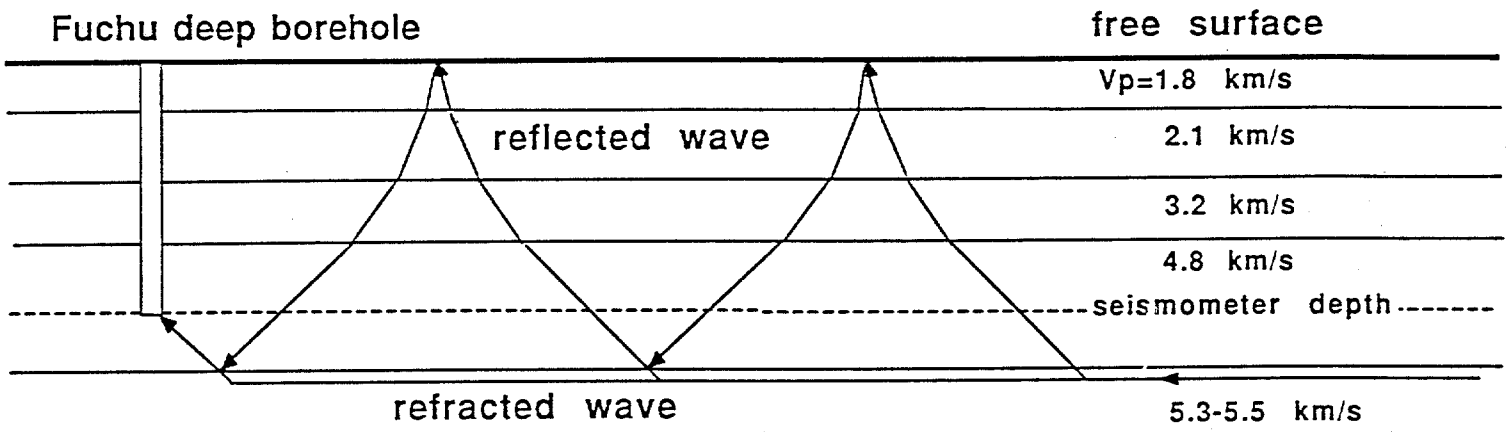

Fig. 3-3. Schematic diagram illustrating the propagation of the multiple reflected and the refracted waves.

plane P-wave incidence were compared. The assumption of the flat layering is plausible near the Fuchu deep borehole as shown in the profile from Yumenoshima to Takao, which is 5 km south of the borehole. Fig. 3-4 shows the reflection and the transmission coefficients at the various interfaces as well as the corresponding ray paths. The incident angle is measured from the vertical. The reflection coefficients in the figure are calculated for each interface as indicated by L1 to L4. The incident angles of the down-going wave at each interface after the reflection at the free surface are indicated by the arrows in the figure. The reflection coefficient at the bottom interface (L4) is unity, because of the critical angle. Since the incident angles to the other upper interfaces become under-critical ones, the reflection coefficients at these interfaces are very small. On the other hand, all the transmission coefficients at the upper interfaces are almost unity and the amplitude of down-going wave does not become small.

Since the location of the explosive source is almost on the free surface, the propagation path of the initial phase discussed here can not be expected for seismic waves from earthquakes. This case, however, gives us an extreme example for shallow earthquakes. This kind of propagation mechanism can be one of the possible explanation for distinct later phases in earthquake records as it is discussed later.

Kinoshita (1986) investigated the similar propagation mechanism using earthquake records at the borehole. Since we used seismic sources with an impulsive waveform and well-defined source parameters, the propagation mechanism for body wave, multiple reflection, could be understood clearer.

3.1.2 Seismograms observed from the other explosions

The seismic waves from the other explosions were also observed at the bottom of the borehole. At first, the incident direction of the initial phases were compared. The particle motions of the initial phases derived at the bottom in the vertical-radial plane are depicted in Fig. 3-5. These particle motions can be classified into two types according to the polarized

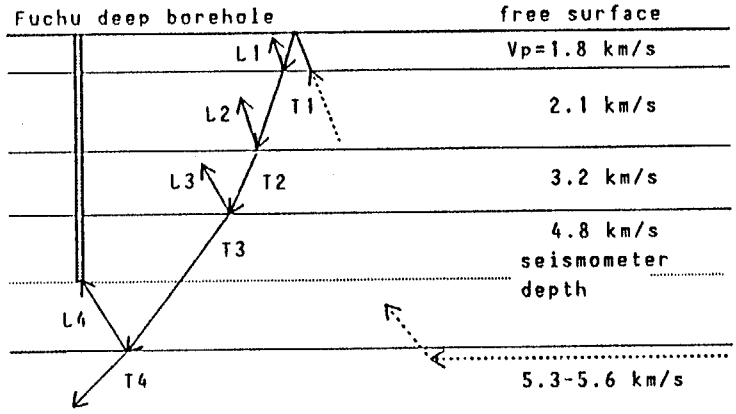

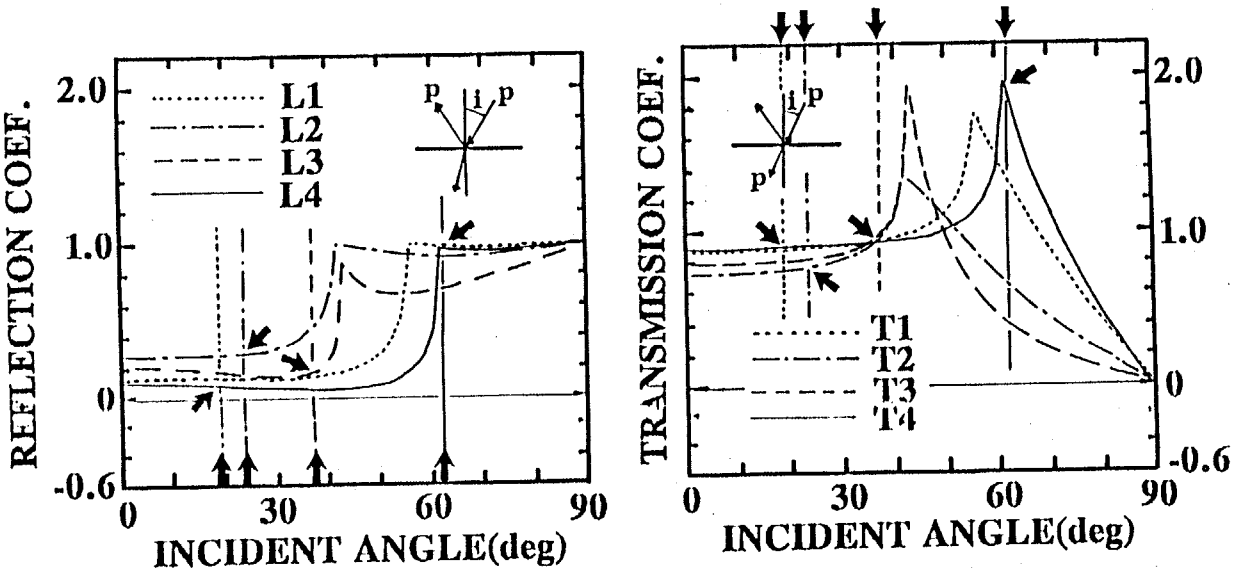

Fig. 3-4. Reflection and transmission coefficients of P-wave due to plane P-wave incidence at interfaces of the Fuchu deep borehole (upper figure). For example, solid line (L4) is reflection coefficient of P-wave at the interface beneath the bottom of the borehole. Incident angle is measured from the vertical.

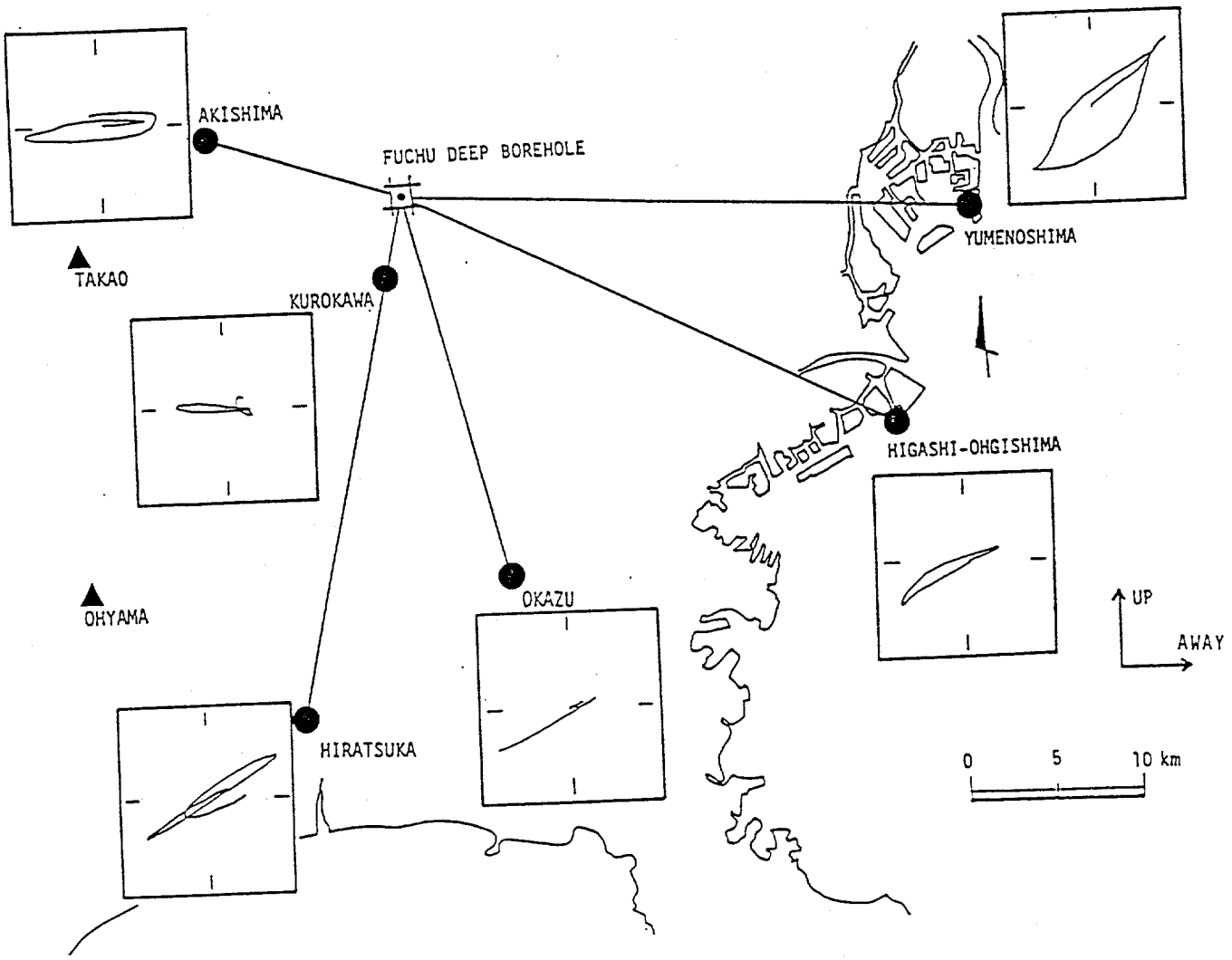

Fig.3-5. Particle motions of the initial P-phases due to explosions obtained at bottom of the Fuchu deep borehole.

directions. The particle motions from the Akishima and the Kurokawa explosions are horizontally polarized. These explosion sites are located near the borehole. On the other hand, the particle motions from the other explosions are polarized in an oblique direction. The initial phases from the explosions far away from the borehole belong to this type. This means that the polarization differences are caused by the differences of the layers through which the initial phases travel; the initial phases from the explosions near the borehole travel through the layer in which the seismometer is installed, while those from the explosions far from the borehole propagate through the lower layer.

The radial components of the explosion seismograms observed at the bottom of the borehole are shown in Fig. 3-6. Fig. 3-7 shows the products of the radial and the vertical components (Sutton and Pomeroy, 1963). Suppose that the up and the away directions are positive, then a motion product is positive for up-going P-wave , negative for down-going P-wave and so on. All the motion products of the initial phases are positive. The later phases in the traces from the explosions are not distinct with an exception of that of the Yumenoshima explosion, though small later arrivals can be seen in the seismogram for the Higashiohgishima explosion which is located off southeast of the borehole. This fact indicates that the refractor has a upward dip from the south towards the Fuchu deep borehole, because the incident angle to the top of the refractor becomes under-critical and the reflection coefficient becomes small. According to the results of the seismic surveys in chapter two, the topography of the layer with a P-wave velocity of 5.5 km/s up-inclines steeply from Nagatsuta to Kurokawa. This topographical feature is consistence with the observational facts.

3.1.3 Travel time analysis of the initial phases

Here, we made the travel time analysis of the initial phases. The observed travel times of the initial phases are shown in Table 3-1. Since we know the differences of the layers through which the initial phases propagate from the comparison of the polarization direction

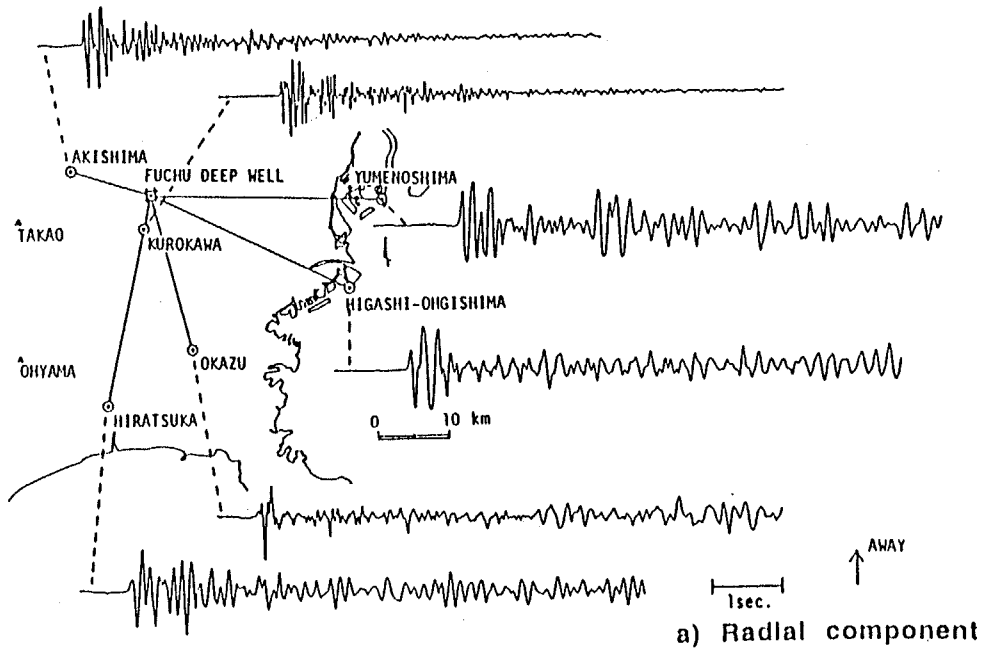

Fig. 3-6. Radial component of observed explosion seismograms at the bottom of the Fuchu deep borehole.

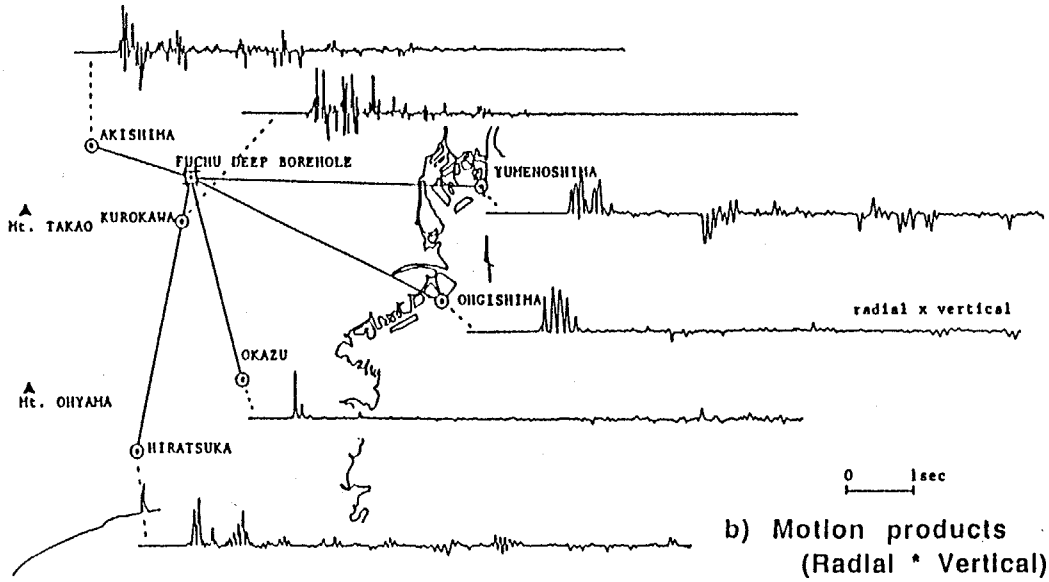

Fig. 3-7. Motion products of radial and vertical components at the bottom of the Fuchu deep borehole.

Table 3-1. Travel times of initial phases obtained at the bottom of the Fuchu deep borehole from explosions

No	EXPLOSION	D_{FCH} (km)	T_{FCH} (s)	$tt_{S4.8}$ (s)	$T_{C4.8}$ (s)
1	YUMENOSHIMA	33.29	7.20	1.03*	7.97
2	HIGASHIOHGISHIMA	31.88	7.02	0.99	7.63
3	KUROKAWA	5.19	1.89	0.96	2.04
4	OKAZU	23.45	5.57	0.80	5.69
5	HIRATSUKA	31.15	6.70	0.76	7.25
6	AKISHIMA	11.94	2.64	0.26	2.62**

*Time-term at Yumenoshima is assumed as 1.03 sec.
**P-wave velocity is 5.07 km/s at AKISHIMA

D_{FCH} :Distance from the explosion sites to the Fuchu deep borehole
T_{FCH} :Travel time of initial phases at the bottom of the borehole
$tt_{S4.8}$:Time-term for the explosion site down to 4.8km/sec layer
$T_{C4.8}$:Calculated travel time of phase propagating through 4.8km/sec layer

of the initial phases, the travel time analysis was carried out using the travel times of the initial phases propagating through the layer with a P-wave velocity of 5.5 km/s. Travel time of initial phase at the bottom of the borehole, T_{FCH} , is

$$T_{FCH} = t_{S5.5} + \frac{D_{FCH}}{Vp} + t_{FCH} \tag{3-1}$$

where $t_{S5.5}$ is a time-term at a explosion site, D_{FCH} is distance between the explosion site and the Fuchu deep borehole, Vp is refractor velocity and t_{FCH} is a time-term from the bottom of the borehole to the top of the refractor. The seismic wave from the Yumenoshima explosion was also observed at each explosion site and its travel time, T_{YMS} , is expressed as

$$T_{YNS} = t_{S5.5} + \frac{D_{YMS}}{Vp} + 1.03 \tag{3-2}$$

where D_{YMS} is distance between each explosion site and the Yumenoshima explosion site. 1.03 sec corresponds to the time-term at the Yumenoshima explosion site. Using (3-1) and (3-2), we obtain

$$(T_{FCH} - T_{YMS}) + 1.03 = \frac{D_{FCH} - D_{YMS}}{Vp} + t_{S5.5} \tag{3-3}$$

From this relation, we can obtain Vp and $t_{S5.5}$. As shown in Fig. 3-8, the refractor velocity of 5.31 km/s and t_{FCH} of -0.05 sec were obtained by a regression analysis. This velocity is a little smaller than that obtained from the seismic surveys and t_{FCH} is negative. Even though the density of the used data is poor and the accuracy is not do high, it can be qualitatively said from this analysis that the layer with a P-wave velocity of 5.5 km/s exists just below the bottom of the borehole.

The observed travel time of the initial phase for the Akishima explosion agrees well with the calculated one, when the refractor velocity is 5.07 km/sec. However, that for the Kurokawa explosion is not coincident with the calculated one. As the explosion site is quite near from the borehole, the initial phase at the bottom, probably, is a direct wave from the source.

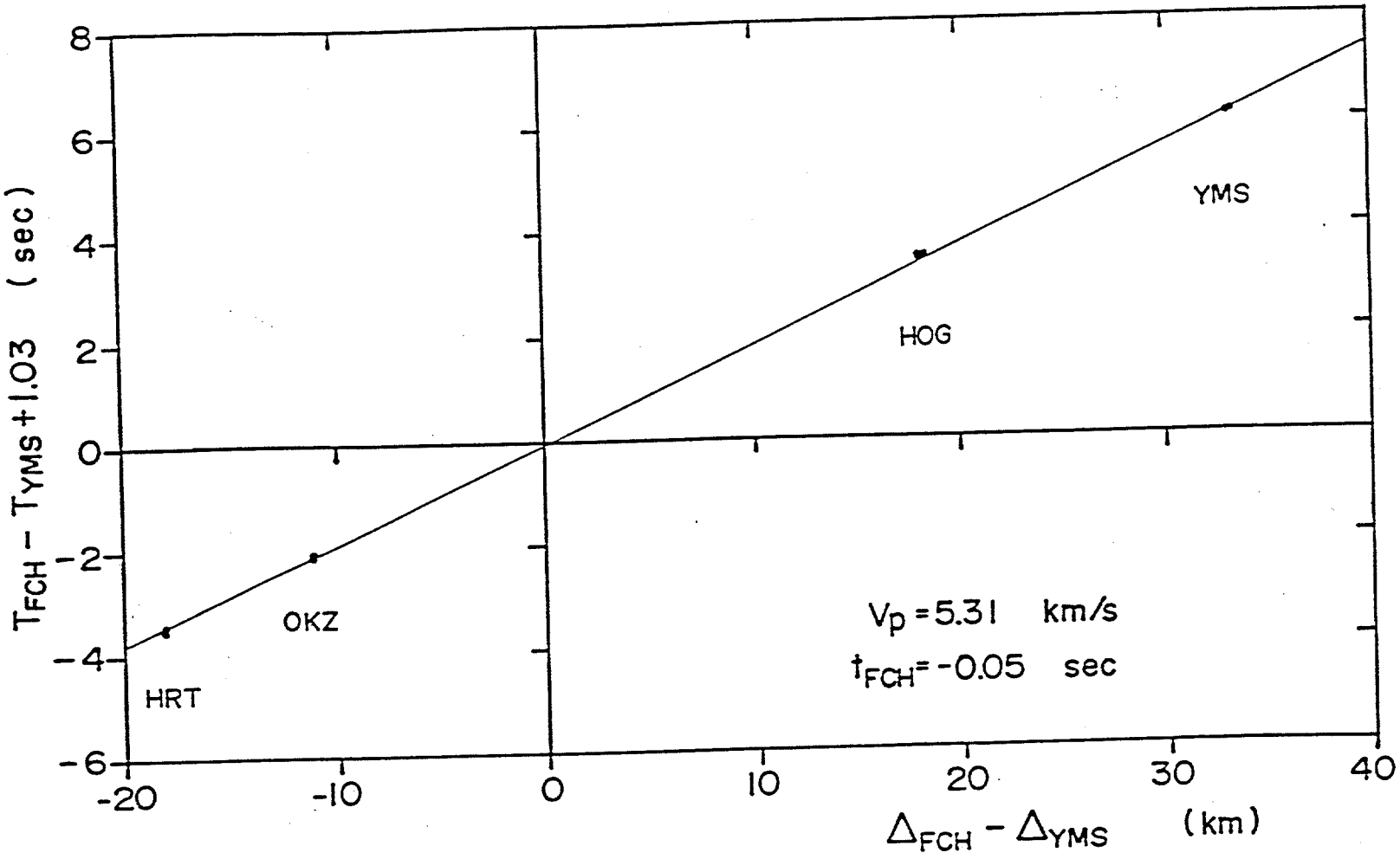

Fig. 3-8. Travel time analysis of the initial phases at the bottom of the Fuchu deep borehole.

3.2 Multiple-reflected Phases in Earthquake Ground Motions

3.2.1 Distinct later phases in earthquake ground motions observed in a seismic array

In the study area of the southwestern Kanto plain, an array observation of earthquake ground motions has been carried out employing three-component velocity type seismometers at the stations indicated by squares in Fig. 3-1. One of the stations called "ASK" is located on a firm rock with a P-wave velocity of more than 5 km/s. The others are set on the sedimentary layers. Some seismograms observed on the sediments exhibit distinct later phases which are obviously related to the propagation mechanism discussed above.

Fig. 3-9 shows the nearly transverse oriented velocities observed during the earthquake of August 12, 1982 with a magnitude of 5.7 and a focal depth of approximately 30 km. The seismogram obtained at the station ASK has an impulsive wave form. The initial motions of the S-waves observed at the other stations are also impulsive. Moreover, some impulsive later phases can be found every 5 to 6 sec in the seismograms observed on the sedimentary layers. The arrival time differences between these later phases are almost equal to the two way-time of the S-wave for the stack of the sedimentary layers known from the seismic surveys. In the case of a P-wave, the corresponding time interval would be 2 to 3 sec. Therefore, it is reasonable to assume that these later phases are also caused by multiple reflections within the sedimentary layers as discussed in the case of the explosion seismograms earlier. In the area, there are two layers with high P- and S-wave velocities of 4.8, 5.5 km/sec and 2.5, 3.0 km/sec, respectively. Furthermore, it is difficult to conclude which layer contributes to the multiple reflections. However, considering the impedance ratios, it is proper that the multiple reflections occur between the free surface and the top of the layer with an S-wave velocity of 2.5 km/sec. Some differences from the case of the explosion, however, should be noted with respect to the propagation path. Since the hypocentral depth is 30 km and is located within the lower earth's crust, the initial S-wave travels in the upper mantle with an S-wave velocity of about 4.4 km/s as the refracted wave (Sn). On the other hand, the initial phase in the explosion seismogram travels as the refracted wave along the top of

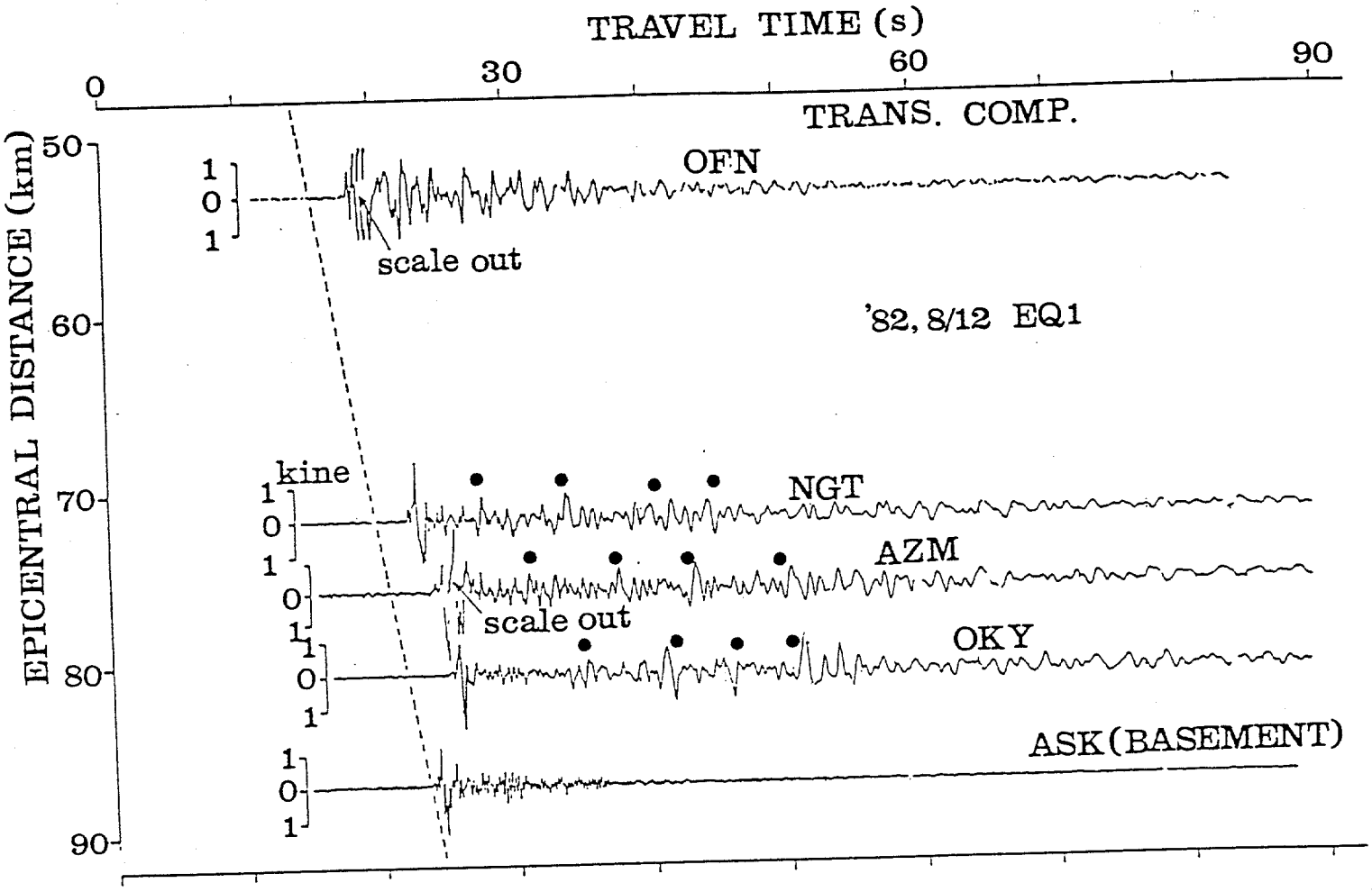

Fig. 3-9. Nearly transversely polarized ground velocities observed in a seismic array during the earthquake of 12/Aug/1982 (M=5.7).

the basement rock which is located considerably shallower than the mantle. This difference leads the different incident angle into the sedimentary layers. The incident angle to the sedimentary layers is somewhat oblique in the case of the earthquakes. While, the explosion wave travels along the top surface of the basement with a velocity of 5.5 km/sec and incidents into the upper layers with the critical angle. If these later phases in the earthquake records are due to multiple reflections between the free surface and the upper boundary of the layer in which the initial S-wave travels, just like the case of the explosion, the arrival time difference would be more than 10 sec and this can not be explained with the obtained data. Thus, the observed later phases are interpreted to be caused by the multiple reflections within the sedimentary layers.

If the strata are horizontally layered, a down-going from the free surface wave can be reflected with a large amplitude at the top of the mantle, while the reflection coefficient at the top of the basement is small; correspondingly the incident angle to the basement is about 35 ° (see, Fig. 3-4). To explain the large later phases observed, the incident angle of the down-going wave to the basement should be near and more than the critical angle. This requires a dipping topography of the layer with an S-wave velocity of 2.5 km/sec to explain the large reflection coefficient.

3.2.2 Variation of amplitudes of multiple-reflected phases

The distinct later phases discussed above can not always be seen in seismograms observed on the sedimentary layers. Here, we investigated the variation of amplitudes of multiple-reflected wave in seismograms observed during several earthquakes.

For this investigation, seismic waves from sources are required to be simple to identify easily the later phases. Next, we compare earthquake ground motions with simple wave forms observed at station OKY during earthquakes from various azimuthes. The 24 earthquake records from 1982 to 1988 were selected as shown in Table 3-2. Since we selected earthquake records whose initial motions are impulsive, the magnitudes of the earthquakes

Table 3-2. List of earthquakes with simple waveform observed at OH-OKAYAMA

No	ORIGIN TIME	LOCATION	LAT.	LONG.	M_{ima}	H(km)
1	12/AUG/82 13:33:00.0	NEAR COAST OF IZU OHSHIMA	34 53	139 34	5.7	30
2	27/JAN/83 18:07:32.6	EASTERN TOKYO BAY	35 45.7	139 37.7	4.6	57
3	22/FEB/83 11:48:51.7	NORTHERN CHIBA PREF.	35 44.0	140 07.9	4.9	70
4	14/FEB/84 01:53:00.8	YAMANASHI KANAGAWA BORDER	35 35.1	139 06.4	5.2	25
5	02/NOV/84 17:45:16.2	NORTHERN TOKYO BAY	35 41.6	139 58.1	4.2	58
6	10/NOV/84 10:40:07.6	SOUTHERN CHIBA PREF.	35 16.7	140 01.5	4.6	95
7	17/DEC/84 23:49:47.7	CENTRAL CHIBA PREF.	35 35.8	140 03.5	4.9	78
8	07/JAN/85 07:08:43.9	CENTRAL CHIBA PREF.	35 32.3	140 06.9	4.7	71
9	07/FEB/85 10:07:08.0	EASTERN KANAGAWA PREF.	35 24.0	139 32.0	4.3	103
10	08/JUN/85 01:29:01.1	CENTRAL CHIBA RREF.	35 32.3	140 14.9	4.8	64
11	04/OCT/85 06:28:01.3	SE OFF BOSO PEN.	34 48.2	140 59.1	5.6	64
12	17/OCT/85 22:06:21.3	SAITAMA CHIBA BORDER	35 52.1	139 52.5	4.5	67
13	22/NOV/86 09:41:44.7	NEAR COAST OF IZU OHSHIMA	34 32.8	139 31.5	6.0	15
14	17/APR/87 16:33:40.3	NORTHERN CHIBA PREF.	35 44.5	140 08.5	5.1	77
15	30/JUN/87 18:17:07.7	SE IBARAGI PREF.	36 11.0	140 05.3	4.9	57
16	18/OCT/87 03:41:----	CENTRAL KANAGAWA PREF.	35 31	139 10	4.9	29
17	16/JAN/88 20:42:----	EAST OFF CHIBA PREF.	35 22	140 27	5.2	53
18	03/FEB/88 14:43:----	SOUTH OFF CHIBA PREF.	34 51	140 11	5.0	75
19	18/MAR/88 05:34:----	EAST TOKYO	35 40	139 39	6.0	99
20	31/JUL/88 08:40:----	EAST OFF IZU PEN.	34 54	139 18	5.4	10
21	02/AUG/88 22:16:----	EAST OFF IZU PEN.	34 54	139 12	5.2	10
22	12/AUG/88 14:15:----	SOUTH CHIBA PREF.	35 06	139 54	5.3	66
23	05/SEP/88 00:49:----	EAST YAMANASHI PREF.	35 29	139 02	5.6	31
24	29/SEP/88 17:23:----	SOUTH SAITAMA PREF.	35 56	139 12	5.0	16

are moderate from 4.2 to 6.0. The source parameters, such as origin time, of the recent earthquakes, No.16 to 24, are roughly determined by Japan Meteorological Agency until now. The epicenters of these earthquakes are shown in Fig. 3-10. All the solid circles and the square indicate the epicenters and the location of the OKY station, respectively. The earthquakes distribute in various directions from the station. Much earthquakes, however, took place in the eastern side of the station, because of, probably, seismo-tectonic reasons. Earthquakes occurred in regions far from the station were not selected, because such earthquakes observed usually were relative large events and had complex initial phases.

The earthquake records obtained at OKY are shown in Figs. 3-11a to 3-11f: two horizontal velocities in the NS and the EW directions for each earthquake. The seismograms of event No.1 were observed during the same earthquake as discussed previously in Fig. 3-9. Some distinct later phases with arrival time differences of approximately 6 sec can be clearly seen in the seismograms as indicated by open circles, specially, in the records during earthquakes of No.1, 4, 11, 13, 16 and 23. Because of the arrival time intervals of the later phases, these later phases can also be interpreted as multiple-reflected waves within the sedimentary layers. In the other seismograms, we can also find the faint later phases about 6 sec after the arrivals of the initial phases in the records of earthquakes of No.8, 12, 14, 19, 20, 21, 24 as denoted by open circles, too.

The focal depths of the earthquakes are shown in Fig. 3-12. The open circles indicate the earthquakes with the large later phases. It is clear that the multiple-reflected phases can have large amplitudes, when the epicenters are located in south and west of the OKY station and focal depths are shallow. On the other hand, no large later phases can not be found in the seismograms from the deep earthquakes.

3.3 Characteristics of Two-dimensional Multiple Reflection

To investigate the proposed propagation mechanism and the variation of the ampli-

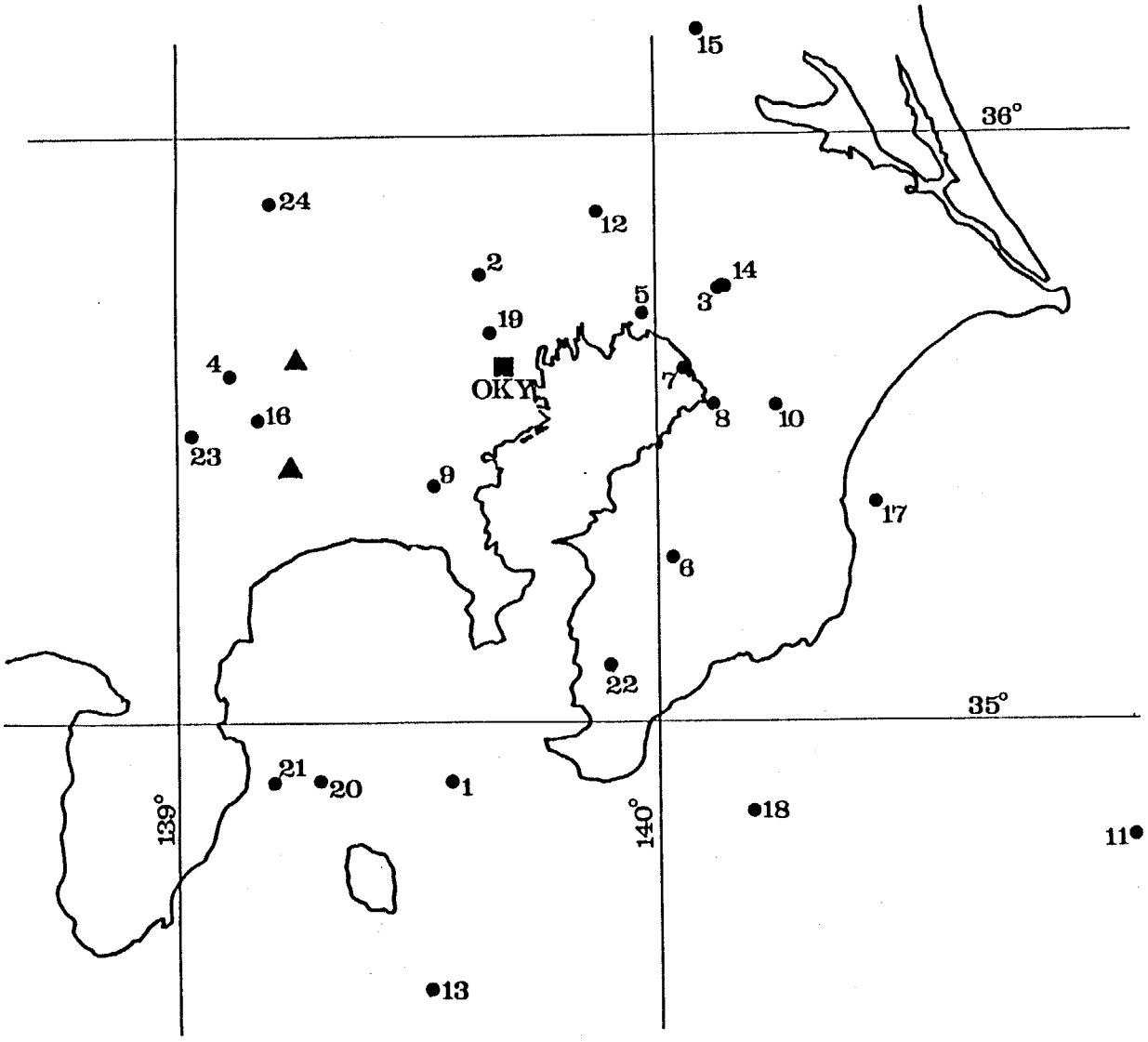

Fig. 3-10. Distribution of epicenters of earthquakes with simple wave forms and location of Oh-okayama station.

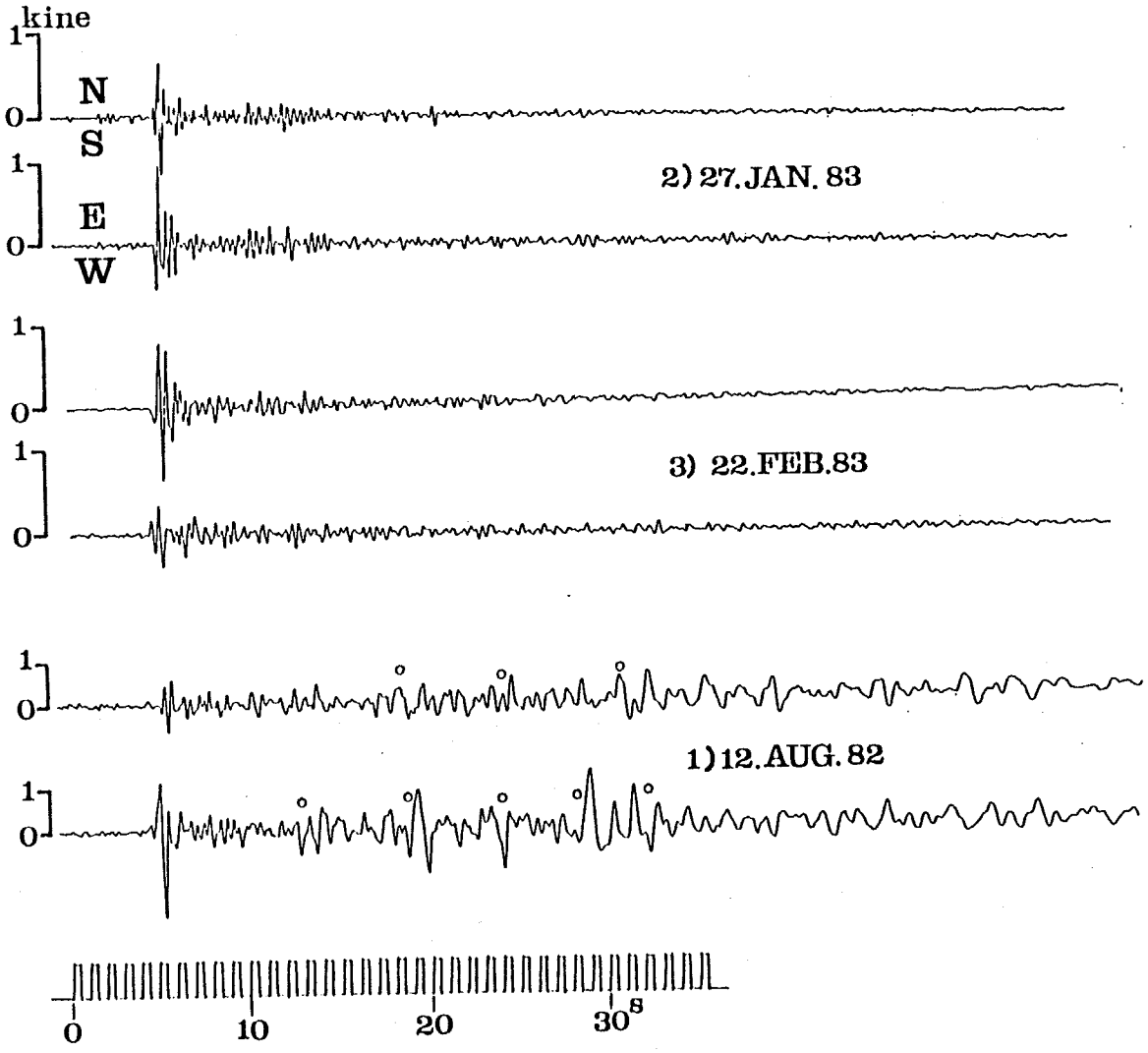

Fig. 3-11a. Horizontal ground velocities observed at Oh-okayama station from 1982 to 1983.

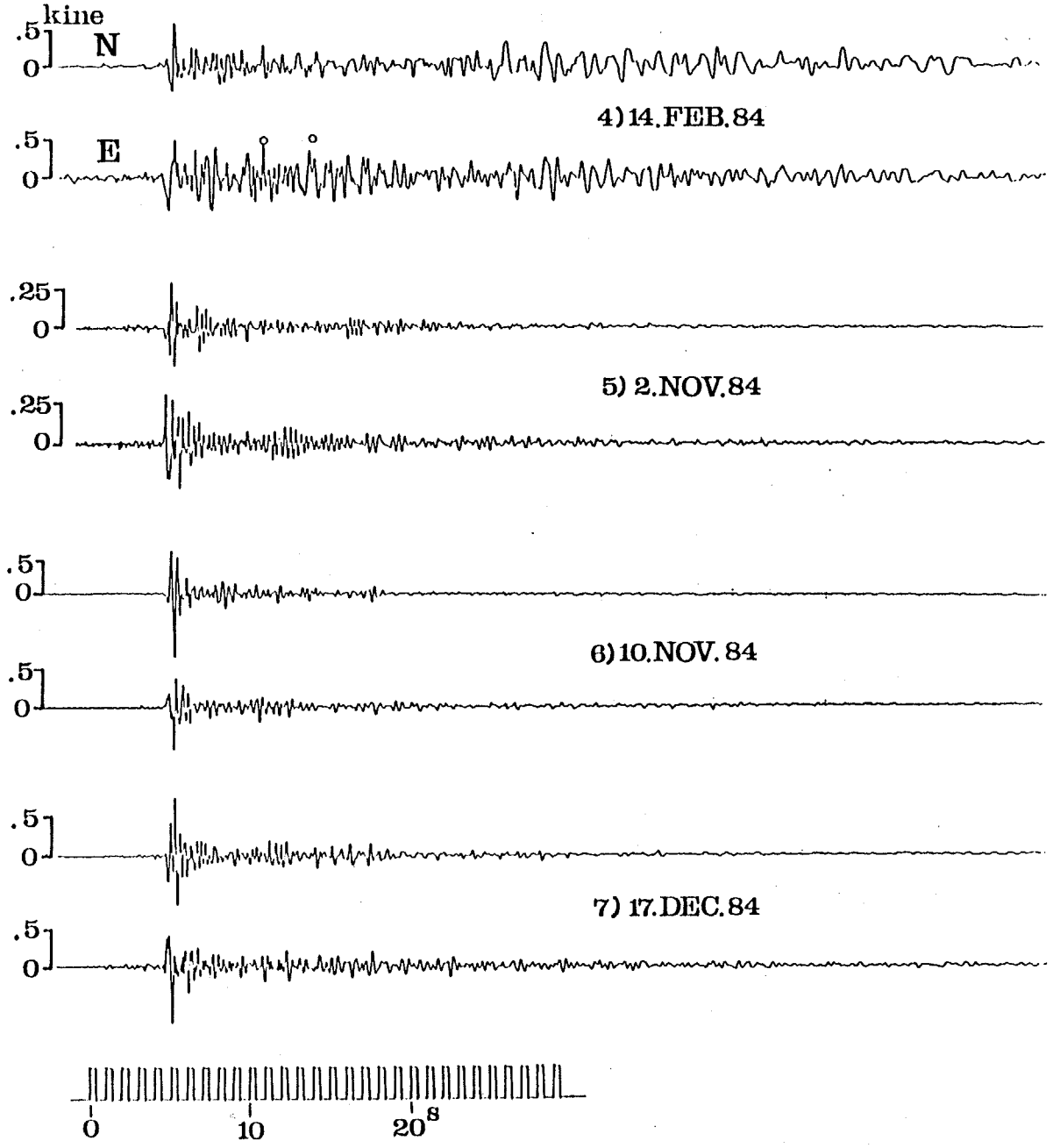

Fig. 3-11b. Horizontal ground velocities observed at Oh-okayama station in 1984.

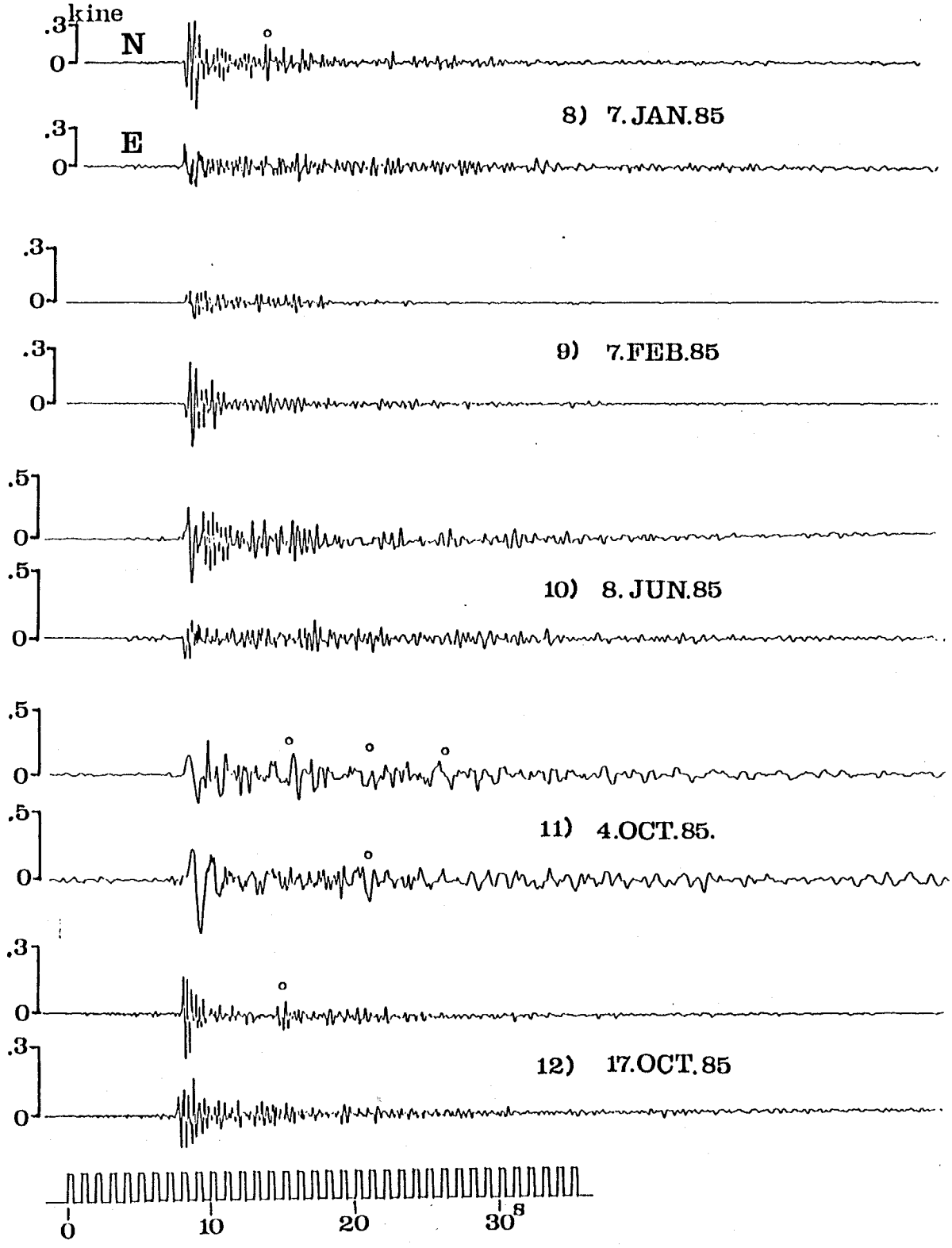

Fig. 3-11c. Horizontal ground velocities observed at Oh-okayama station in 1985.

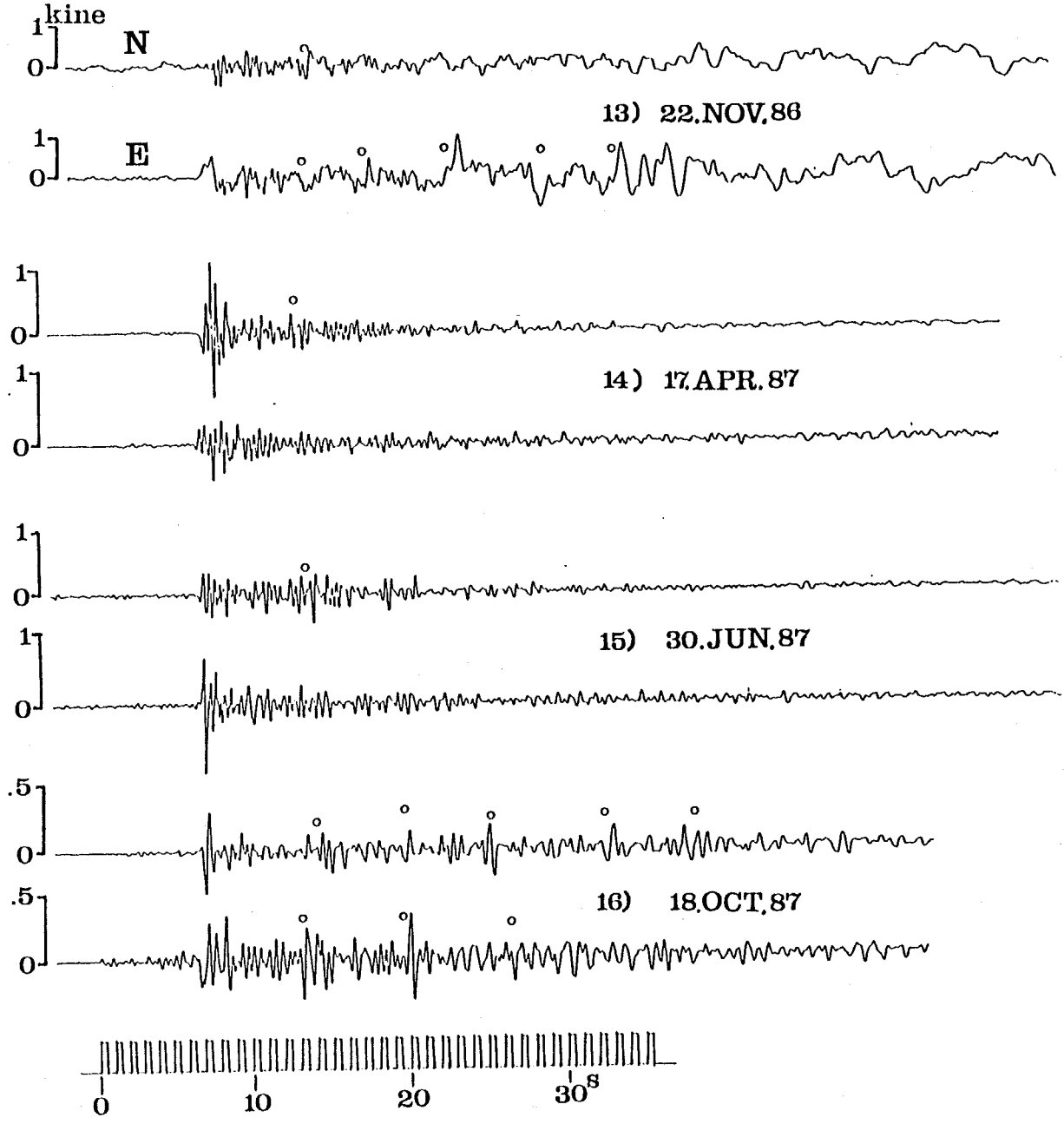

Fig. 3-11d. Horizontal ground velocities observed at Oh-okayama station from 1986 to 1987.

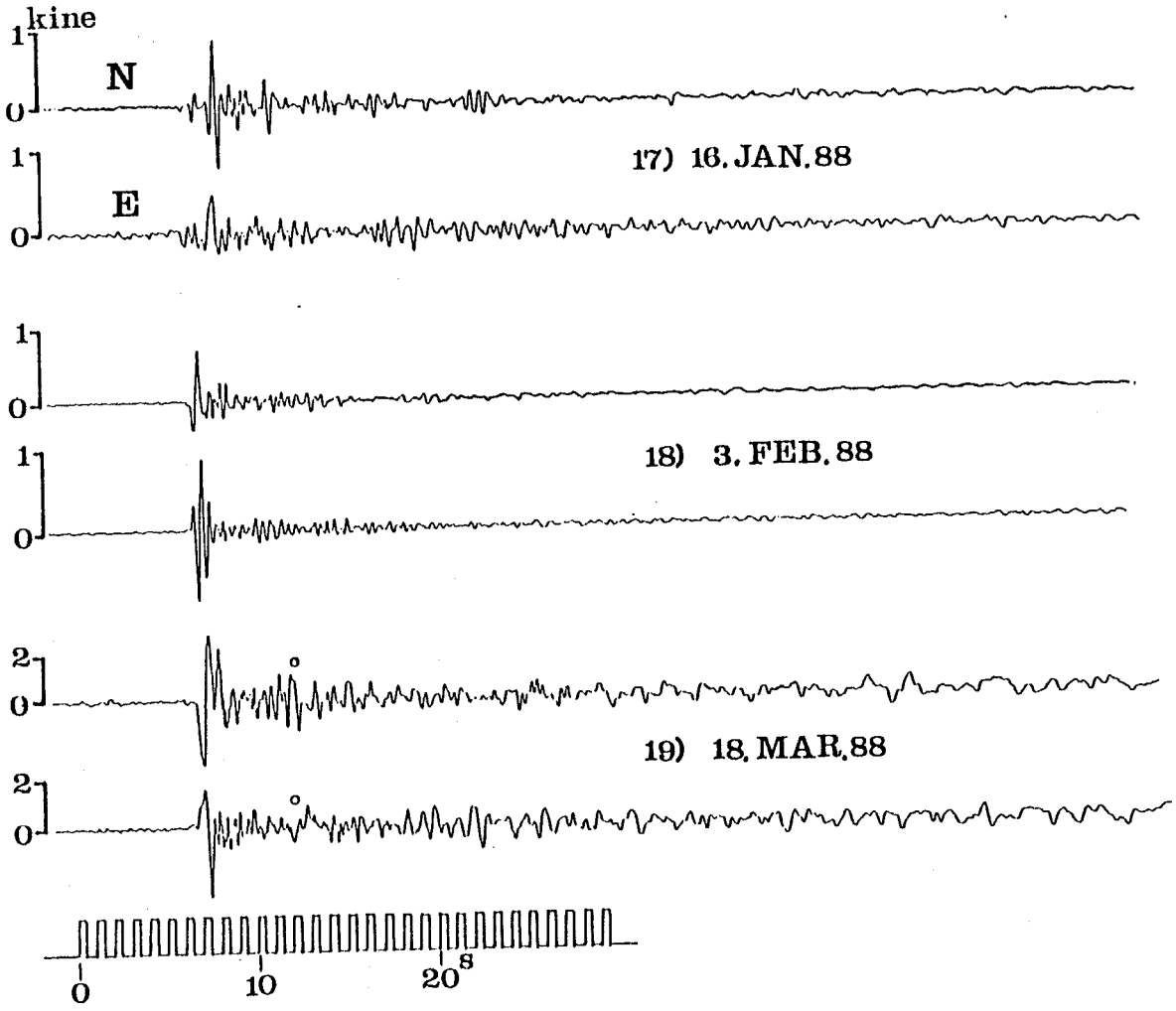

Fig. 3-11e. Horizontal ground velocities observed at Oh-okayama station in 1888.

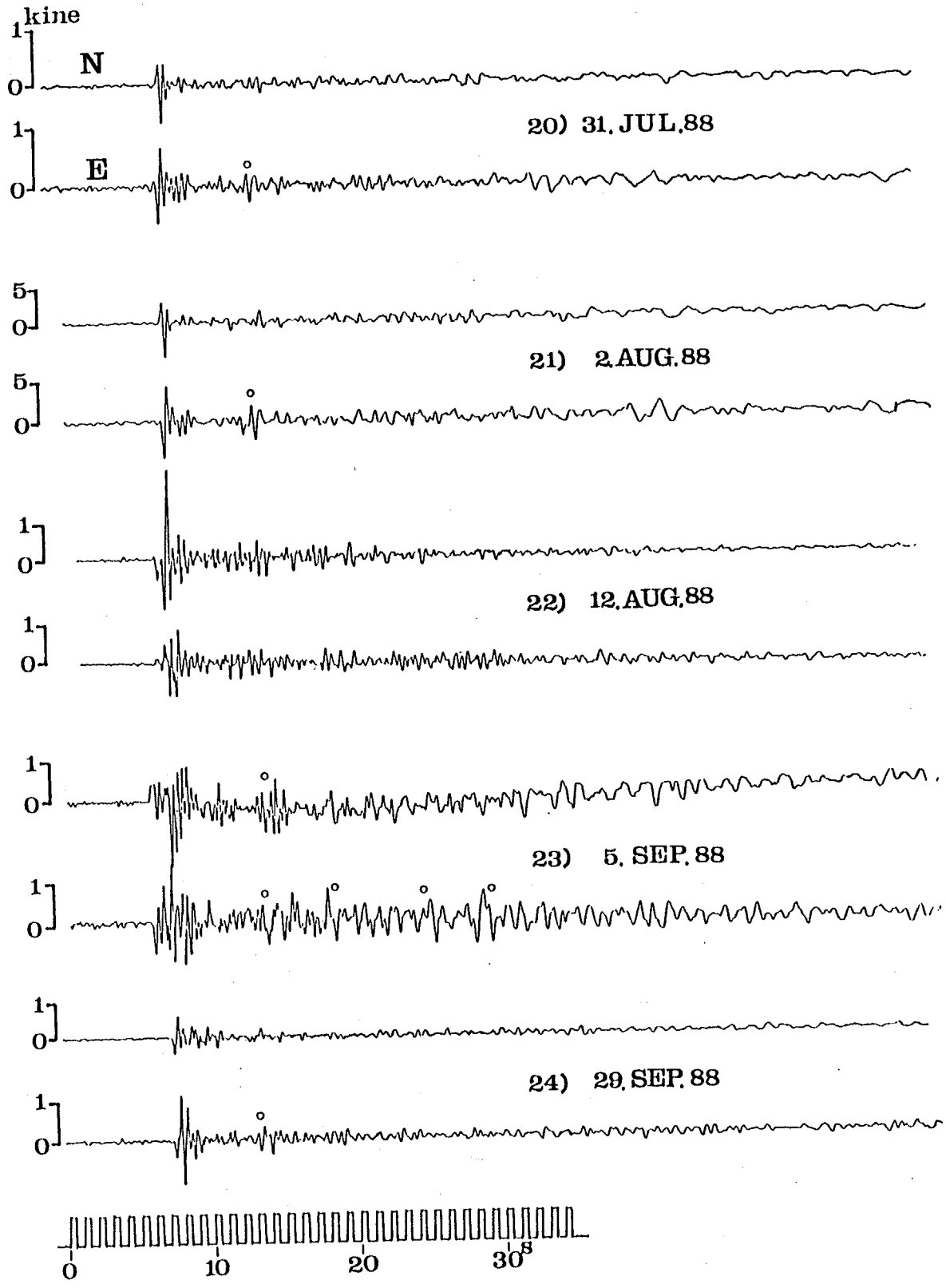

Fig. 3-11f. Horizontal ground velocities observed at Oh-okayama station in 1988.

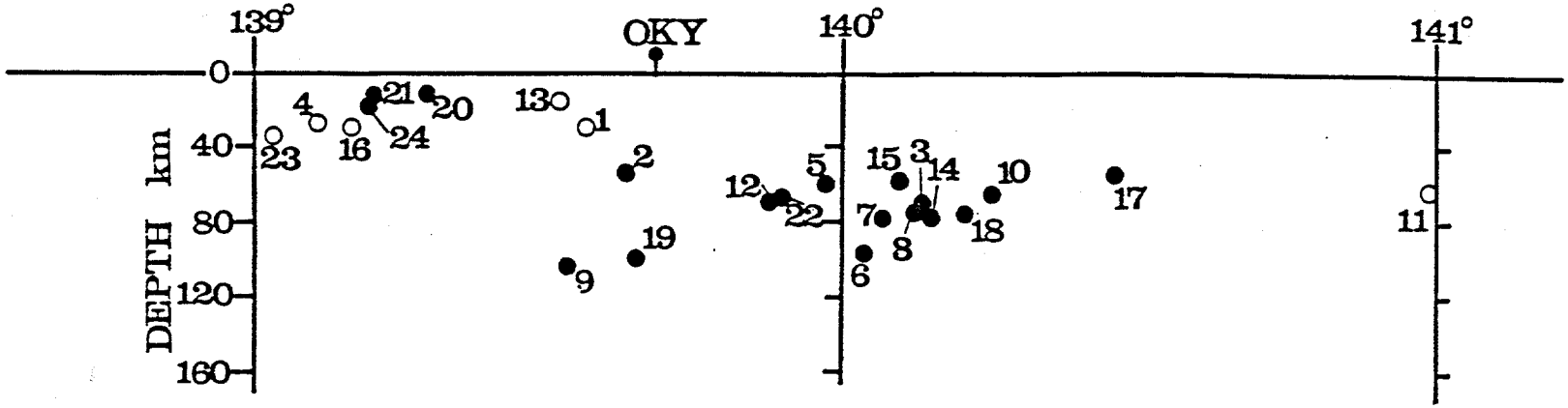

Fig. 3-12. Distribution of focal depth of the earthquakes. Open circles denote focal depth of earthquakes which can generate large multiple reflected phases, while solid ones does those of earthquakes which can not.

tudes of later phases discussed in the previous section, a simple computation based on a ray theory (Ishii and Ellis, 1970) was used here.

The model consists of a surface layer overlying a half-space with a dipping interface (dip angle θ_d ; see Fig.3-13). The response of the structure is represented as the superposition of multiple-reflected phases within the surface layer due to a plane SH-wave incidence from the half-space below.

Accordingly, a plane SH-wave, V_0, which incidents from the half-space into the surface layer is expressed in a polar coordinate system (r,θ) as shown in Fig. 3-13:

$$V_0 = A_0 exp\,[ik_2 r\cos(\theta-\alpha)] \tag{3-4}$$

where A_0 and α denote the amplitude and the incident angle, respectively; k_2 denotes the wave number in the half-space. After the incidence of the wave, the wave multiply reflects in the surface layer with amplitude A_m and with the propagating direction γ_m or γ'_m , which satisfy the boundary conditions at the free surface and at the interface between two media. Then, the waves reflecting j times at the interface between the surface layer and half-space are given by;

$$V_j = A_0 \prod_{m=1}^{j} \exp[ik_1 r\cos(\theta-\gamma_m)] \tag{3-5}$$

for up-going wave from the interface

$$V'_j = A_0 \prod_{m=1}^{j} \exp[ik_1 r\cos(\theta-\gamma'_m)] \tag{3-6}$$

for down-going wave from the free surface where k_1 denotes the wave number in the surface layer. The response is obtained by summing the contributions of all the up- and the down-going waves. The synthetic seismogram is obtained using an inverse Fast Fourier Transformation (FFT).

The multiple reflections continue until the propagation direction becomes between π and $\pi+\theta_d$ or the amplitude becomes a certain small value. The ray reaching this propagation direction leaves the wedge and never reflect at the free surface or the interface. This

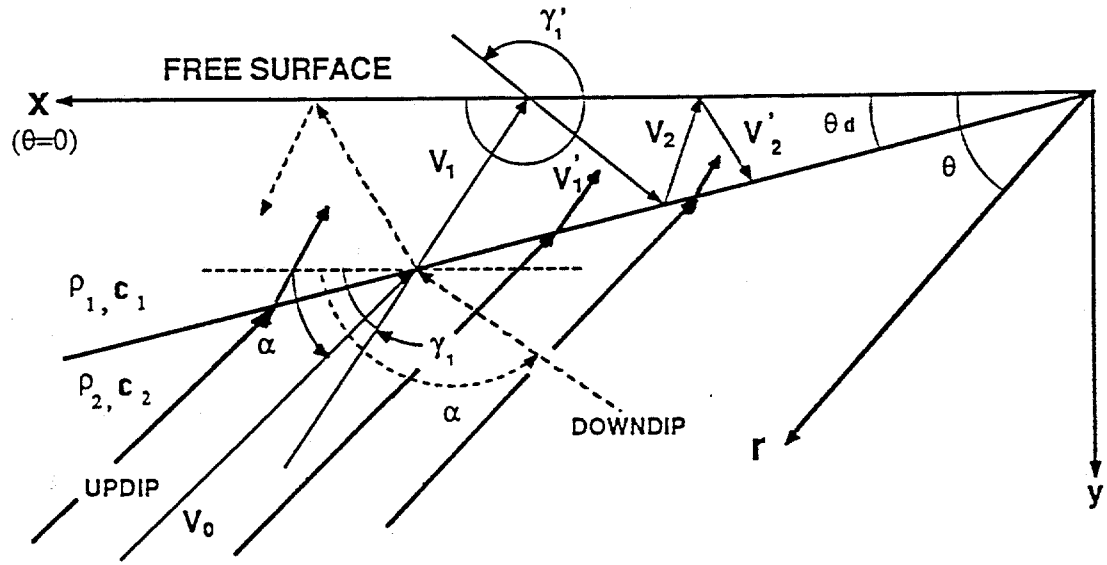

Fig. 3-13. Computational model with a dipping interface to interpret multiple reflections. Parameters for calculations are $\rho_1,\rho_2=1.9,2.3 g/cm^3$ and $C_1,C_2=1.0,2.5 km/sec$.

last ray makes a displacement discontinuity from which the diffracted wave can be derived. Ishii and Ellis (1970) concluded that the discontinuity is significant in the case of down-dip propagation, because the wave reflects a few time in the surface layer and the amplitude of the wave out-going from the wedge is still large. Since the understanding of the propagation mechanism of the multiple reflections is of major interest in this study, diffracted waves which might contribute considerably in some cases were not considered in this modeling.

In the calculation, S-wave velocities for the surface layer and the basement are 1.0 and 2.5 km/s, and densities are 1.9 and 2.3 g/cm**3, respectively. The S-wave velocity of 2.5 km/sec is assumed as the P-wave velocity of 4.8 km/sec. The calculated points are situated on the free surface of a layer and are chosen such that they always lie 3.0 km above the half-space. In order to understand the characteristics of multiple reflections clearer, a Ricker wavelet (ν_d = 1 Hz),

$$f(t) = (1-2\pi^2\nu_d^2t^2)e^{-\pi^2\nu_d^2t^2} \tag{3-7}$$

was used as an input wave.

At first, the multiple reflection of an SH-wave with a down-dip propagation direction is examined; phases propagate in the direction to which a layer becomes thicker (cf. Fig. 3-13). The incident angle (α) was set constant as 125 ° considering the propagation path of the initial S-wave from the earthquake discussed in 3.2.1. Fig. 3-14 shows the calculated seismograms on the free surface with the dip angles of the interface (θ_d) from 2 ° to 10 °. Each trace in the figure is normalized to a maximum amplitude of all the traces. An example of the ray paths of the multiple-reflected phases is also shown in Fig. 3-15 (θ_d = 7 ° and α =125 °). Although the initial phases are almost the same at all the stations, the multiple-reflected phases with large amplitudes and phase distortions can be seen only when the dip angles are equal and greater than 7 °. This is caused by the over-critical reflection of the first down-going wave. On the other hand, the traces for dip angles less than 6 ° have no distinct later phases, because of the under-critical reflection at the boundary. The minimum amplitude of the first multiple-reflected phase can be seen in the case of a dip

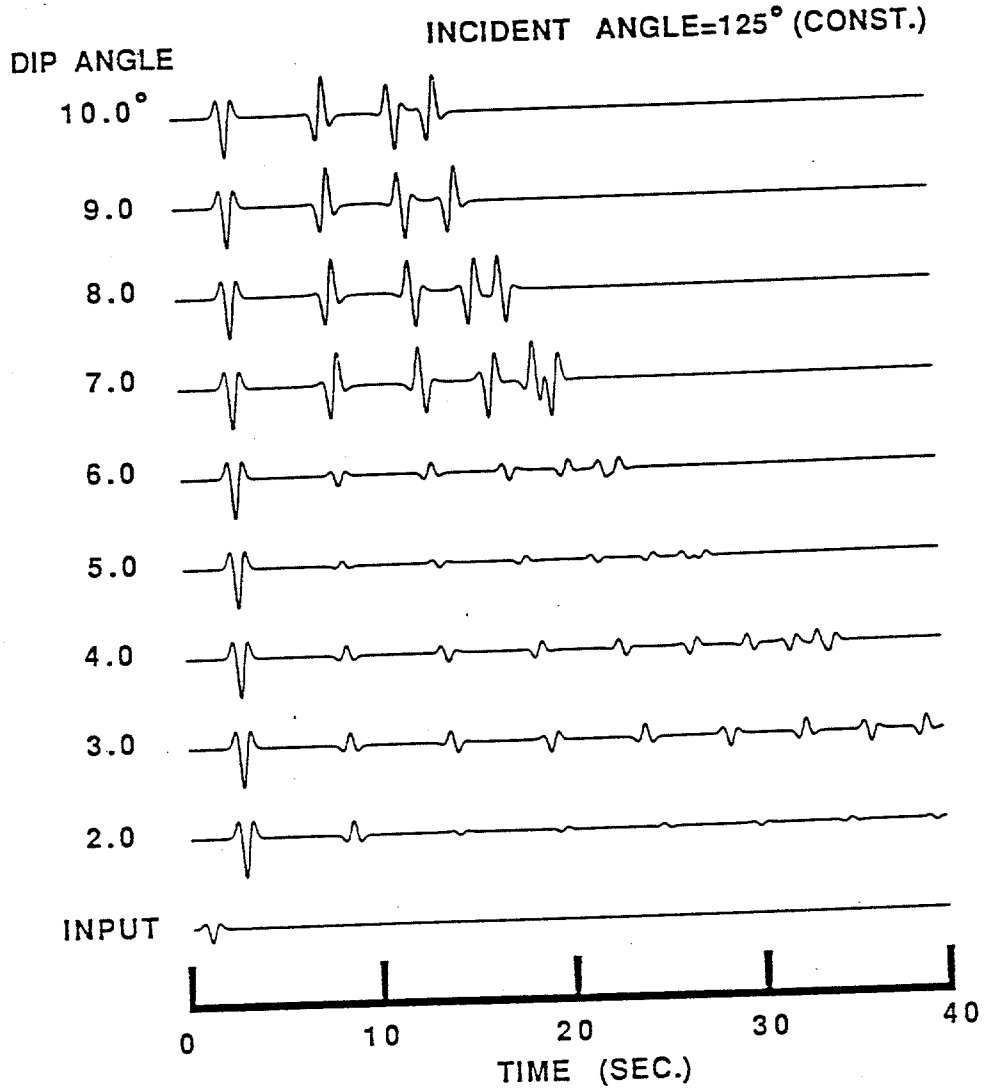

Fig. 3-14. Calculated seismograms (SH-waves) on the free surface at stations with a depth of 3 km to the half-space. Dip angles are varied from 2 to 10 ° and incident angle is constant as 125 °. Amplitude are normalized to that of input wave. A ricker wavelet (t = 1 sec) is used as an input wave.

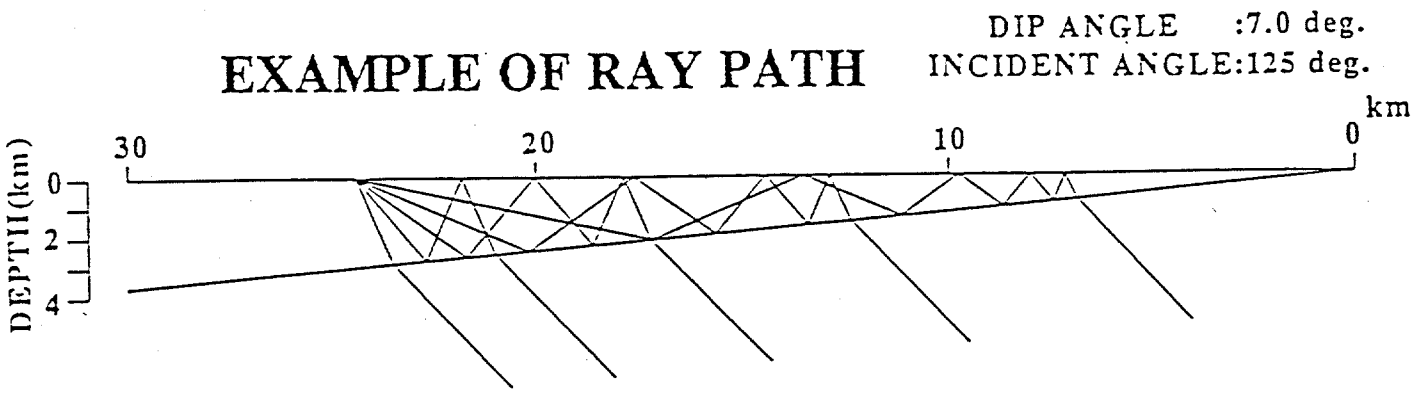

Fig. 3-15. A example of ray path of multiple reflected phases in a computational model. Dip and incident angles are 7 and 125 °.

angle of 5 °. This corresponds to the small reflection coefficient between the over-critical and the normal reflections. Although the model is very simple, the basement topography is required to have a downwards dip angle of several degrees from the south to the north for the over-critical reflection to explain the large later phases in the observed seismograms.

The influences of the variation of the incident angle (α) were examined with a constant dip angle (θ_d) of 7 ° as shown in Fig. 3-16. They are also normalized to the same scale as in Fig. 3-14. The cases with incident angles less than 90 ° correspond to up-dip propagation, the others do the down-dip propagation. The wave forms with incident angles equal or greater than 130 ° are very different from those with those less than 120 ° with respect to later phases.

These results clearly show that the amplitude of the multiple-reflected phases depend considerably on the dip angles of the interface between the basement and the sedimentary layers and on the incident angles. This means that the focal depth is an important for the amplitudes of the multiple-reflected phases. As discussed in 3.2, the multiple-reflected waves with large amplitudes could be seen in the seismograms of shallow earthquakes. It is considered that the incident angles of seismic waves from the shallow earthquakes to the sedimentary layers is oblique and seismic waves reflect over-critically at the top of the basement, while the seismic waves from deeper earthquakes incident almost vertically and amplitudes of reflected waves become small. There would be also variation of amplitudes of the reflected phases according to dipping of the interface between the basement and the sedimentary layers. We, however, could not find such variation from the observations, because our earthquake records are limited; shallow earthquakes are considerably rare in the eastern side of the field.

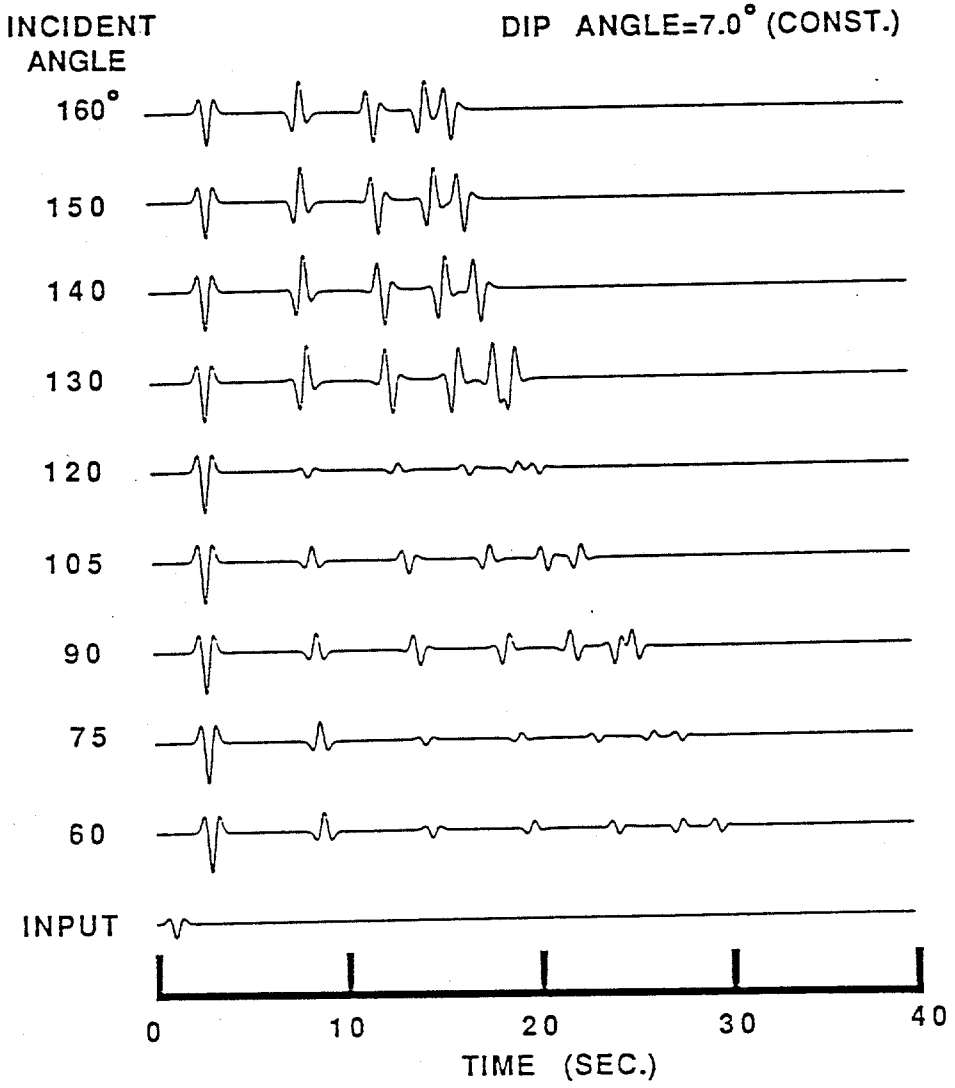

Fig. 3-16. Calculated seismograms (SH-waves) on the free surface at stations with a depth of 3 km to the half-space. Incident angles are varied from 60 to 160 ° and dip angle is constant as 7 °. Amplitude are normalized to that of input wave. A Ricker wavelet (t_o = 1 sec) is used as an input wave.

CHAPTER 4. EFFECTS OF A STEP-LIKE TOPOGRAPHY OF BASEMENT ON SEISMIC WAVE PROPAGATION

As it was shown in chapter two, there is a step-like topography of the basement with a P-wave velocity of 5.5 km/sec. In this chapter, body wave propagation in the underground structure with a step-like topography of basement is discussed. In particular, we pay attention to the characteristics of later phases in the time domain. At first, later phases in explosion seismograms are investigated. Then, the same later phases are pointed out in the earthquake records obtained in a seismic array. Finally, numerical forward modeling is carried out to interpret the later phases on seismograms.

4.1 Array Observation of Seismic Waves from an explosion at Yumenoshima in the Northern Part of Yokohama

The location of the step-like topography of the basement, namely a fault, revealed by the seismic surveys is depicted by a broken line in Fig. 4-1. The possibility of this feature was first suggested by Seo (1981) from the observation of the Yumenoshima explosion at a station between Yumenoshima and Ohyama in northern part of Yokohama. The station is indicated by an arrow in Fig. 4-1. Fig. 4-2 shows the vertical velocities obtained from the Yumenoshima explosion, which is reproduced from a paper of Seo (1981). The travel time delay of the initial phases can be seen in the trace named No.10, which was obtained at Kawawa in Yokohama. In the trace, the large later phase with a time delay of about 0.7 sec after the initial phase can be seen, too. Seo (1981) suggested that this later phase was a phase affected by the step-like topography of the basement. However, observation of the explosion was not so sufficient that detailed investigations and clear understanding could not be performed.

In order to confirm the existence of the step-like topography of the basement and to understand what the later phase is, relative dense observation of an explosion at Yumenoshima was carried out on the same line as Seo (1981): the Ohyama line.

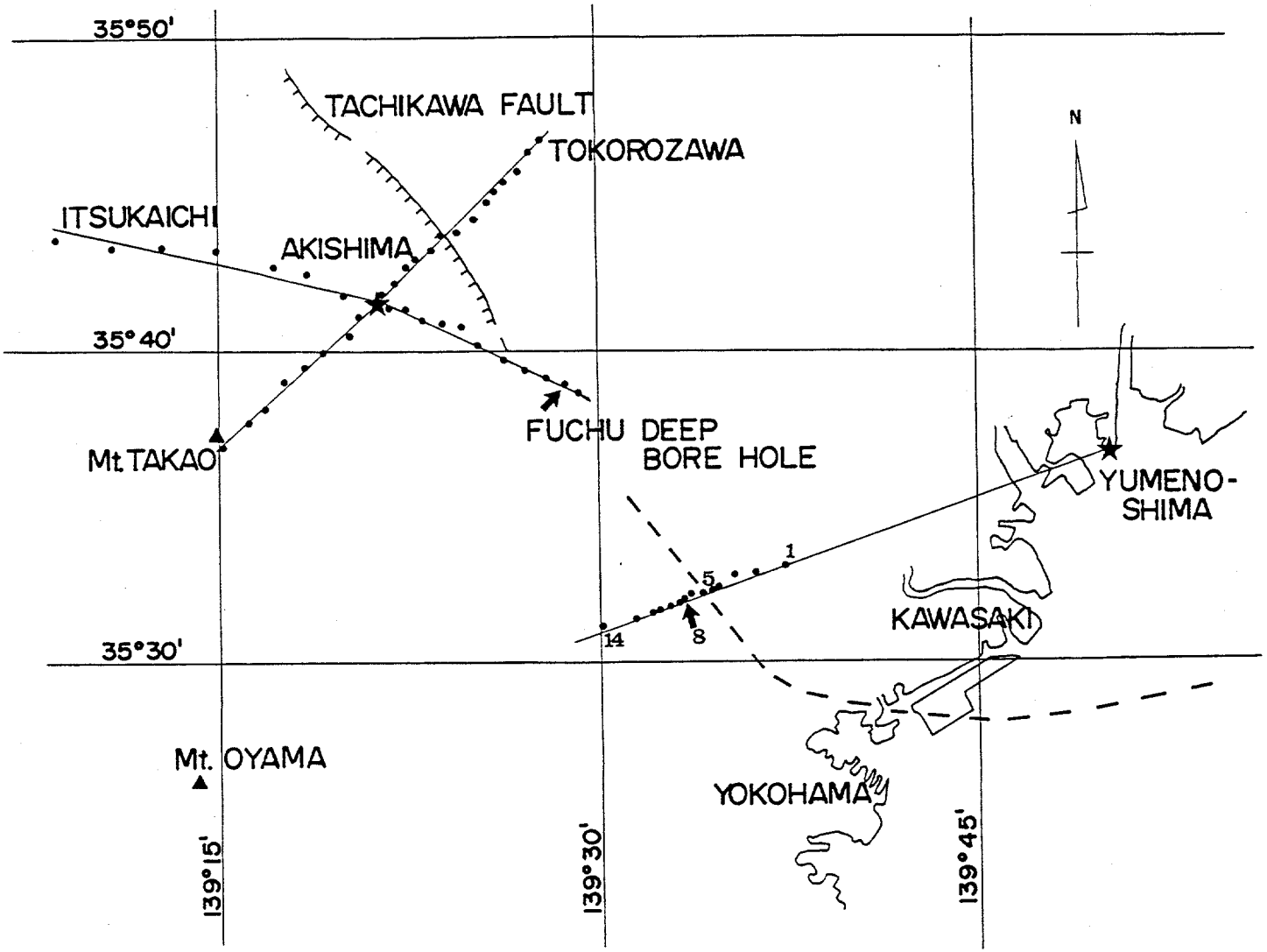

Fig. 4-1. Location of step-like topography of basement deduced from seismic refraction surveys, observation stations of an explosion at Yumenoshima and the Tachikawa active fault.

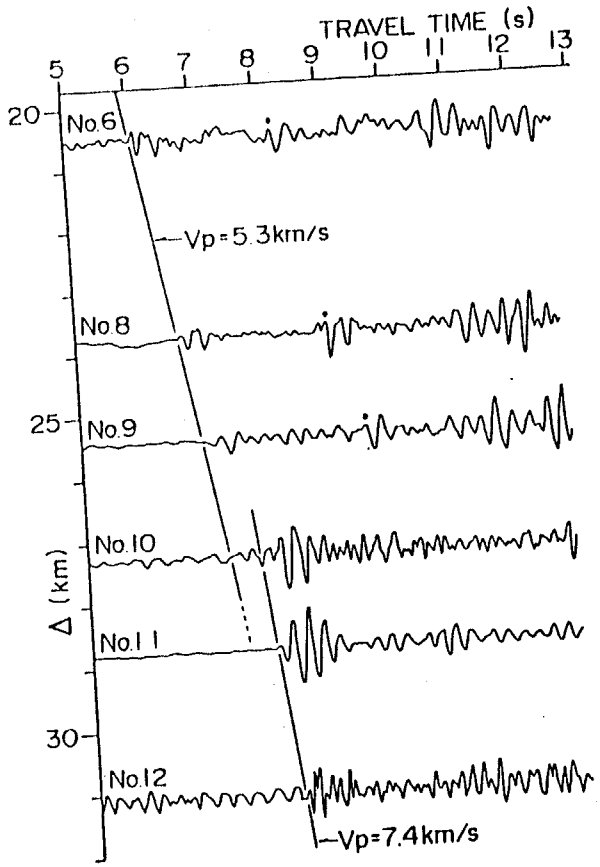

Fig. 4-2. Partial details of seismograms obtained during the Yumenoshima explosion [Reproduction of Seo (1981)]. Station of No.10 (Kawawa) in the figure is the same one of No.8 in Fig. 4-1.

The explosion with 500 kg dynamite was detonated at Yumenoshima on March, 16, 1986. The observation sites are listed in Table 4-1 and are indicated by circles in Fig. 4-1. The station spacing is less than one kilometer. A station of No.8 is the same location as Seo's station No.10 (cf. Fig. 4-2). Each seismometer used has the same characteristics with a natural frequency of 4.5 Hz and a damping coefficient of 0.7, except for the seismometer for station No.1, whose natural frequency is 1.0 Hz. Therefore, observed waveforms including variation of amplitudes can be compared with each other.

At first, the seismogram observed at Kawawa was compared with Seo's observations, because the estimated arrival time of the initial phase differs from Seo's result. The upper trace in Fig. 4-3 shows the vertical seismogram observed in this study and the lower one is the seismogram observed by Seo (1981) using a seismometer with a natural frequency of 1.0 Hz. The circles attached indicate the arrivals of initial phases. The initial phase of the lower seismogram seems to be disturbed by the ground noise of around 0.5 second. To eliminate the effects of the seismometer, the response of single-degree-of-freedom system with a natural frequency of 4.5 Hz and a damping coefficient of 0.7 was calculated, when the lower trace was loaded. The middle trace indicates the response. The circle for this trace is the newly estimated onset of the initial phase. The comparison of the middle trace with the upper trace shows that the arrival times in the upper and the middle traces are proper and that the later phases with large amplitudes are stable phenomena.

The vertical velocities observed the Yumenoshima explosion of 1986 are shown in Fig. 4-4. All the traces in the figure are normalized to the same value. Solid circle for each trace indicates the initial phase arrival. One of notable features is the travel time delay of the initial phase which arrivals at stations between 26 and 28 km. Another interesting feature of the observed seismograms is the large later phases arriving approximately 0.5 sec after the initial phases at stations where the arrival delays of initial phases can be seen. These arrival times of the later phases lie in the branch of the travel time curve for the arrivals of the initial phases at the stations with distances more than 29 km. As for the amplitudes, these

Table 4-1. Travel time of initial phases
obtained from the 27th Yumenoshima explosion

No	STATION	LOCATION LONG.	LOCATION LAT.	YUMENOSHIMA D(km)	YUMENOSHIMA T(s)
0	YUMENOSHIMA S.P.	139 50 20.0	35 36 40.0	0.00	
1	TAKADA SHO	139 37 23.4	35 33 11.3	20.58	6.10
2	MINAMI YAMADA	139 36 17.6	35 32 54.5	22.32	6.44
3	NAKAGAWA SHO	139 35 26.6	35 32 50.9	23.57	6.54
4	CHIGASAKI CHO	139 34 50.8	35 32 30.8	24.62	6.77
5	KOHHOKU NEW TOWN 1	139 34 29.7	35 32 26.2	25.17	6.92
6	KOHHOKU NEW TOWN 2	139 34 09.8	35 32 19.5	25.71	7.12
7	KOHHOKU NEW TOWN 3	139 33 40.5	35 32 14.0	26.47	7.30
8	KAWAWA KOH	139 33 20.2	35 32 07.6	27.01	7.48
9	KAWAWA CHO	139 33 09.6	35 31 57.8	27.36	7.51
10	TANIMOTO GAWA	139 32 45.9	35 31 51.8	27.99	7.58
11	KITA HASSAKU CHO	139 32 19.7	35 31 49.1	28.64	7.75
12	YOKOHAMA SHO DAI	139 31 54.7	35 31 36.6	29.36	8.05
13	TOHKAICHIBA	139 31 20.2	35 31 27.5	30.27	8.17
14	NAGATSUTA	139 30 05.6	35 31 14.2	32.18	8.41

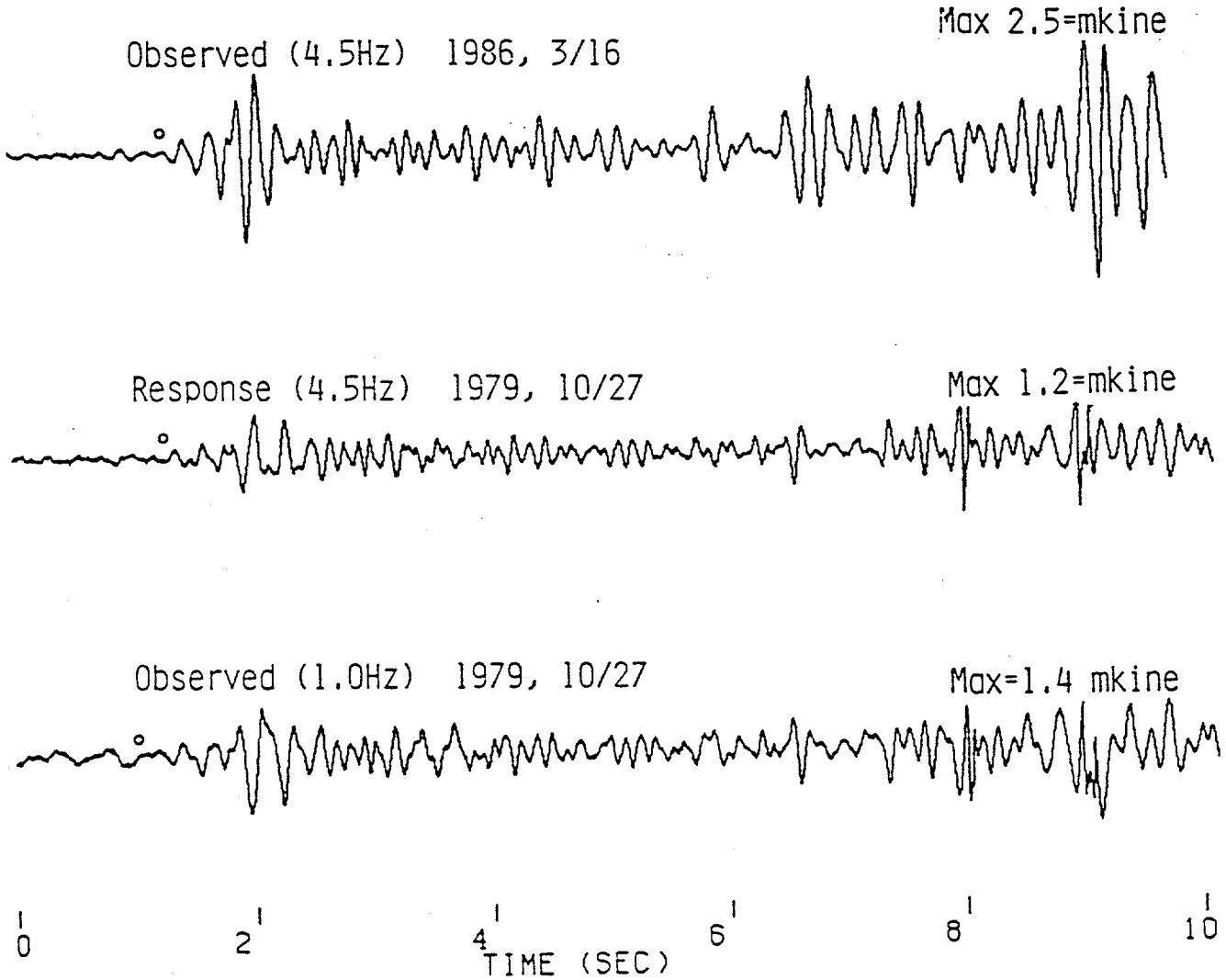

Fig. 4-3. Comparison between seismograms obtained at Kawawa during the Yumenoshima explosion by Seo (1981) and in this study. Lower trace indicates vertical velocity observed by Seo (1981) using a seismometer with a natural frequency of 1.0 Hz. Middle trace is a response of SDOF with a natural frequency of 4.5 Hz. Upper one is the observed seismograms using a seismometer with a natural period of 4.5 Hz in this study.

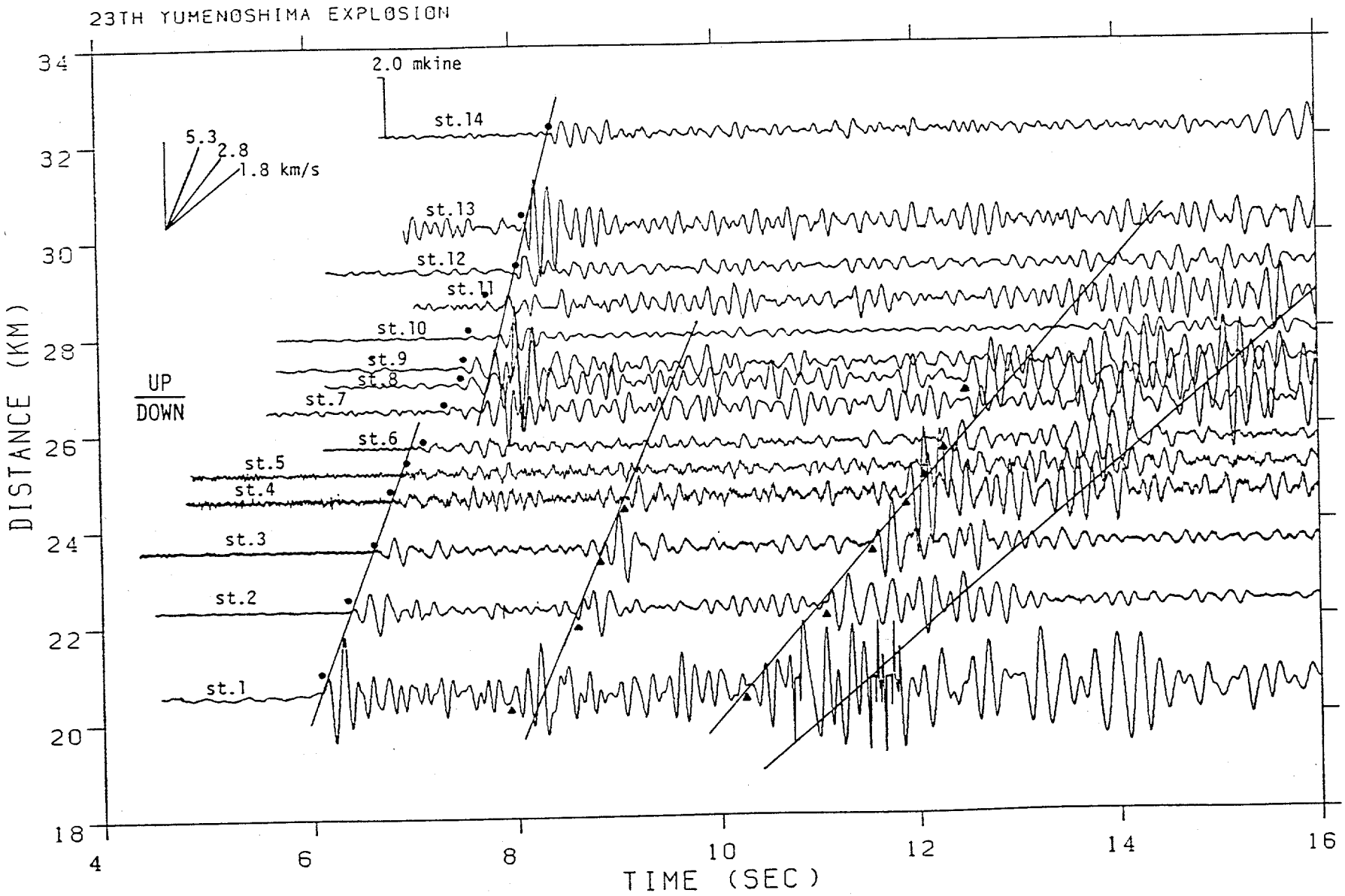

Fig. 4-4. Vertical velocities observed during an explosion at Yumenoshima.

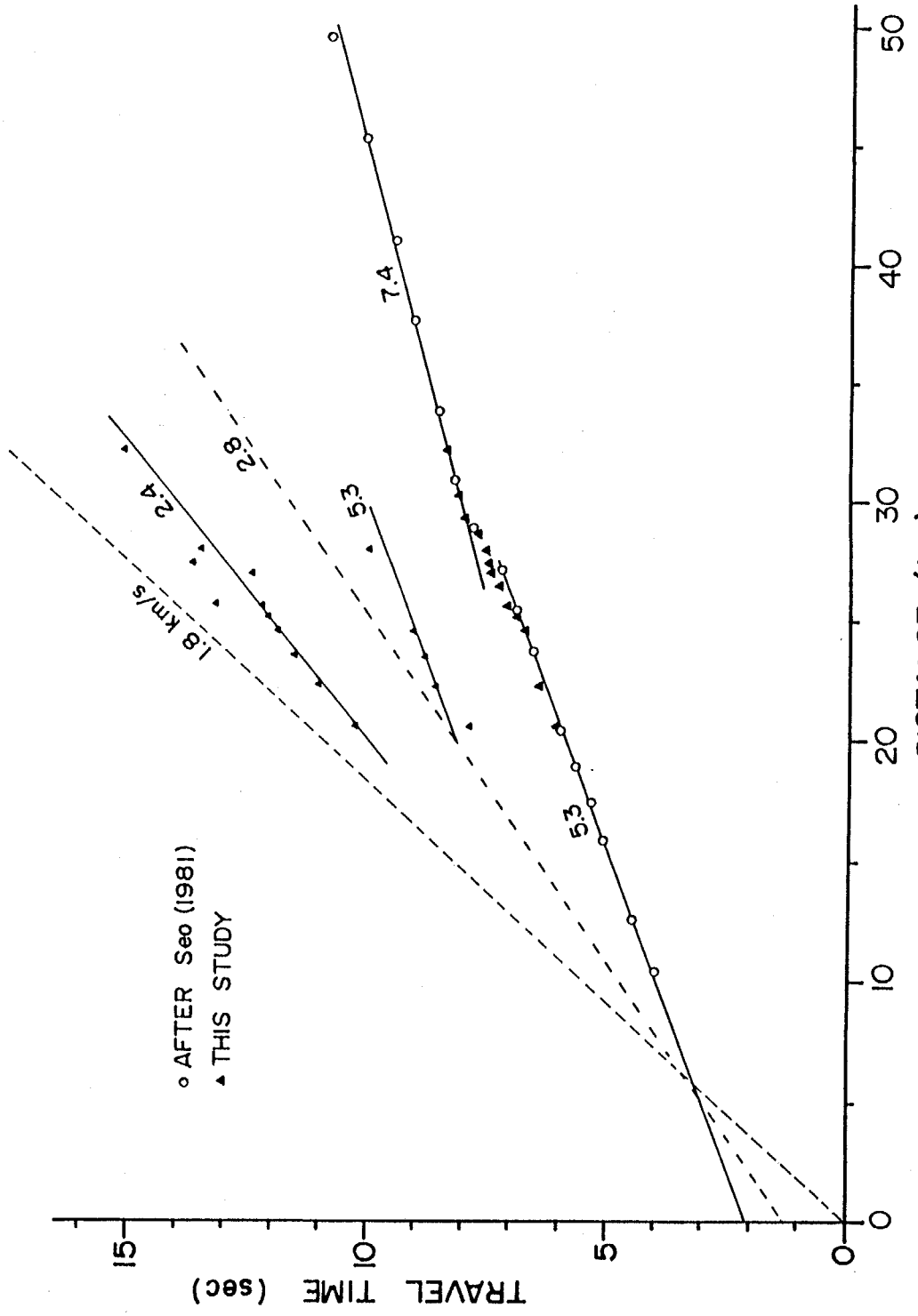

Fig. 4-5. Travel time diagram of initial and later phases of the Yumenoshima explosion. Solid triangles denote the arrivals of the initial and later phases obtained in this study. Open circles do those of the initial phases obtained by Seo (1981).

later phases have 2 to 3 times larger amplitudes than amplitudes of the initial phases. These features can be recognized not only at one station, Kawawa, but also at several stations which are located within 2 km of Kawawa. This means that these features of the initial part of the seismograms can not be explained by the effects of superficial layers at each station, but by the effects of the common propagation path.

The travel time curve is shown in Fig. 4-5 including the travel time data of the Yumenoshima explosion by Seo (1981). The above characteristics of the initial phase arrivals can be also seen in the figure. The apparent velocity of the initial phases changes from 5.3 km/sec to 7.4 km/sec at the stations where the travel time delays were found. The higher apparent velocity was considered to be caused by the inclination of the basement of a P-wave velocity of 5.5 km/sec as discussed before.

These features with respect to the arrival time delay of initial phases are typical ones of a fault or a step-like topography of the basement as it is well described in textbooks on geophysical prospectings (e.g., Dobrin, 1976; Tajime, 1981). It is considered in this case that the basement is down-faulted to the west.

4.2 Array Observation of Earthquake Ground Motions

4.2.1 Outline of earthquake observation

As discussed in the previous section, the dense observation of the Yumenoshima explosion clearly suggested the existence of the step-like topography of the basement. Moreover, the distinct later phases which appear 0.5 sec after the initial phases could be seen at the stations where the step can be expected. Since the nature of the later phases would be concerned with the existence of the step, the same kind of the later phases can be expected to be found in earthquake records, too. Several earthquake records are examined in this respect.

Investigations on effects of a subsurface step-like topography on earthquake ground motions are few, though those of a surface step-like topography or a cliff were well studied

(e.g., Ohbo, 1986; Zama, 1981a). One of the reasons is uncertainty on subsurface ground structure. Irikura and Kasuga (1980) and Kasuga and Irikura (1982) systematically investigated amplification characteristics in such an underground structure in the Kyoto basin where the underground structure down to the basement was known and a fault was also detected. They concluded through the observations and the computations that the subsurface step-like topography gives considerable effects on ground motions in the neighborhood of the step. The effects, however, were mainly evaluated in the frequency domain.

In this study, an array observation of earthquake ground motions was carried out along the same surveying line for the observation of the Yumenoshima explosion. The observational array consists of the stationary and the temporary stations which are listed in Table 4-2 and are depicted in Fig. 4-6. A station called Kawawa (KWW) is the same location as the observation point No.8 in the explosion experiment, where the step-like subsurface structure could be postulated. Although the station named ASK on a firm rock is away from the array, records obtained at the station were used for the investigation. At each station, three-component seismometers and an analog or digital data recorder were installed. The seismometer used at each temporary station was of velocity-type with a natural period of 10 sec and a damping coefficient of 0.7. The velocity-type strong motion seismometers whose frequency characteristics are flat more than 40 sec are used at the stationary stations. The temporary observation was continued around a year from June, 1985, to July, 1986.

4.2.2 Observed records of near-by earthquakes

Earthquake records observed are more or less limited, because of the short term for the observation and the seismo-tectonic reasons in this area. Shallow earthquakes are very rare in the eastern side and locations of epicenters concentrate in some limited regions. The earthquakes discussed here are listed in Table 4-3, whose epicenters are depicted by stars in Fig. 4-6. Since later phases in the seismograms are of our major interest as discussed in 4.1, the seismograms used have relative simple wave forms and the sizes of the earthquakes are moderate except for EQ5. EQ5 is an example of relative large earthquakes. The observed

Table 4-2. List of earthquake used

No	ORIGIN TIME	LOCATION	LAT.	LONG.	M_{jma}	DEP.(km)
1	08/JUN/85 01:29:01.1	CENTRAL CHIBA PREF.	35 32.3	140 14.9	4.8	64
2	15/JUL/85 07:21:48.6	NORTHERN CHIBA PREF.	35 44.5	140 08.4	4.3	74
3	11/OCT/85 22:39:45.4	NORTHERN CHIBA PREF.	35 50.0	140 07.3	4.4	77
4	06/NOV/85 00:30:50.0	CENTRAL CHIBA PREF.	35 21.3	140 14.6	4.4	50
5	25/MAR/86 13:10:11.5	E. OFF FUKUSHIMA PREF.	37 08.6	141 27.8	4.4	50
6	04/JUL/86 08:28:54.7	E. SAITAMA PREF.	35 52.1	139 26.9	4.9	150
7	09/JUL/86 01:17:57.7	W. KANAGAWA PREF.	35 13.5	139 05.7	4.1	15

Table 4-3. List of earthquake observation station

No	LOCATION		LAT.	LONG.
1*	KAWASAKI	(KWS)	35 30.5	139 42.7
2*	OHOKAYAMA	(OKY)	35 36.3	139 40.9
3**	TAKADA	(TKD)	35 33.2	139 37.4
4**	NAKAGAWA	(NKG)	35 32.8	139 35.4
5**	KAWAWA	(KWW)	35 32.0	139 33.3
6*	NAGATSUTA	(NGT)	35 30.6	139 29.3
7*	ASAKAWA	(ASK)	35 38.1	139 17.0

* STATIONARY STATION
**TEMPORARY STATION

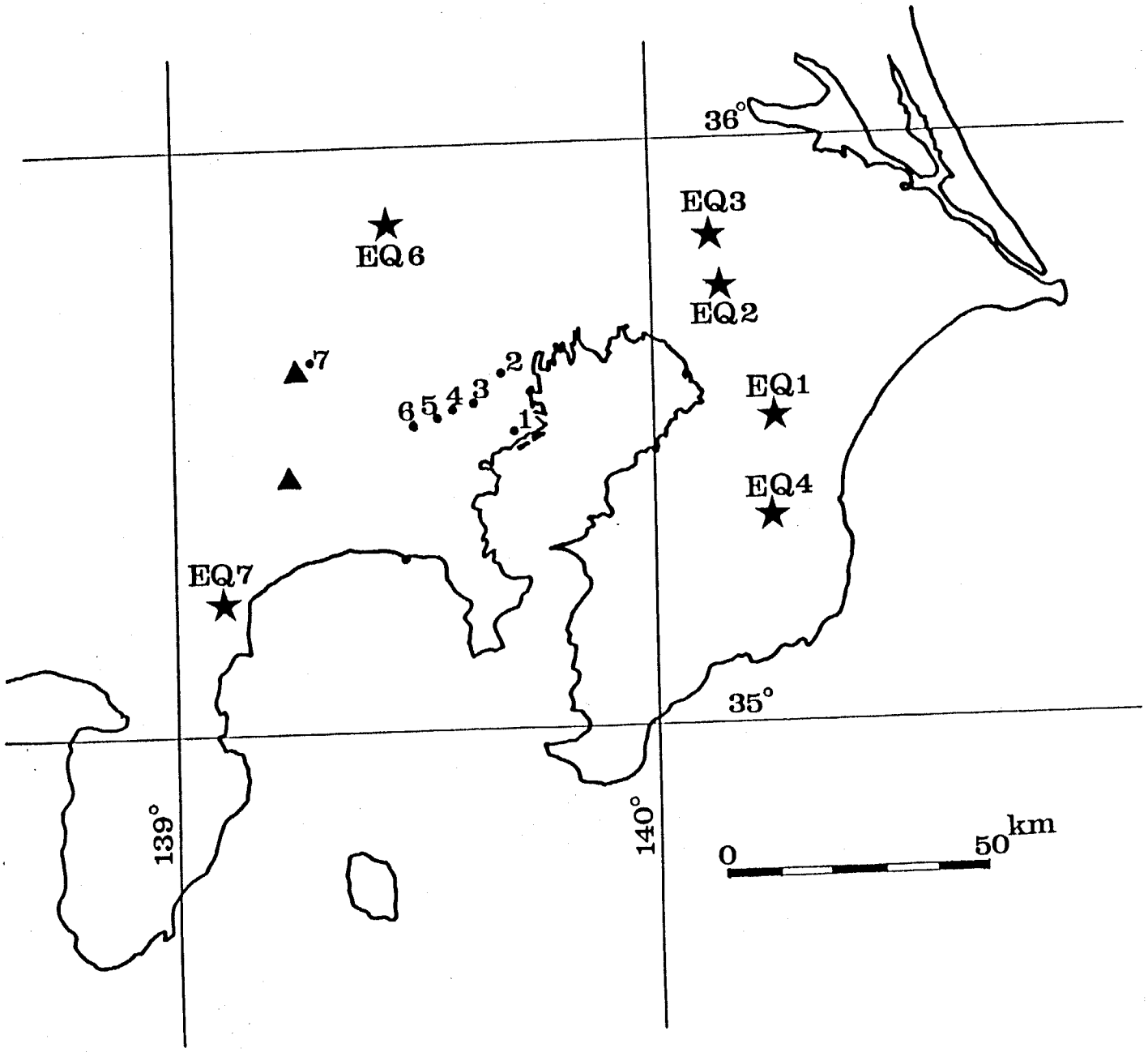

Fig. 4-6. Location of earthquake observation stations and epicenters observed at the stations.

seismograms in the NS direction are shown in Fig. 4-7. They have complex features, maybe, according to the source process which can be speculated as a cause to the main part of the initial S-wave with a period of about two sec. This kind of ground motions is not suitable for the investigation which we are going to do, because they make it difficult to identify the later phases clearly. In the following, the seismograms observed during a)deep earthquakes and b)shallow earthquake are investigated with respect to the later phases.

(a) Seismograms of deep earthquakes

At first, we pay our attention to the seismograms observed during an earthquake in the central Chiba region, EQ1. The observed velocities are shown in Fig. 4-8. Since the seismogram at TKD is over-scaled, all traces in Fig. 4-8 are polarized in a direction of 11 ° east from the north. The direction, as a result, can be almost regarded as the transverse direction. The initial S-phases obtained at OKY and TKD show considerably simple wave forms with durations of around one sec. Although the initial S-phase at KWW shows also the same characteristic, a large later phase (Phase B in Fig. 4-8) ,whose amplitude is 2 to 3 times larger than that of the initial phase (Phase A), can be seen approximately one sec after the initial phase. The one-sec travel time delay of S-wave is considered approximately to correspond to the 0.5-sec time delay of P-wave; it is consistence with the delay seen in the explosion seismograms as discussed before. This large later phase can not be found in the seismograms at any other stations in the array. Since the focal depth of the earthquake is relatively deep as 64 km and the epicentral distance is short as around 60 km, it can be regarded that the seismic wave incidents almost vertically to the sedimentary layers from the basement. Therefore, the underground structure just beneath the KWW station would be a cause of the later phase at KWW. As for the radial component as shown in Fig. 4-9, the later phase can not be clearly seen. The initial phase, however, seems to have a long duration; this suggests the arrival of the later phase.

Ground motions observed during the other earthquakes are shown in Fig. 4-10 to Fig.4-13. Fig. 4-10 shows the nearly radially polarized velocities obtained during EQ4:

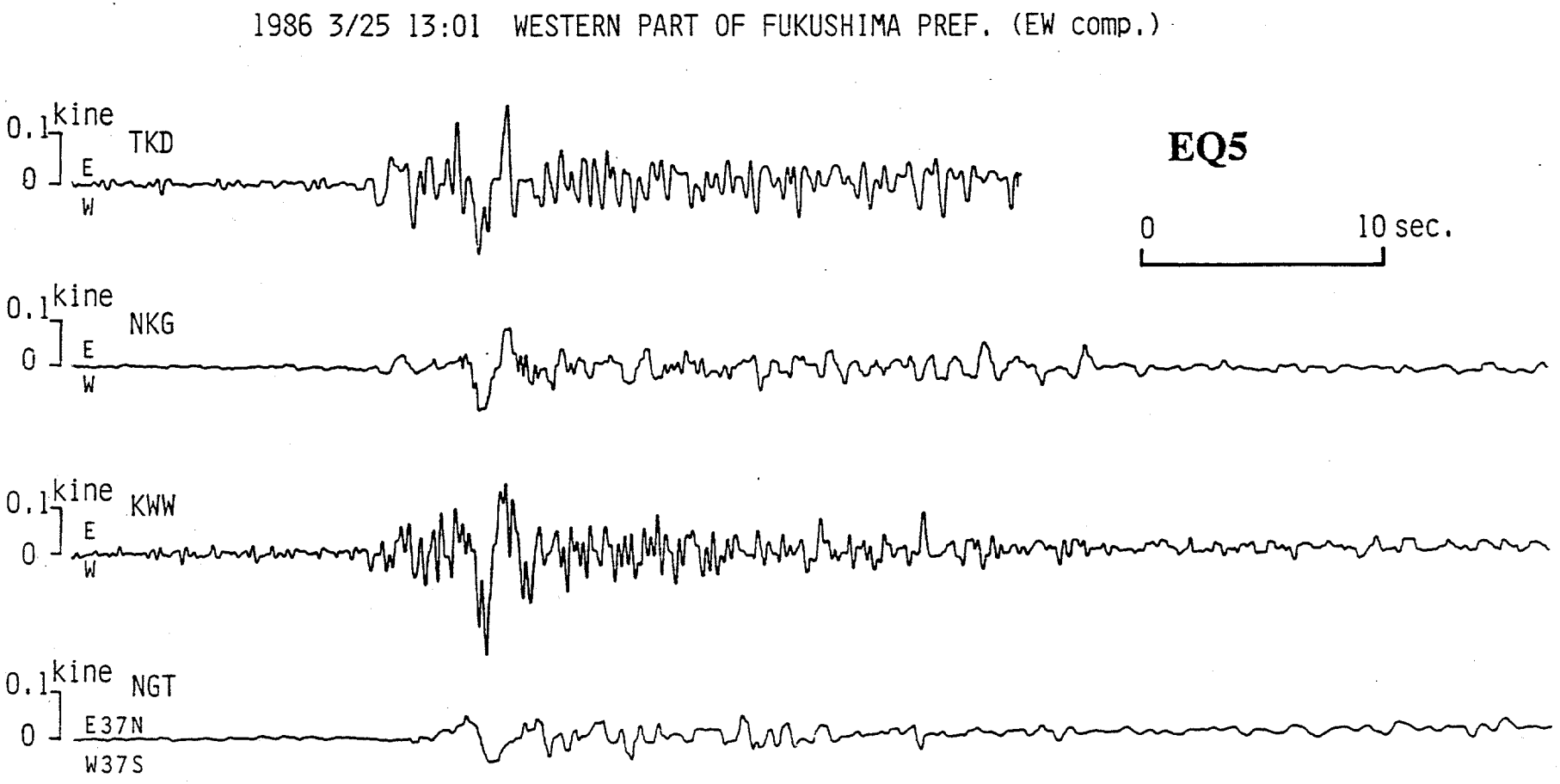

Fig. 4-7. Seismograms observed in a seismic array during a earthquake of 25/MAR/1986 (EQ5). Each trace indicate transversely polarized velocity.

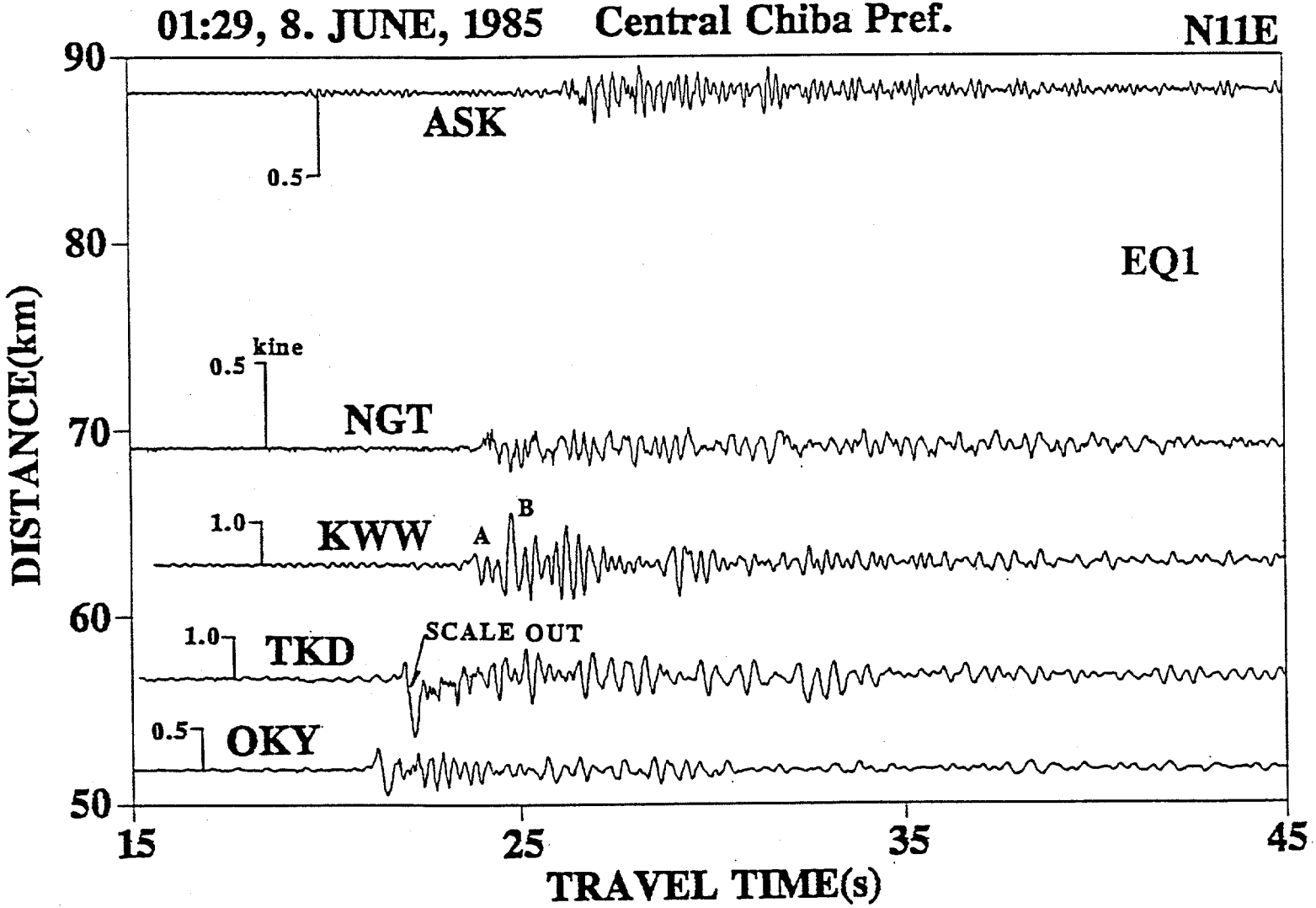

Fig. 4-8. Seismograms observed in a seismic array during a earthquake of 8/JUN/1986 (EQ1) Each trace indicate nearly transversely polarized velocity.

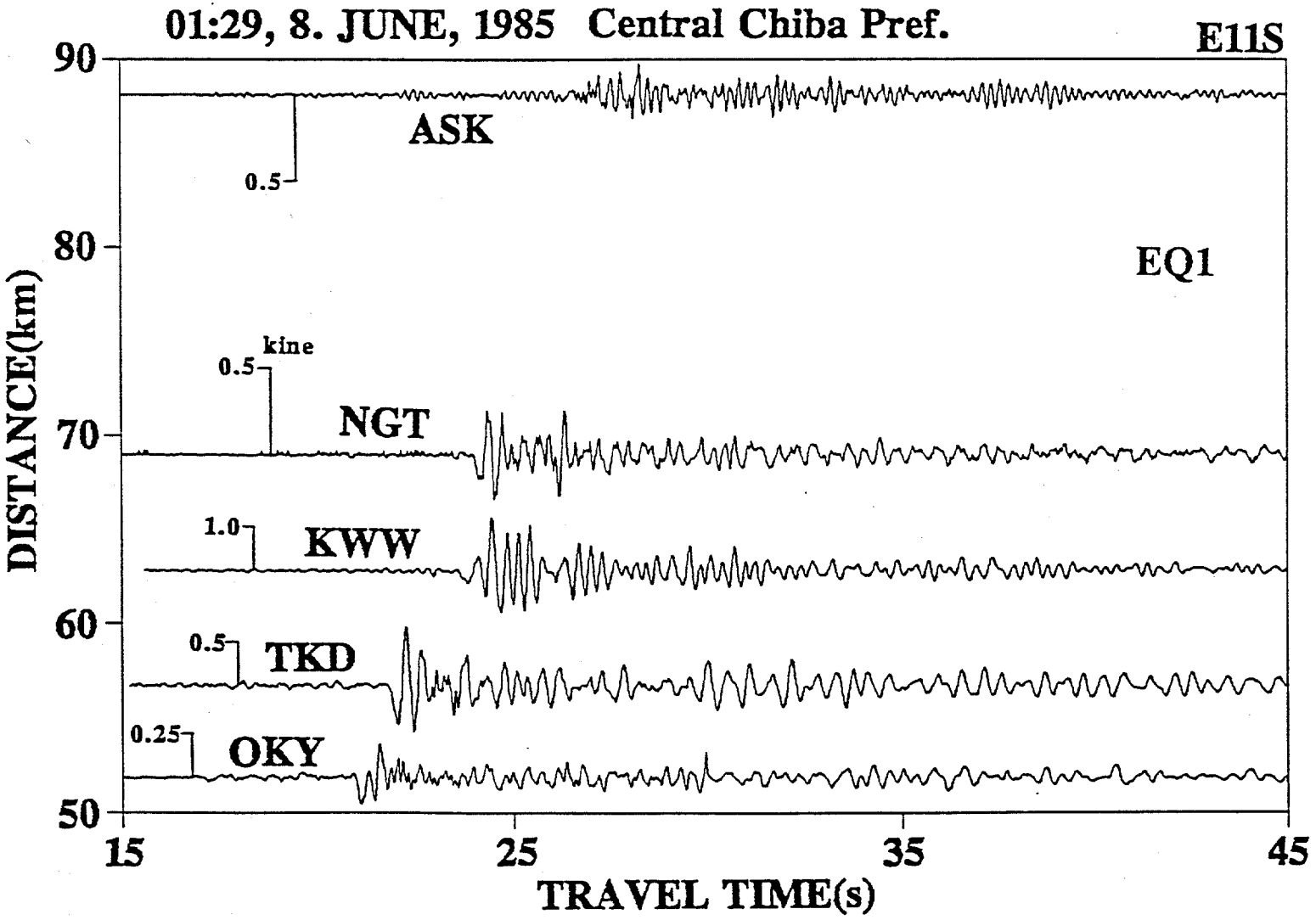

Fig. 4-9. Seismograms observed in a seismic array during a earthquake of 8/JUN/1985 (EQ1). Each trace indicate nearly radially polarized velocity.

earthquake in the central Chiba region. The location of the hypocenter is almost the same as EQ1. Unfortunately, the nearly transverse velocity at KWW is over-scaled. We can see two phases in the initial portion of the S-wave arrival at KWW. The transverse velocities from earthquakes whose epicenters are located in the northern Chiba region are shown in Figs. 4-11 and 4-12. The later phase about one second after the initial S-wave can be seen in the seismogram of EQ3 at KWW in Fig. 4-12. Although the initial phase is small and not clear, the distinct later phase can be also seen in the seismogram of EQ2 at KWW. These observational facts indicate that the later phase just after the initial phase can be well observed during a deep earthquake occurred in the eastern side of the array. On the other hand, no distinct later phases can be clearly found in the seismograms obtained at KWW during EQ6 which occurred in the northern region of the array. Fig. 4-13 shows the transverse velocities of EQ6: earthquake in the northern Saitama region. As the clocks could not be calibrated at some stations during this earthquake, the absolute time was not recovered. Hence, all traces in the figure are not synchronized. These records suggest that the appearance of the later phase depends on the propagation direction of the initial phases.

(b) Seismograms of shallow earthquake

Only one shallow earthquake was observed in the array during the observational period. EQ7 is an earthquake which occurred in the western Kanagawa region, the western side of the array, with a focal depth of 20 km. The transversely polarized velocities are shown in Fig. 4-14. Because the initial phases at all the stations are impulsive, they can be easily identified as indicated by open circles in the figure. The later phase having amplitude two to three times larger than that of the initial phase can not be found in the seismogram obtained at KWW, as well as the other stations.

Since the focal depth of the earthquake is shallow, the incident angle of the initial phase to the sedimentary layers is no longer vertical; the initial phases incident somewhat obliquely. Moreover, they propagate from the west to the stations: just opposite to the propagation direction of the seismic waves from EQ1 as mentioned before. Therefore, it is

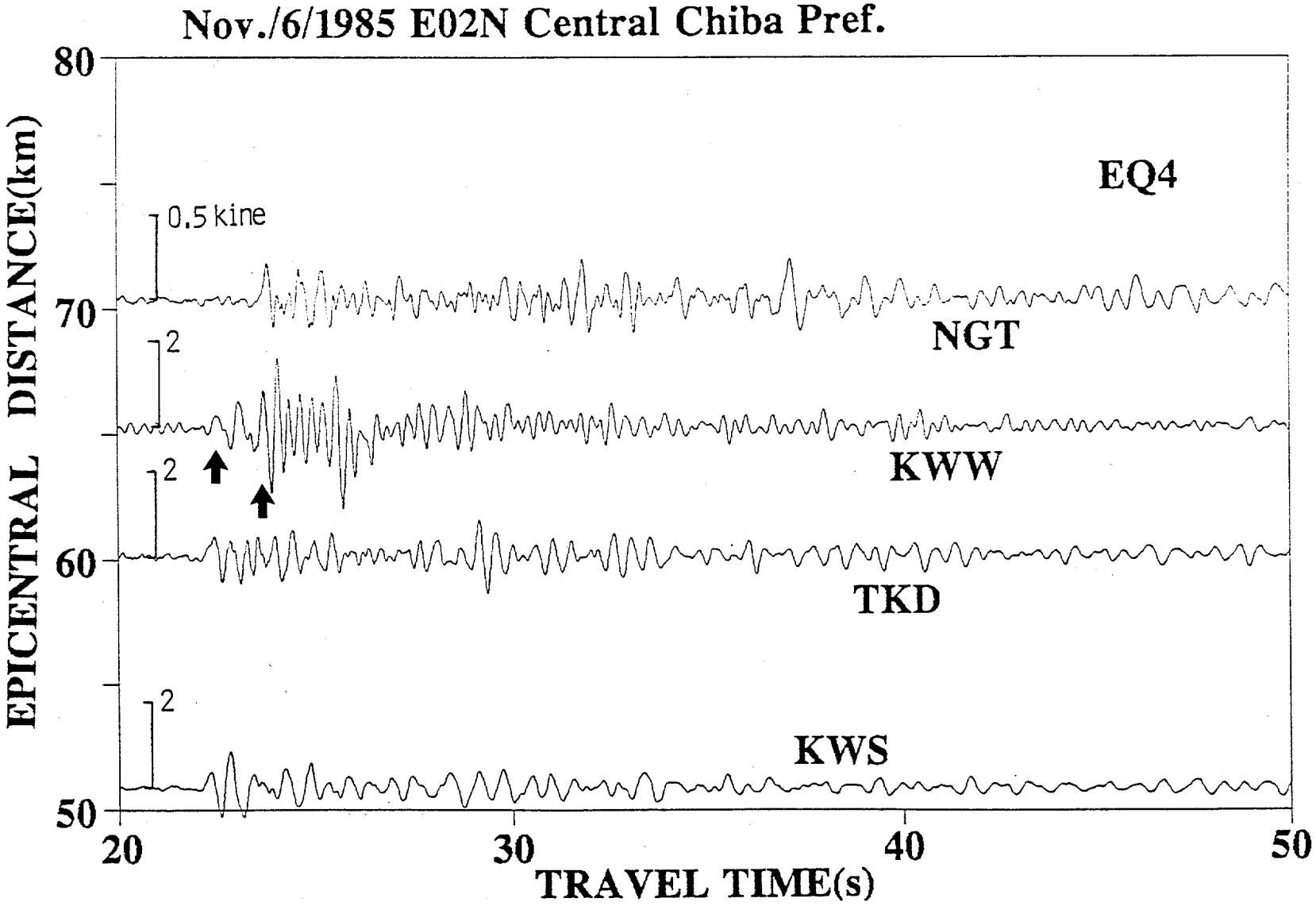

Fig. 4-10. Seismograms observed in a seismic array during a earthquake of 6/NOV/1985 (EQ4). Each trace indicate radially polarized velocity.

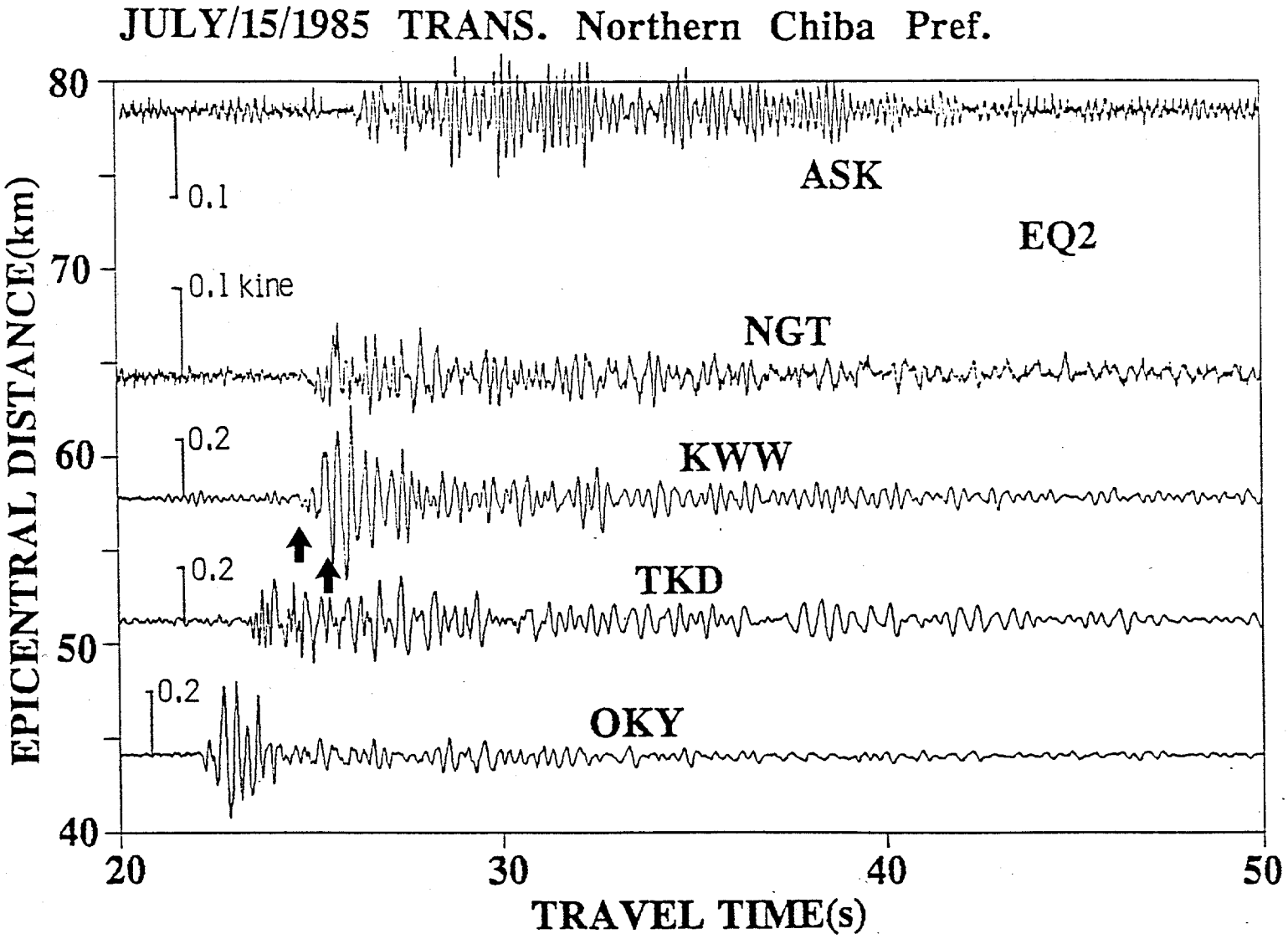

Fig. 4-11. Seismograms observed in a seismic array during a earthquake of 15/JUL/1985 (EQ2). Each trace indicate transversely polarized velocity.

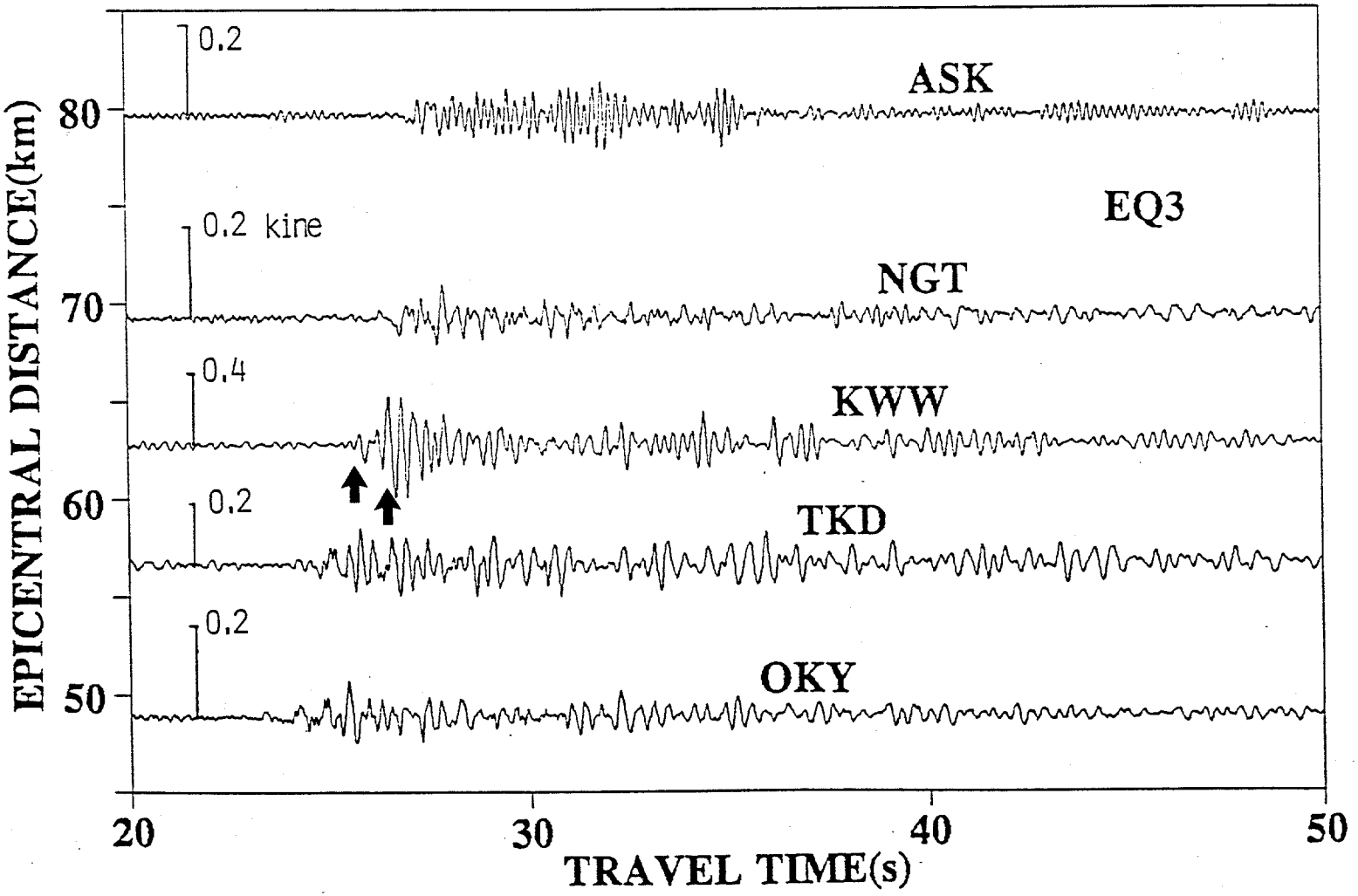

Fig. 4-12. Seismograms observed in a seismic array during a earthquake of 11/OCT/1985 (EQ3). Each trace indicate transversely polarized velocity.

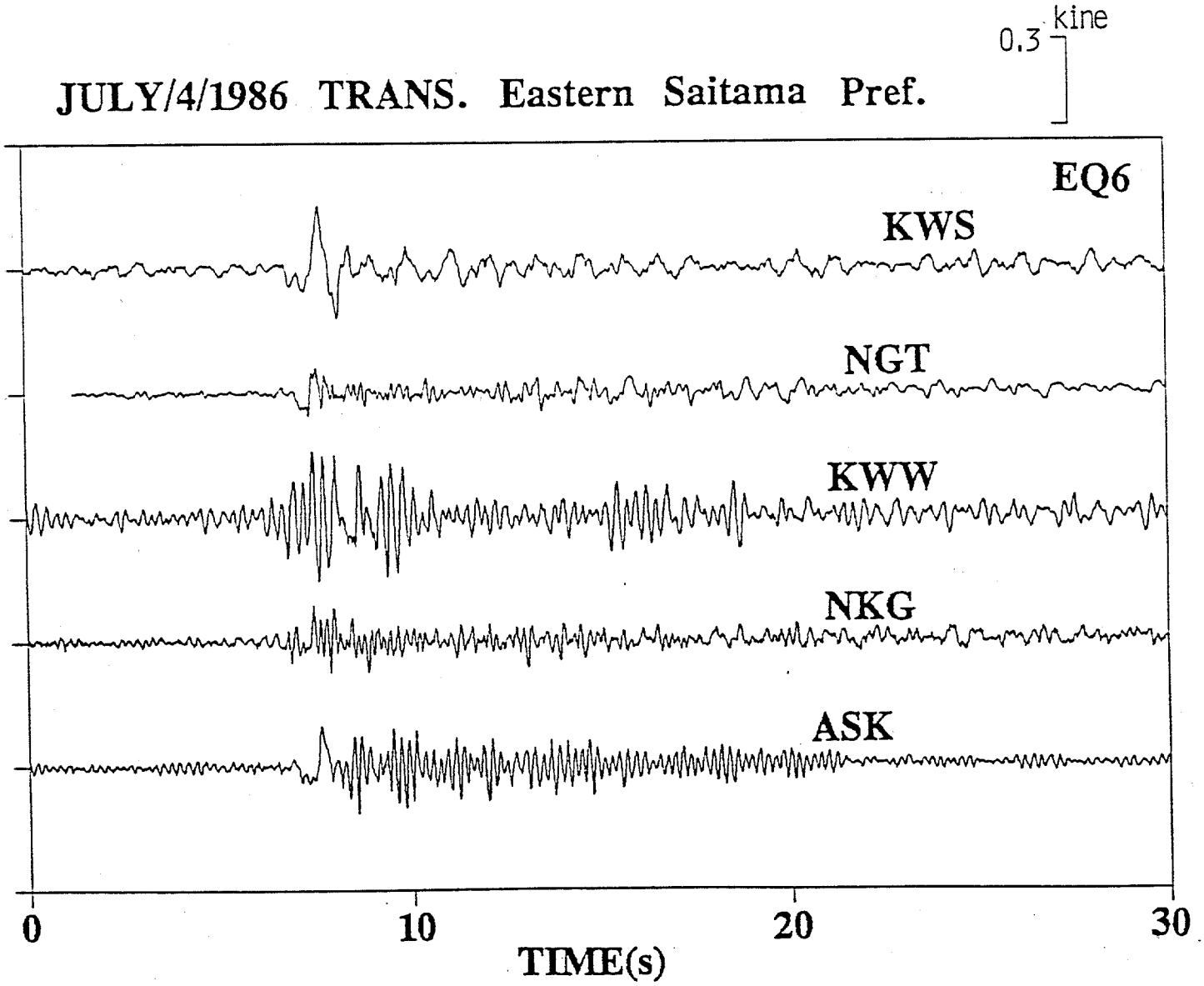

Fig. 4-13. Seismograms observed in a seismic array during a earthquake of 4/JUL/1986 (EQ6). Each trace indicate transversely polarized velocity.

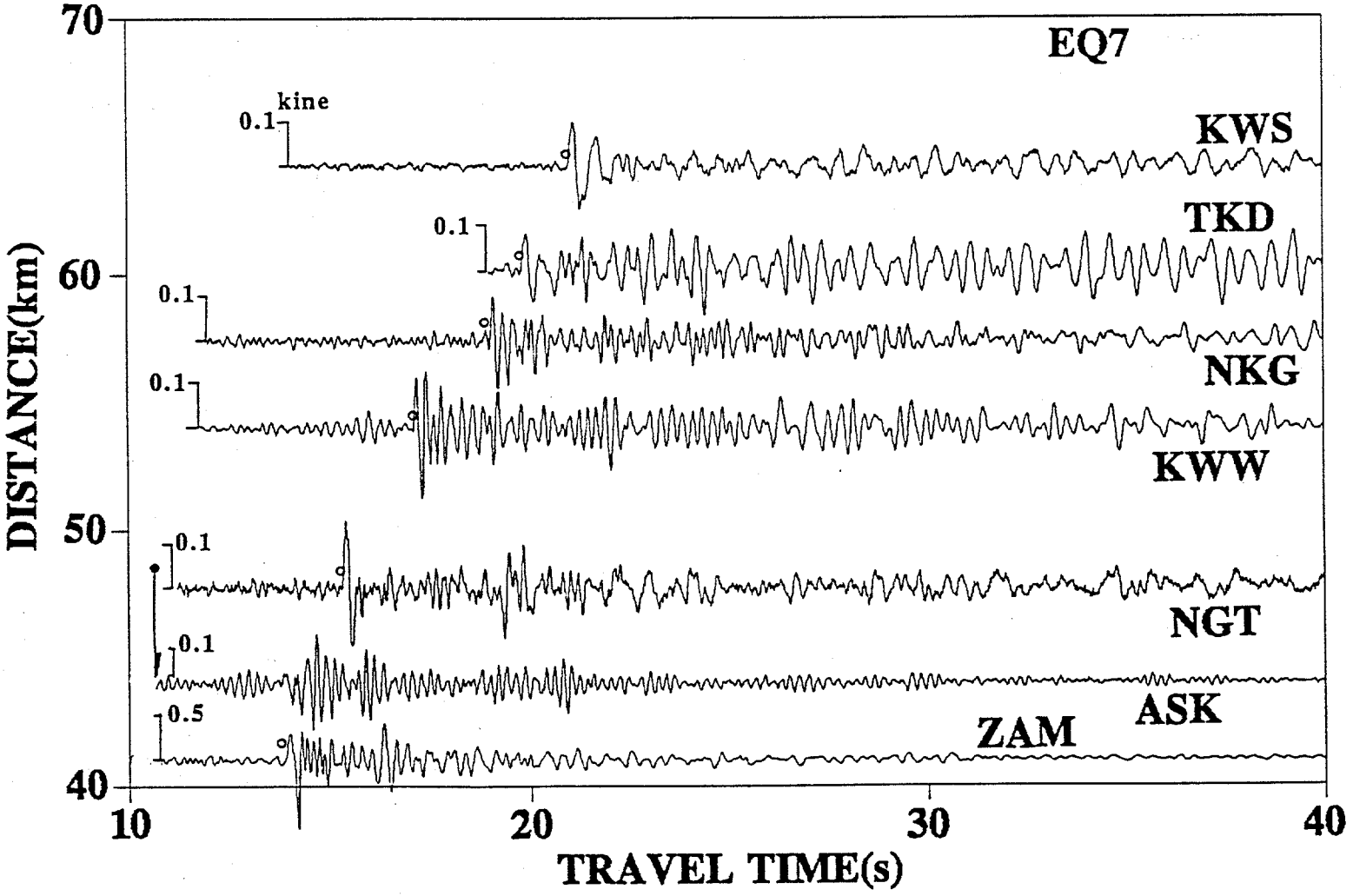

Fig. 4-14. Seismograms observed in a seismic array during a earthquake of 9/JUL/1986 (EQ7). Each trace indicate transversely polarized velocity.

considered that the behavior of the distinct later phase just after the initial phase depends on the propagation direction and the incident angle.

4.2.3 Elimination of the effects of superficial layers

In the seismic surveys discussed in chapter two, the layer with a P-wave velocity of 1.8 km/sec, corresponding to 0.7 km/sec in an S-wave velocity, was regarded as the top layer. In fact, there are superficial layers overlaying the top layer with a P-wave velocity of 1.8 km/sec. As far as we consider ground motions in the longer period range, effects of such layers are negligible. On the contrary, it is considered that these layers affect short period ground motions. In particular, amplitudes are strongly amplified. It is , however, permissible to assume that superficial layers have little effects on propagations of phases in short periods as it is discussed here and in chapter three. In order to confirm this, the effects of superficial layers having S-wave velocities less than 0.7 km/sec are eliminated by simple one-dimensional multiple reflections.

It is very difficult to eliminate the effects of superficial layers from ground motions observed on the free surface exactly. We, here, assume that seismic waves incident vertically to the superficial layers from the layer with an S-wave velocity of 0.7 km/sec and the superficial layers extend horizontally to the infinite. Under these assumptions, the influences of the superficial layers can be easily estimated by one-dimensional multiple reflections of S-waves propagating vertically.

S-wave profiles to a depth of the top of the layer with an S-wave velocity of 0.7 km/sec are not known at all the stations of interest. The available data rely on geotechnical measurements to a layer with a standard penetration test (SPT) N-value more than 50. At first, S-wave profiles were supposed from the geotechnical data. Several empirical correlations between S-wave velocities and the other geotechnical data were proposed by Ohta and Goto (1976). In this study, the following empirical equation for deducing an S-wave velocity (Vs: m/sec) from SPT N-value (N) and depth (H: meter) was used,

$$V_s = 61.62N^{0.254}H^{0.222} \tag{4-1}$$

We assumed the S-wave velocity for the bottom layer with a SPT N-value more than 50 is 0.7 km/sec, except for the ASK station. There are superficial layers just over the basement with an S-wave velocity of 2.5 km/sec at ASK. Therefore, the S-wave velocity for the bottom layer was set as 2.5 km/sec at ASK. Quality factors (Q) were assumed to be

$$Q \doteq \frac{V_s}{15} \tag{4-2}$$

Density was set as 1.7 or 1.8 g/cm**3, according to STP N-value.

After the S-wave profile has been made, transfer function due to multiple reflections of vertical incidence of S-wave was calculated in the frequency domain. Then, the spectra of the observed records were multiplied by the inverse of the transfer function in the frequency domain. Finally, corrected seismograms were obtained through an inverse Fourier transformation back to the time domain. At the same time, the filter cutting frequencies higher than 10 Hz was applied. Resultant seismograms are considered to correspond to ground motions on the top of the layer having an S-wave velocity of 0.7 km/sec, except for those at the ASK station.

The S-wave profiles assumed and transfer functions due to vertical incidence of plane S-wave at the stations of interest are shown in Figs. 4-15. The S-wave velocities at OKY and NGT were directly obtained by board banging measurements. As seen in the figures, the superficial layers have no significant influences on ground motions in a period range more than one sec. The large amplification factor at a period of 0.24 sec appears in transfer function for the ASK station. In seismograms observed at the ASK station, we can also find strong high frequency ripples which correspond to the large amplification factor. Therefore, it is permissible to consider ground motions observed at ASK as those on the free surface of the basement, except for the ripples.

The seismograms from EQ1 and EQ7 were processed here, because they exhibit clearly the important features as discussed before. The traces in Fig. 4-16 indicate the processed seismograms of EQ1. The trace at TKD is the original record, since it is over-scaled.

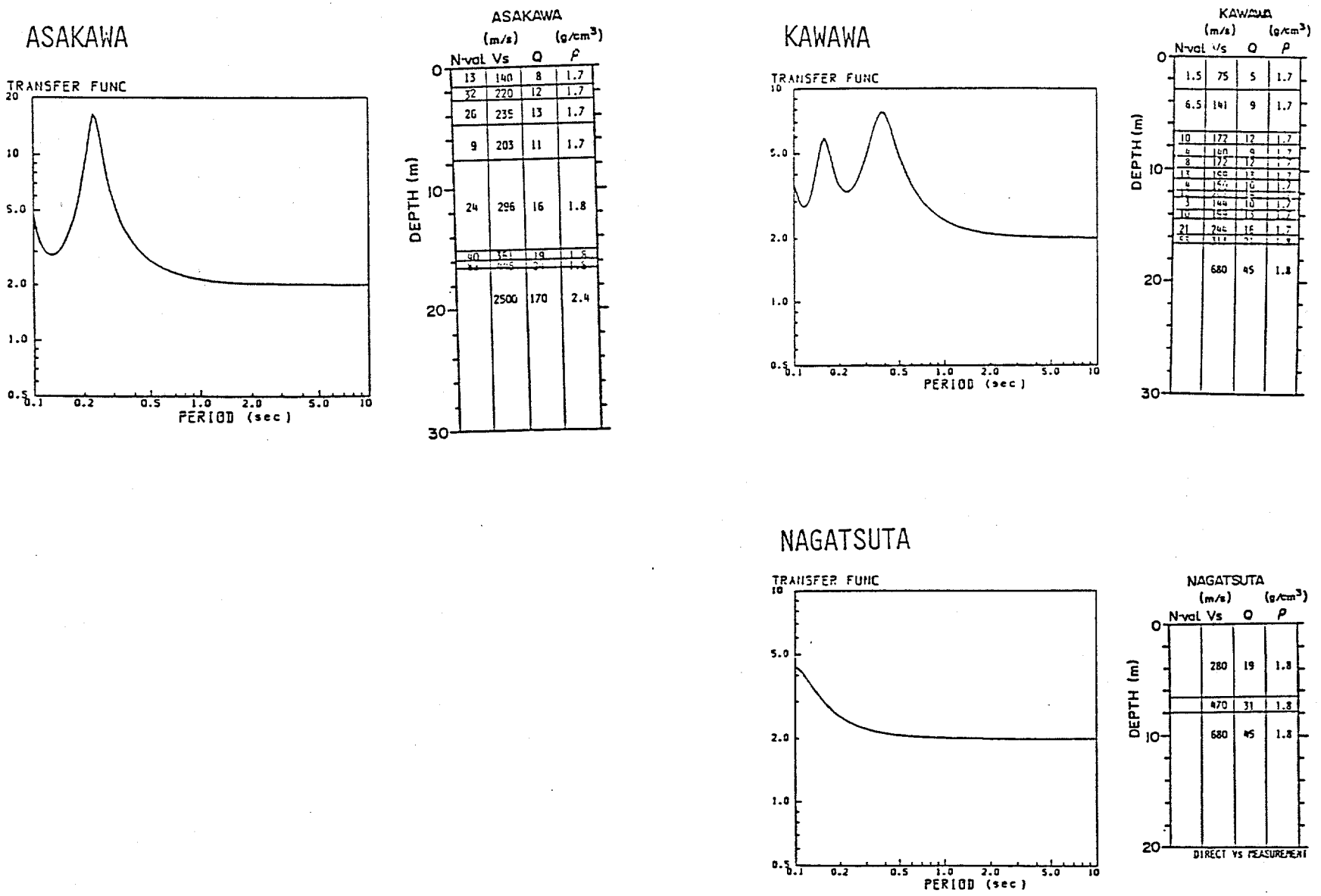

Fig. 4-15. Structure of superficial layers with S-wave velocities less than 0.7 km/sec at the stations in Fig. 4-6 and their amplification factors.

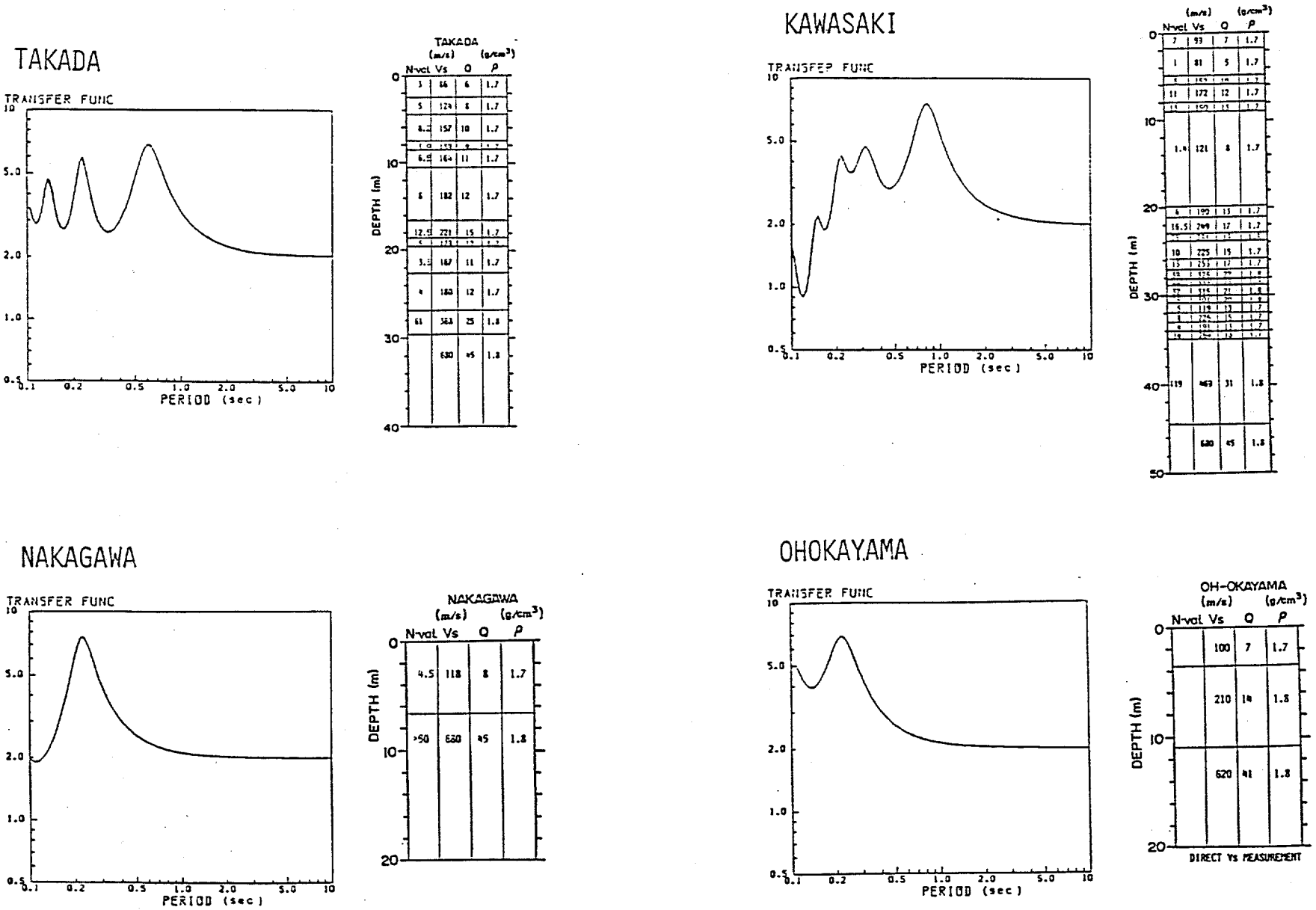

Fig. 4-15. Structure of superficial layers with S-wave velocities less than 0.7 km/sec at the stations in Fig. 4-6 and their amplification factors (continued).

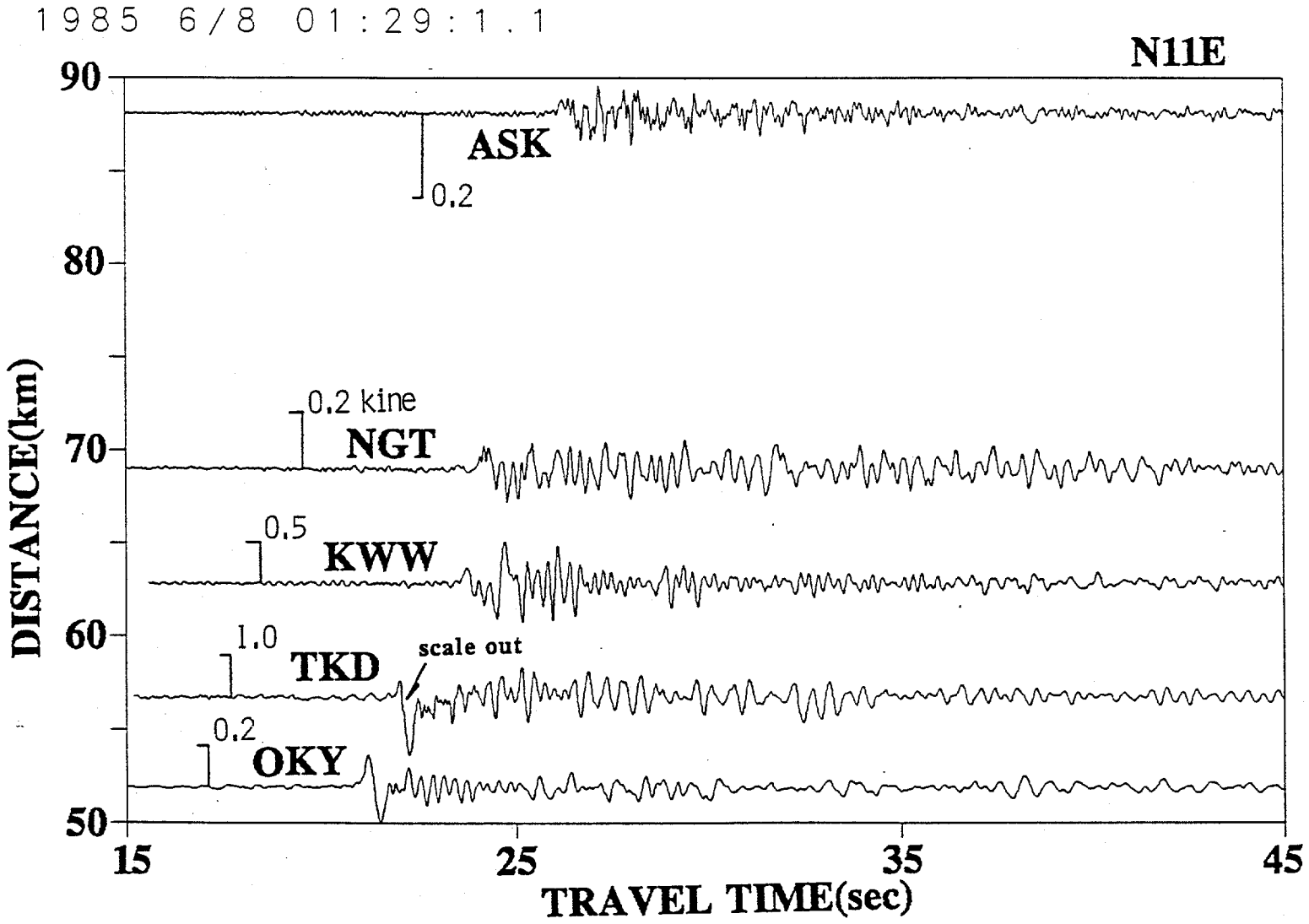

Fig. 4-16. Nearly transverse velocities of earthquake of 6/JUN/1985 after elimination of effects of superficial layers.

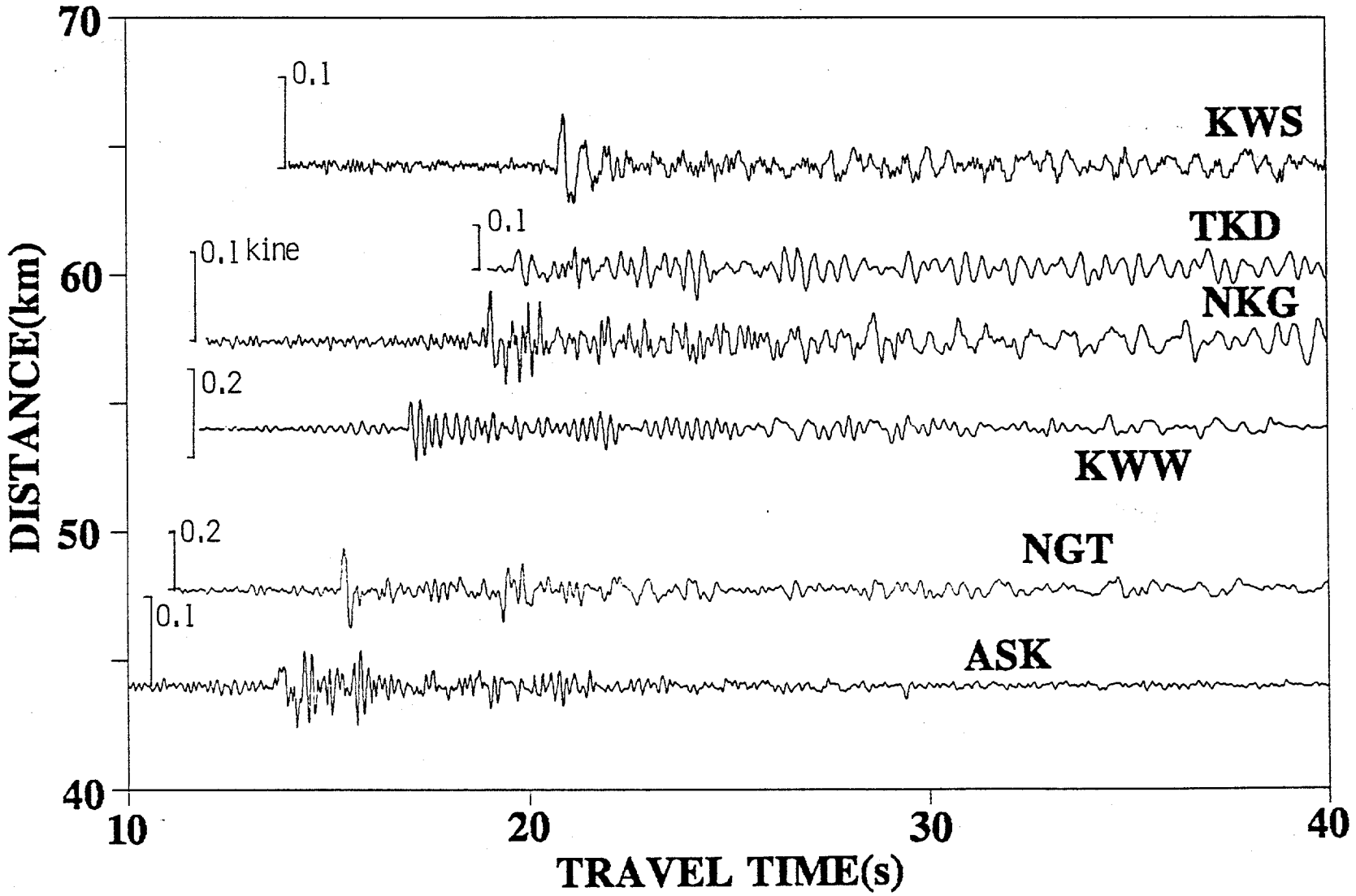

Fig. 4-17. Transverse velocities of earthquake of 9/JUL/1986 after elimination of effects of superficial layers.

It can be seen that the high frequency components are diminished and wave forms are slightly different from the original traces. However, the fundamental characters of the traces are the same as the original ones. The large later phase one-sec after the initial S-wave can be clearly seen in the processed record at KWW. Fig. 4-17 shows the transversely polarized velocities after the above processings. The processed traces have the same features as the original ones and we can not find no later phases which can be seen in the record at KWW during EQ1.

These simple consideration lead us to confirm that the superficial layers can not be a cause of the large later phases in the seismogarms at KWW.

4.3 Interpretation for the Later Phases by Numerical Modeling

In this section, numerical forward modelings are carried out to understand the nature of the later phases identified in the seismograms discussed in the previous sections.

4.3.1 Finite difference modeling

In this study, a finite difference method is employed to interpret the later phases, because of its simplicity. The finite difference method is a purely numerical method for solving differential equations in an algebraic way and has been successfully applied to many seismological problems (e.g. Boore, 1972; Kelly et al., 1976).

The two-dimensional SH-wave equation in a homogeneous medium can be written as

$$\rho \frac{\partial^2 u}{\partial t^2} = \mu\left(\frac{\partial^2 u}{\partial x^2} + \frac{\partial^2 u}{\partial z^2}\right) \tag{4-3}$$

where u is displacement and ρ and μ are density and rigidity of the medium, respectively. Each derivative in the wave equation with respect to time and space is replaced by the following central difference approximation;

$$\frac{\partial^2 u}{\partial t^2} = \frac{1}{dt^2}\left(u^{l-1}_{m,n} - 2u^{l}_{m,n} + u^{l+1}_{m,n}\right) \tag{4-4}$$

$$\frac{\partial^2 u}{\partial x^2} = \frac{1}{dx^2}\left(u^{l}_{m-1,n} - 2u^{l}_{m,n} + u^{l}_{m+1,n}\right) \tag{4-5}$$

$$\frac{\partial^2 u}{\partial z^2} = \frac{1}{dz^2}(u^l_{m,n-1} - 2u^l_{m,n} + u^l_{m,n+1}) \tag{4-6}$$

where dx , dz are spacings of grids in x and z direction and dt is interval of time. When the two grid spacings are equal, we denote the displacement in certain position at certain time steps in the following way;

$$u(mh, nh, ldt) = u^l_{m,n} \tag{4-7}$$
$$h = dx = dz$$

Then, substitution of equations (4-4) to (4-6) into (4-3) gives

$$u^{l+1}_{m,n} = -u^{l-1}_{m,n} + \gamma^2(u^l_{m+1,n} + u^l_{m-1,n} + u^l_{m.n+1} + u^l_{m,n-1}) + 2(1-2\gamma^2)u^l_{m,n} \tag{4-8}$$

where;

$$\gamma = \frac{\beta dt}{h}, \quad \beta = \sqrt{\mu/\rho}$$

According to this explicit form of the wave equation, the displacement at new time step $l+1$ can be derived from those at the previous time step l and $l-1$.

In inhomogeneous media, boundary conditions between grids are imposed. The following formulation after Korn and Stoeckl(1982) was used in this study. Assuming that a horizontal interface divides upper medium 1 and lower medium 2 at $z=(N+\frac{1}{2})h$, the following boundary conditions for continuities of stress and displacement have to be satisfied at the interface;

$$u_1 = u_2 , \quad \mu_1 \frac{\partial u_1}{\partial z} = \mu_2 \frac{\partial u_2}{\partial z} \tag{4-9}$$

We assume the virtual displacement as $\hat{u}_{m,N+1}$ in Fig. 4-18. $\hat{u}_{m,N+1}$ is placed at $z=(N+1)h$ indicating displacement with the assumption that the upper medium still continue under the boundary. Then, the formulation in homogeneous medium can be applied to the relation between $u_{m,N}$ and $\hat{u}_{m,N+1}$. Stress at the boundary can be expressed by the central difference approximation;

$$\mu_1 \frac{\partial u_1}{\partial z}\Big|_{z=(N+\frac{1}{2})h} = \frac{\mu_1}{h}(\hat{u}_{m,N+1} - u_{m,N}) \tag{4-10}$$

Calculating the virtual displacement $\hat{u}_{m,N}$ in the upper medium in the same way, the stress

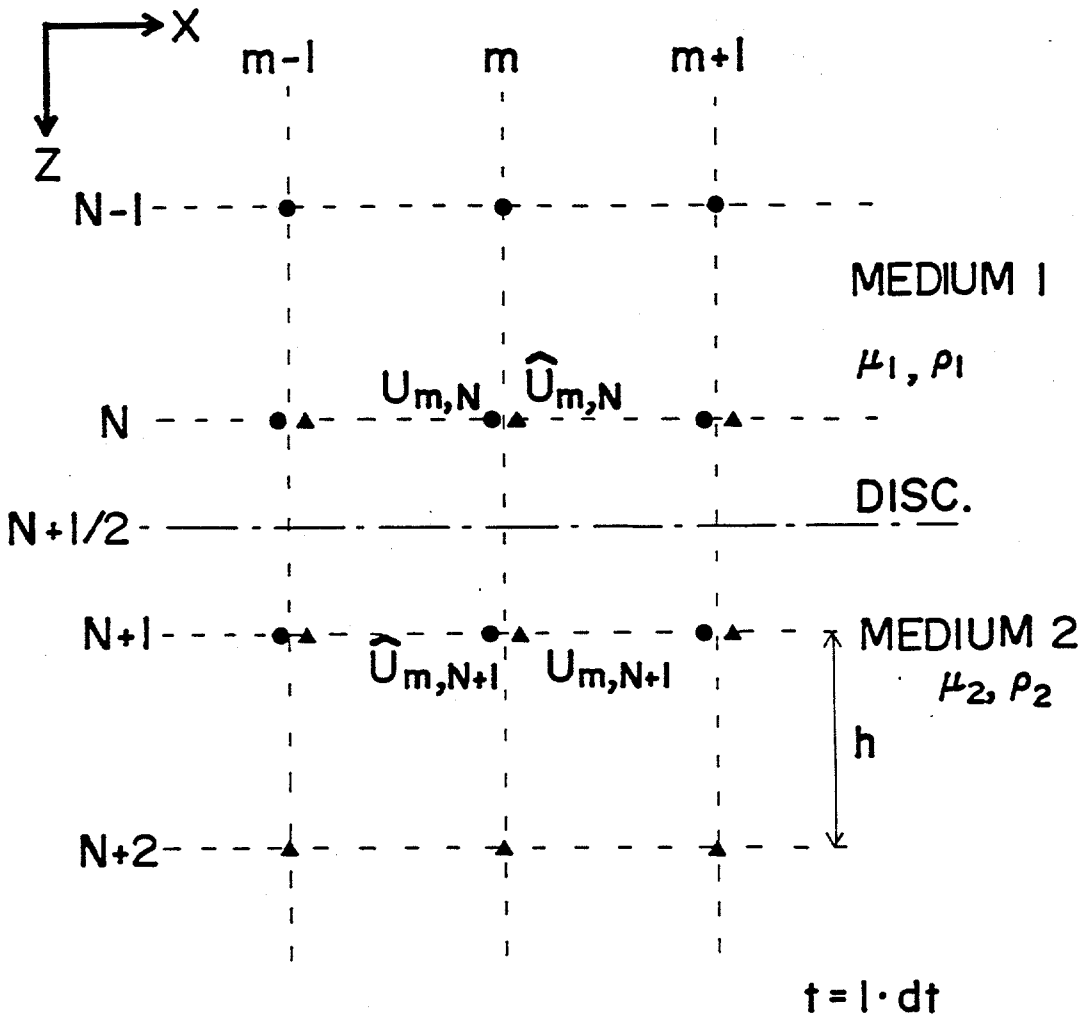

Fig. 4-18. Treatment of continuities of displacement and stress at a boundary in finite difference method.

at the boundary is

$$\mu_2 \frac{\partial u_2}{\partial z} \Big|_{z=(N+\frac{1}{2})h} = \frac{\mu_2}{h}(u_{m,N+1} - \hat{u}_{m,N}) \tag{4-11}$$

From (4-10) and (4-11), the boundary condition on stress is expressed as follows;

$$\frac{\mu_1}{h}(\hat{u}_{m,N+1} - u_{m,N}) = \frac{\mu_2}{h}(u_{m,N+1} - \hat{u}_{m,N}) \tag{4-12}$$

Similarly, the boundary condition on continuity of displacement is written, using the virtual displacements and central difference approximation as;

$$\frac{1}{2}(u_{m,N} + \hat{u}_{m,N+1}) = \frac{1}{2}(\hat{u}_{m,N} + u_{m,N+1}) \tag{4-13}$$

Equation (4-12) and (4-13) yield the representation of the virtual displacements by real displacements as follows;

$$\hat{u}_{m,N} = (2\mu_1 u_{m,N} - (\mu_1 - \mu_2)u_{m,N+1})/(\mu_1 + \mu_2) \tag{4-14}$$

$$\hat{u}_{m,N+1} = (2\mu_1 u_{m,N+1} + (\mu_1 - \mu_2)u_{m,N})/(\mu_1 + \mu_2) \tag{4-15}$$

The same kind of representation for vertical interface can be obtained similarly. Then, four virtual points surround a real grid point. Since all the virtual points were assumed to exist in the same medium, the finite difference formulation for homogeneous medium (4-8) can be used as a relation between displacement at a grid point of interest and the virtual displacements at grid points surrounding it. Finally, after eliminating virtual displacements by employing the relation between real and virtual displacements, the finite difference formulation for inhomogeneous media can be obtained as follows;

$$= -u_{m,n}^{l-1} + 2\left(\frac{\beta_{m,n} dt}{h}\right)^2 [M_1(u_{m+1,n}^l - u_{m,n}^l) - M_2(u_{m,n}^l - u_{m-1,n}^l) + M_3(u_{m,n+1}^l - u_{m,n}^l) - M_4(u_{m,n}^l - u_{m,n-1}^l)] + 2u_{m,n}^l$$

$$M_1 = \frac{\mu_{m+1,n}}{\mu_{m+1,n} + \mu_{m,n}}, \quad M_2 = \frac{\mu_{m-1,n}}{\mu_{m-1,n} + \mu_{m,n}} \tag{4-16}$$

$$M_3 = \frac{\mu_{m,n+1}}{\mu_{m,n+1} + \mu_{m,n}}, \quad M_4 = \frac{\mu_{m,n-1}}{\mu_{m,n-1} + \mu_{m,n}}$$

According to this formulation, each grid point can have arbitrary rigidity and density and the displacement at a grid point is expressed by using those at the grid point and the grid

points surrounding it in the two previous time steps. If the initial displacements at $l=1, 2$ are given, we can recursively solve the two dimensional inhomogeneous wave equation at any other time steps by a time marching process.

Both in the finite difference method and in the finite element method, the generation of undesired reflections from artificial boundaries of the computation model is the most important problem and several methods have been proposed to eliminate them. In this study, the artificial boundaries of the model were dealt as absorbing boundaries based on the method proposed by Reynolds(1978). This formulation is based on the paraxial approximation of the wave equation. For example, at the bottom artificial boundary, the displacement is obtained so that the following equation is satisfied.

$$\frac{1}{\beta}\frac{\partial^2 u}{\partial t \partial z}+\frac{\partial^2 u}{\partial z^2}+\left(\frac{\gamma}{1+\gamma}\right)\frac{\partial^2 u}{\partial z^2}=0 \qquad (4\text{-}17)$$

This is approximated as follows:

$$u_{m,N+1}^{l+1}=u_{m,N+1}^{l}+u_{m,N}^{l}-u_{m,N}^{l-1}+\gamma\left(u_{m,N+1}^{l}-u_{m,N}^{l}-\left(u_{m,N}^{l-1}-u_{m,N-1}^{l-1}\right)\right) \quad 2\le m\le M \qquad (4\text{-}18)$$

During the computations, the following stable conditions for the grid spacing (h) and the time increment (dt) must be satisfied to avoid numerical dispersion and divergence.

$$h \le \frac{\lambda_0}{10-15} \qquad (4\text{-}19a)$$

$$dt \le \frac{h}{\sqrt{2}\,\beta_{max}} \qquad (4\text{-}19b)$$

where λ_0 is wave length considered and β_{max} is maximum velocity in the model.

4.3.2 Interpretation for the later phases in explosion seismograms

Here, the later phases of the explosion seismograms are interpreted using the finite difference forward modeling. Since major phases radiated by explosion can be considered as P-waves, the finite difference formulation for acoustic wave field was used; SV-waves and Rayleigh-waves were neglected. Although anelasticity is a crucial factor to describe the behavior of short period seismic waves, the effects were not taken into account in the

computations.

The used model is displayed in Fig. 4-19. Since the principle object of this modeling is to interpret the cause of the later phases and to understand wave propagation phenomena in an underground structure with a step-like topography of basement, such a simple underground structural model was made. The model is 9.0 km long and 2.0 km deep, and consists of a surface layer and a basement which is down-thrown 1 km to the right side. The P-wave velocities and the densities of the surface layer and the basement are 2.0, 2.1 and 5.0 km/sec, 2.5 g/cm**3, respectively. The four artificial boundaries of the model were dealt the absorbing boundaries (Reynold 1978). Although the free stress condition should be imposed on the upper surface for realistic situations, the absorbing boundary condition was applied to suppress the multiple reflections within the surface layer which might overshadow the step's effects.

The source was set at 0.36 km deep. Actually, the Yumenoshima explosion was fired at a depth of 0.1 km and approximately 30 km away from the stations of interest. The applied source time function is;

$$f(t)=\sin(\frac{2\pi}{T_0}t)-\frac{1}{2}\sin(\frac{4\pi}{T_0}t) \qquad t<T_0 \qquad (4\text{-}20)$$

where t is time and T_0 was taken as 0.15 sec. The function is displayed in Fig. 4-20. The grid spacing and the time increment were set 0.02 km and 0.002828 sec, respectively, according to the criteria of (4-19).

The synthetic seismograms on the upper surface are shown in Fig.4-21. Each trace is normalized to the maximum value of all the traces. Only a large phase can be seen in the synthetic seismograms. The large phase is a superposition of the direct wave and the phase reflected from the interface between the surface layer and the basement. The other phases do not have large amplitudes. For example, the amplitude of the refracted wave (i.e., head wave) which plays an important roll in seismic refraction surveys is considerably small as compared with the direct and the reflected waves. In fact, the difference between the ampli-

tudes of the refracted wave and the direct wave is not as large as shown in the computational result (cf. seismogarms in Fig. 4-4), when the distance from the source is large. This is probably because the refracted wave, usually, propagates along the basement whose quality factor is higher than that of the surface layer.

The close-up of the region indicated by a dotted square is shown in Fig. 4-22. Travel time curves in Fig. 4-22 are for the rays denoted in Fig. 4-19. D_r and L denote the direct wave and the reflected wave from the interface. R_1 is the refracted wave; the wave form is different from the source time function. It is one of the characteristics of a refracted wave. The initial phase is the refracted wave until it reaches at the step. Then, the diffracted wave at the upper edge of the step (D_1) becomes the initial phase and the arrival time delay appears at distances more than 4.5 km. The amplitude of the diffracted wave from the upper edge in the down-thrown side (right) is considerably larger than that in the up-thrown side (left). This indicates that the behavior of the diffracted wave depends on the direction of propagation and the geometry of the underground structure. Later phase whose amplitude is comparable to or larger than that of the initial phase can be seen at the stations within a distance of 5 km, where the travel time delay appears. This is considered to be the superposition of the diffracted wave at the lower edge (D_2) and the refracted wave traveling along the down-thrown basement (R_2). Because the apparent velocities of these two phases are different, they are apart each other at the stations away from the step. Then, the refracted wave becomes the initial phase at the stations with distances more than around 2 km. These features are just the same as mentioned for the observed explosion seismogarms.

In order to understand the propagation mechanism of the seismic waves visually, the so-called "snapshots," distribution of amplitude at a certain time step, are displayed in Fig. 4-23. In the upper two snapshots at 0.51 and 0.99 sec, we can see the transmitted wave to the basement characterized by a circular wave front. On the other hand, the wave front of the refracted wave is characterized by a plane wave front. The large phases with a low apparent velocity is the contribution of direct and reflected waves. The circular wave front

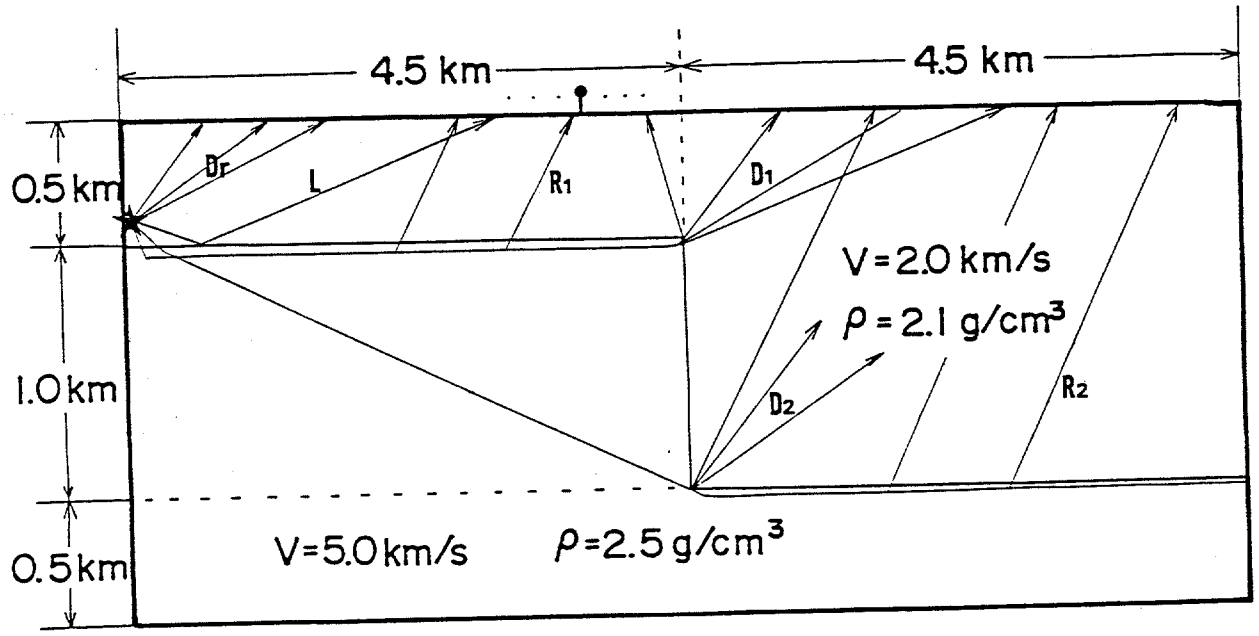

$\Delta X = \Delta Z = 0.02$ km

$\Delta t = 0.002828$ sec.

Fig. 4-19. Underground structural model to interpret the later phases in the explosion seismograms in Fig. 4-4. A line source source is set at the location of the star. Propagation paths of some rays are also shown in the figure.

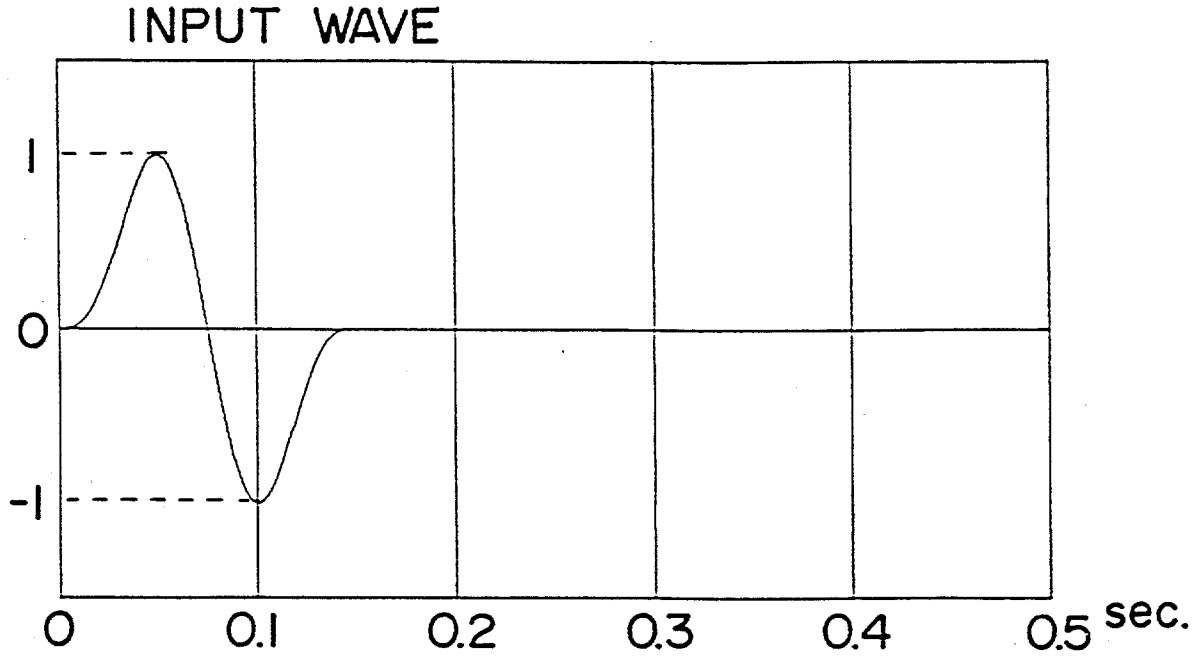

$$\mathrm{SIN}\left(\frac{2\pi}{0.15}t\right)-\frac{1}{2}\mathrm{SIN}\left(\frac{4\pi}{0.15}t\right)$$

Fig. 4-20. Input wave.

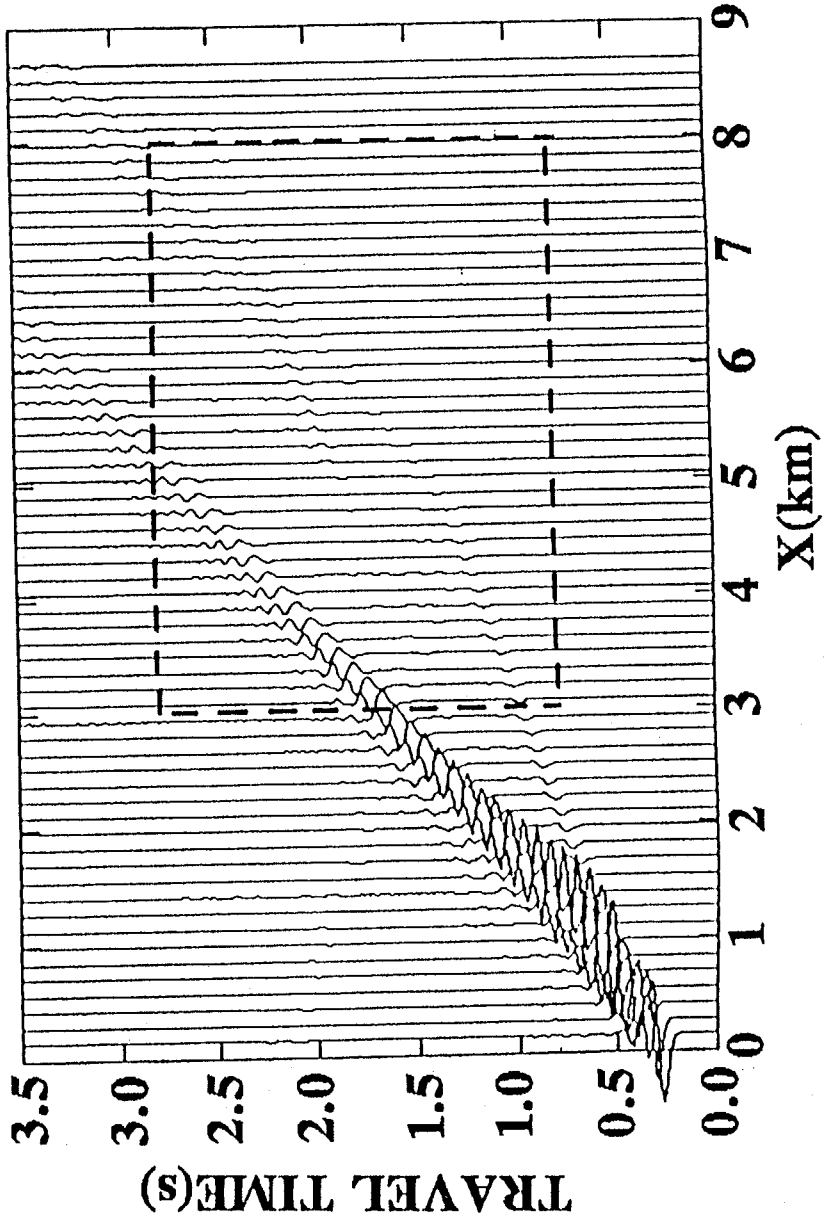

Fig. 4-21. Synthetic seismograms on the upper surface of the model in Fig. 4-19.

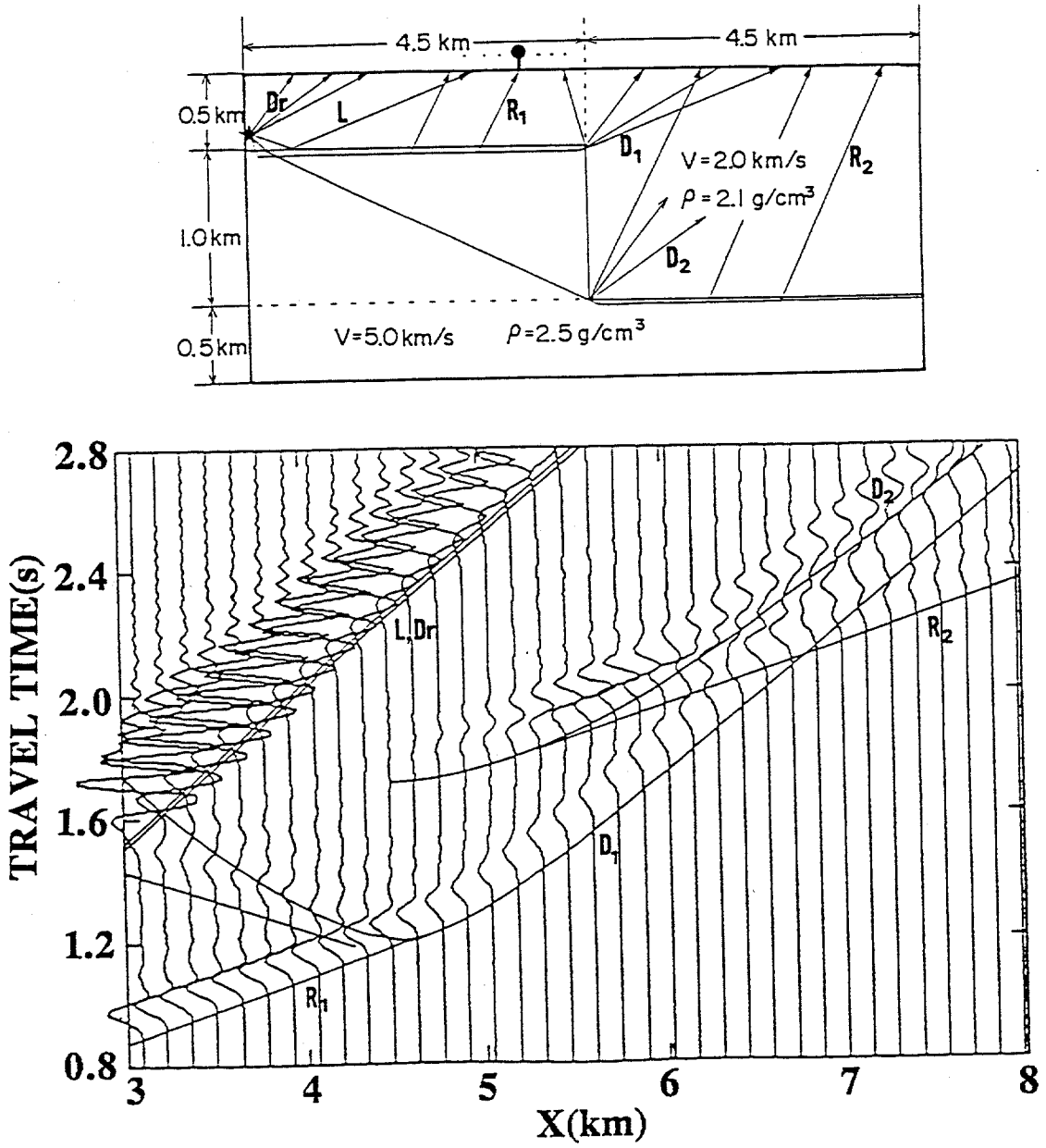

Fig. 4-22. Partial details of Fig.4-21. Travel time curves for rays indicated in Fig. 4-19 are also shown.

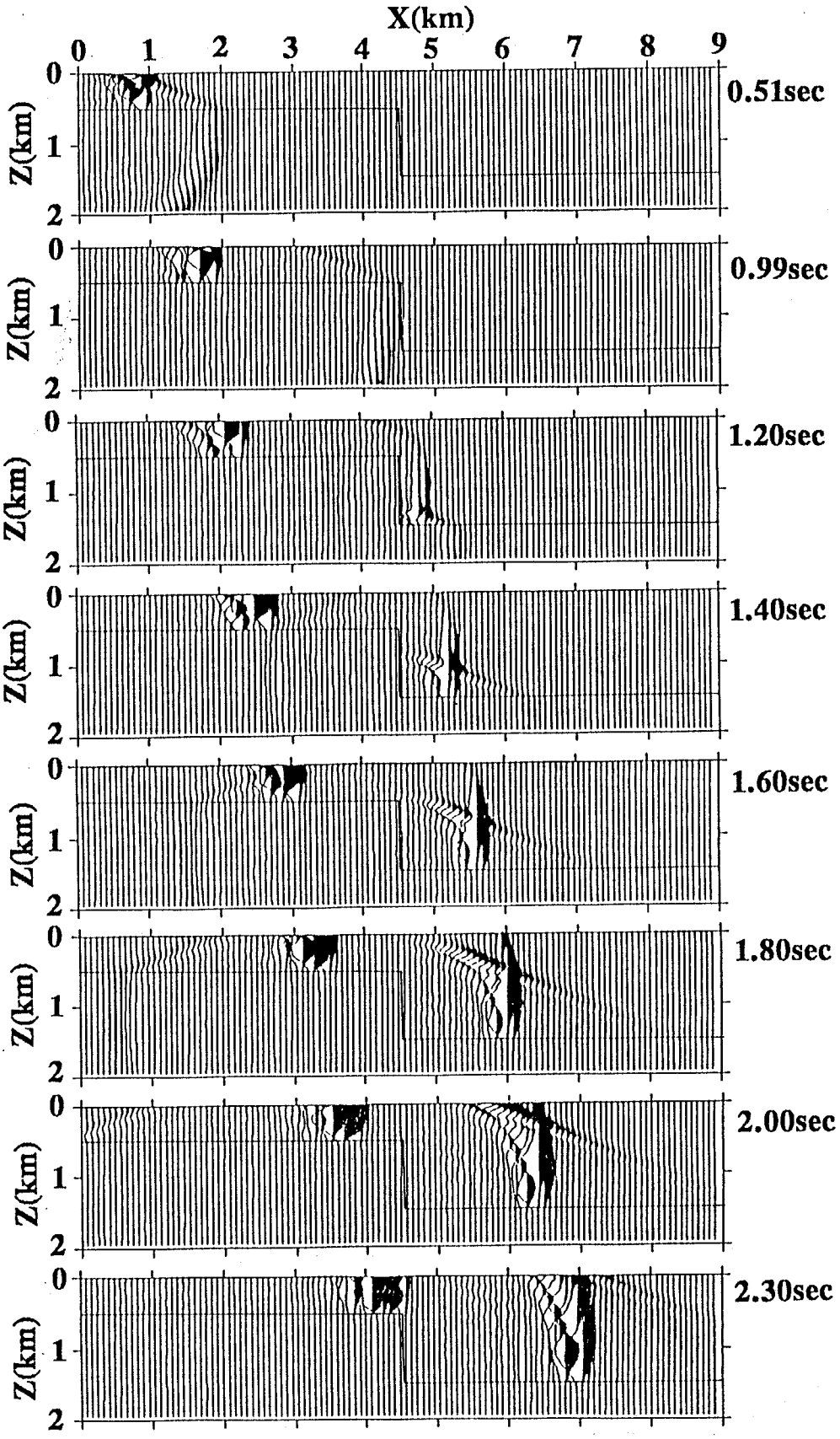

Fig. 4-23. Snapshots for Fig. 4-21.

having a center at the upper edge of the step indicates the radiation of the diffracted wave as shown by the third snapshot. The diffracted wave at the lower edge with a circular wave front and the refracted wave from the down faulted side of the basement with a plane wave front appear in the snapshots at time more than 1.40 sec. The large phase traveling horizontally towards the right direction is considered to be the transmitted wave beyond the vertical interface at the step; this phase can not reach at the upper surface. Although the amplitude is small, we can also see phases reflecting at the step and traveling towards the left in the 1.2- and 1.8-sec snapshots.

Thus, we can understand the nature of the later phases in the explosion seismograms. Moreover, it becomes clear that the appearance of the later phase gives the certain evidence to the existence of the step-like topography of the basement. It is well-known that the travel time of the diffracted wave plays an important roll in interpreting seismic data from faults. In particular, the behavior of the reflected-diffracted wave (i.e., diffracted wave due to hitting edge of direct or reflected wave) is investigated in detail in the field of reflection seismology (e.g., Angona, 1960; Trorey, 1970). On the other hand, only the kinematic aspects of the refracted-diffracted wave (i.e., diffracted wave due to hitting edge of refracted wave) is usually of interest in the field of refraction seismology (e.g., Dobrin, 1976), and the dynamic characteristics, such as amplitudes, are not sufficiently studied. However, the characteristics of the later phase can provide a lot of valuable information about the fault.

Next, results of some seismic refraction surveys are referred in order to see whether later phases exist or not just after the initial phases. The first example is shown in Fig. 4-24; vertical velocities observed on the line from Akishima to Tokorozawa from the Akishima explosion discussed in chapter two. The presence of a fault on the basement was deduced by the seismic surveys. Travel time delay of the initial phases can be seen at a distance of 9 km. Although the stations were not densely set, later phase just after the initial phases can be pointed out as indicated by the arrow. Another example is the result of the

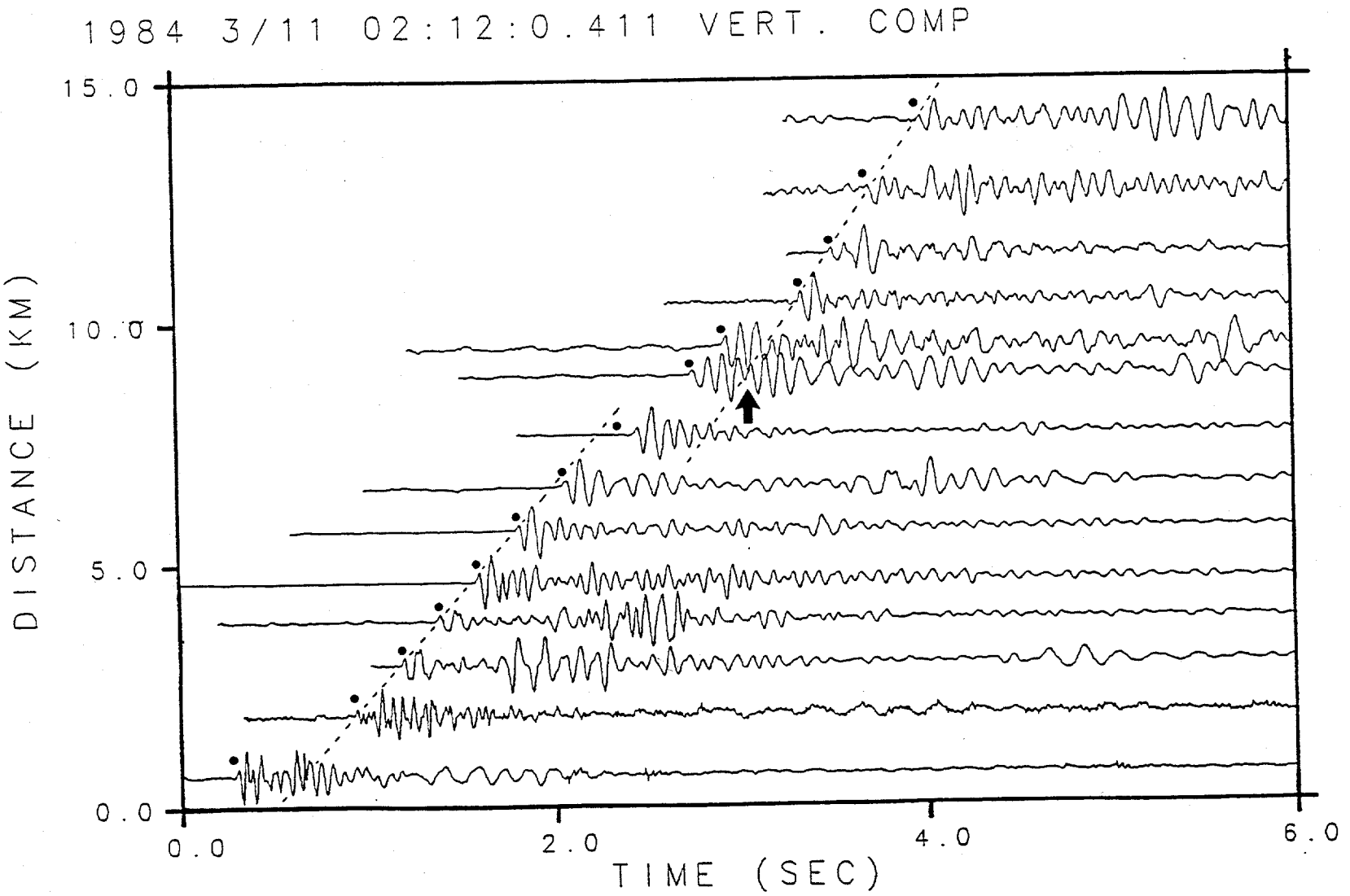

Fig. 4-24. Vertical velocities observed between Akishima and Tokorozawa during the Akishima explosion.

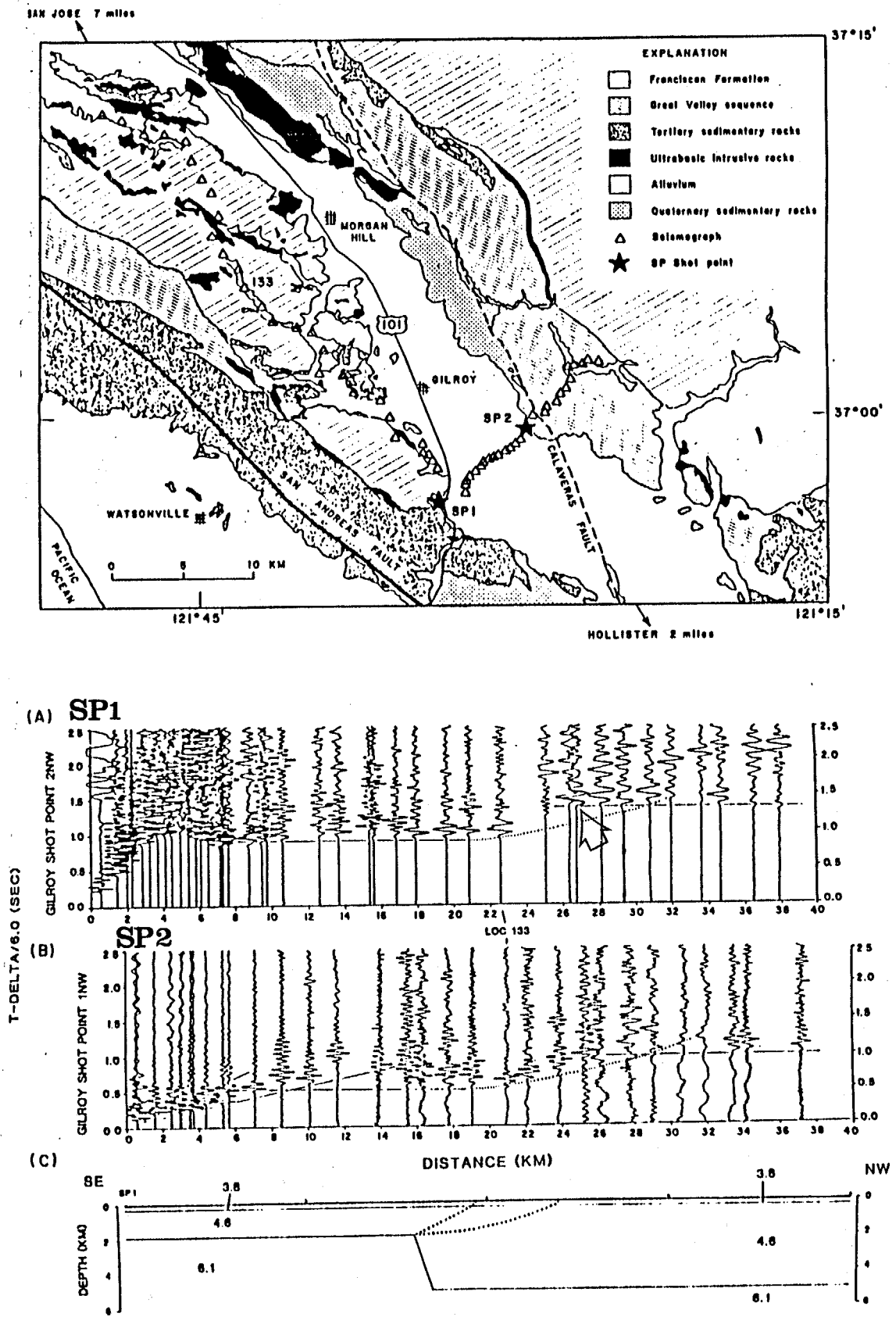

Fig. 4-25. Results of seismic refraction work in California, USA (After Mooney and Leutgert, 1982).

refraction survey in the Santa Clara Valley region, USA, by Mooney and Luetgert (1982) shown in Fig. 4-25. The layer with a velocity of 6 km/sec was deduced to be down-thrown to a distance of 25 km. In the record sections of the explosions SP1, the later phases can be clearly seen as indicated by an arrow. Hence, the appearance of distinct later phases just after the initial phases can facilitate the interpretations of refraction data.

4.3.3 Interpretation for the later phases in earthquake ground motions

A diffracted wave plays an important roll in describing the seismic wave field in an underground structure with a step-like topography as was mentioned in the case of the explosion seismic waves earlier. Here, the forward modeling is used in order to interpret the later phases seen in earthquake ground motions, too.

(a) Modeling of seismic wave propagation for deep earthquake

At first, the nature of later phases in the seismograms obtained during the deep near-by earthquakes was investigated. We used, here, the same finite difference method as before, but SH-wave field was assumed. A simple model depicted in Fig. 4-26 was adopted for the computation, because of the same reasons described earlier. The shear wave velocities for the upper and the lower layers are 1.0 and 3.0 km/sec and the densities are 2.0 and 2.5 g/cm**3, respectively. The same source time function expressed by (4-20) was employed as the input wave, but T_0 was set as 0.35 sec.

Since the hypocenters of the earthquakes are deep and near, the incident wave to the sedimentary layers can be regard to propagate almost vertically. Assuming vertical plane wave incidence, the source time function was applied at grid points arranged in a horizontal line at a certain depth. We call this horizontal line "input plane." If the source time function applies as a forced displacement, the input plane becomes a rigid reflector and make undesired reflections of scattering waves from physical interfaces inside the model. In order to avoid the reflections, the following procedure (Yuan et al., 1986) was used. The explicit finite difference method needs time marching calculation of displacements at all grid points

in the model. After the new displacements at all grid points were calculated, the source time function was added to the new displacements at the grid points on the input plane. The same source time function was also substructed from the new displacements at the grid points in a horizontal line which is one grid lower than the input line. These newly defined displacements were used for calculations at the next time step. Then, the scattering waves from physical interfaces can propagate downwards beyond the input plane and they are suppressed by the absorbing boundary at the bottom. The result of a simple test model can be seen in section 5.2.

Because of the assumption of plane wave incidence, the left and right end sides of the model were treated as symmetric boundaries on which stress free condition is imposed. The absorbing condition was applied to the top and the bottom end sides of the model, because of preventing disturbances of multiple reflections which make it difficult to understand synthetic seismograms.

The synthetic seismograms on the upper surface of the model are shown in Fig. 4-27. The snapshots are also displayed in Fig. 4-28. The direct waves arrive first at the points $x <= 1$km and $x >= 1$km with the arrival times depending on the thickness of the surface layer. Since the initial phases near the left and right end sides have similar wave forms, the step at $x = 2$km gives no influences on the initial phases of the seismograms at the points far from the step. The effects of the step, however, are clearly seen in the initial part of the seismograms at the points of $1 < x < 2$km, where belong to the down-thrown side. A smaller initial phase arrives with travel time delay; the wave front of these phases is circular with a center at the upper edge of the model as shown in the snapshot at a time of 0.75 sec. This is the diffracted wave generated by direct wave impinging the upper edge of the step. Distinct later phases having amplitudes two to three times larger than those of the initial phases can be seen just after the initial phases. From the snapshots, this is considered to be a contributions of the diffracted wave from the lower edge of the step and the direct wave which propagates in the down-faulted side (right). Such later phases can not appear at the stations in

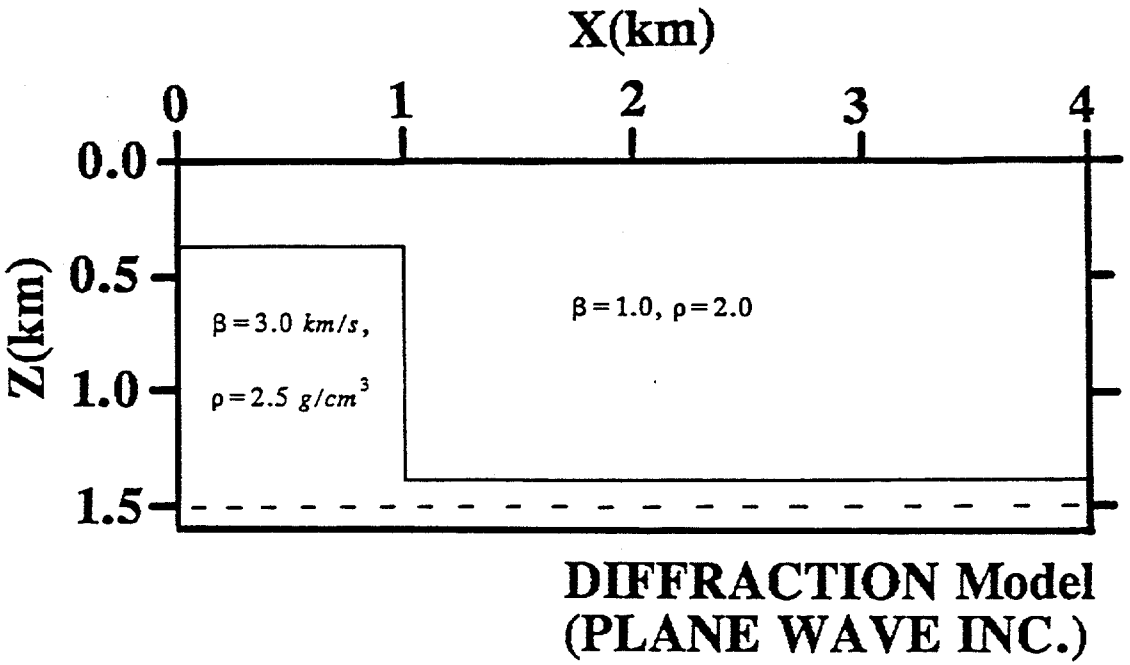

Fig. 4-26. Underground structural model to interpret the later phases in the earthquake records. A vertically plane wave incidence is assumed.

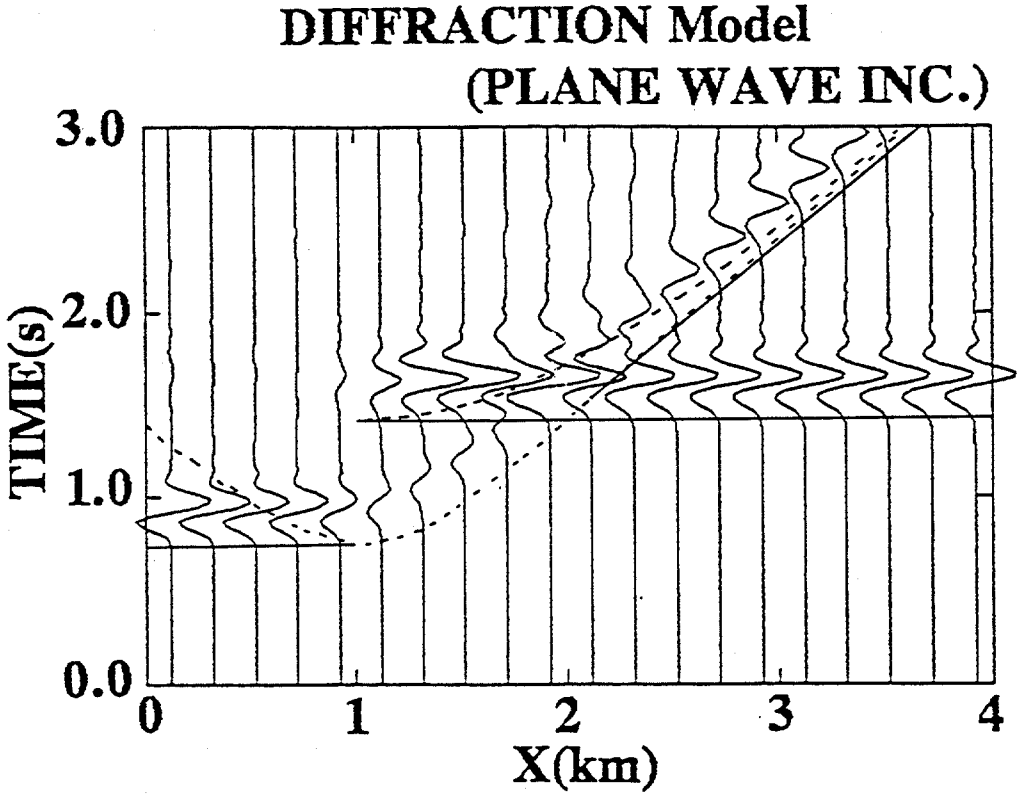

Fig. 4-27. Synthetic seismograms on the upper surface of a model in Fig. 4-26.

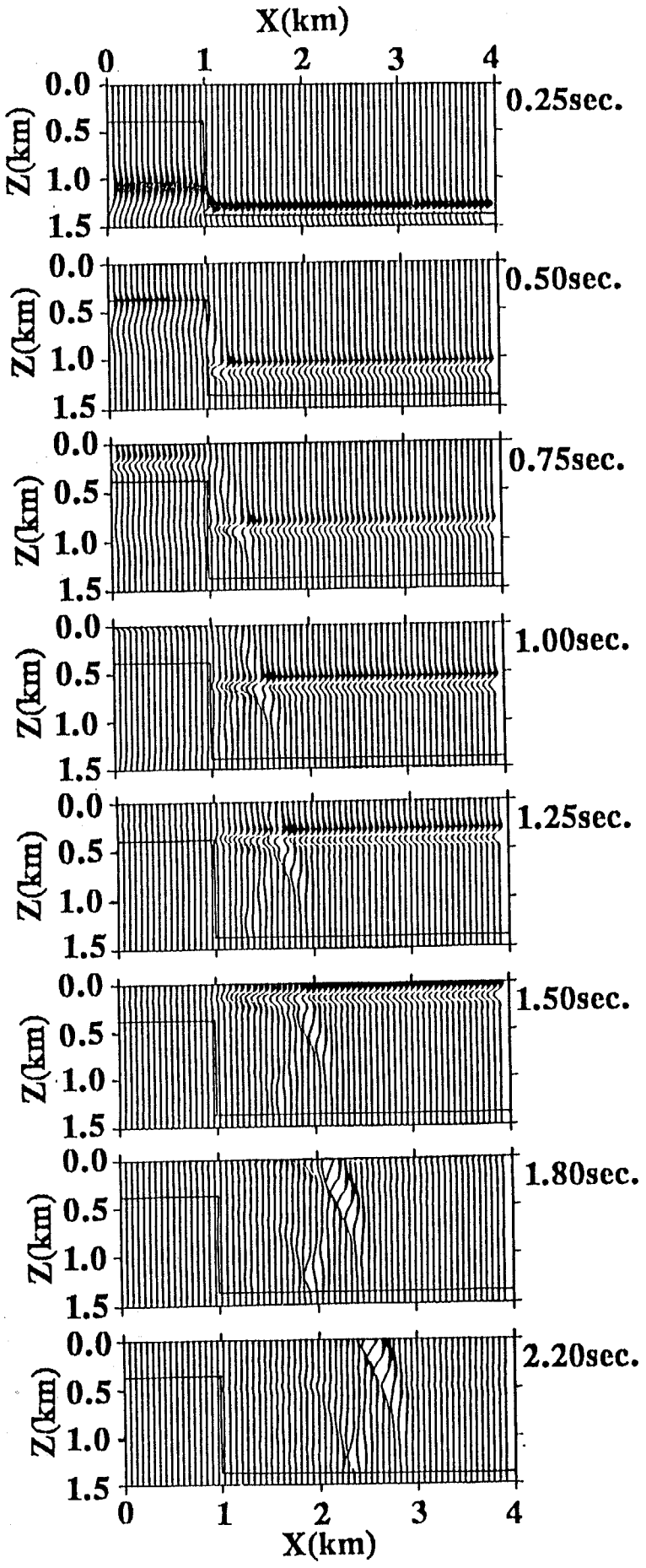

Fig. 4-28. Snapshots for Fig. 4-27.

the up-faulted side (left). These computational results can give the interpretation of the later phases seen in the seismograms observed during the deep earthquakes, such as EQ1. They also support the existence of the subsurface step-like topography. Moreover, it is suggested that the station KWW can be located in the western side of the step.

The character of diffracted waves, generally, depends on the shape of the diffractor, in this case, the step-like subsurface topography. In the following, the effects of the shape of the step were investigated by the modeling for an underground structure as shown in Fig. 4-29; dip angle of the step is 45 ° from the vertical. The physical parameters of the model and the treatment for the input plane and artificial boundaries was the same as used for the previous model; only the geometries of the model was changed.

The synthetic seismograms for the model are shown in Fig. 4-30. The snapshots are also depicted in Fig. 4-31. The arrival time delays at stations of $1<x<2$km and large initial phases at x of 2km show the same characters as in the previous modeling. However, no distinct later phases just after the initial phases can be seen, except for small later phase around 2 km. As seen in the snapshots in Fig. 4-31, the diffracted waves having a circular wave front are not dominant. The bending direct wave by the dipping interface of the step has more horizontal wave front than that in the case of the vertical step. In other words, the response becomes more similar to that of flat layering. The phases which arrive at 1.5 sec at 1 km are caused by the symmetric boundary conditions imposed at the right and the left sides of the model. The comparison between these two modelings due to the vertical incident plane wave suggests that the basement should have a steep step-like topography to elucidate the observed large later phase just after the initial phase.

(b) Modeling of seismic wave propagation for shallow earthquake

Propagation of seismic waves from a shallow earthquake, such as EQ7, are investigated here. The most important difference between deep and shallow events is considered to be the incident angle to sedimentary layers. Because of a shallow focal depth, seismic waves incident obliquely. In the following, forward modelings for wave propagation due to

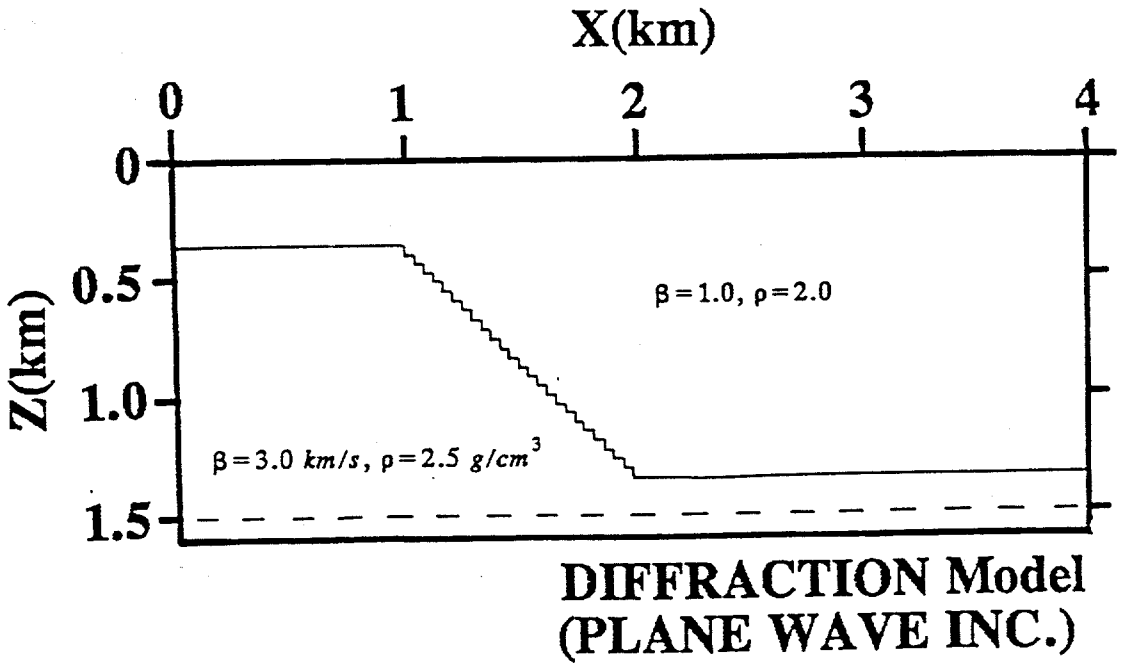

Fig. 4-29. Underground structural models. A vertical plane wave incidence is assumed.

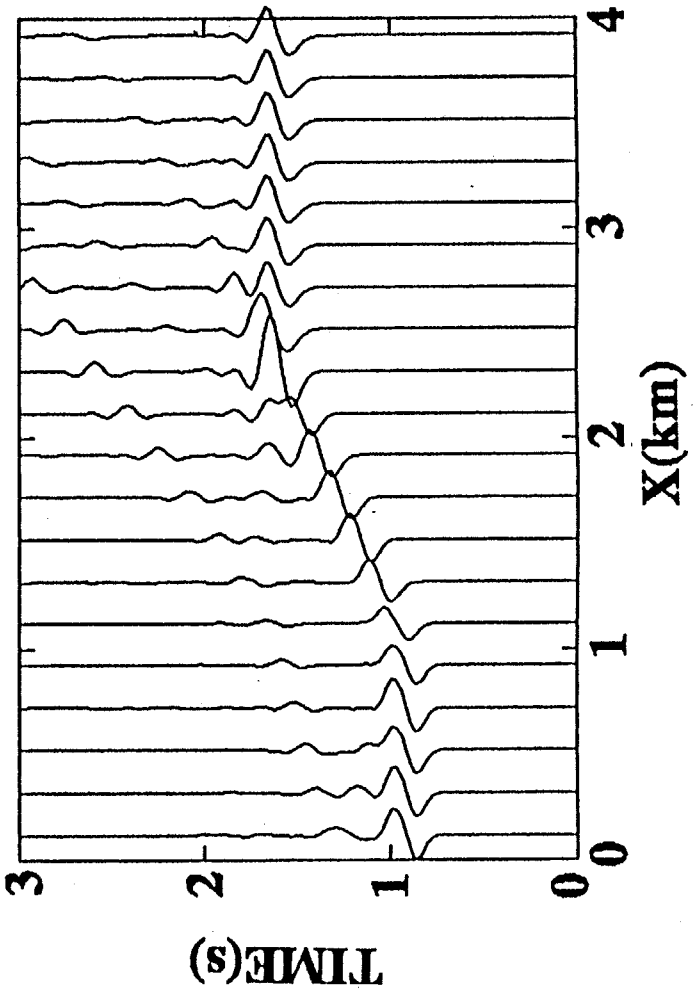

Fig. 4-30. Synthetic seismograms on the upper surface of the model indicated by solid line in Fig. 4-29.

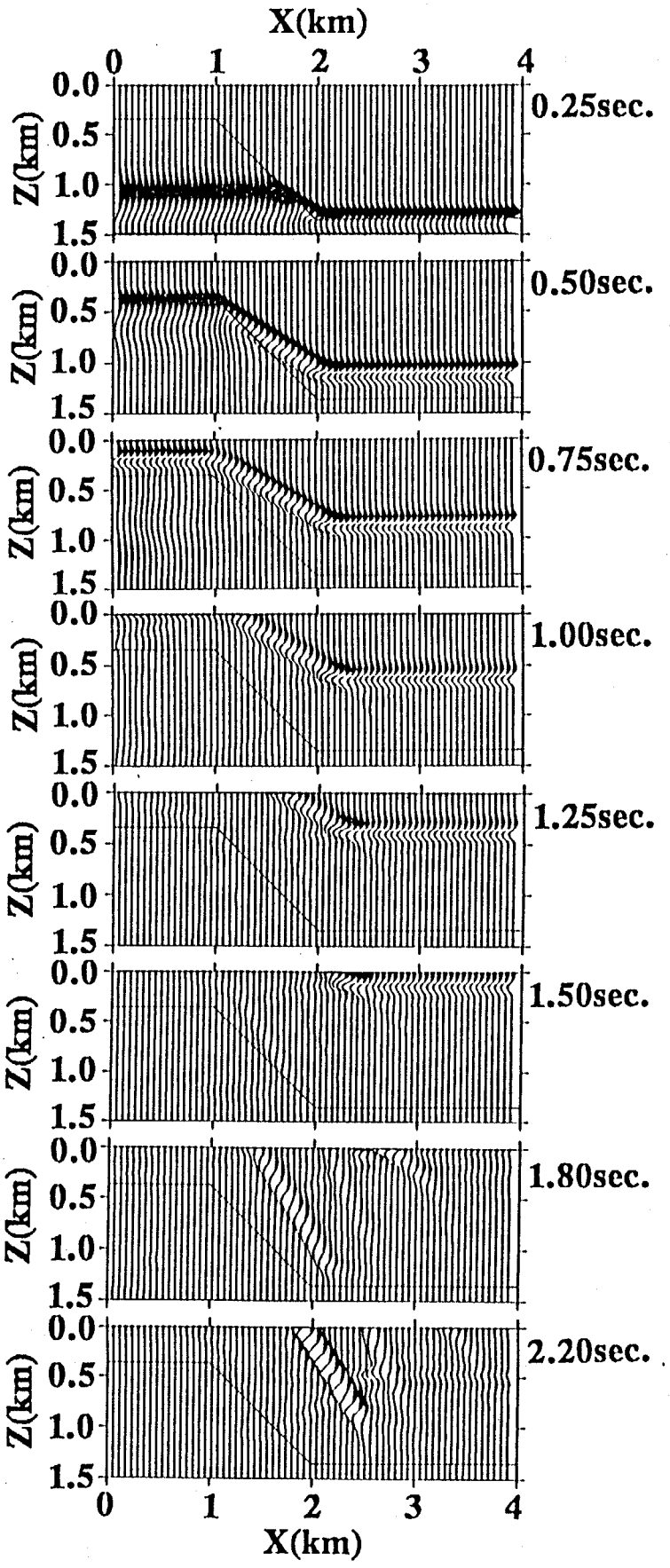

Fig. 4-31. Snapshots for Fig. 4-30.

oblique incident SH-wave in an underground structure with a step-like topography of basement are carried out.

The geometry and physical parameters of the model for the computations were the same as used in the above investigations. In order to describe oblique incidence, the following treatment was applied. Let us consider an SH plane wave propagating with a velocity β in homogeneous media and having a wave front with an angle of θ from the vertical as shown in Fig. 4-32a. The input source time function $f(t)$ at the individual grid points on the input plane varys with a time delay as

$$f(t-\tau_x) \qquad \tau_x = \frac{x\cos\theta}{\beta} \quad \textit{in x direction}$$

$$f(t-\tau_z) \qquad \tau_z = \frac{z\sin\theta}{\beta} \quad \textit{in z direction} \tag{4-21}$$

Since there is a surface layer overlying the basement in the model discussed here, the time delay was changed according to the ray path as shown in Fig. 4-32b. Moreover, the source time function applied at the grid points belonging to the surface layer was multiplied by the transmission coefficient between two layers. The epicenter of EQ7 is located in the western side of the seismic array, namely, the down-faulted side. Therefore, the plane wave incidents from the right side of the model with a incident angle of 45 °. The model used is the same as shown in Fig. 4-26. The step exists at x=1km. The boundaries were dealt with the same manner as the previous modeling.

The synthetic seismograms on the upper surface are shown in Fig. 4-33. The travel time curves of the important rays are also shown in the figure; solid and dotted lines are those for the direct and the diffracted waves, respectively. The seismograms exhibit different features, as compared with the synthetics ones for vertical incidence (cf. Fig.4-27). The initial phase is considerably small at x=1km where the step exists, though the later phase have large amplitude. As seen in the snapshots of Fig. 4-34, the initial phase at x=1 km is a phase diffracted twice at the lower and the upper edge of the step. Because of the twice conversions to the diffracted waves, the amplitude of the initial phase can not be dis-

tinct. The large later phase is caused by the focusing of the diffracted wave at the lower edge and the direct wave as well as the case of the vertical incident. It is considered that the existences of considerable small initial phase and large later phase lead us the absence of the later phase. They also can give us the explanation why the initial portion of S-wave observed at KWW during EQ7 was not different from those observed at the other stations.

In order to investigate effects of the propagation direction, we calculate wave field due to a SH plane wave with the incident direction opposite to that in the previous case: incidence from the up-faulted side (left) with an incident angle of 45 °. Considering actual situations, this corresponds to ground motions due to shallow earthquakes which occur in the eastern side of the seismic array. The same model in Fig. 4.26 was adopted. The synthetic seismograms with travel times of the important rays, diffracted waves and direct waves, are shown in Fig. 4-35. The snapshots are also shown in Fig. 4-36. The seismograms exhibit the similar characters as recognized in the case of the vertical incidence in Fig. 4-27. The later phases with comparable or large amplitudes than those of initial phases appear at positions with x between 1 and 2 km. It can be understood from the snapshots that what contributes to these later phases is the same as the vertical incidence case: focusing of the direct waves from the down-faulted basement and the diffracted waves from the lower edge of the step. The results of the above two modelings for the oblique incidences implies that incident angle is an important factor for seismic wave propagation in the vicinity of a step-like topography of the basement, particularly, during shallow earthquakes.

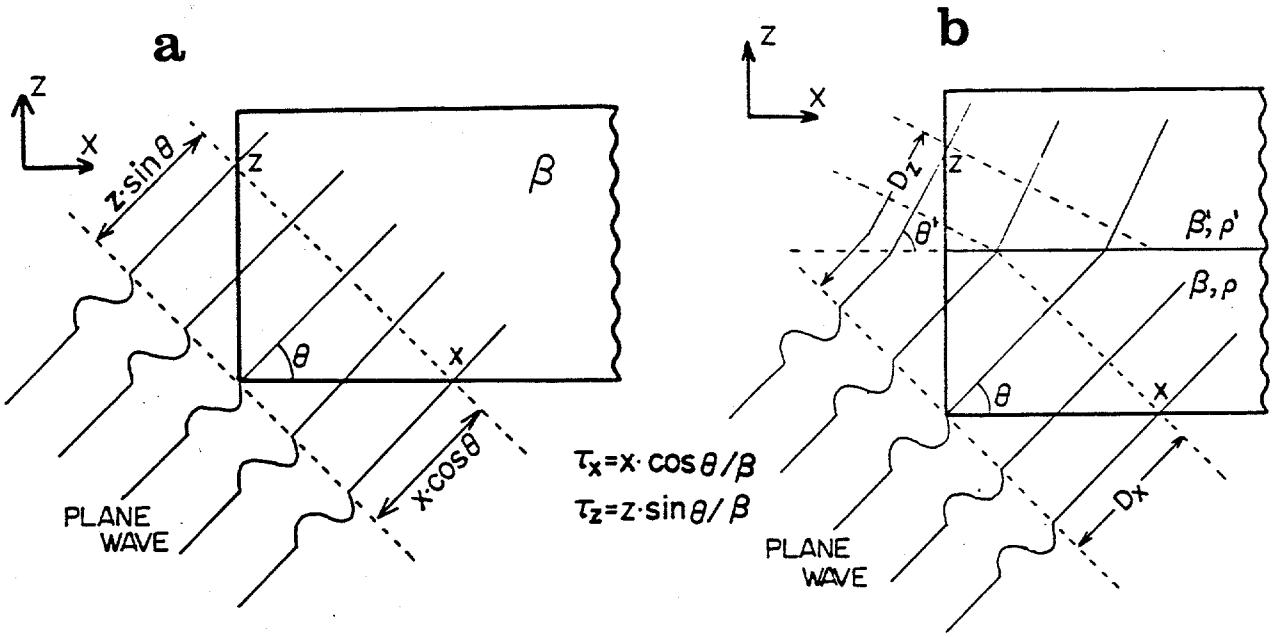

Fig. 4-32. Schematic illustration of oblique plane wave incidence in (a) a homogeneous media and (b) a media consisting of two layers.

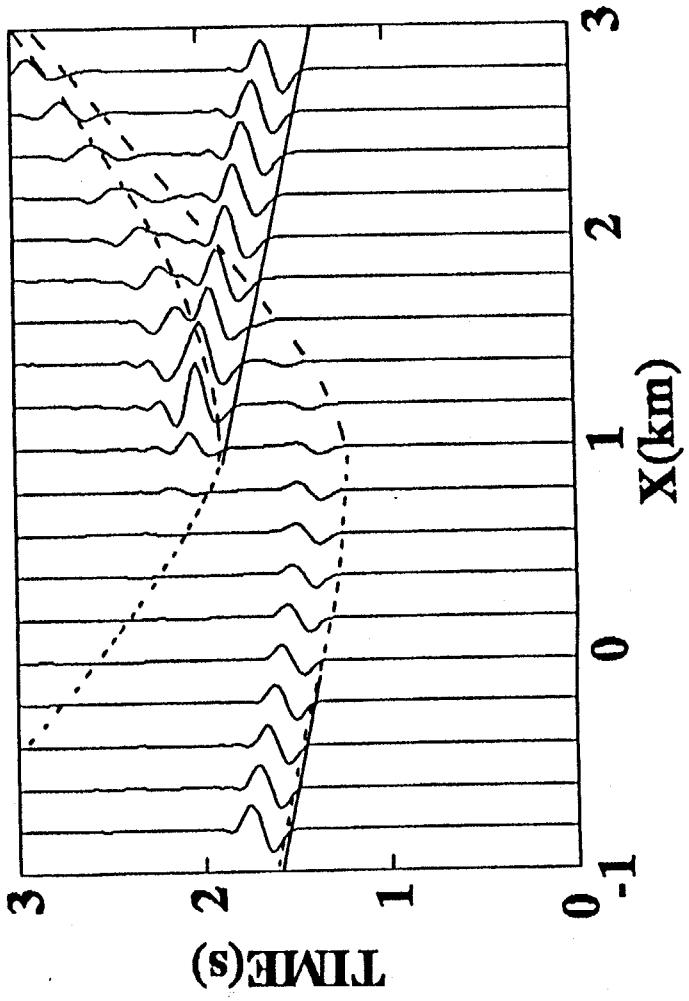

Fig. 4-33. Synthetic seismograms on the upper surface of the model in Fig. 4-26. Incident angle is 45 ° from the down-faulted side (right).

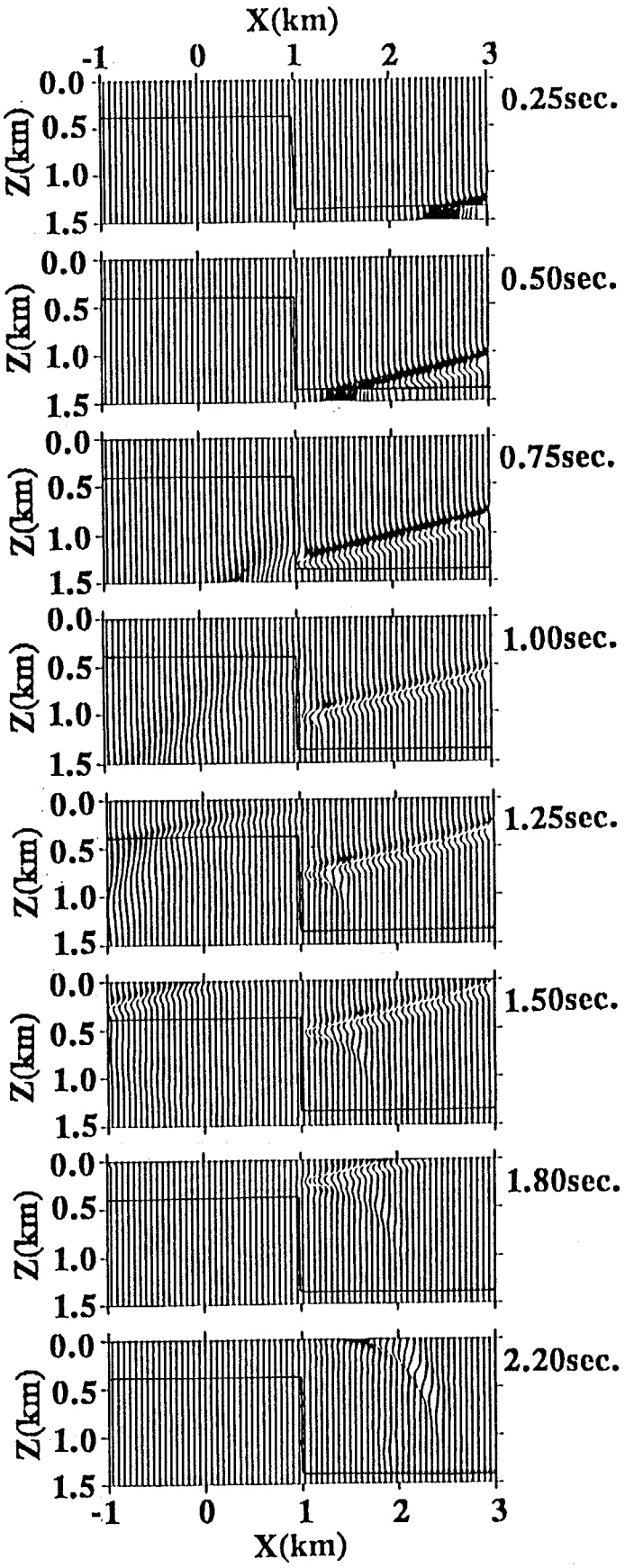

Fig. 4-34. Snapshots for Fig.4-33.

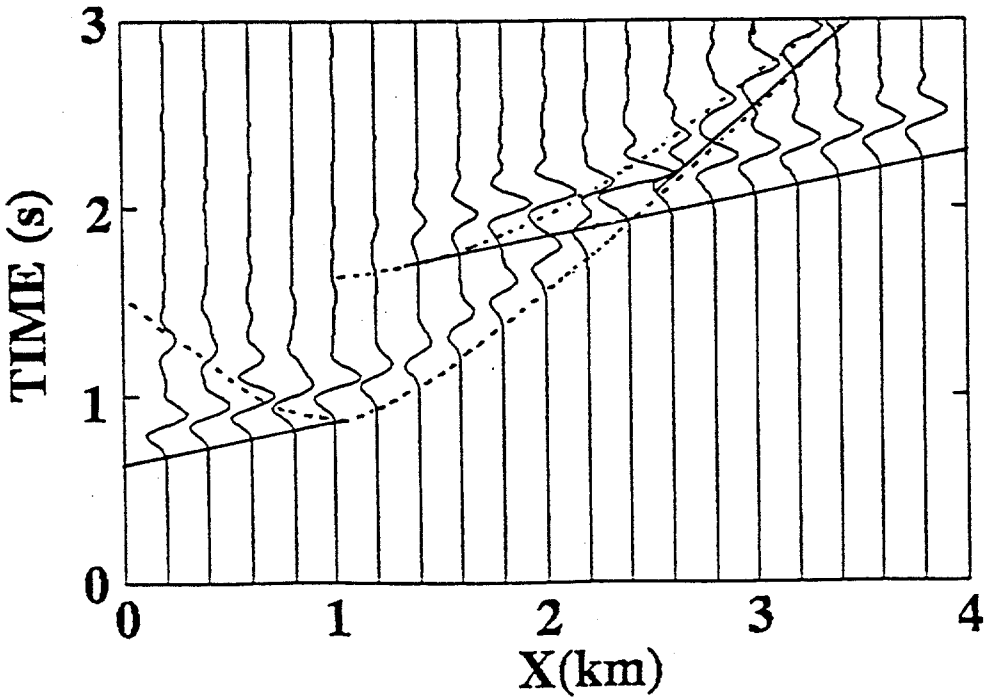

Fig. 4-35. Synthetic seismograms on the upper surface of the model in Fig. 4-26. Incident angle is 45 ° from the up-faulted side (left).

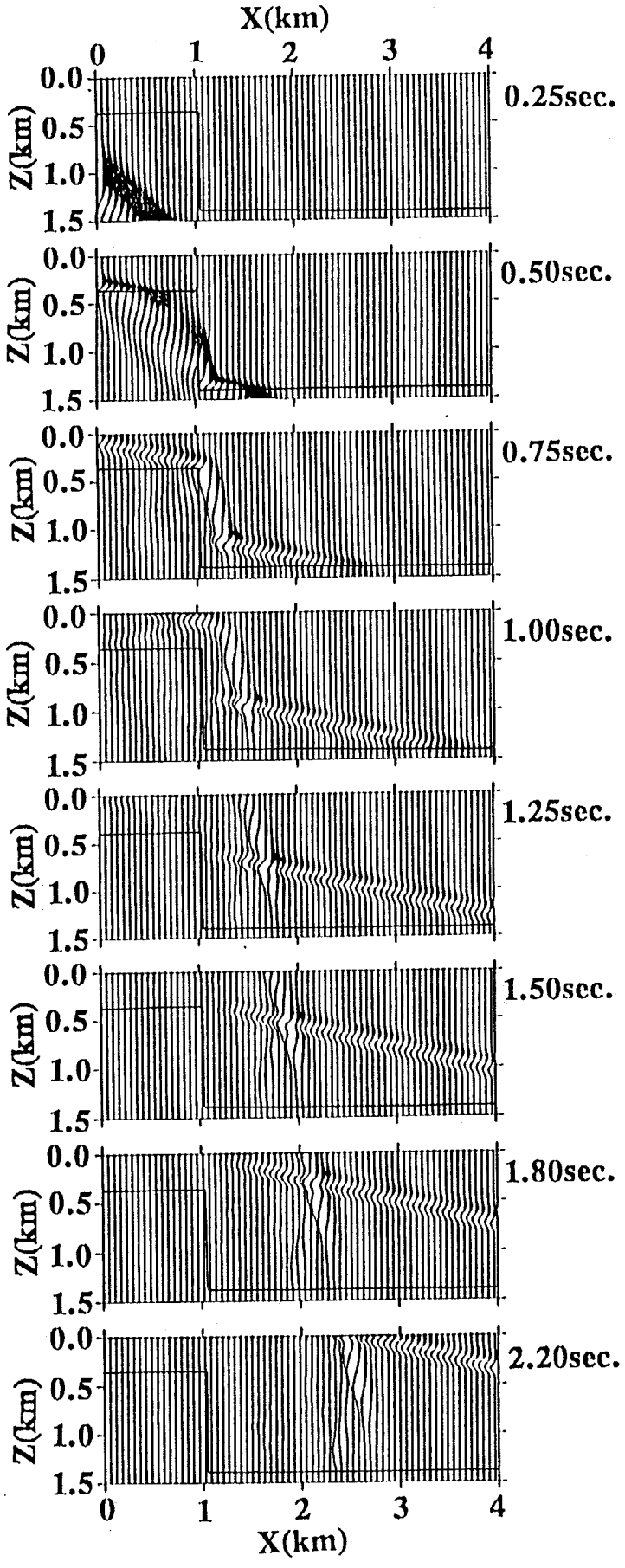

Fig. 4-36. Snapshots for Fig. 4-35.

CHAPTER 5. SURFACE WAVE PROPAGATION WITHIN SEDIMENTARY LAYERS

In this chapter, characteristics of surface wave propagation within sedimentary layers are discussed by considering the underground structure which was made clear in chapter two. At first, ground motions in the longer period range observed during the Western Nagano earthquake of 1984 are analyzed in respect to dispersion characteristics. Then, forward modeling based on two-dimensional finite difference method is applied to simulate the surface wave propagation within the sedimentary layers. Finally, the effects of sedimentary layers on surface wave propagation are investigated for various underground structural models.

5.1 Surface Wave Modified by Sedimentary Layers

5.1.1 Surface wave observed during the Western Nagano earthquake of 1984

The Western Nagano earthquake on September 14, 1984, had a strike slip mechanism, which occurred in Central Japan with JMA magnitude of 6.8 as shown in Fig. 5-1 (Takeo and Mikami, 1987). Ground motions were observed during the Western Nagano earthquake in a seismic array in the southwestern part of the Kanto plain, Japan, as indicated in Fig. 5-1. There is the Kanto Mountains in the western side of the studied area. The station called ASK is located on a firm rock which belongs to Pre-Neogene basement. The other stations are set on the sedimentary layers. Comparisons of ground motions at the stations on the sedimentary layers with that at ASK can make it easy to evaluate effects of the sedimentary layers on earthquake ground motions.

Each station consists of velocity type seismometers in three components, whose frequency characteristics are flat to around 40 sec, and an analog or digital data recorder. Therefore, records obtained are reliable even in the longer periods where acceleration seismometers, such as SMAC, usually loose accuracy. A calibrated time signal is also recorded.

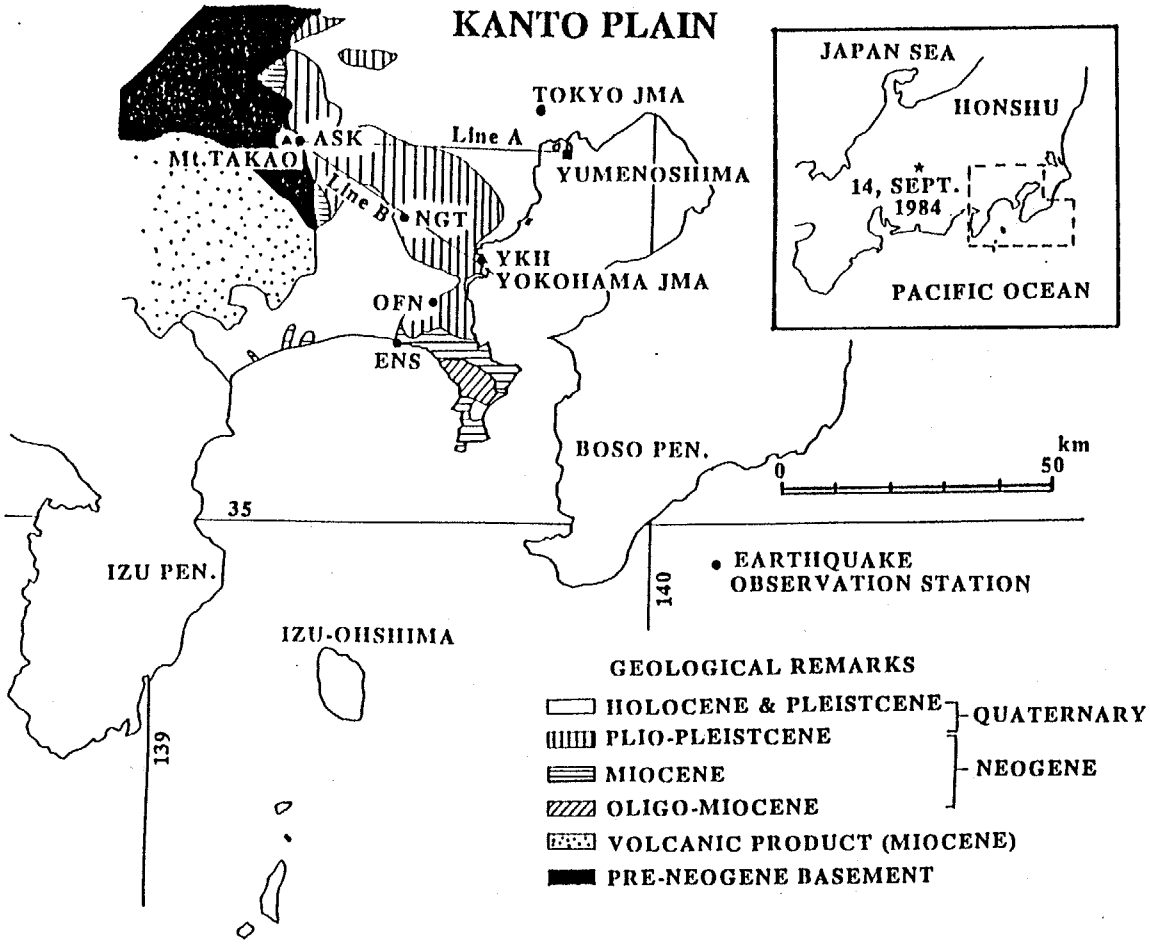

Fig. 5-1. Earthquake observation stations (solid circles) in the south-western Kanto, district, Japan, and location of the epicenter of the Western Nagano earthquake of 1984. Surface geological conditions are also indicated.

The transverse velocities obtained in the array are shown in Fig. 5-2. All the traces are filtered in periods from 2 to 20 sec. The seismogram at ASK on the firm rock is simple and has short duration. On the other hand, the seismograms at the stations on the sediments show large amplitudes and long durations, despite of longer epicentral distance than that of ASK. In particular, two distinct well-dispersed wave trains in the long period range are seen in the traces obtained at NGT and YKH. The travel time curve of these two phases are indicated by solid lines in Fig. 5-2. The first phase arrives after the initial S-wave onset. The other is a phase with a low apparent velocity of 0.6km/s in the latter part of the traces. The period of the second phase is shorter than the former one. The second phase can not be clearly seen in the seismogram at ASK. These facts imply that the sedimentary layers have considerable influences on the amplification of the second phase.

The seismogram at ENS also shows that no well-dispersive wave trains appear. Outcrop of relatively hard sedimentary layer which geologically belongs to the Miocene age can be seen on the free surface near ENS. Therefore, it would be considered that a little energy of seismic wave could be transmitted towards ENS. In the following, the transverse components of the records observed at ASK, NGT and YKH were investigated.

The displacement response spectra (damping coefficient 2%) of the three records are shown in Fig. 5-3. The spectral amplitudes of the records obtained at stations on the sediments, NGT and YKH, are several times larger than that at the firm rock site, ASK. The spectral peak of the record at ASK is only seen at a period of about 7 seconds. The spectra at NGT and YKH, however, have two peaks at the same period and the shorter period of 4 sec.

To investigate the nature of the dispersive later phases, the multi-filtering technique was adopted (Dziewonski et al., 1969). Figs. 5-4a, b and c are the results of processing the transverse records at ASK, NGT and YKH, respectively. The amplitude contours of the envelopes of the filtered records are drawn at 20% intervals of the maximum amplitude. Dispersion is clearly seen for the period range of 3 to 10 sec. It implies that the seismic

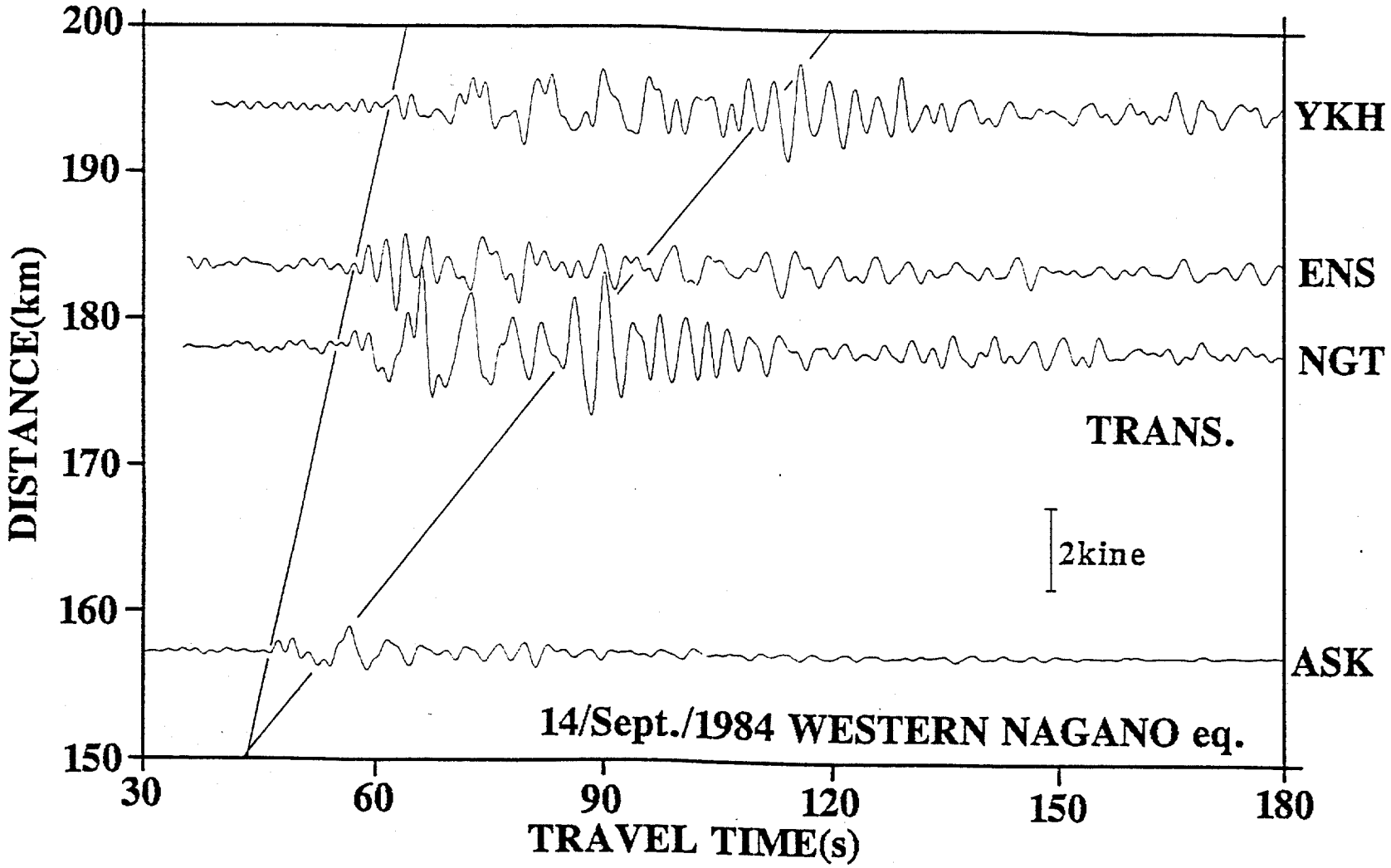

Fig. 5-2. Observed seismograms obtained at the array stations during the Western Nagano earthquake. Each trace indicates nearly transverse velocity.

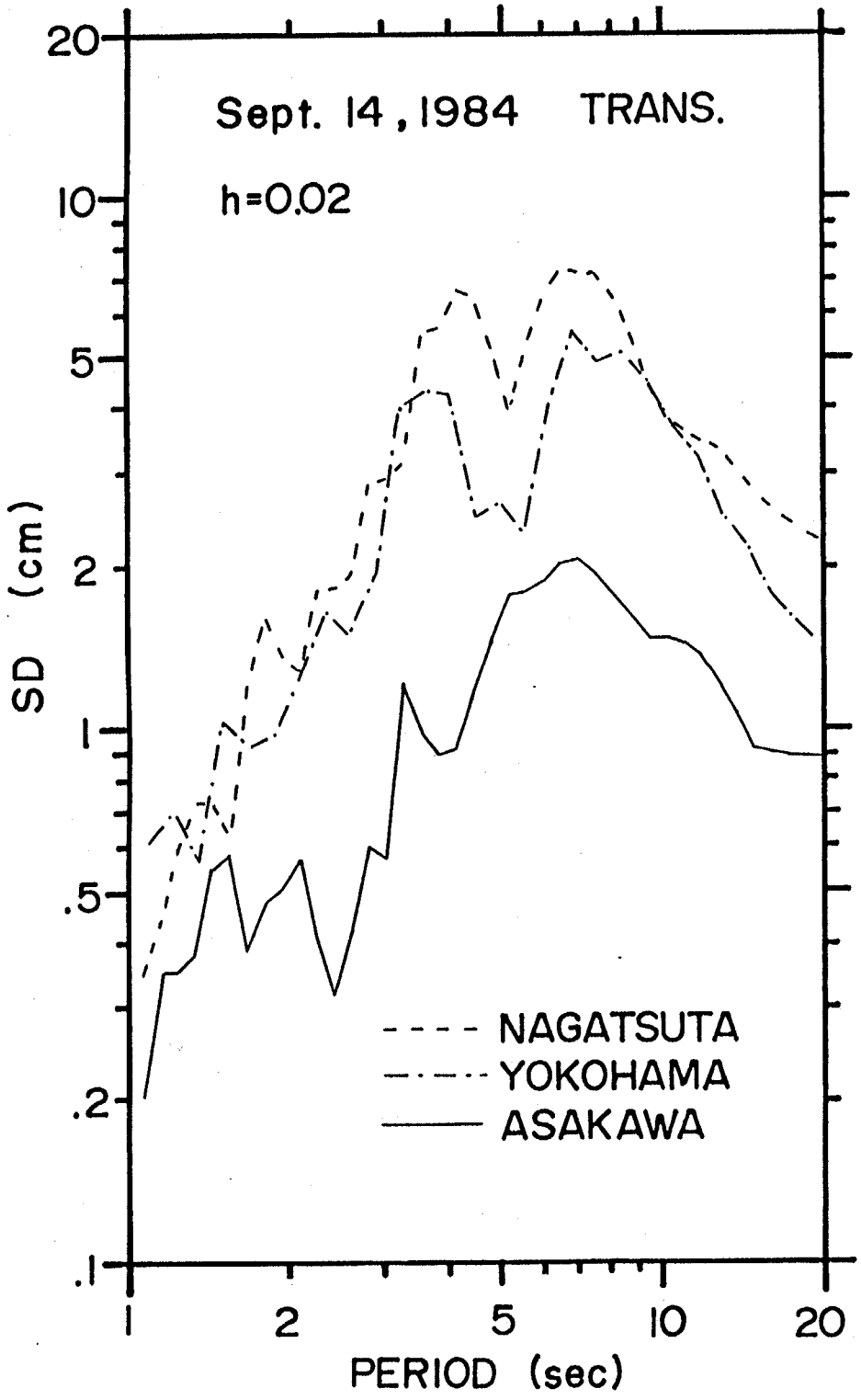

Fig. 5-3. Displacement response spectra with damping coefficient of 2% for the transverse components at ASK, NGT and YKH.

waves of the transverse components can be taken as surface waves. The two predominant peaks at periods of 4 and 7 sec seen in the spectrum of NGT and YKH are the contributions of the two distinct wave trains, respectively.

Using the arrival time difference of the maximum peaks of the envelopes at NGT and YKH, the group velocities for the sedimentary layers between the two stations are obtained as indicated by solid circles in Fig. 5-5. The group velocities for periods less than 7 sec concentrate around 0.6km/s. The underground structure in the middle of the two observation sites is known from the results of the seismic surveys as shown in Fig. 5-6a. The Shear wave velocities of the layers were assumed from the P-wave ones. The solid line in Fig. 5-5 represents the dispersion curve of group velocities of fundamental Love wave for this horizontally layered model. The calculated group velocities are in good agreement with the observed ones in the periods of 3 to 10 sec. It should be noted that the model is obtained with no iterations. The period for the Airy phase in which large amplitude can be expected is 4 to 5 sec. This period corresponds to the predominant one of the second later phase in the observed seismograms on the sedimentary layers. The dotted line in Fig. 5-5 indicates the group velocity dispersion curve of fundamental Love wave for the underground structure at Yumenoshima as shown in Fig. 5-6b This model is considered as a typical underground structure for the Kanto plain. The observational group velocities, however, can not be explained by the Yumenoshima model. In particular, the period for the Airy phase is considerably different from the model which fits the observational result.

Thus, the dispersive later phases at the stations on the sediments can be interpreted as surface waves developed within the sedimentary layers, in which the waves propagate. Since the seismogram obtained on the firm rock also shows the dispersive characteristics as be seen in Fig. 5-4c, it is considered that the main portion of the seismic waves which incident into the sedimentary layers can be regarded as surface wave. This can be interpreted as the surface waves traveling from the source through the crust and the mantle where no thick sedimentary layers exist. Then, the surface waves propagate and are ampli-

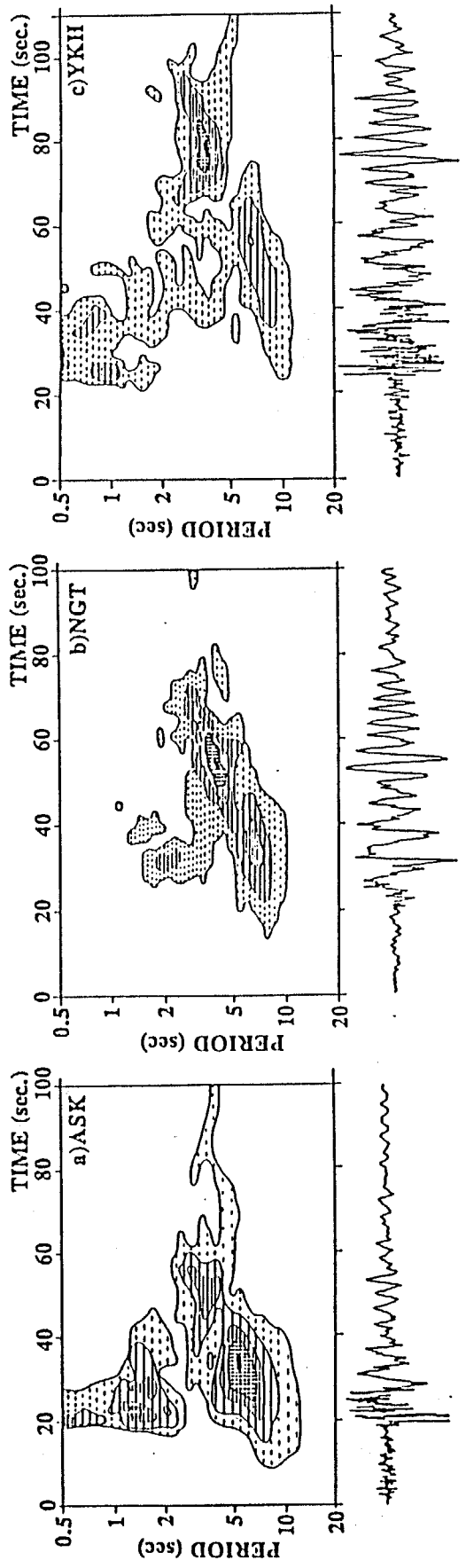

Fig. 5-4. Multi-filter analysis of the transverse components at a)ASK, b)NGT, and c)YKH.

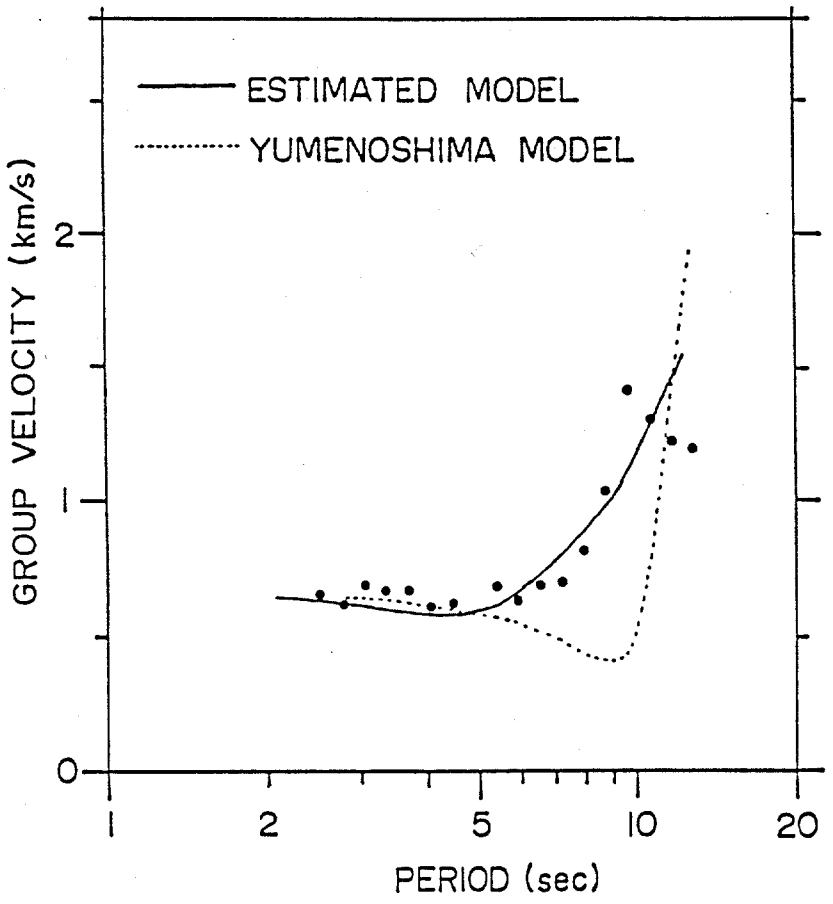

Fig. 5-5. Comparison of observed and calculated group velocities. Solid circles indicate observed group velocities derived from the records at NGT and YKH. Solid line indicates calculated group velocity of fundamental Love wave for the underground structure shown in Fig. 5-6(a). The dotted line shows that calculated for the underground structure shown in Fig. 5-6(b).

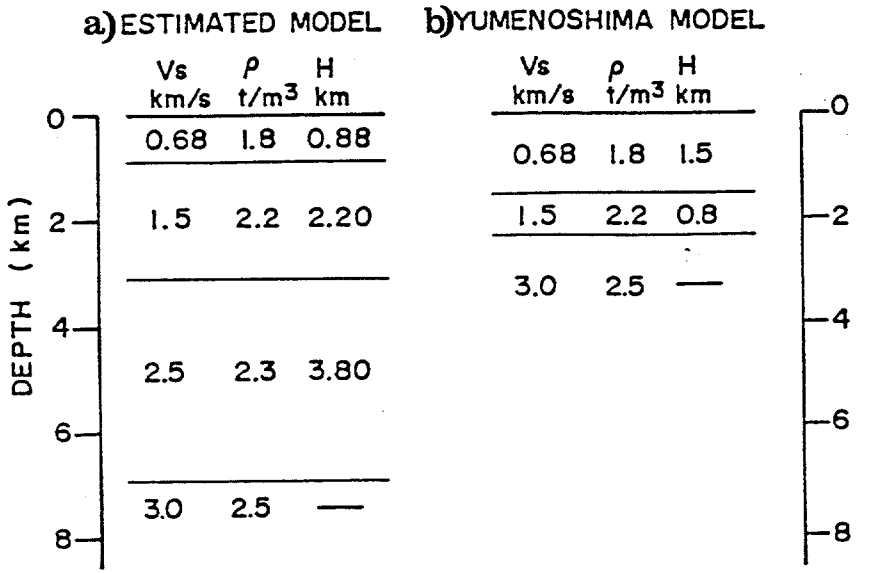

Fig. 5-6. Underground structure model derived from seismic surveys for (a) the middle between NGT and YKH and (b) at Yumenoshima.

fied within the sedimentary layers, and the well-dispersive wave trains with long durations appear in the seismograms. Vidale and Helmberger (1988) concluded from finite difference modeling that the ground motion at a firm rock site is a Love wave pulse and it generates local surface waves in a basin. This differs from our interpretation. The source-site geometry in their discussion belongs to the near-field, while our geometry does to the far-field. Then, surface wave trapped in the crust can appear even at a firm rock site like Lg wave. Therefore, our interpretation does not stand for near-field problems.

5.1.2 Digitization of records obtained by the JMA strong motion seismometer

In all over Japan, Japan Meteorological Agency (JMA) has installed displacement type strong motion seismometers. Its magnification factor is unity, and the natural periods of the horizontal and the vertical seismometers are 6 and 5 sec., respectively. Therefore, longer period ground motions can be recorded well by this seismometers. Records by the seismometers provide us a number of useful information about the characteristics of the longer period ground motions for engineering purposes (e.g., Okada et al., 1978). There are, however, some restriction in the use of such records, because of the paper-recording system.

The ground motions from the Western Nagano earthquake were also observed at the stations of JMA. Our seismometer at YKH is set on the same position of the JMA strong motion seismometer (JMAS) at the Yokohama JMA observatory. Our seismometer (SF101) is of a velocity type strong motion seismometer whose frequency characteristics is flat for more than 40 sec. Here, the accuracy of the digitization of records derived by the JMA strong seismometers was examined by a comparison of the earthquake record at the Yokohama JMA station with that at YKH in our seismic array. The comparison was done using the N-S component which shows the maximum amplitude.

Since the seismograms by the JMA seismometers are recorded on paper, they were digitized according to a method by Omote(1978). At first, peaks and troughs of a trace were digitized. Then, effects of the finiteness of the arm length of the seismometer and drift

of a baseline of the digitized data were removed. Finally, these unequally digitized data were sampled with equal interval of 0.2 sec. by cosine function interpolation.

Since the natural period of the JMA seismometer is 6 seconds, the magnification decreases to 34% at 10 sec and 9% at 20 sec as shown in Fig. 5-7. In order to discuss characteristics of ground motion in periods more than several seconds using such records, it is necessary to correct for the instrumental characteristics. The instrumental correction was applied to the equally sampled data by the frequency domain deconvolution. At the same time, differentiation was done to obtain ground velocity.

Velocity Fourier spectra of the two records are shown in Fig. 5-8. The spectral amplitudes in a period range from two to 13 sec are similar and the periods of the spectral peaks and troughs are also coincident. However, the spectral amplitudes of the record by the seismometer of our seismic array (SF101) are larger than that obtained by JMA seismometer (JMAS) in periods less than two sec. On the other hand, spectral amplitudes longer than ten several seconds by JMAS are overestimated by the instrumental correction. Therefore, cosine taper band pass filtering in periods of 2 to 20 sec was applied in the frequency domain to the sampled data. Similar conclusions were reported by Sino and Katayama (1985) and Yamada et al. (1988) using shaking table experiments. The total frequency characteristic of the instrumental correction and the band pass filtering is depicted in Fig. 5-9. To get a velocity in the time domain, phase delay of the seismometer was also corrected. The upper trace in Fig. 5-10 indicates the corrected velocity obtained by JMAS. The lower one is the velocity observed in our seismic array, which was filtered with a period range of 2 to 20 sec. Although the corrected JMA record shows a smooth waveform, compared with the record by SF101, the coincidence of arrival times of main phases is obvious. The comparison clearly shows that the seismograms by JMA strong motion seismometers can be used in this analysis with an accuracy similar to that of the records obtained in our seismic array.

5.1.3 Difference of seismograms at Tokyo and Yokohama

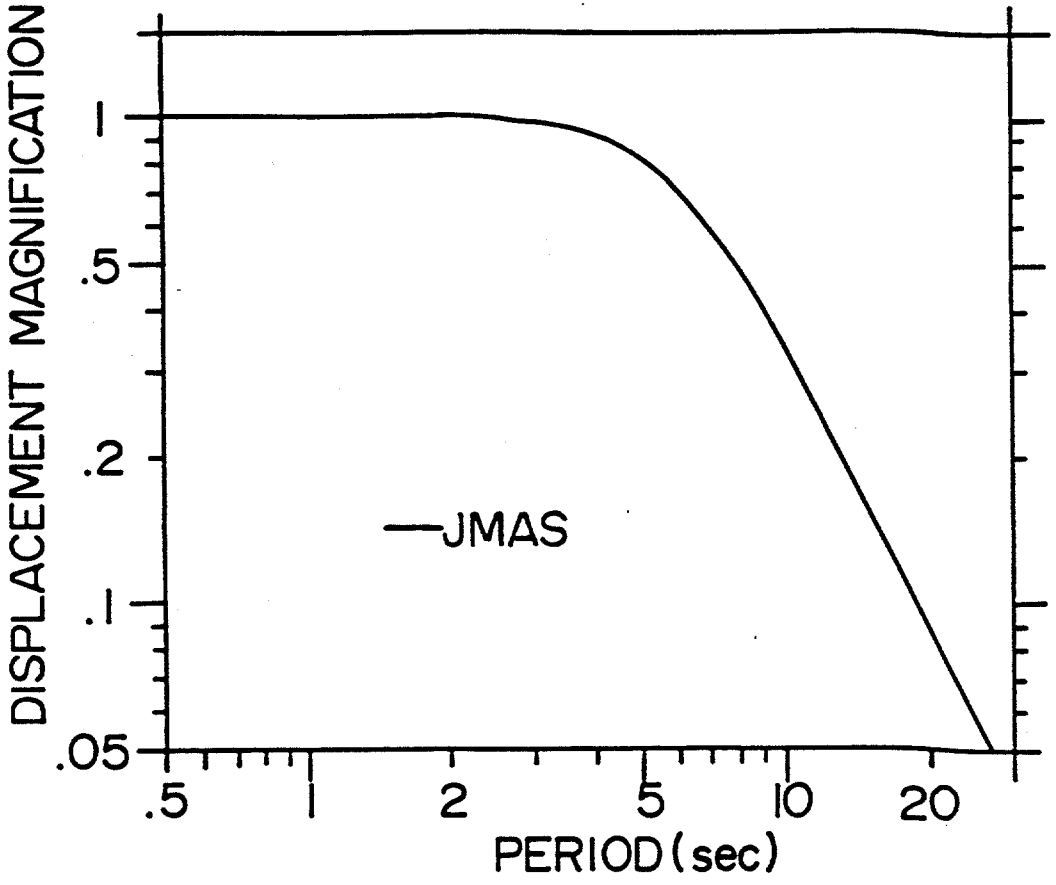

Fig. 5-7. Instrumental response of the strong motion seismometer installed by the Japan Meteorological Agency. The natural period is 6 sec for horizontal component and the magnification is unity.

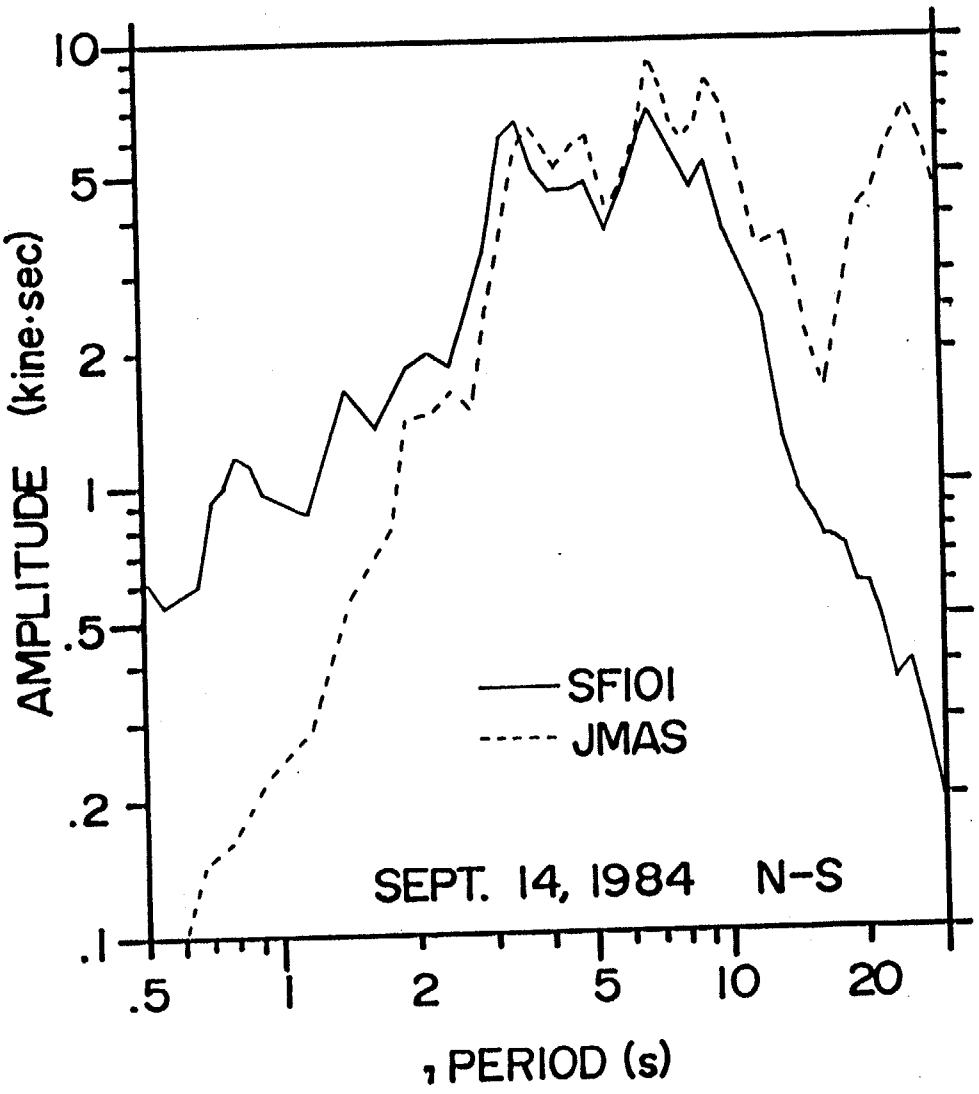

Fig. 5-8. Comparison of Fourier spectra of records obtained at Yokohama by a JMA strong motion seismometer (JMAS) and a velocity type strong motion seismometer (SF101).

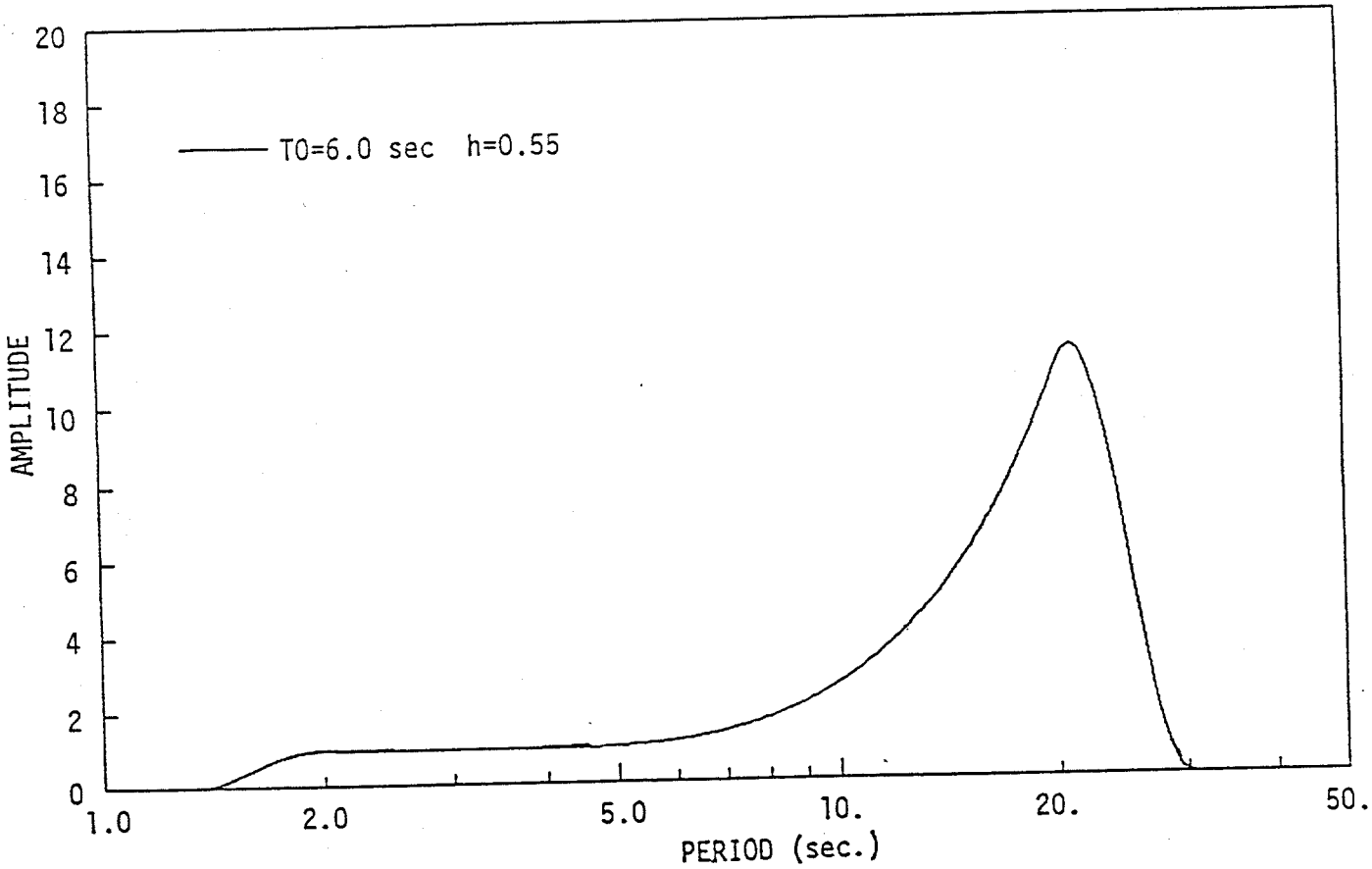

Fig. 5-9. Filter used in digitization of JMAS records.

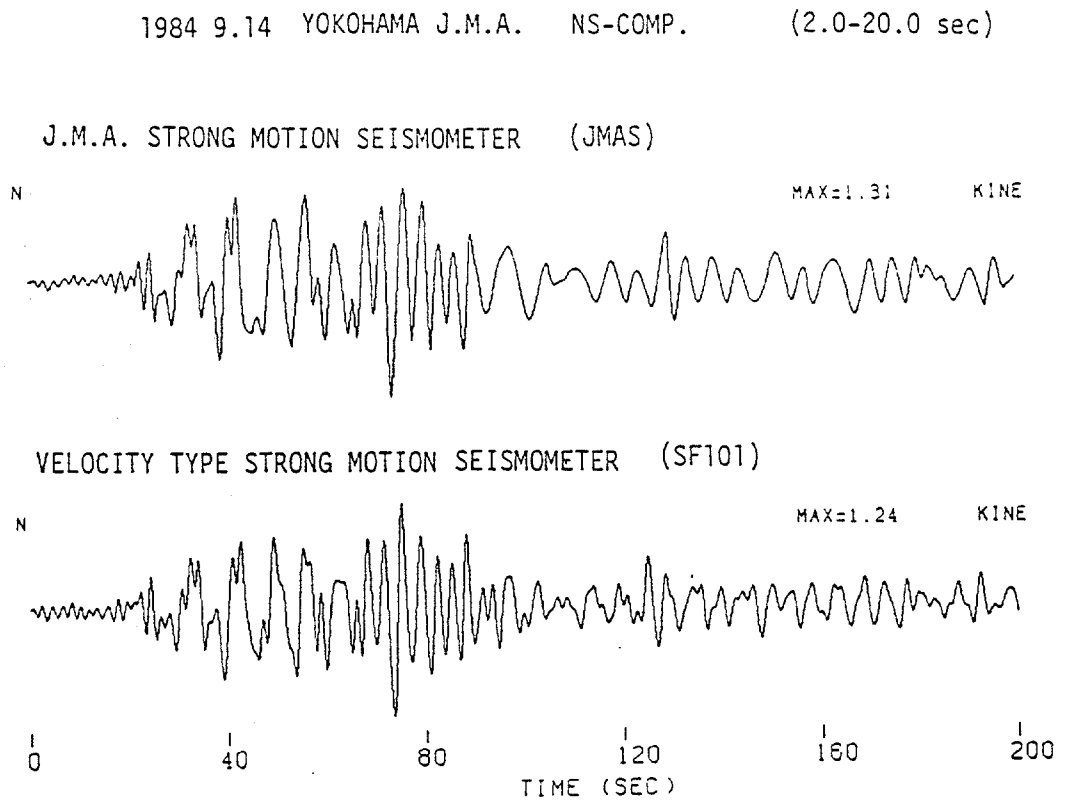

Fig. 5-10. Comparison of seismograms obtained at Yokohama obtained by a JMA strong motion seismometer (JMAS) and a velocity type strong motion seismometer (SF101).

During the Western Nagano earthquake, the ground motion was well observed at the Tokyo JMA station, too. The location of Tokyo station is about 10km away in the north-west of the Yumenoshima explosion site as shown in Fig. 5-1.

The observed displacements at the Tokyo and the Yokohama JMA stations are depicted in Fig. 5-11. Each trace indicates displacement in the north-south direction which almost corresponds to the transverse direction. Despite of the nearly equal epicentral distances, the waveforms at the two sites show different features. Although the dispersive wave trains can be seen in both seismograms, the pattern of dispersion is considerably different. The response displacement spectra of the transverse components at Tokyo and Yokohama are shown in Fig. 5-12. The response spectrum of Tokyo has one peak. That of Yokohama has two peaks in periods of 3 or 4 sec and 7 sec. Although the predominant period at 7 sec is common for the both records, the amplitudes are different; spectral amplitude at Tokyo is three or 4 times as large as that at Yokohama. These different features of seismograms obtained at Tokyo and Yokohama were investigated in the followings.

The multi-filter analysis is also applied to the corrected ground velocity at the Tokyo JMA station in order to investigate the dispersion characteristics. The contour map of the record at the Tokyo station in Fig. 5-13 indicates the different characteristics compared with that at YKH (cf. Fig. 5-4b). As pointed out above, the spectral peak of the record at the Tokyo station can be found only at period of around 7 sec. However, peak with a period of 3-4 sec. is seen at YKH as well as the second peak at 7 sec. Moreover, the ridge line of the maximum value of the envelope for each period for the Tokyo station changes more steeper than that for YKH. This means that the group velocity changes rapidly against the period. As explained above using the dispersion curve of group velocity in Fig. 5-5, the different features of seismograms at the two sites can be elucidated by considering the difference configurations of the underground structures around Yokohama and Yumenoshima.

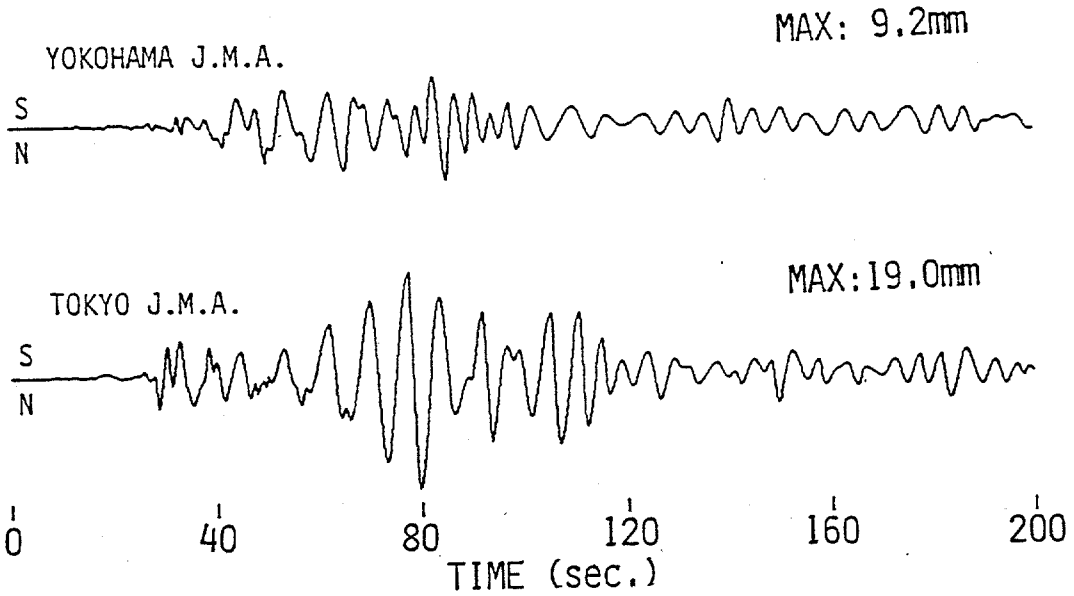

Fig. 5-11. Displacements observed at the Tokyo and the Yokohama JMA observatories during the Western Nagano earthquake of 1984. Each trace indicates N-S component which corresponds nearly to the transverse direction.

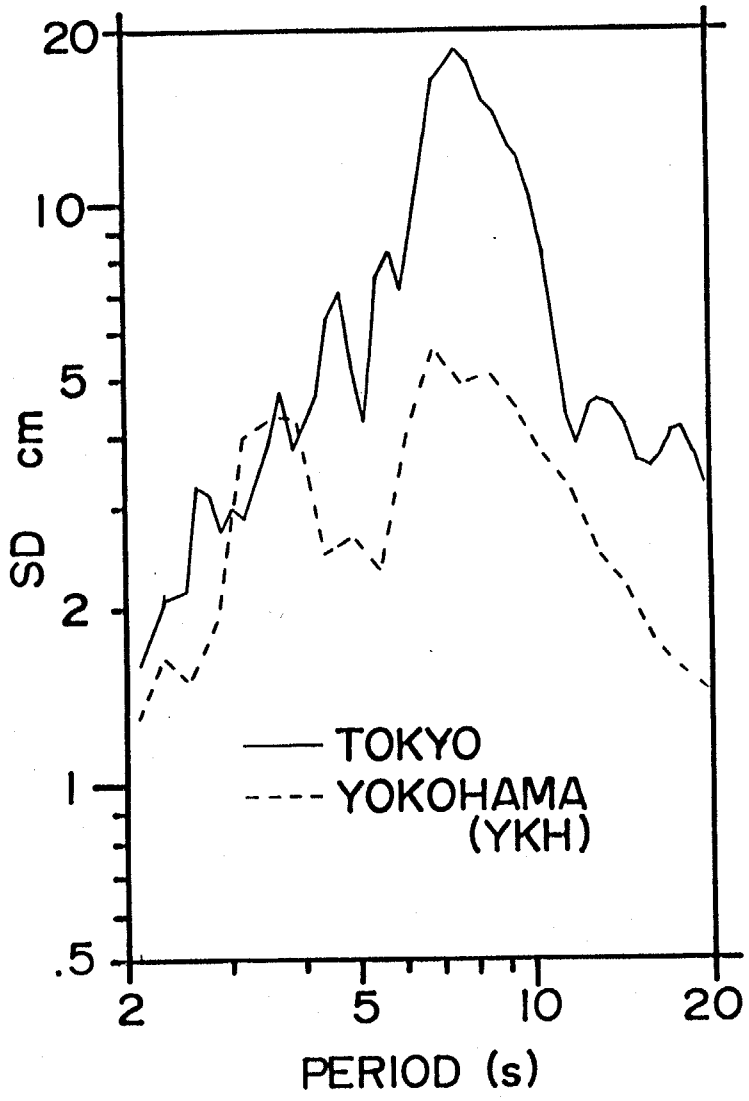

Fig. 5-12. Displacement response spectra with damping coefficient of 2% for the transverse components at Tokyo and Yokohama.

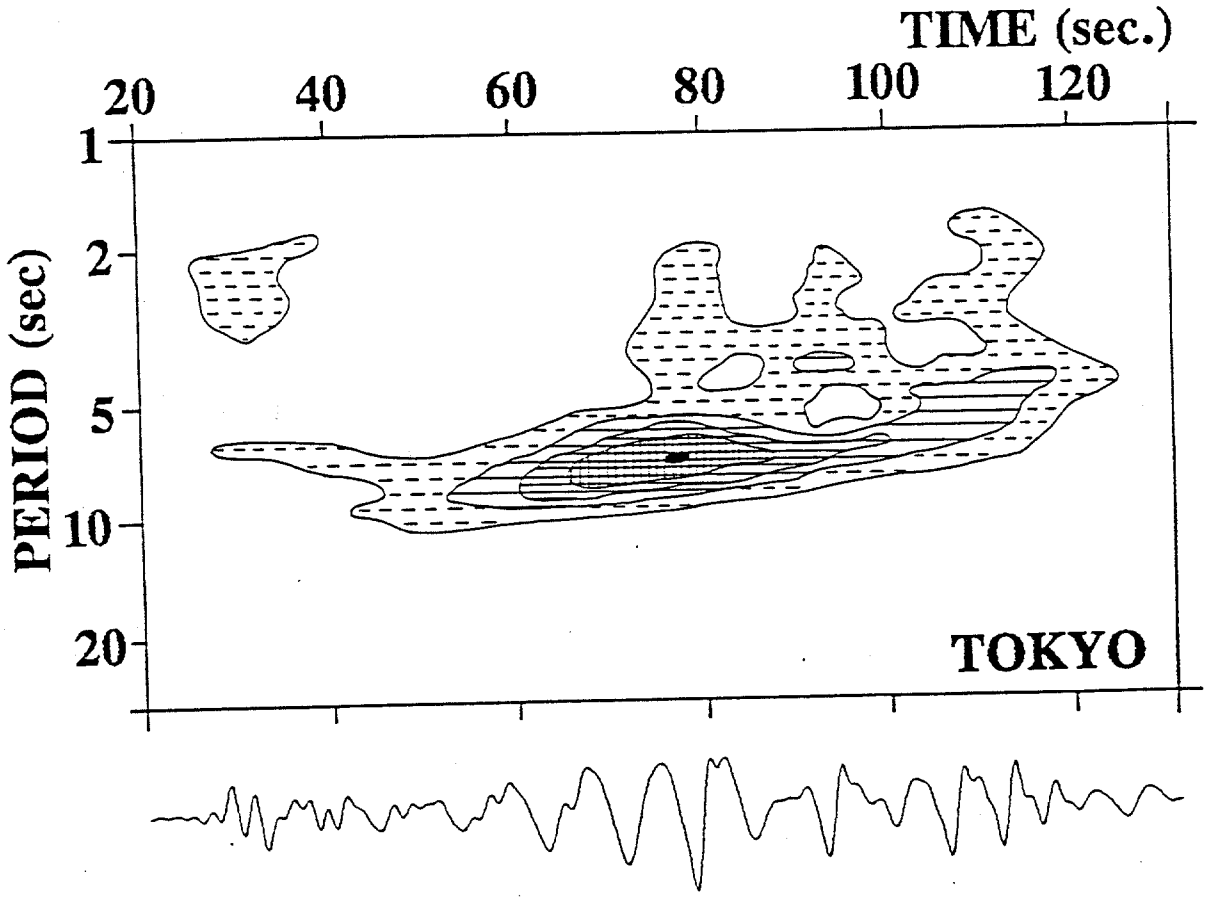

Fig. 5-13. Multi-filter analysis of the transverse components at Tokyo.

5.2 Numerical Modeling of Surface Wave Propagation within Sedimentary Layers.

It became clear in the previous section that the observed seismograms are considerably affected by the sedimentary layers corresponding to the propagation paths. In this section, numerical forward modelings are carried out to simulate surface wave propagation within the sedimentary layers.

5.2.1 Computational procedure

Many kinds of numerical forward modeling for seismic wave propagation in inhomogeneous media have been developed until now. The most interesting point of numerical modeling here is how we can simulate the ground motions observed on the sediments during the Western Nagano earthquake by taking into consideration realistic deep sedimentary layers' structures. The finite difference method employed in the chapter 4 was also used for the surface wave propagation problems. However, different treatment in the computation is needed, especially for the description of the input wave, because of differences in the propagation mechanism.

It is reasonable as a source in a computation to set a certain wavelet or force at fault region according to the fault mechanism of an earthquake considered. However, such treatment in a large model with epicentral distance around 200 km long, as discussed here, requires large computational facilities for the longer period range in the finite difference modeling. Moreover, wave propagation within the sedimentary layers is of our major interest. In this study, the source in the computation was dealt with as follows.

We supposed that the observed seismogram at the ASK station can be regarded as the incident wave to the sedimentary layers. The transverse displacement record at ASK is used as the incident wave in the modeling. Since the main portion of the seismogram consists of Love waves which propagate horizontally along the free surface of the earth from the source, it is better to set the incident wave not as a point source, but as a plane wave with a certain weight function in the vertical direction. We call this vertical row of the grids "input

plane" in the following. As the weight function, we employed the vertical distribution of the displacement for the fundamental-mode Love wave at a period of 6.5 sec in the simple horizontally layered crustal structure which was assumed as a structure near the ASK station as shown in Fig. 5-14. The period of 6.5 sec corresponds to the predominant one of the record at ASK.

The criteria for the grid spacing and the time increment (eq. 4-19) must be satisfied to get stable computation and to avoid numerical error. Hence, a band pass filtering should be applied to the incident wave. Fig. 5-15 shows the original velocity observed at ASK (lower trace) and the records filtered with various frequency bands. The shortest period in which the major features of the original record in the long period range are not reduced or not deformed is considered to be 4 sec. In the computation, therefore, the cosine-tapered band pass filter with cut-off periods of 3.57 and 16.5 sec was used to provide the incident wave. The characteristic of the band pass filter is shown in Fig. 5-16. The resultant filtered dispacement with a duration of 60 sec as displayed in Fig. 5-17 was used as the input wave.

To avoid scattering waves at the input plane, the same kind of treatment used in the chapter 4 was applied for the displacements at the grid points on the input plane. The artificial boundaries on the both sides and the bottom of models were treated as absorbing boundaries based on the method proposed by Reynolds (1978). Free stress condition is imposed at the upper boundary. Throughout this study, the grid spacing and the time increment were set 0.2 km and 0.04714 sec, respectively, considering the period range as determined above.

Before going to simulate ground motions using realistic underground structure, the procedure was tested for a simple model which consists of two media with a vertical interface as shown in Fig. 5-18. An input wave has a short duration. The input plane is indicated by a broken line in the model. The displacements calculated on the free surface are depicted in the lower part of Fig. 5-18. The phases scattering back towards the input plane propagate beyond the input plane and the reflections from the artificial boundary at the left

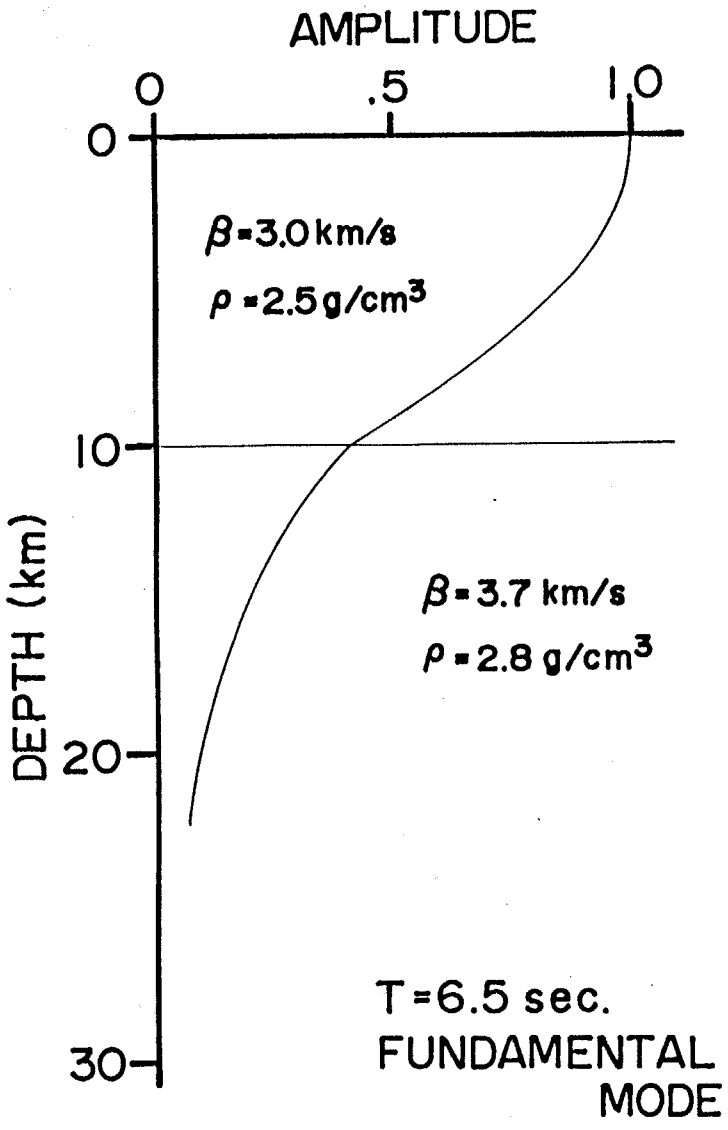

Fig. 5-14. Vertical distribution of normalized displacement amplitude of fundamental Love wave at a period of 6.5 sec. for crustal structure model depicted. This distribution is used for a weight function of source in FD computations.

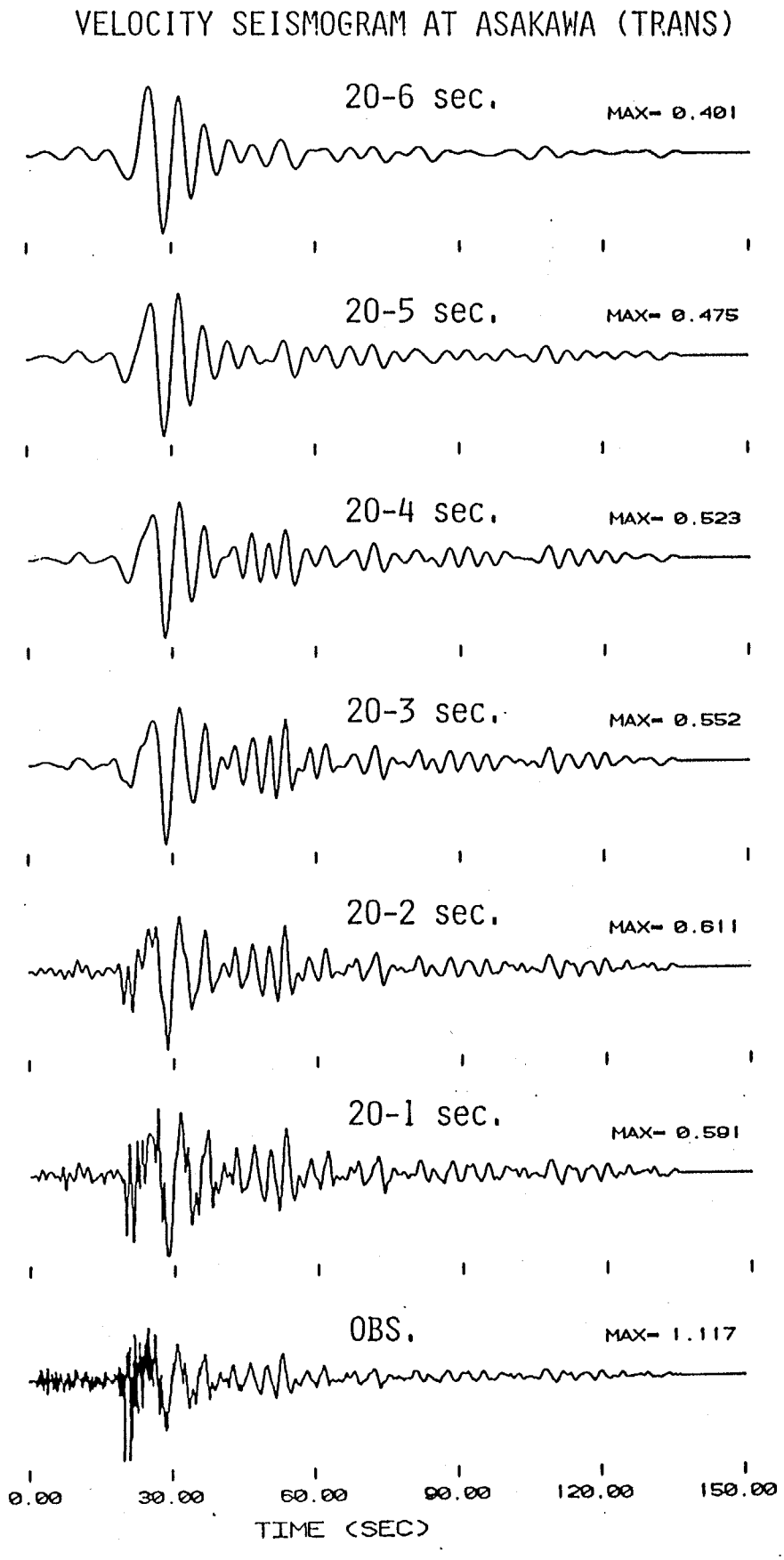

Fig. 5-15. Transversely polarized velocity observed at ASk (top trace) and its filtered seismograms with various frequency bands (lower traces).

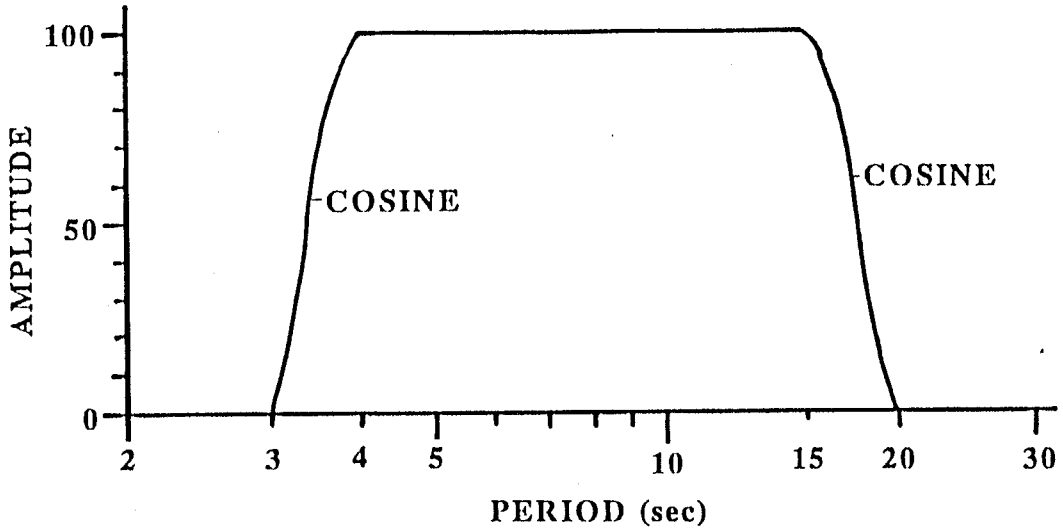

Fig. 5-16. Band pass filter applied to the record at ASK during the Western Nagano earthquake to make input wave for the FD computations.

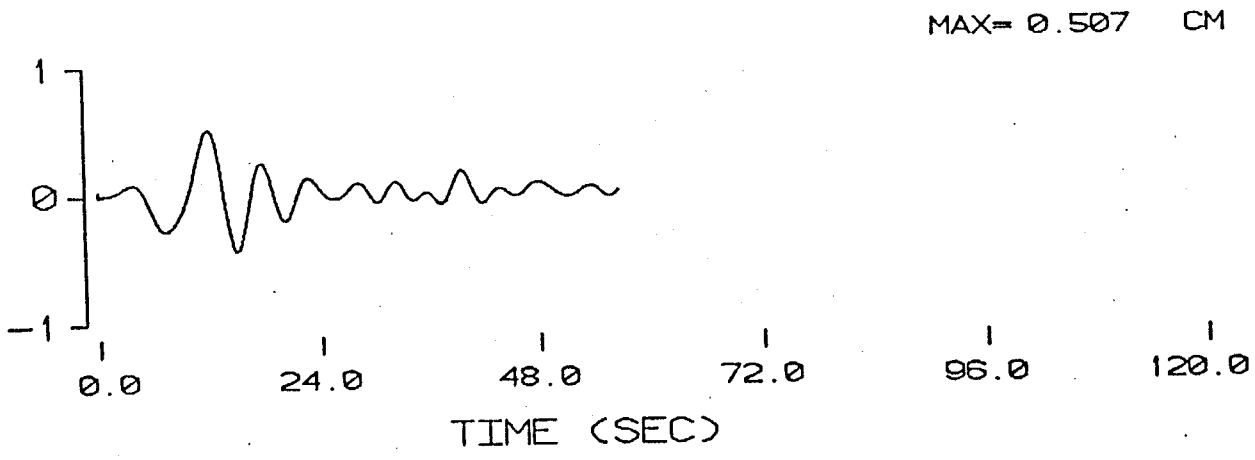

Fig. 5-17. Filtered transverse displacement observed at ASK used for the input wave in the FD computations.

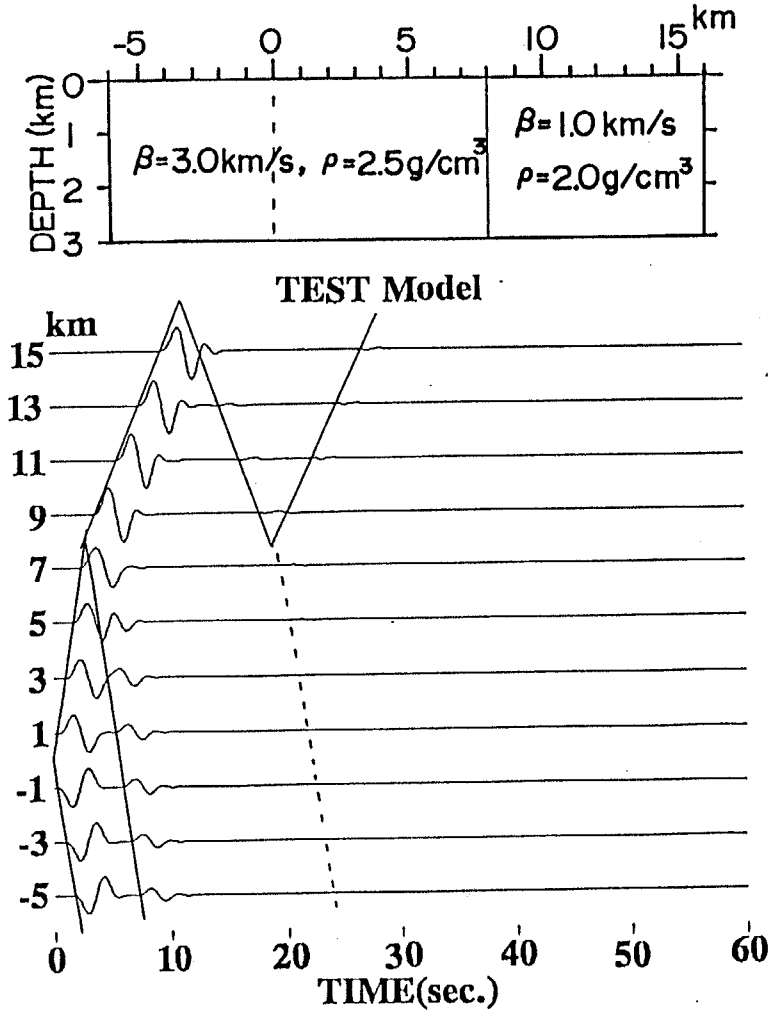

Fig. 5-18. Model used to test effects of the source treatment and computed displacements on free surface of the model.

end of the model are suppressed.

5.2.2 Numerical results for Yokohama model

The numerical modeling of surface wave propagation within sedimentary layer between ASK and YKH (line B in Fig. 5-1) is discussed here. First, the underground structural model is constructed by using results of the seismic surveys in the chapter two, then, the modeling is carried out.

The underground structure between NGT and YKH was accurately made clear by the seismic surveys. The two-dimensional underground structure between NGT and YKH is depicted by a thick line in Fig. 5-19. However, the underground structure between NGT and ASK has not been revealed in detail. The data available to construct the structural model between NGT and ASK only relay on the observation of the Yumenoshima explosion which was detonated more than 30 km far from the area under consideration. The temporary observation sites were set like an array of fan shooting as shown in Fig. 5-20. The travel times of the initial phases are listed in Table 5-1. The travel time data of Yumenoshima explosion obtained between NGT and YKH are also shown in this figure. Since there are no observations of reversed shots, it is difficult to deduce the detailed underground structure. In order to get gross features of the structure, the time-terms for the sedimentary layers overlying the refractor were derived by assuming that the refractor velocity is 5.45 km/sec and the time-term at the shot point, Yumenoshima, is 1.03 sec. The time-terms are shown by solid and broken lines in Fig. 5-19; they can be divided to two groups according to the locations of the observation sites. Although the configuration of the sedimentary layers can not be deduced only from the distribution of the time-terms, it is evident that the sedimentary layers become gradually thinner toward ASK. Considering these circumstances, the following two models were made for this profile.

The first model is depicted in Fig. 5-21. Hereafter, we call the model "Yokohama model 1." The S-wave velocities and densities are the same ones as used in the calculation of the theoretical dispersion curve which could accomplish a good agreement with the

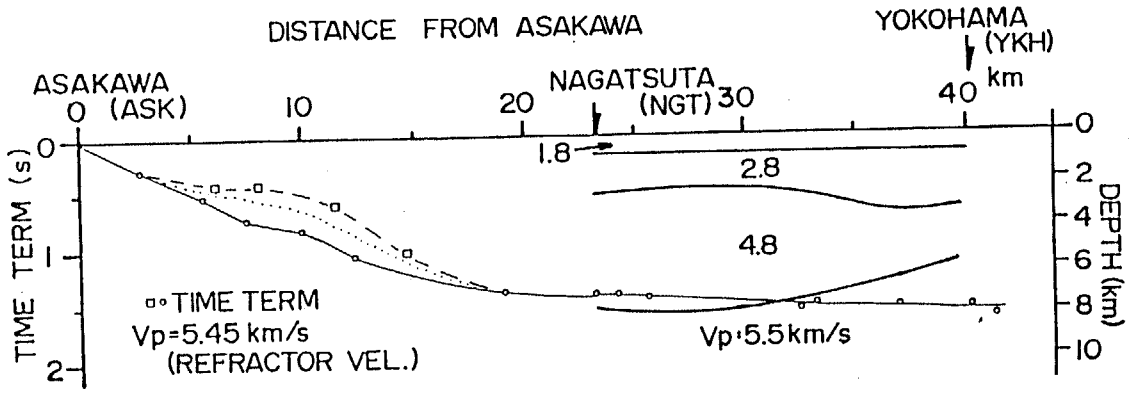

Fig. 5-19. Underground structure between NGT and YKH along Line B (in Fig. 5-1) revealed by seismic refraction prospectings and time-terms along Line B obtained from explosion at Yumenoshima assuming that the refractor velocity is 5.45 km/s and time-term at Yumenoshima is 1.03 sec. Time-terms indicated by dotted and solid lines are obtained at stations along dotted and solid lines in Fig. 5-20, respectively.

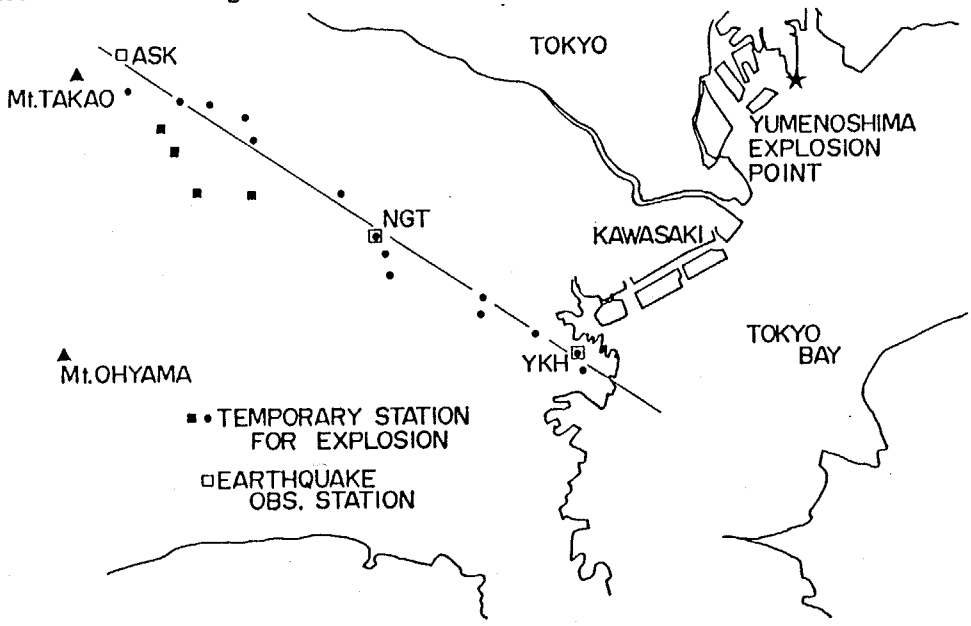

Fig. 5-20. Location of observation points of the Yumenoshima explosion between ASK and YKH.

Table 5-1. Location and travel times of initial phases
obtained from Yumenoshima explosion between ASK and YKH

No	STATION	LAT.	LONG.	DISTANCE(km)	TRAVEL TIME(s)	TIME TERM(s)
1	OHTO	35 36 41.9	139 17 30.5	49.48	10.39	0.28
2	AIHARA	35 36 14.3	139 19 49.5	45.99	9.99	0.52
3	KUBOGAHARA	35 36 03.4	139 21 18.0	43.78	9.78	0.72
4	OYAMA CHO	35 35 33.2	139 20 50.0	41.50	9.46	0.82
5	FUCHINOBE	35 34 28.4	139 23 47.2	40.08	9.43	1.05
6	MACHIDA 6 SHO	35 32 44.6	139 21 47.9	34.74	8.76	1.38
7	NAGATSUTA	35 30 31.4	139 29 16.9	33.73	8.63	1.41
8	WAKABADAI	35 30 13.4	139 29 46.3	33.31	8.55	1.41
9	HODOGAYA C.C.	35 29 16.9	139 30 02.9	33.62	8.64	1.44
10	KAMIHOSI KAWA SHO	35 28 21.8	139 34 52.5	28.09	7.74	1.56
11	NISHI CHU	35 26 56.5	139 37 16.9	26.90	7.50	1.53
12	YOKOHAMA JMA	35 26 13.6	139 39 19.8	25.92	7.33	1.54
13	HOSIIGAOKA	35 27 34.9	139 34 49.2	28.88	7.84	1.51
14	OSHIMA SHO	35 25 26.9	139 39 36.7	26.39	7.51	1.64
15	NIHONMATSU SHO	35 35 19.8	139 19 13.1	46.97	10.61	0.41
16	OSAWA SHO	35 34 21.6	139 19 42.4	46.40	9.97	0.43
17	SAGAMI G.C.	35 32 37.6	139 24 11.4	40.13	9.42	1.03

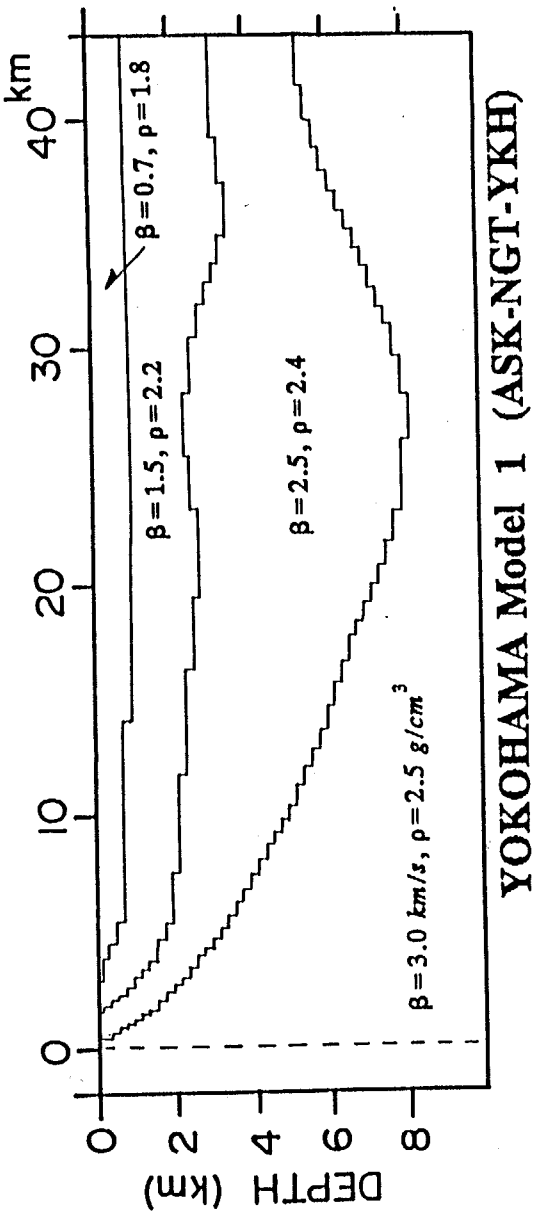

Fig. 5-21. Underground structure model between ASK and YKH (Yokohama model 1).

observed one. The underground structural model from 20 to 40 km distance from the input plane is almost the same as the surveyed profile shown in Fig. 5-19. The model within a distance of less than 20 km is based on the following interpretation for the nature of the later phase in the seismograms observed on the sediments. It can be seen in Fig. 5-2 that the later phase has an apparent velocity of around 0.6 km/sec, which is approximately the same as that of the top sedimentary layer, and its travel time curve meets that of the initial S-wave near ASK. This observation leads us that the later phase might be generated in the margin of the basin near ASK and propagate toward the center of the basin. This interpretation requires that the thickness of the first layer should be large even from ASK and NGT, in order to get low propagation velocity of 0.6 km/sec. Therefore, the sedimentary layers in the Yokohama model 1 have a thickness of 2-3 km at the points with distance of more than 5 km from the input plane.

The computed displacements on the upper free surface of the model are shown in Fig. 5-22. The amplitudes are normalized to the maximum of all the traces. The maximum amplitudes for the traces at the points where the top layer with a low S-wave velocity of 0.7 km/sec exists are three or four times as large as that of the incident wave. Because of dispersion, the durations of the synthetic seismograms become longer with increasing distance from the input plane. The apparent velocity of the first arrivals is nearly equal to the velocity of the bottom layer. As compared with the features of the observed seismograms seen in Fig. 5-2, it can be considered that the synthetic seismograms show considerable different characteristics; the two later phases are not divided into two wave trains.

In order to improve this inconsistency with the observation, the second model for the profile was constructed. The second model is shown in Fig. 5-23 (Yokohama model 2 in the following). The S-wave velocities and densities of the layers are identical with those of Yokohama model 1. Although the structural model between 20 and 40 km distances is almost the same as the previous model, it shows different features at distances of less than 20 km. The topography of the layer with an S-wave velocity of 2.5 km/sec has a steep incli-

Table5-2. Shear wave velocity and density of Yokohama model 1

No	S-WAVE VEL. *km/sec*	DENSITY g/cm^3
1	0.7	1.8
2	1.5	2.2
3	2.5	2.4
4	3.0	2.5

Table5-3 Shear wave velocity and density of Tokyo model

No	S-WAVE VEL. *km/sec*	DENSITY g/cm^3
1	0.7	1.8
2	1.5	2.2
3	3.0	2.5

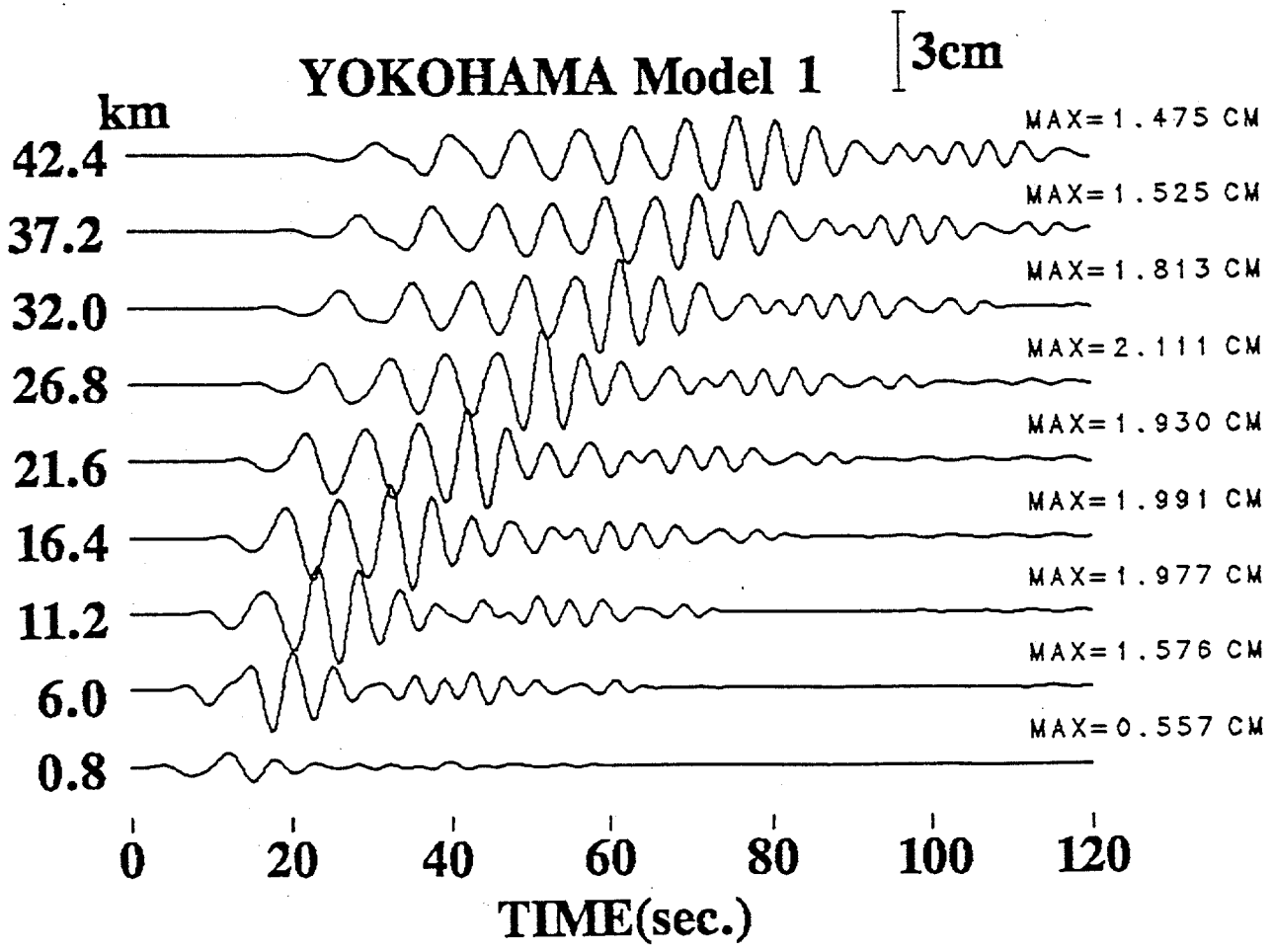

Fig. 5-22. Synthetic displacements on free surface of the Yokohama model 1 (Fig. 5-21). Each trace is normalized to maximum of all traces.

nation at distance of 15 km from the input plane, considering the results of the seismic survey around NGT. The layer having an S-wave velocity of 0.7 km/sec does not exist within 15 km distance from the input plane. This profile gives better correlation with the distribution of time-terms in Fig. 5-19 than that of the Yokohama model 1.

The computed displacements on the free surface of the model are shown in Fig. 5-24. Each trace is normalized with the same amplitude scale as used for plotting of the synthetic seismograms of the Yokohama model 1 in Fig. 5-22. The synthetic seismograms at the points with distances less than 15 km from the input plane have small amplitudes and no well dispersive characteristics. On the other hand, the amplitudes of the seismograms at the points far 15 km from the input plane become about three times larger than that of the input wave, and durations become longer, because of the dispersion. This implies that the surface layer with an S-wave velocity of 0.7 km/sec has significant influence on the characteristics of earthquake ground motion in the long period range. Two wave trains can be seen in the synthetic seismograms. The apparent velocity of the latter phase is about 0.65 km/sec at the points where the surface layer has a velocity of 0.7 km/sec. The extended line of the travel time curve for the latter phase indicated by a broken line in Fig. 5-24 crosses with that of the first arrivals near the position of the input plane. These features are in good agreement with the observation.

The synthetic seismograms for Yokohama model 2 were compared with the observed displacements at NGT and YKH in Fig. 5-25. The integration and the same filter as used for the input wave were applied to the observed velocities. The predominant period of the second phase is less than that of the first one. This characteristic is consistent with the observations. Since the absolute time of the observed records is adjusted, the arrival time of each phase can be also compared. The first distinct phases of the observed and synthetic seismograms arrive at the same time. The arrival time of the second ones, however, are slightly different. The synthetic seismograms have larger amplitudes than the observed ones, perhaps, because of the ignorance of the effects of anelasticity in computation. Neverthe-

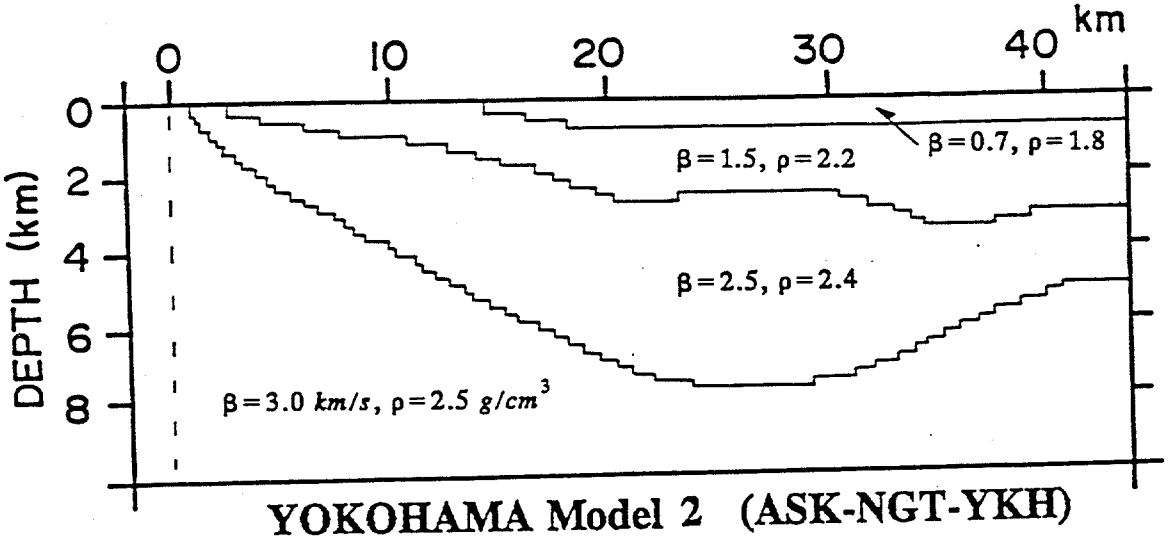

Fig. 5-23. Underground structure model between ASK and YKH (Yokohama model 2).

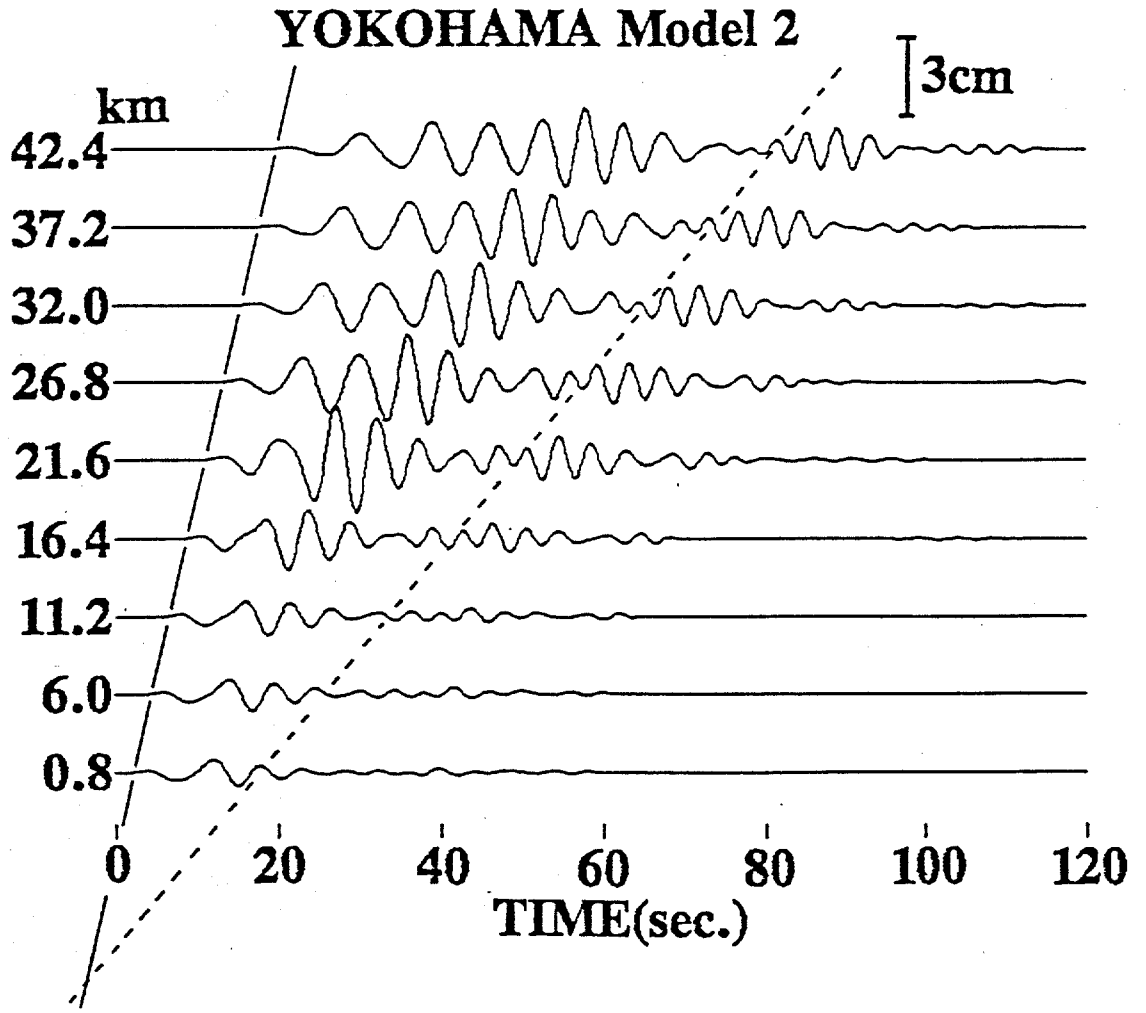

Fig. 5-24. Synthetic displacements on free surface of the Yokohama model 2 (Fig. 5-23). Each trace is normalized to the same value as used in Fig. 5-22.

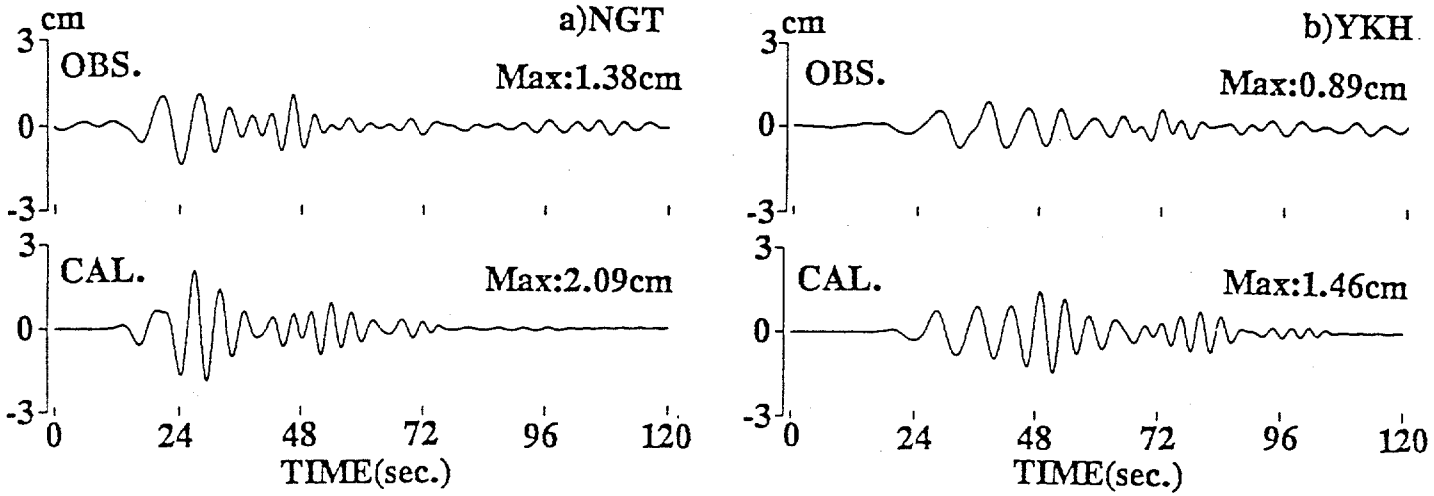

Fig. 5-25. Comparisons of observed and synthetic displacements at a)NGT and b)YKH. Observed seismograms are filtered in periods of 3 to 20 sec.

less, the general features of the observed seismograms are well explained by the numerical modeling and the knowledge of the underground structure clarified by the seismic surveys.

As compared with the synthetic seismograms from Yokohama model 1, it is found that the location where the top layer with an S-wave velocity of 0.7 km/sec begins to appear is of important for describing the characteristics of earthquake ground motions in the time domain. In particular, durations of earthquake ground motions observed in the area discussed would be roughly estimated by considering how long seismic waves propagate within the layer having an S-wave velocity of 0.7 km/sec.

5.2.3 Numerical results for Tokyo model

The same kind of the numerical forward modeling was applied to simulate the earthquake ground motions at Tokyo. It is not so difficult to make a reasonable underground structural model for the profile between the ASK and the Tokyo JMA stations, because Yumenoshima-Takao line (line C in Fig. 2-1) from Yumenoshima to Takao is applicable to this modeling. As can be seen in Fig. 2-17, the depth to the last layer with a P-wave velocity of 5.35 km/sec, the basement, becomes gradually larger from the foot of Mt. Takao toward the east, until it reaches around 2.5 km. Then, the thickness of the sedimentary layers becomes nearly constant toward the Yumenoshima explosion point. Therefore, this underground structure was used for the numerical modeling, though the Tokyo JMA station is apart about 10 km toward the north from this surveyed profile.

Fig. 5-26 shows the model for the underground structure between the ASK and the Tokyo JMA stations (Tokyo model in the following). The physical parameters of the layers are the same as those for the model for Yokohama, except for a lack of the layer having an S-wave of 2.5 km/sec. The upper two layers with P-wave velocities of less than 2 km/sec in the surveyed profile were treated as the same surface layer with an S-wave velocity of 0.7 km/sec in the computational model. The surface layer appears at a distance of about 10 km from the input plane and the thickness of the sedimentary layers becomes almost constant after it reaches about 2.5 km.

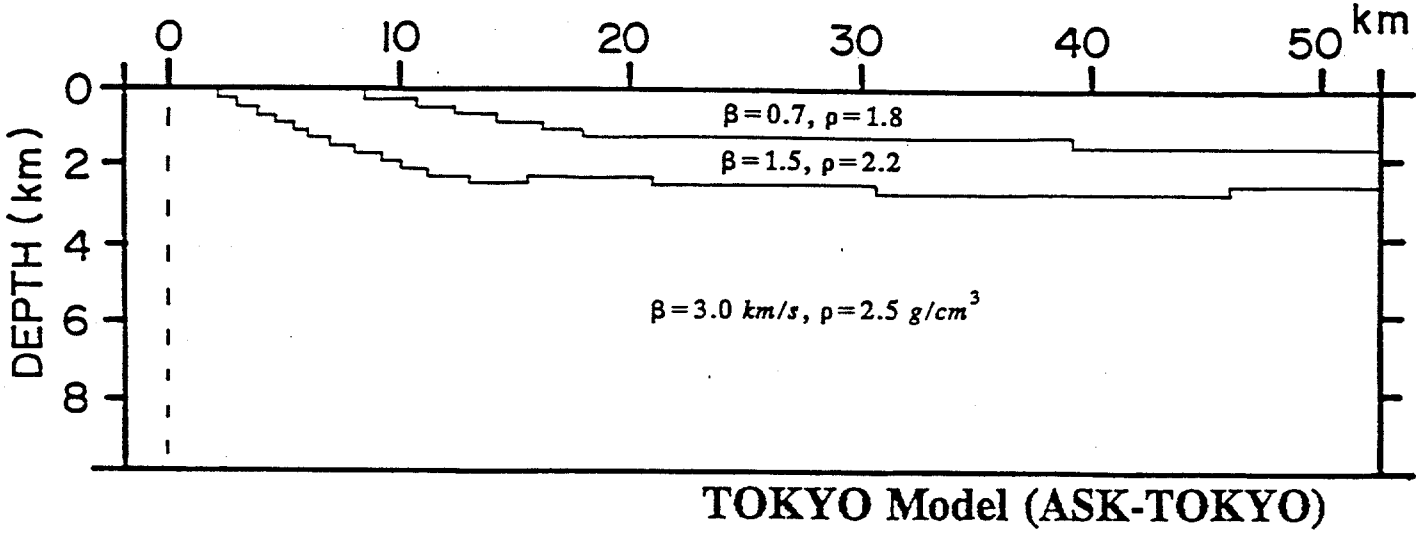

Fig. 5-26. Underground structure model between the ASK station and Tokyo JMA station (Tokyo model).

The synthetic displacements on the free surface of the Tokyo model are shown in Fig. 5-27. Each trace is normalized with the same amplitude scale as used in Fig. 5-22. The well dispersive wave trains with large amplitudes can be seen as well as the results for the Yokohama model 2. The pattern of the dispersion, however, are different between the Tokyo and the Yokohama models. As for the Tokyo model, most of the energy of the waves travel with a lower apparent velocity of about 0.6 km/sec concentrating on the latter part of the wave trains. This corresponds to the Airy phase as seen in the dispersion curve of the structure model at the Yumenoshima explosion site (see, dotted line in Fig. 5-5). Since the minimum group velocity around the Airy phase is strikingly low as seen in the dispersion curve, it is considered that most of the energy of the surface waves concentrate on the stationary period. The differences of the observed seismograms at Tokyo and Yokohama, which are considered to be mainly caused by the configuration of the sedimentary layers, could be well estimated by the numerical modelings.

The comparison between the synthetic and the observed displacements with filtering in the periods from 3 to 20 sec is shown in Fig. 5-28. Maximum amplitudes of the both traces show quite well coincidence. Although the arrival times of the phases indicating the maximum amplitudes are slightly different, the feature of the observed seismograms that energy concentrates on the latter part of the wave trains is well simulated.

It is concluded that the seismograms observed at the sedimentary layers are well explained by the two-dimensional numerical forward modelings based on the finite difference approximation with consideration of the realistic underground structure known by the seismic surveys, despite of ignorance of the contributions of some kind of body wave (e.g., refracted wave along the Moho discontinuities) and effects of inelasticity.

These results indicate the possibilities of prediction of earthquake ground motions in the longer period by considering realistic deep underground structure. For this engeneering purpose, it should be noted that sedimentary layers' structure must be clarified in the area of consideration and be included, at least, two-dimensionally in evaluation of ground motions.

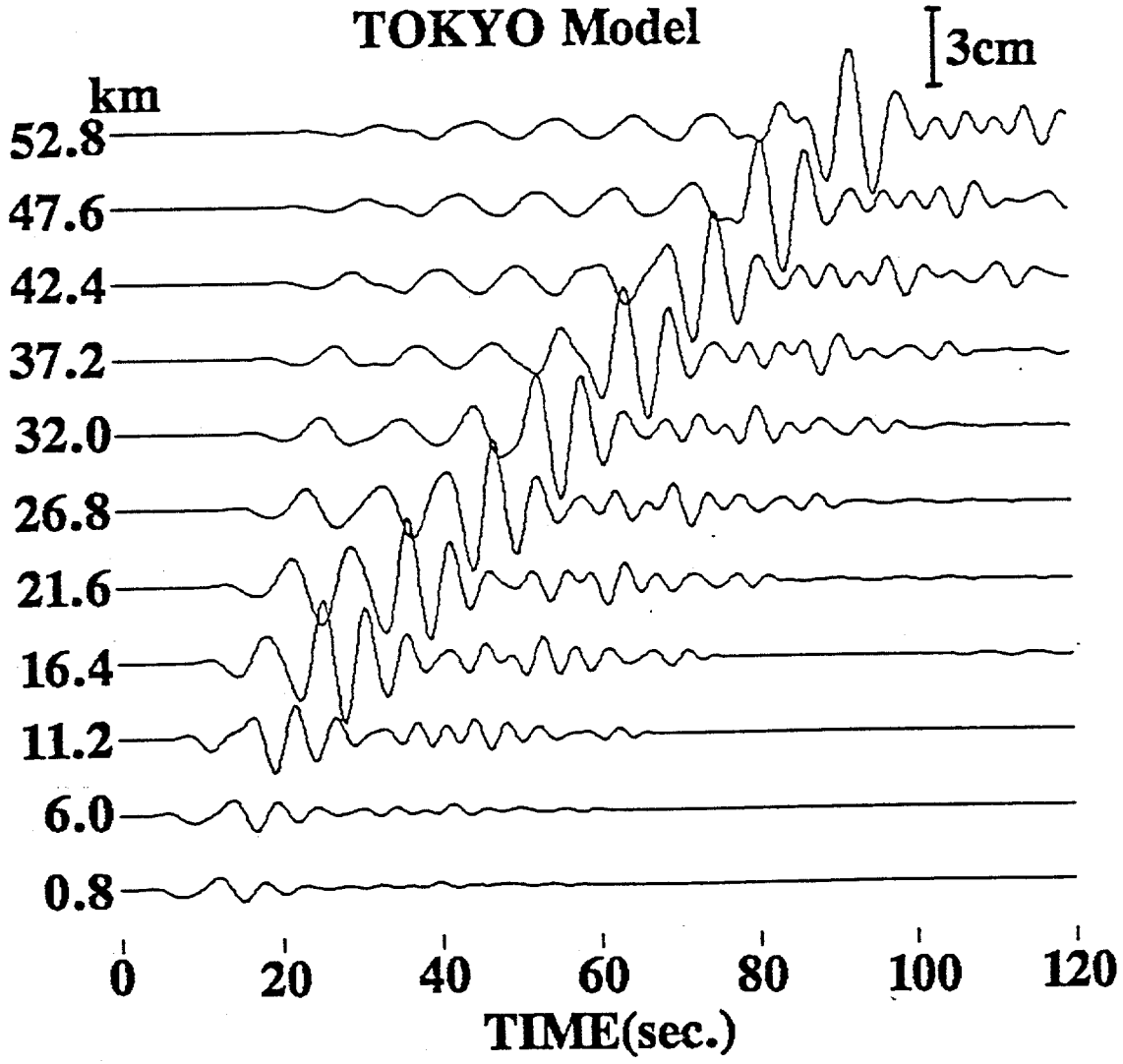

Fig. 5-27. Synthetic displacements on free surface of the Tokyo model (Fig. 5-26). Each trace is normalized to the same value as used in Fig. 5-22.

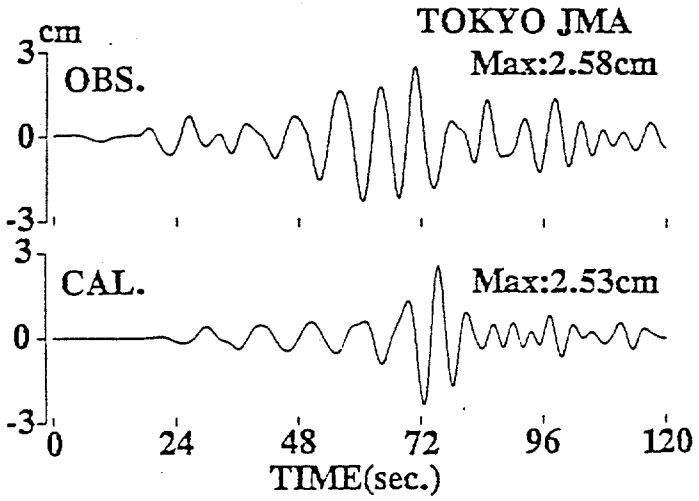

Fig. 5-28. Comparisons of observed and synthetic displacements at Tokyo JMA station. Observed seismograms are instrumentally corrected and filtered in periods of 3 to 20 sec.

5.3 Effects of Sedimentary Layers on Surface Wave Propagation

5.3.1 Surface wave propagation in flat layered underground structure

Surface wave propagation in layered media has been well investigated by employing various numerical methods. One of the typical ones is the normal mode summation method based on excitation theory of surface waves. As this method requires small computational efforts, compared with finite element and finite difference methods, it has been successfully applied for estimation of longer period ground motions (e.g., Kudo, 1978). Despite of some improvements (Kudo, 1980), it can not deal with problems requiring general inhomogeneity. Even in simulations of ground motions by methods in which two-dimensional inhomogeneities are allowed, flat layered structural models are often used, because detailed knowledge on underground structure is not available. Here, the synthetic seismograms for realistic model approximated by flat layers are compared by using the finite difference modeling.

The investigations were carried out using the profile for Tokyo and Yokohama as discussed in the previous section. At first, the synthetic seismograms for the realistic model for Tokyo were compared with those for a model approximated by flat layering. As seen in Fig. 5-26, most of the underground structure for this profile can be regarded as flat layered one. Therefore, it is expected that flat layering could be a well approximation of the realistic model. Fig. 5-29 shows the approximated model. The physical parameters of the model are the same as used in the realistic Tokyo model. The significant differences between the realistic and approximated underground structural models can be seen in a distance range less than 15 km from the input plane, where the depth to the basement becomes gradually larger in the realistic model. On the other hand, the approximated layered structure for the sedimentary layers is similar to that at the Yumenoshima explosion site.

The synthetic seismograms on the free surface of the flat layered model are shown in Fig. 5-30. The seismograms at distances less than 6 km are almost the same as those obtained for the realistic model in Fig. 5-27, which should be compared. At distances of

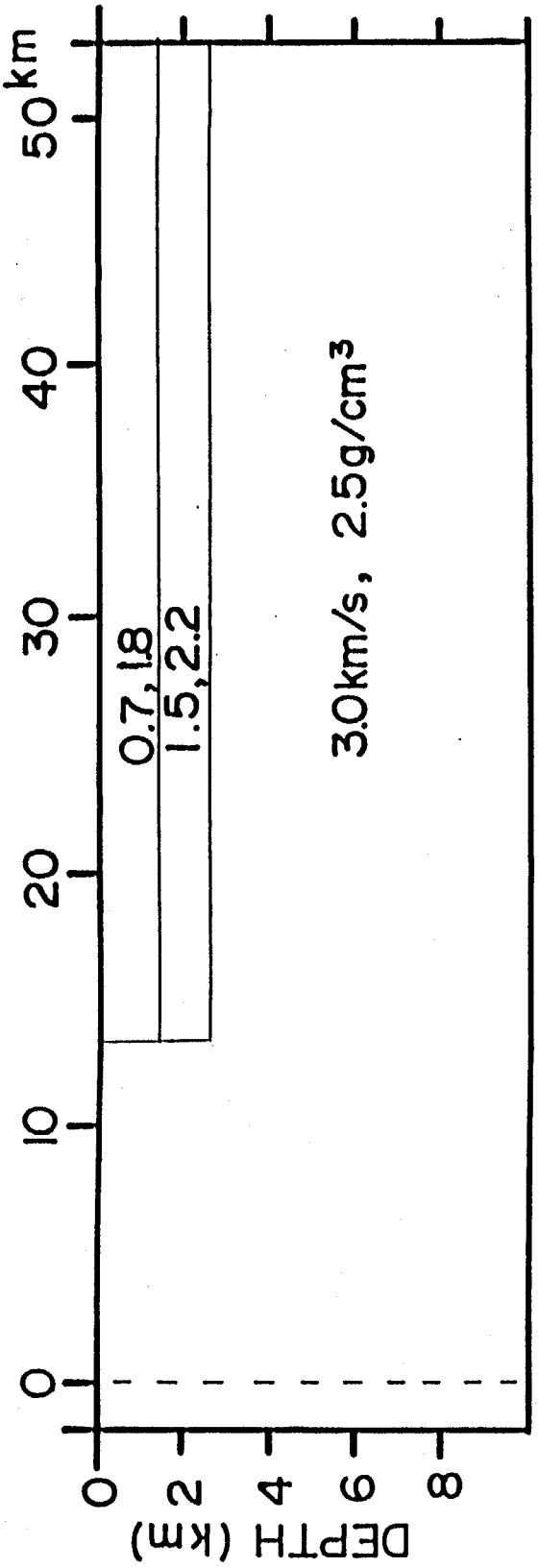

Fig. 5-29. A model approximated from Tokyo model in Fig. 5-26 by flat layers.

11.2 and 16.2 km, where the differences between the two models are seen, the synthetic seismograms for the flat model are smaller and are not dispersed like those for the realistic model. In a distance range more than 21.6 km, the features of both synthetic seismograms are similar to each other, except for the absolute amplitudes. In particular, the concentration of the energy of the seismic waves in the latter part of the seismograms is in good agreement. However, the amplitudes of the seismograms for the flat model are 60 to 70% of those for the realistic model. Additionally, the synthetic seismograms for the flat model seem to exhibit the dispersion characteristics not so smooth as those for the realistic model does, especially for the time before the large phase arrivals.

In order to compare these two kinds of synthetic seismograms from an engineering point of view, more quantitative evaluations are required. Since we consider surface waves in the longer period range, responses of large-scale structures are much concerned with this investigations. Therefore, three parameters were compared: maximum amplitude, duration and frequency content. The distributions of maximum displacements against the distances from the input plane are shown in the upper part of Fig. 5-31. The thin and thick solid lines indicate maximum displacements for the flat layered and the realistic Tokyo models, respectively. Significant differences of the amplitudes of the two kinds of the seismograms can be seen for distances less than 15 km. However, both distributions of maximum displacements show similar patterns; maximum amplitudes become larger with increasing distance to about 20 km, then, they maintain certain levels of the amplitude. The distributions of durations are shown in the lower part of Fig. 5-31, The duration, here, was calculated according to the definition by Trifunac and Brady (1975): the time interval for which the square amplitude of the displacement lies between 5 % and 95 % of the total integrals. Although there is fluctuation in the curve of the durations for the flat layered model, they are both consistent. As for the frequency content, spectral ratios of the synthetic seismograms to the input wave, displacement observed at ASK, were calculated at several points as shown in Fig. 5-32. The spectral ratios for the flat layered and the realistic models are not different

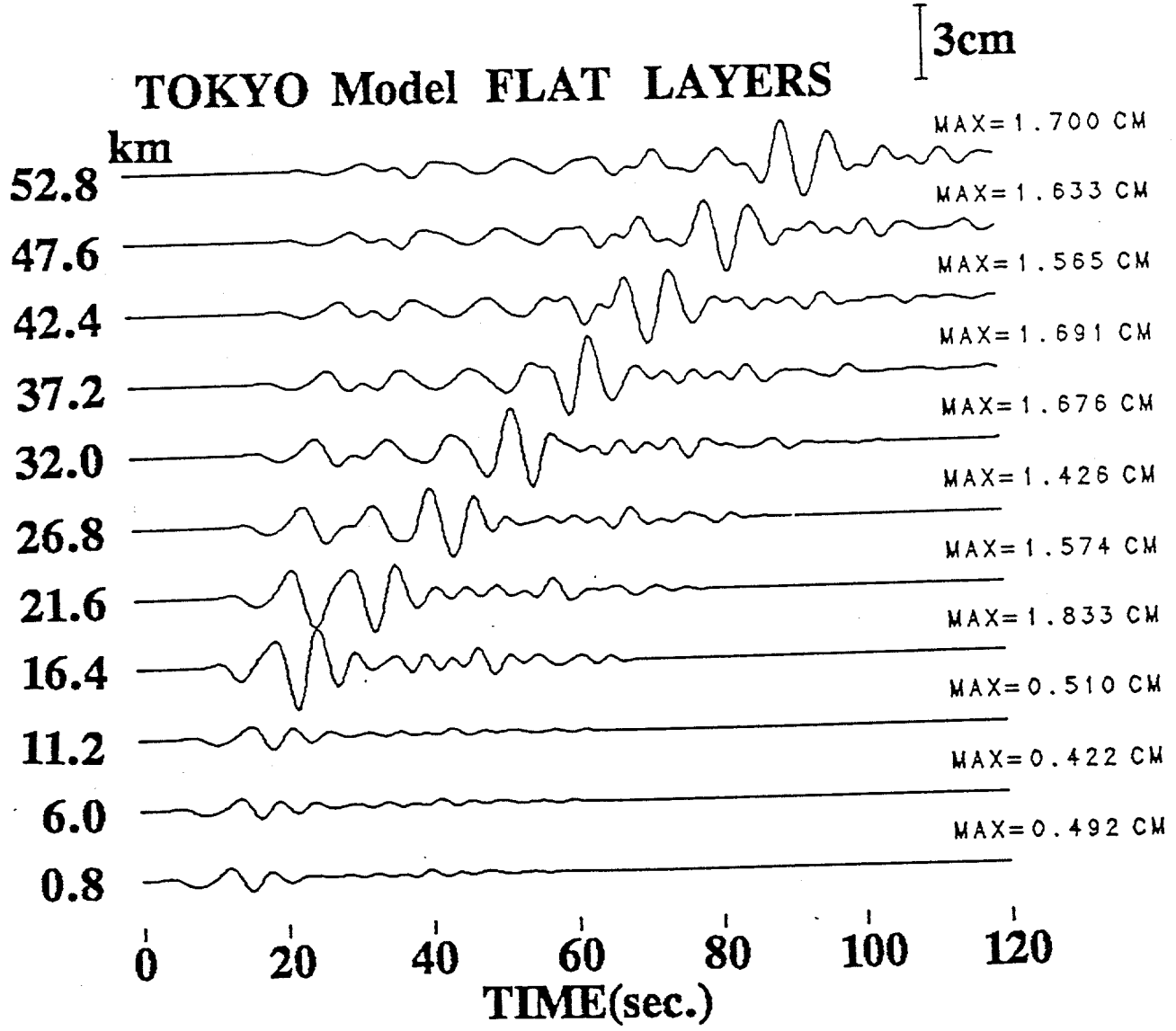

Fig. 5-30. Synthetic displacements on the free surface of the model in Fig. 5-29. Each trace is normalized to the same value as used in Fig. 5-22.

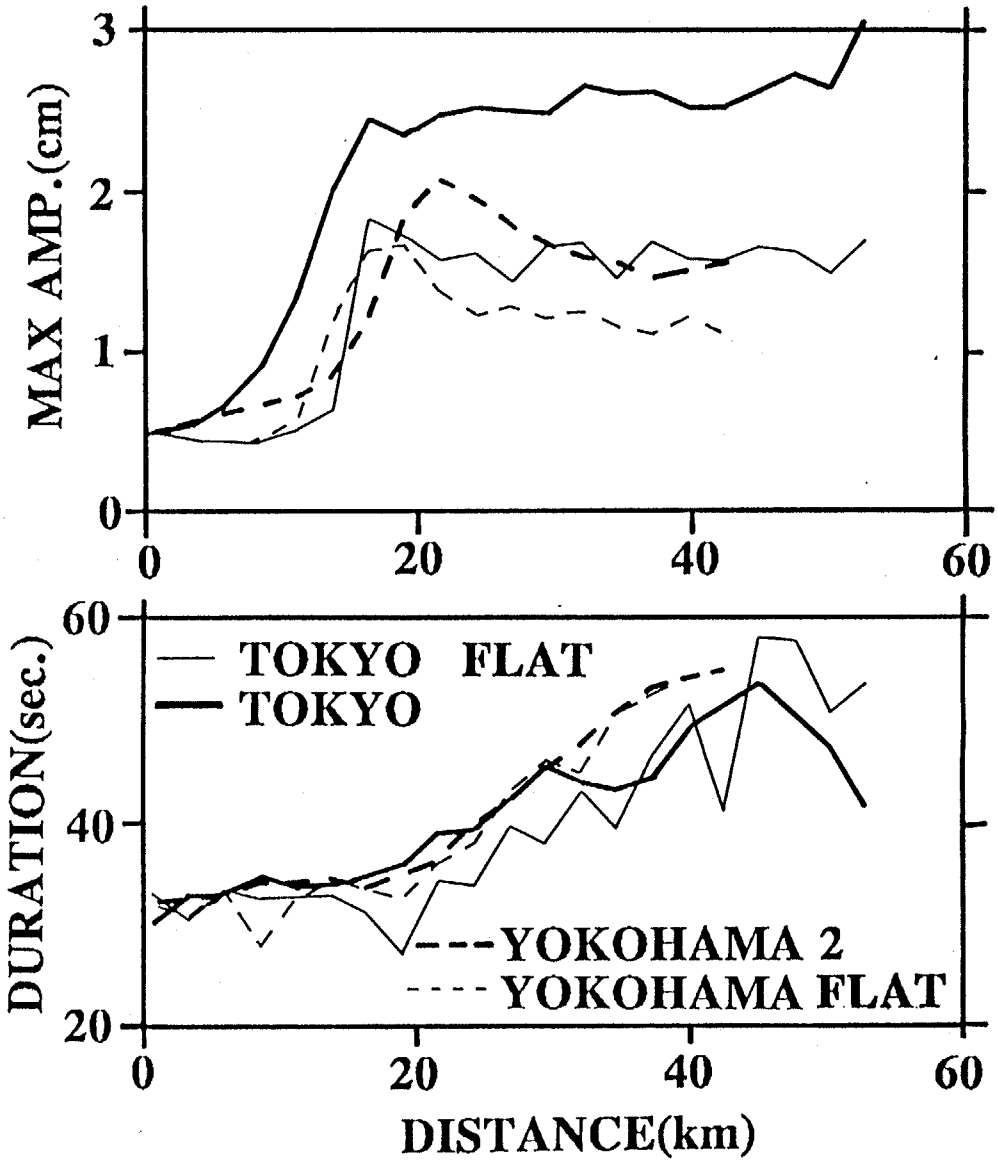

Fig. 5-31. Distribution of maximum displacements and durations for the synthetic seismograms in Fig. 5-30 as well as those in Fig. 5-34.

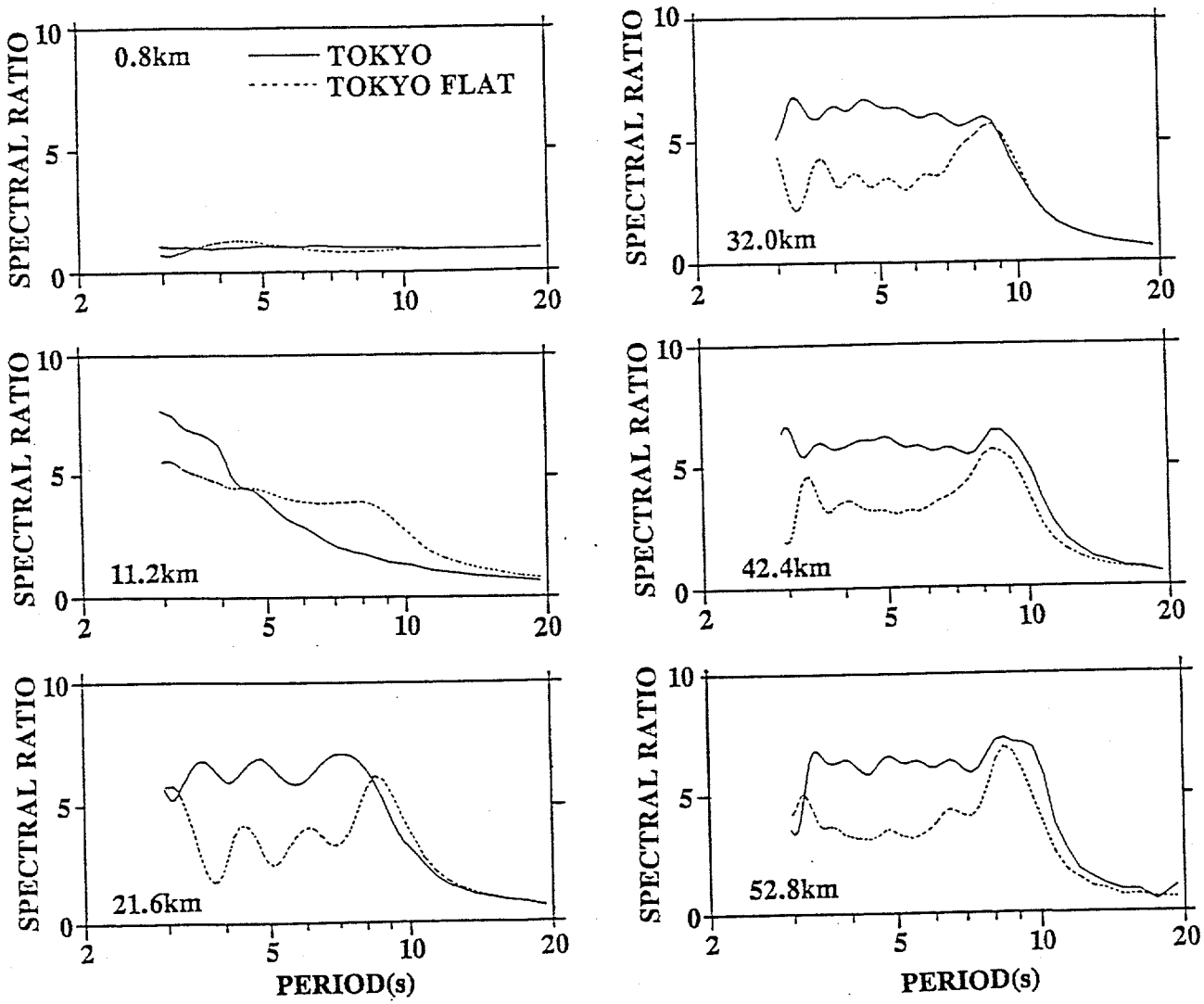

Fig. 5-32. Spectral ratios of the synthetic seismograms in Fig. 5-30 to the input wave shown in Fig. 5-17.

in a period range more than 8 sec. At the points with distances more than 21.6 km, the same tendency of the spectral ratios can be seen; peaks with the same spectral amplitudes appear at around 8 sec for the both models and the ratios for the flat layered model are characterized by an absence of short period components. This indicates that the realistic underground structure in distances less than 20 km contributes to the amplification of the short period components, because of their thin sedimentary layers.

The same investigation was carried out for the profile of Yokohama. The model, approximated by flat layers, shown in Fig. 5-33 was derived from the underground structure model which could satisfy the observed group velocities.

The synthetic seismograms for the flat layered model are depicted in Fig. 5-34. Compared with the synthetic seismograms for the realistic model in Fig. 5-24, we obtained that both displacements are similar. Probably, this is due to the similarity of the low velocity top layer. The thickness of the second layer varys significantly as it is seen in the realistic model. The shear wave velocity for the second layer is relative high and wave lengths become also longer in this layer. Therefore, it is considered that the variation of the thickness of the second layer gives less influences to the ground motions in the long period range. The maximum displacements and the durations for the flat layered and the realistic models were plotted by thin and thick broken lines in Fig. 5-31, respectively. More similar distributions of maximum displacements and the durations for the realistic and flat layered models can be obtained than the case for the models of Tokyo. The comparisons of spectral ratios are shown in Fig. 5-35. The synthetic seismograms for the realistic model have larger spectral amplitudes than the flat layered model does in the shorter periods less than around 5 sec at all the stations. The reasons mentioned for the models of Tokyo can also stand for this differences. The absence of the spectral peak at 8 sec seen in the ratios of Tokyo model is due to the difference of the underground structure between Tokyo and Yokohama models.

Through these two comparisons, it is concluded that the approximation of sedimentary

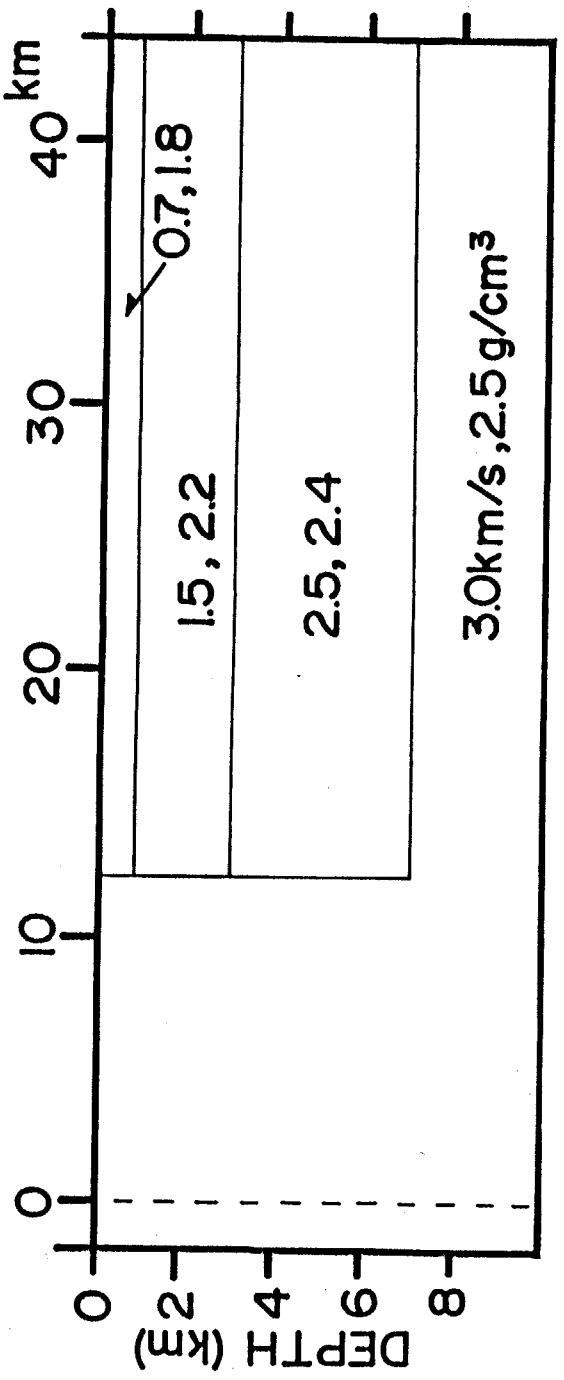

Fig. 5-33. A model approximated from Yokohama model 2 in Fig. 5-23 by flat layers.

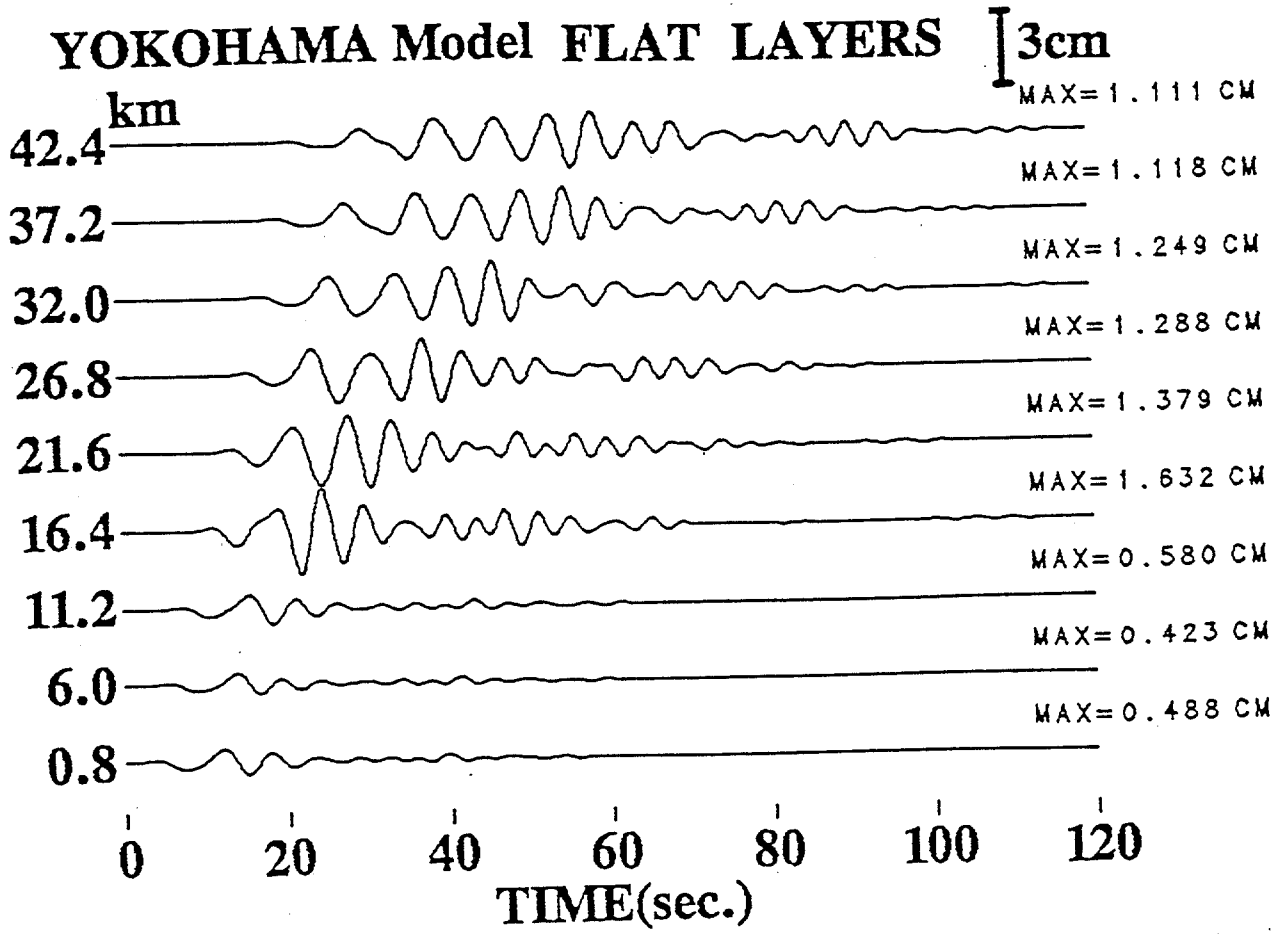

Fig. 5-34. Synthetic displacements on the free surface of the model in Fig. 5-33. Each trace is normalized to the same value as used in Fig. 5-22.

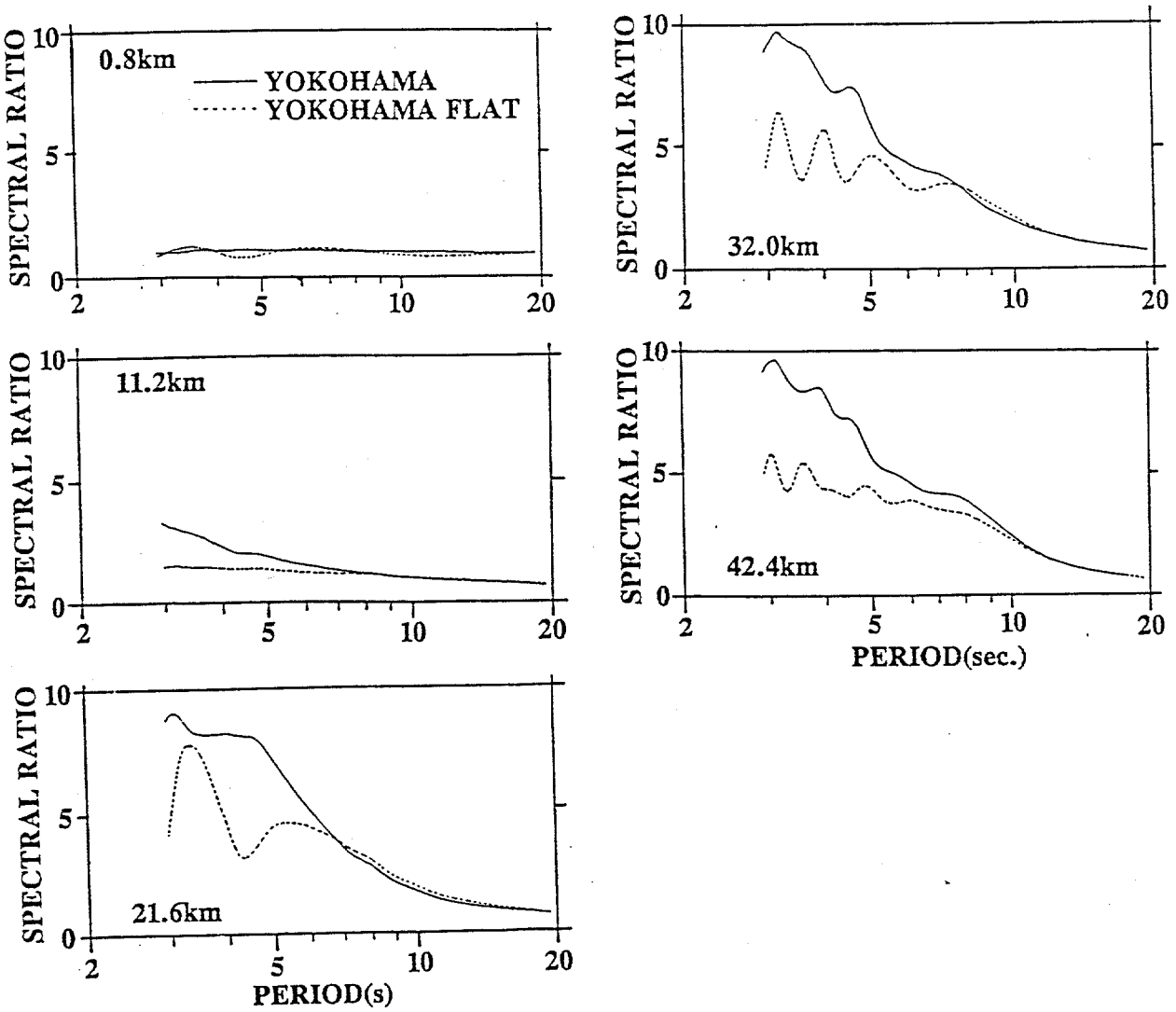

Fig. 5-35. Spectral ratios of the synthetic seismograms in Fig. 5-34 to the input wave shown in Fig. 5-17.

layers by flat layered structure can give reasonable estimations for the duration and arrival time of later phases, but, spectral ratios in a short period range and maximum amplitudes can not be well estimated.

5.3.2 Contribution of low-velocity surface layers to the amplification of surface waves

The differences of the synthetic seismograms for Yokohama model 1 and 2 were considered to be caused by the different condition of top layer with an S-wave velocity of 0.7 km/sec. As it is well-known, low-velocity surface layers give significant influences to the amplification of seismic waves. However, such effects on surface wave propagation are not well known. We, here, investigate how the surface layers affect surface wave propagation by the numerical modelings for the Tokyo model.

Since the Tokyo model has two sedimentary layers overlying the basement as shown in Fig. 5-26, two models were examined. The first one consists of a surface layer and the basement whose S-wave velocities are 0.7 and 3.0 km/sec, respectively. The geometry of the model was derived by replacing the layer with an S-wave velocity of 1.5 km/sec in the Tokyo model by the basement with a velocity of 3.0 km/sec. Namely, the thickness of the layer with an S-wave velocity of 0.7 km/sec is the same as that in the Tokyo model. Hereafter, we call this model "Tokyo model A." In the second one called "Tokyo model B," the depth to the basement is the same as that in the Tokyo model. However, the top layer with a velocity of 0.7 km/sec was replaced by the second layer with a velocity of 1.5 km/sec. We can understand the effects of each sedimentary layer by comparing the synthetic seismograms for these two models.

The synthetic displacements on the free surface of the Tokyo model A are shown in Fig. 5-36. Each trace is normalized to the same scale used in the case of the realistic Tokyo model. The time-variant characteristics seem to be similar to the synthetic seismograms for the Tokyo model; the energy of seismic waves concentrates in the latter part of the wave trains and the large amplitude phases arrive at the similar time. The amplitudes, however, are around two-third of those for the realistic model. On the other hand, synthetic

seismograms for the Tokyo model B in Fig. 5-37 show no similarity. The later phases with a low velocity do not appear unlike the Tokyo model A. The amplitudes of the seismograms become one-third of the original amplitude.

The distributions of maximal amplitudes and durations of the synthetic displacements are shown in Fig. 5-38 against the distance from the input plane. The pattern of the maximum amplitude distribution for the Tokyo model A is similar to that for the realistic model; the amplitudes become larger with increasing distances between 10 and 15 km, then they maintain a constant value. The amplitudes of the Tokyo model B do not significantly vary with increasing distances. The durations for the Tokyo model A are estimated longer than those for the realistic model. Because the distinct later phases in the model A is not so predominant as those in the realistic model, the resultant durations become longer according to the definition of the duration. The spectral ratios of synthetic seismograms to the input wave were calculated as shown in Fig. 5-39. The spectral ratios for the model B show no distinct predominant periods. In the spectral ratio for the model A indicated by a thin solid line, the spectral peak can be seen at a period of 7-8 sec as seen in the realistic model indicated by the thick line. The spectral ratios for a period range less than 7 sec for the model A are smaller than those for the realistic model.

It is concluded from these comparisons that the effects of the layer with an S-wave velocity of 0.7 km/sec on surface wave propagation are considerably large and the fundamental characteristics of surface waves on the sedimentary layers can be determined by the thickness of the top layers, although the layer with an S-wave velocity of 1.5 km/sec also has an influence. Therefore, the variation of the thickness of the layer having an S-wave velocity of 0.7 km/sec should be known in detail.

5.3.3 Construction of underground structural model for engineering use

In 5.2, the good fittings of the synthetic seismograms with the observed ones were accomplished using two-dimensional model determined by using the data from the seismic refraction surveys. However, such areas where details of the underground structure are

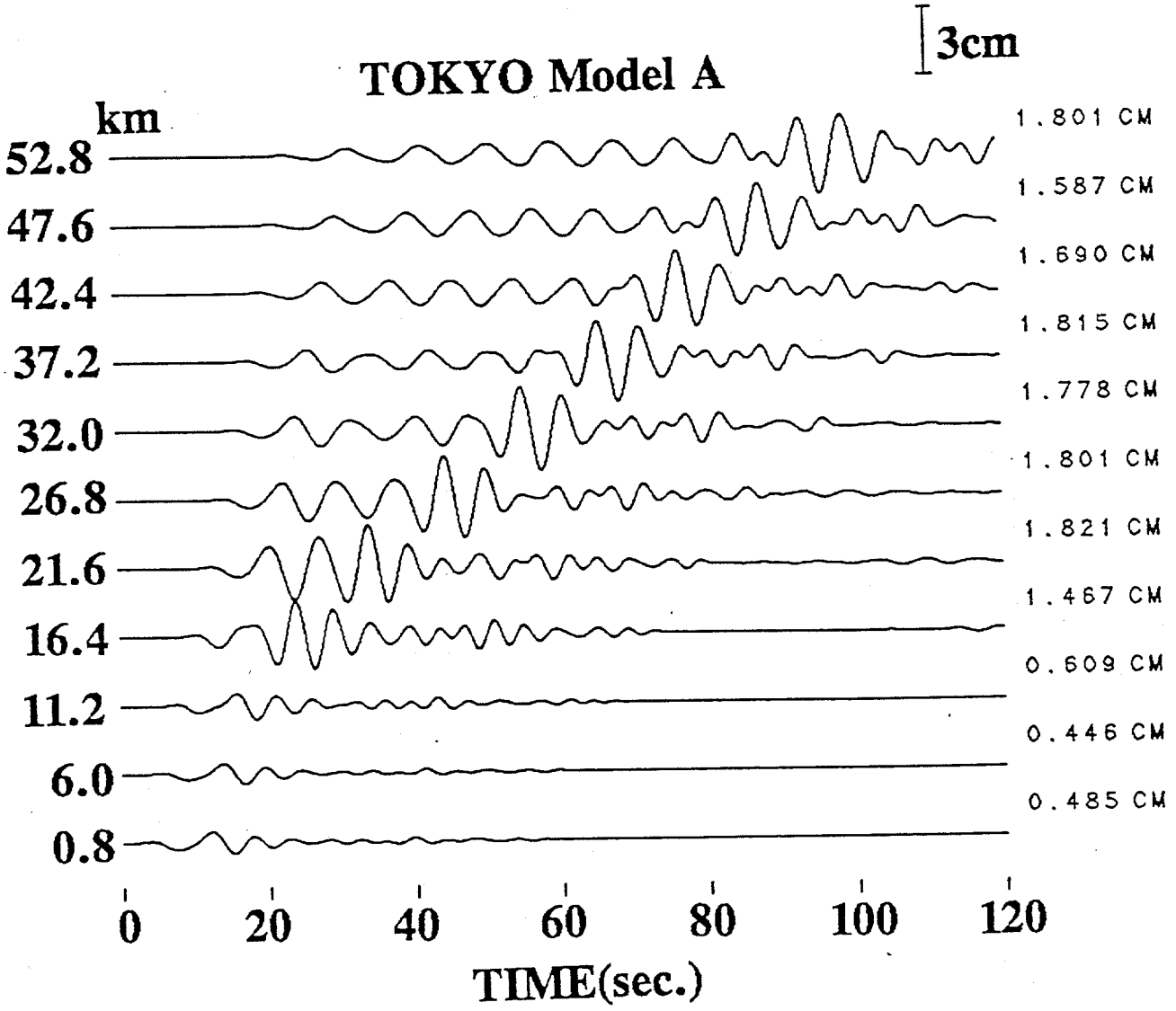

Fig. 5-36. Synthetic displacements on the free surface of the model (Tokyo model A), in which the second layer in Fig. 5-26 is replaced by the third layer in the same figure. Each trace is normalized to the same value as used in Fig. 5-22.

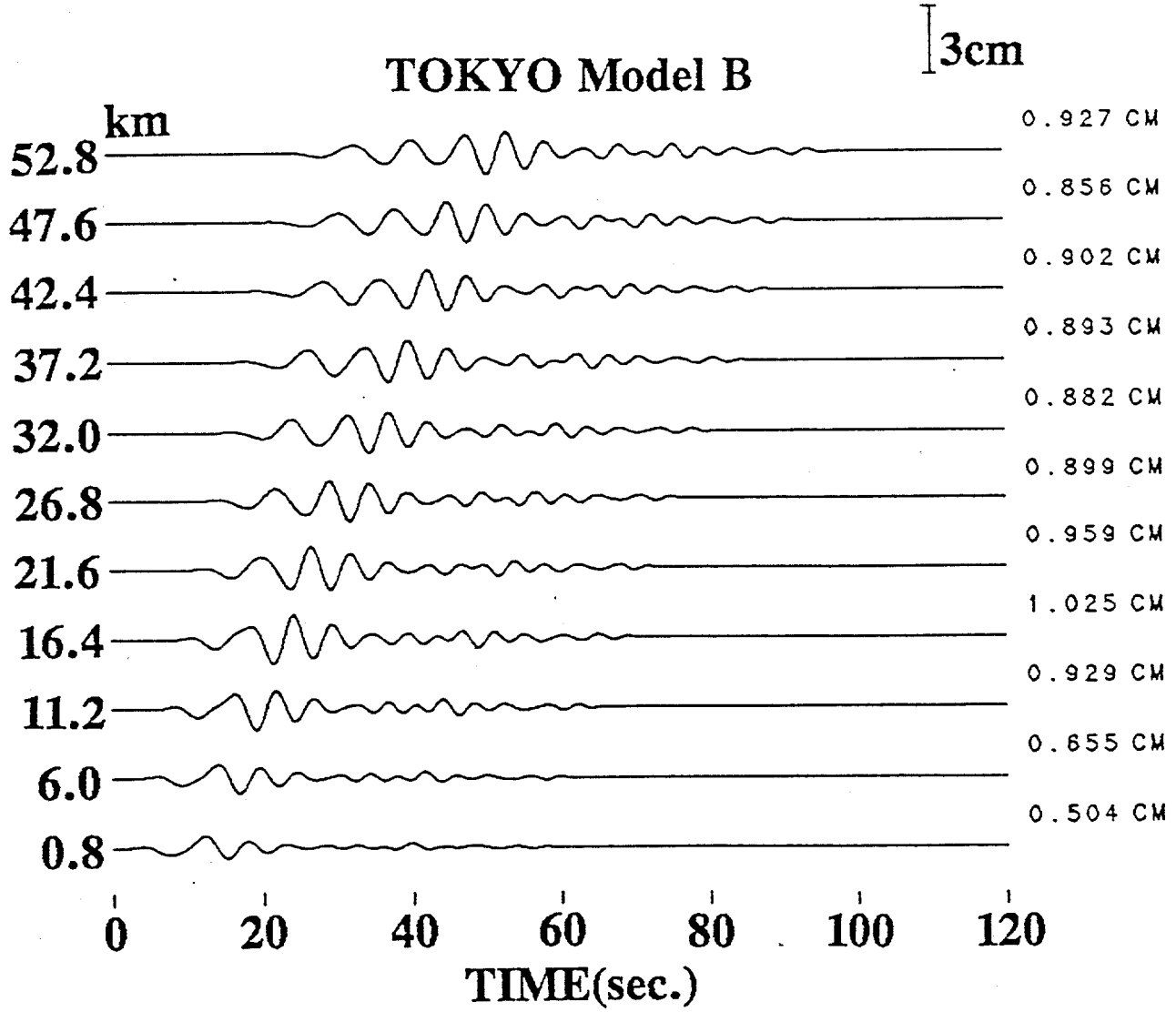

Fig. 5-37. Synthetic displacements on the free surface of the model (Tokyo model B), in which the top layer in Fig. 5-26 is replaced by the second layer in the same figure. Each trace is normalized to the same value as used in Fig. 5-22.

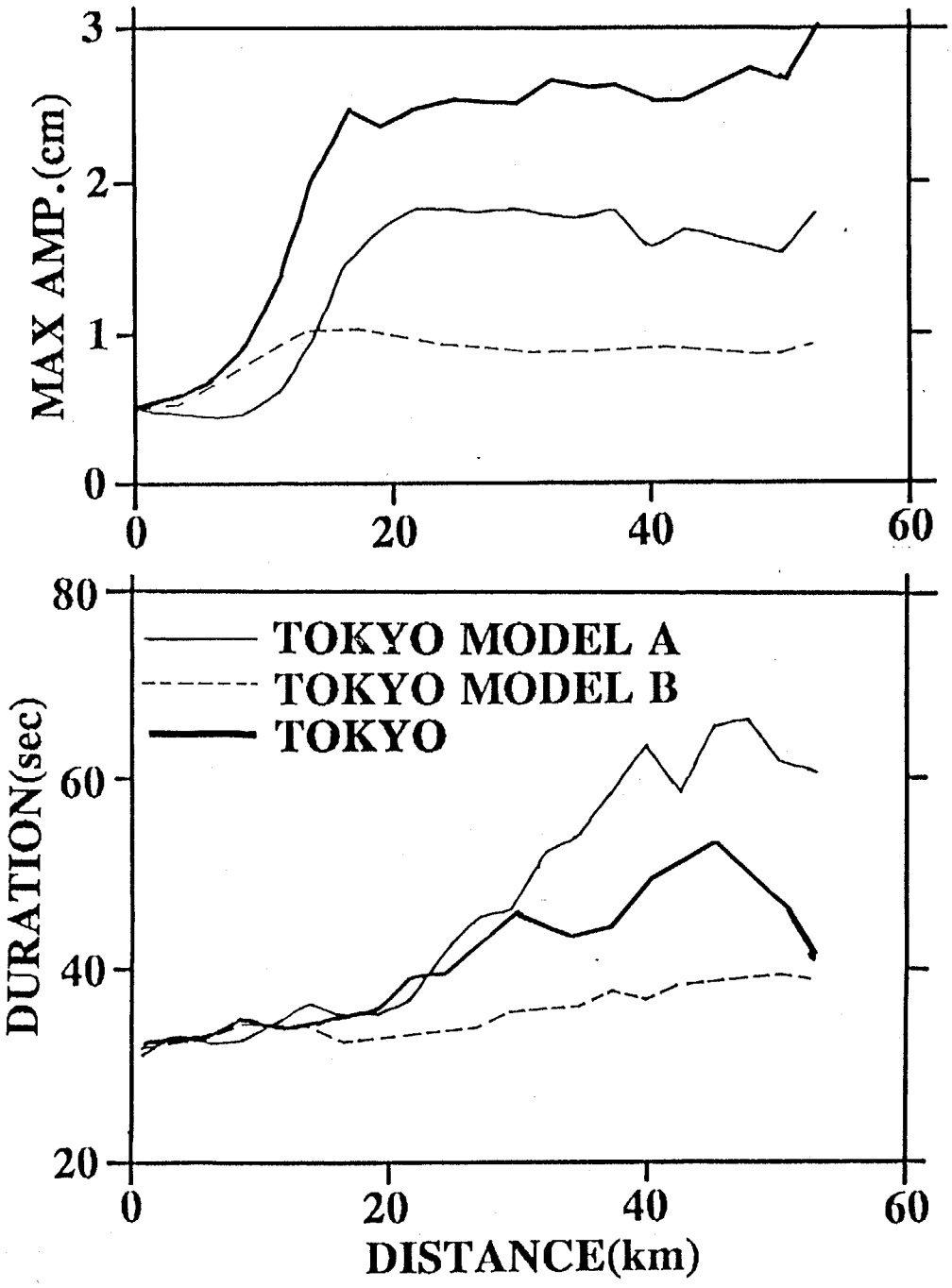

Fig. 5-38. Distribution of maximum displacements and durations for the synthetic seismograms for the Yokohama model A and B.

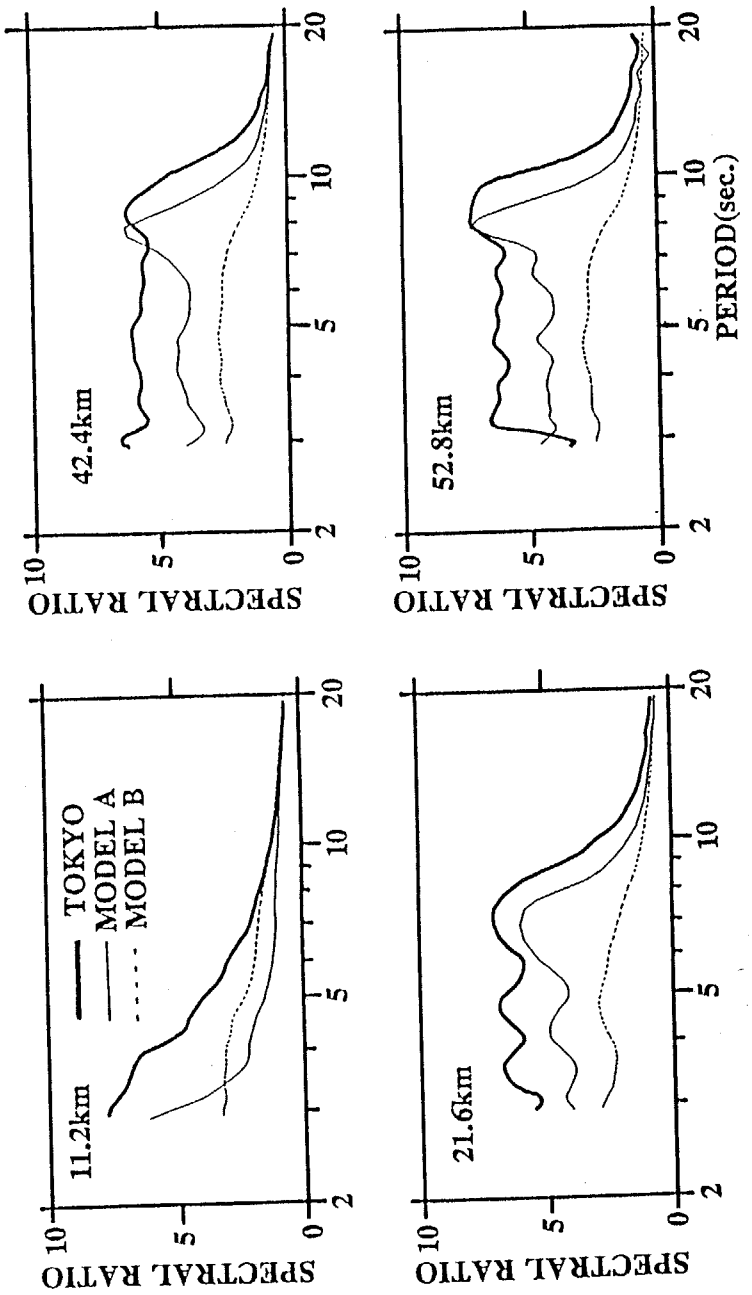

Fig. 5-39. Spectral ratios of synthetic seismograms in Figs. 5-37 and 5-38 to the input wave in Fig. 5-17.

available are very rare. Usually, the available knowledge on the underground structure is limited.

The data which is likely to be available with ease are considered to be time-terms from the refraction surveys. In the whole of the Kanto plain, the distribution of time-terms corresponding roughly to the depth of the basement is already served from the elaborate work by the Research Group for the Basement Structure of Tokyo Metropolis (Shima, 1980; Seo et al., 1982). As stated before, a time-term is an approximated index for a thickness of surface layers overlying the basement.

We discuss here how we can construct reasonable underground structural models from the time-terms for engineering purpose. The investigation was carried out by making some underground structural models according to criteria for the conversion of the time-terms to the thickness of the sedimentary layers and computing synthetic seismograms by the method employed in 5.2. The same input wave was employed. The profile from ASK to YKH was used for the investigation. The realistic model for the profile can be referred as Yokohama model 2 in Fig. 5-23 (in the following, Yokohama model) and the distribution of the time-terms are shown in Fig. 5-19.

Since the most of the time-terms at stations in the Kanto plain were derived from the travel time data from the Yumenoshima explosion, the underground structure at the Yumenoshima explosion site was assumed to be a standard model, namely, the thickness of the sedimentary layers is 2.5 km corresponding to time-terms of 1.03 sec. At first, a two-layers model was examined. The thickness of a surface layer overlying the basement is derived by multiplying a constant of 2.5 by the ratio of the time-term at each site to that at the Yumenoshima explosion site. The distribution of the time-terms used from ASK and NGT is indicated by dotted line in Fig. 5-19, which was derived by taking the average of time-terms on the solid and broken lines in this figure. The resultant model is depicted in Fig. 5-40. The S-wave velocities for the surface layer and the basement are 1.0 and 3.0 km/sec and densitied are 2.0 and 2.5 g/cm**3, respectively. Hereafter, we call it "SMP1".

The depth to the basement becomes gradually larger and the maximum thickness of the surface layer is around 4 km. Fig. 5-41 shows the synthetic seismograms for the SMP1 model. The appearance times of the maximum amplitudes seem to be similar to those of the realistic model in Fig. 5-24. The wave forms, however, are simple and not so dispersive, and the second phases are not distinct. This is caused by the same reason discussed in the section of 5.3.2. It also suggests that the low velocity layer with a velocity of 0.7 km/sec should be included in the modeling of propagation of surface waves.

The ratio of the first and the second surface layers at the Yumenoshima explosion site were kept at every site. The thickness of each sedimentary layer is obtained by the multiplication of the ratio of the time-term at each site to the time-term at Yumenoshima by each thickness of the sedimentary layers at Yumenoshima. The S-wave velocities and densities for each layer are the same as those for the Tokyo model. The proposed model is depicted in Fig. 5-42 (SMP2 in followings). The calculated seismograms in Fig. 5-43 seem to be similar to those for the Tokyo model in Fig. 5-27. The SMP2 model can not give a well approximation of the realistic model for Yokohama. This implies that the underground structure in the Kanto plain can not be represented only by the model at Yumenoshima.

In the third case, the underground structure at the Nagatsuta explosion site was chosen as the standard model instead of that at the Yumenoshima explosion site. The other procedures remain the same as for the previous case of the approximation. We call the resultant structural model in Fig. 5-44 "SMP3." The low-velocity surface layer begins to appear at a distance of 10 km, where the time-term becomes suddenly larger. Comparing the synthetic seismograms in Fig. 5-45 with those for the realistic model, we obtain that amplitudes are almost the same, but the durations seem to be longer. A better similarity to synthetic seismograms for the realistic model than those for the SMP 2 can be seen.

To summarize the results of the three modelings, distributions of the maximum amplitudes, durations and spectral ratios to the input wave were compared as shown in Figs. 5-46 and 5-47. The solid lines in the figures denote the distributions for the realistic model. The

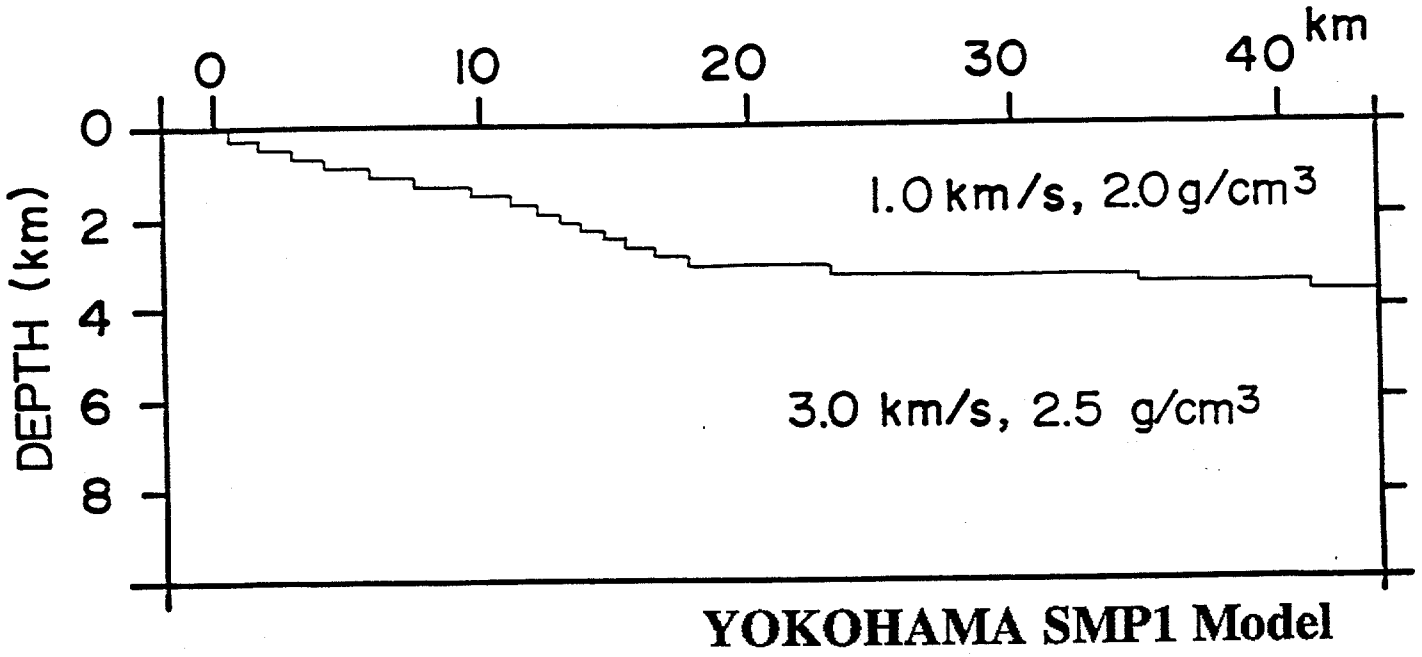

Fig. 5-40. SMP1 model. The underground structural model is approximated from the time-terms.

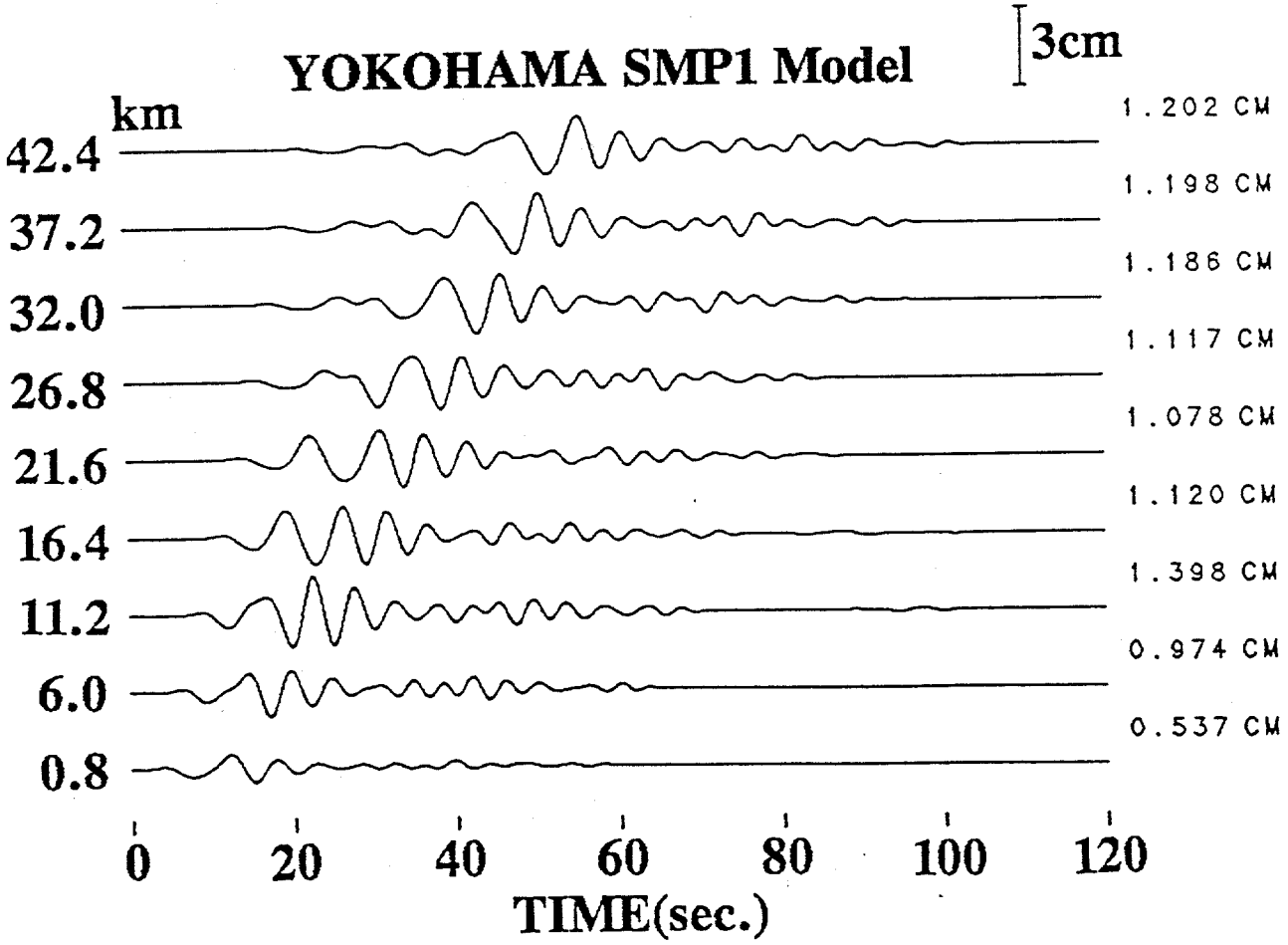

Fig. 5-41. Synthetic displacements on the free surface of the SMP1 model in Fig.5-40. Each trace is normalized to the same value as used in Fig. 5-22.

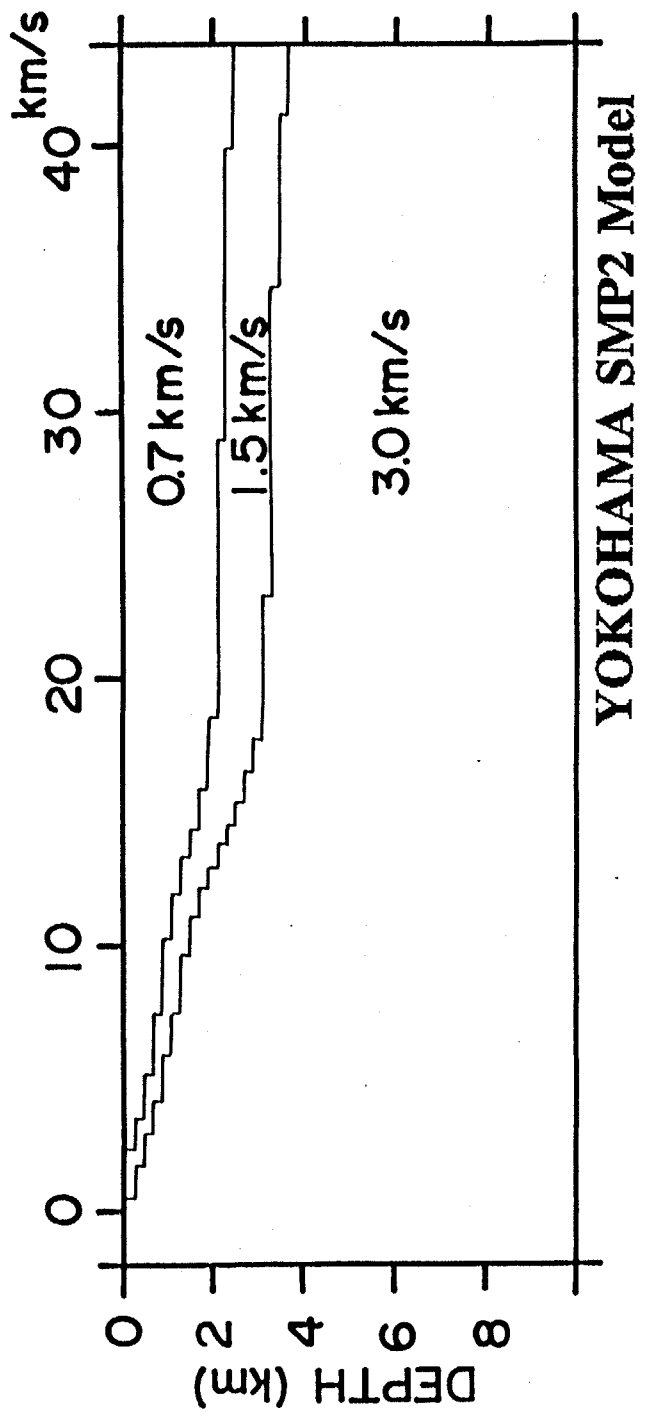

Fig. 5-42. SMP2 model. The underground structural model is approximated from the time-terms.

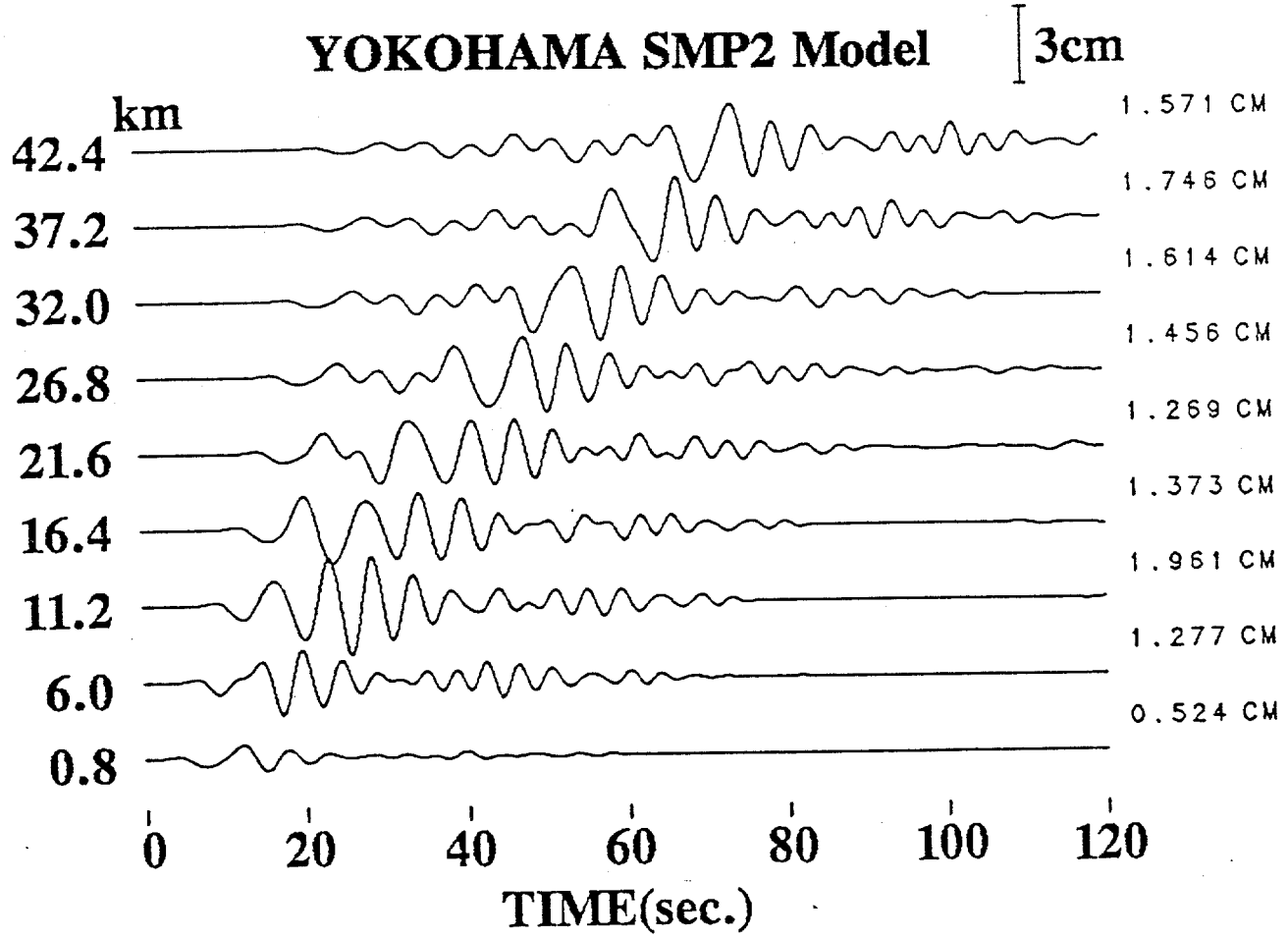

Fig. 5-43. Synthetic displacements on the free surface of the SMP2 model in Fig. 5-42. Each trace is normalized to the same value as used in Fig. 5-22.

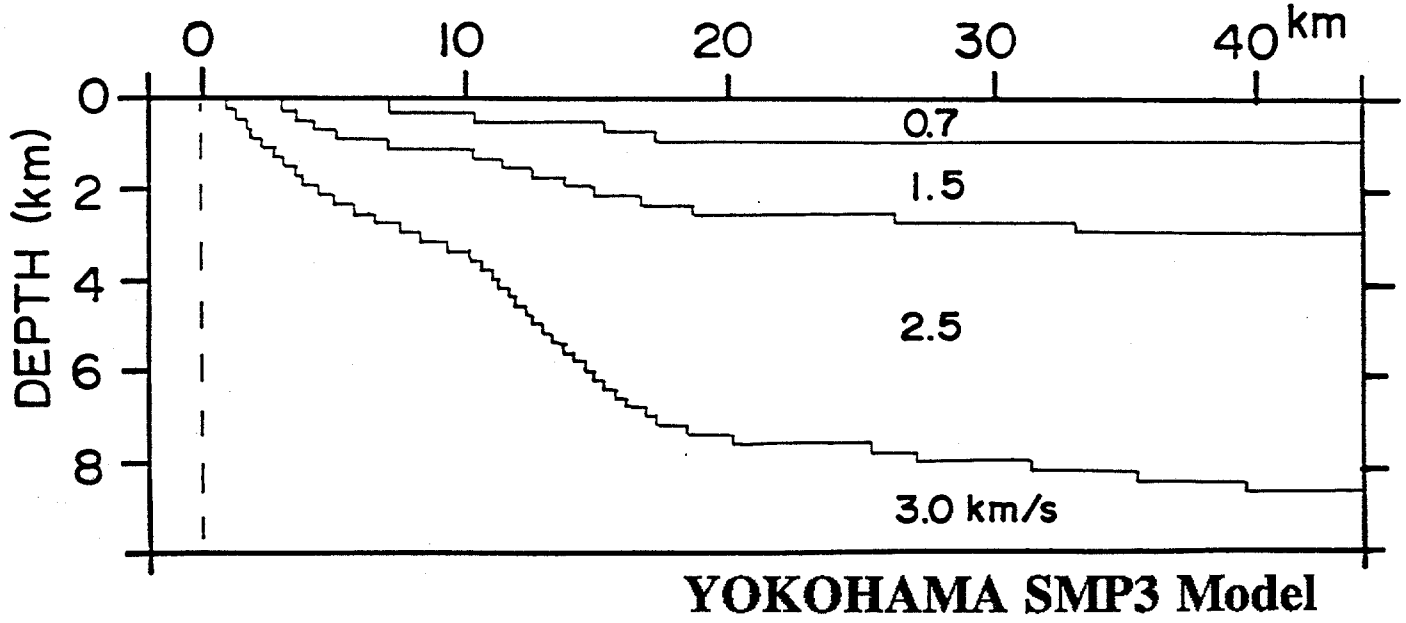

Fig. 5-44. SMP3 model. The underground structural model is approximated from the time-terms.

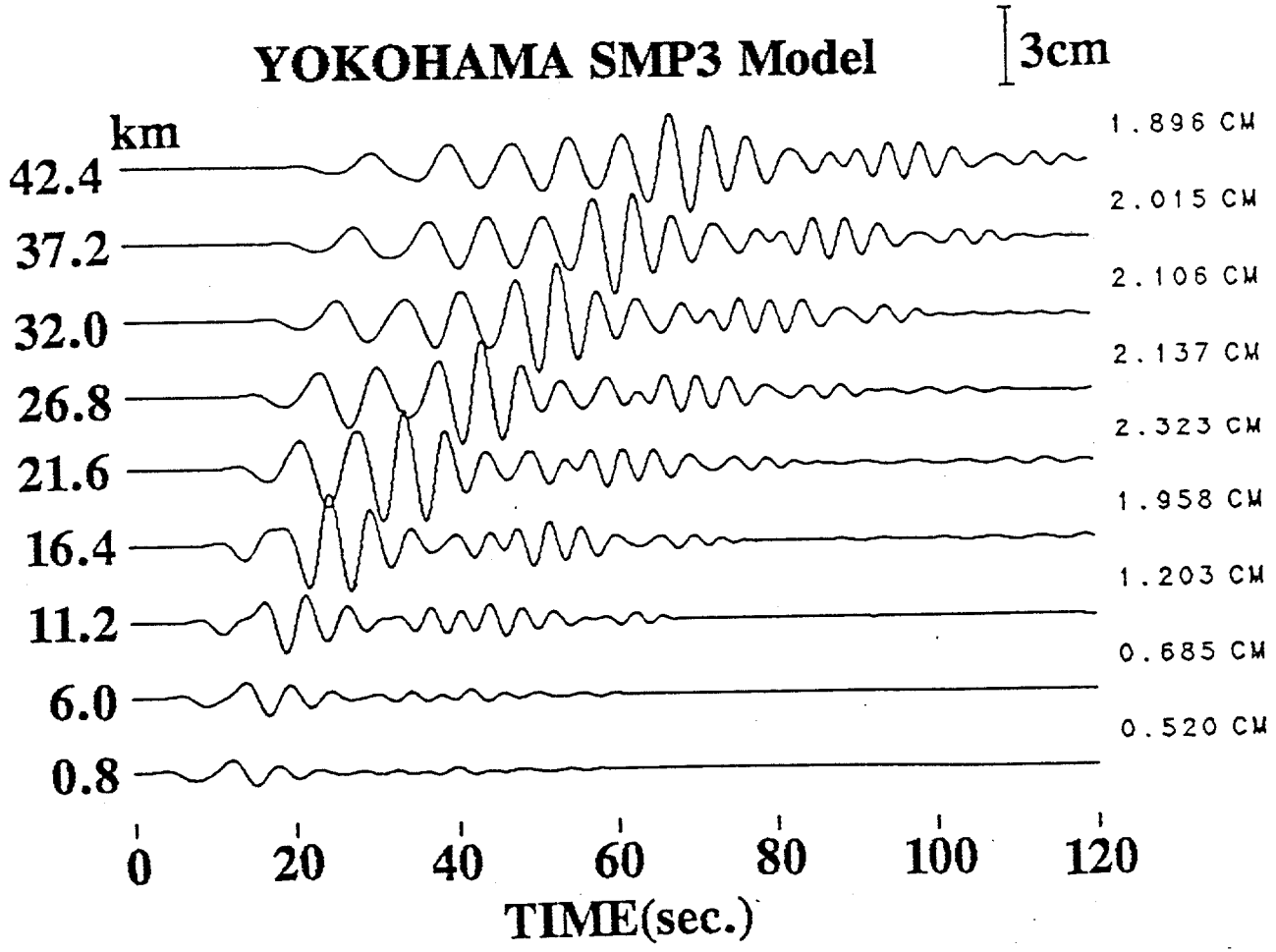

Fig. 5-45. Synthetic displacements on the free surface of the SMP3 model. Each trace is normalized to the same value as used in Fig. 5-22.

variations of the maximum amplitudes and durations for the model SMP3 are most similar to those of the realistic model. The spectral ratios indicate also the same, except for ratio near the input plane. In particular, spectral peaks in a period range more than 10 sec can be seen in the spectral ratios for the SMP1 and 2 models; this is not seen in the ratios of the realistic model.

From these investigations, it can be concluded that reasonable underground structures at arbitrary sites can not be derived only from the distribution of the time-terms and the underground structural model at the Yumenoshima explosion site. However, the seismic waves from the explosions at Yumenoshima have been observed in the whole of the Kanto district and the accumulation of the travel time data becomes considerably larger. Therefore, the distribution of the time-terms is considered to be a powerful basic tool to make models of two-dimensional arbitrary profiles or three-dimensional models. The crucial point is how to convert the time-terms which express the total thickness of sedimentary layers to underground structural models applicable enough for engineering use. In order to perform such a task, as seen in the modeling of SMP3, suitable reference points should be prepared. Then they can be interpolated by the time-terms. More seismic surveys and observations and analyses of earthquake ground motions, such as dispersion analysis, are required to increase the reference points and to know the underground structure three-dimensionally.

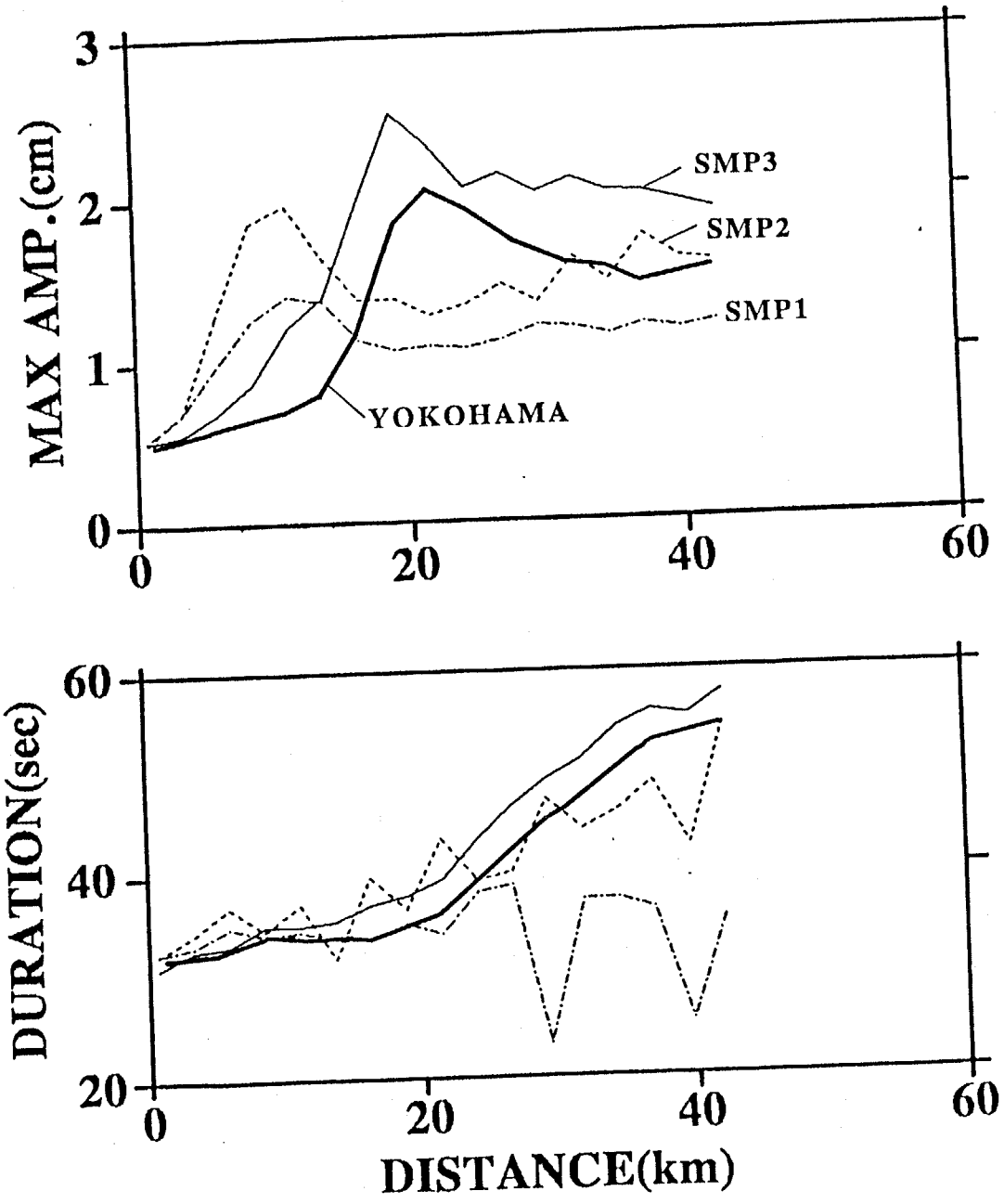

Fig. 5-46. Distributions of maximum displacements and duration of the synthetic seismograms for the SMP1, SMP2 and SMP3 models.

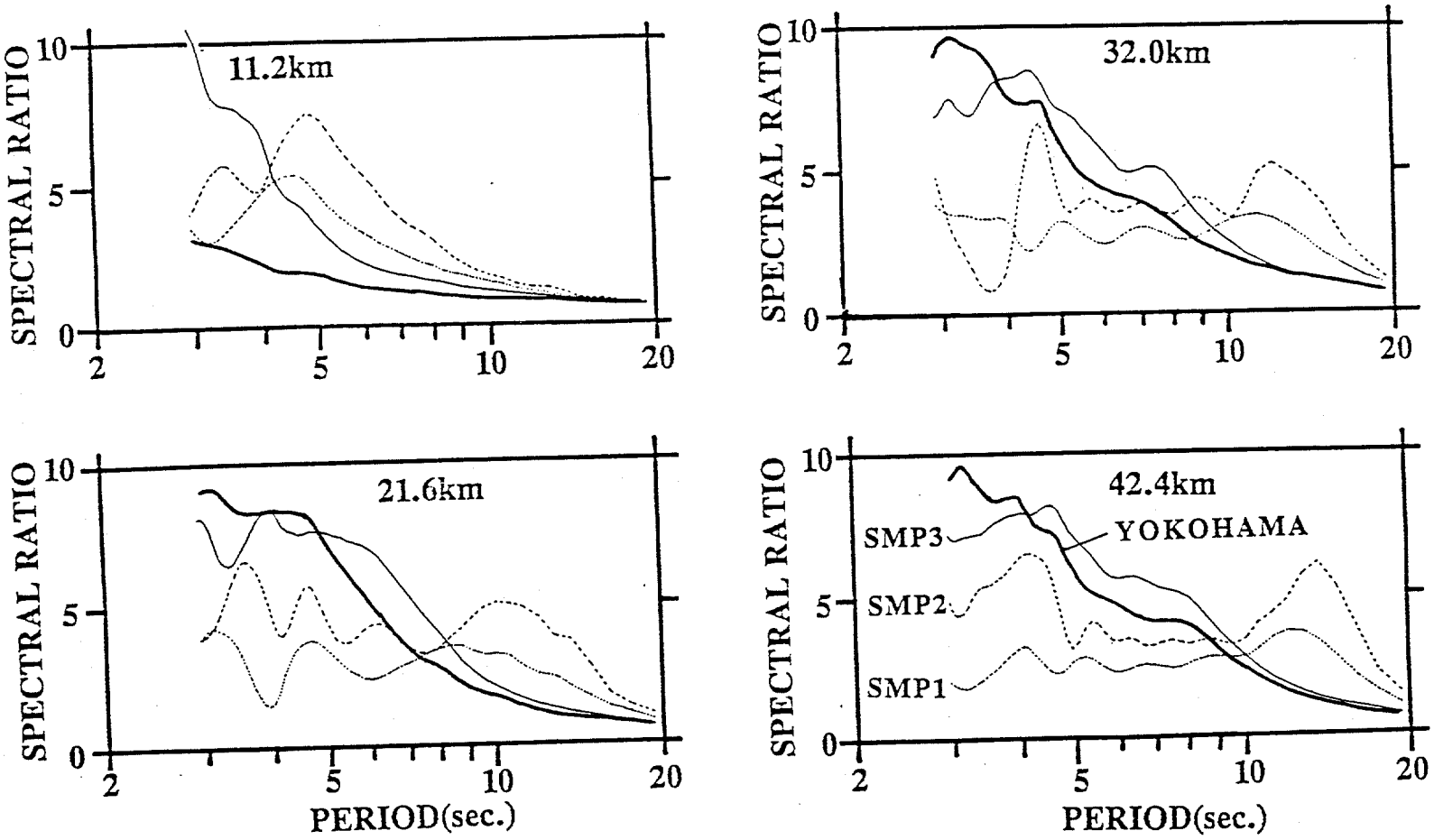

Fig. 5-47. Spectral ratios of the synthetic seismograms for the SMP1, SMP2 and SMP3 models.

CHAPTER 6. CONCLUSIONS

In this research, we discussed the propagation of seismic waves in sedimentary layers overlying a firm rock. First, seismic refraction surveys were conducted in the area of southwestern Kanto district, Japan. Since the area is densely populated, the results of the seismic surveys become the basic data for assessing the seismic hazard in the area. The explosion seismograms observed during the seismic surveys were used not only for travel time analyses, but also to facilitate the understanding of the propagation mechanisms of seismic waves. Distinct later phases in explosion seismograms and earthquake records observed on the sedimentary layers were interpreted by the knowledge of the underground structure and numerical forward modelings. In this study, major attention was paid only to site effects. The conclusions in this study could be summarized as follows:

(1) The seismic refraction surveys with explosions were carried out in the southwestern Kanto district. The underground structure down to the upper most layer of the earth's crust was made clear three-dimensionally. It consists of four layers with P-wave velocities of 1.8, 2.8, 4.8 and 5.5 km/sec, top to down. It was pointed out from the results of the survey that the underground structure around Tokyo differs from that around Yokohama. The maximum depth to the layer with a velocity of 4.8 km/sec is more than 4 km near the Yokohama harbor. On the other hand, the layer with a velocity of 4.8 km/sec is very thin around Tokyo. A step-like topography of the basement could be found in the southeastern extension of the Tachikawa active fault. It was speculated to continue towards the Tokyo bay area by considering the results of reflection surveys in the Tokyo bay (Kato, 1984). The revealed underground structure, as a whole, was in good agreement with results of the other geophysical and geological investigations.

(2) Distinct later phases at the free surface and the bottom of the Fuchu deep borehole were interpreted as two-dimensional multiple-reflected P-waves within the sedimentary layers. The same kind of the later S-wave phases were recognized in ground motions of shallow

earthquakes. A simple forward modeling based on ray theory was applied to understand the characteristics of the proposed propagation mechanism. It was pointed out that the amplitudes of the multiple-reflected phases depend on the incident angle to the sedimentary layers and the dip angle of the interface between the sedimentary layers and the basement. In particular, multiple-reflected phases with large amplitudes can be expected, when seismic waves incident obliquely and propagate towards down-dip directions. This result explains well the observation. Namely, seismic waves from the shallow earthquakes incident obliquely to the sedimentary layers, while the incident angle is almost vertical in the case of deep earthquakes. Since such multiple-reflected phases make durations of ground motions long and generate surface waves by constructive interfaces, they are not negligible from an engineering point of view.

(3) Another propagation mechanism of seismic waves was also discussed using explosion seismic waves. A later phase 0.5 sec after the initial phase was pointed out in seismograms observed during the explosion at Yumenoshima at several stations where the step-like topography on the basement was deduced. The same kind of later phase with an amplitude two or three times larger than that of the initial phase could be recognized one second after the initial S-wave in seismograms of deep earthquakes. A finite difference modeling was applied to interpret the nature of the later phase. It was clarified that diffracted wave plays an important role in describing a wave field in an underground structure with a step-like topography of a basement. Moreover, they are interpreted as superposition of diffracted waves from the lower edge of step and direct waves from the down-thrown side. The existence of a step-like topography of the basement was confirmed through these investigation.

(4) Thirdly, surface wave propagation in the longer period range was investigated which is of considerable importance in engineering practice. Distinct well-dispersive later phases were observed in the seismic array during the Western Nagano earthquake of 1984.

These dispersive wave trains in a period range of 2 to 20 sec could be explained as Love waves affected by the sedimentary layers. The surface waves observed at Tokyo and Yokohama show different characteristics reflecting the difference of the configuration of the sedimentary layers. A good agreement of the synthetic seismograms with the observed ones was accomplished by two-dimensional SH finite difference modelings and the detailed knowledge of underground structure from the seismic surveys. It was concluded through numerical modelings of various underground structural models that the configuration of the sedimentary layers is quite important for amplification of surface waves, specially, the thickness of the upper layer with an S-wave velocity of 0.7 km/sec has crucial effects. Moreover, these results suggest the possibility of predicting the longer period ground motion at arbitrary sites on basins by considering realistic underground structure. For this engineering purpose, structure of sedimentary layers should be known in the area under consideration.

REFERENCES

Aki, K. and K.L. Larner (1970). Surface motion of a layered medium having an irregular interface due to incident plane SH waves, J. Geophy. Res. Vol.75, No.5, 933-954.

Alsop, L.E. (1966). Transmission and reflection of Love waves at a vertical discontinuity, J. Geophy. Res., Vol.71, No.16, 3969-3984.

Amaike, F., S. Kasuga, K. Kisimoto, T. Iwata, K. Irikura and Y. Kobayashi (1982). Estimation of base rock structure using reflected waves, Proc. 6th Japan. Earthq. Eng. Sym., 57-64.

Angona, F.A. (1960). Two-dimensional modeling and its application to seismic problems, Geophysics, Vol.15, No.2, 468-482.

Bard, P.Y. and M. Bouchon (1980a). The seismic response of sedimentary-filled valleys. Part.1. The case of incident SH waves, Bull. Seism. Soc. Am., Vol.70, No.4, 1263-1286.

Bard, P.Y. and M. Bouchon (1980b). The seismic response of sedimentary-filled valleys. Part.2. The case of incident P and SV waves, Bull. Seism. Soc. Am., Vol.70, No.5, 1921-1941.

Bard, P.Y. and M. Bouchon (1985). The two-dimensional resonance of sediment-filled valleys, Bull. Seism. Soc. Am., Vol.75, No.2, 519-541.

Boore, D.M. (1972). Finite difference methods for seismic wave propagation in heterogeneous materials, in methods in computational physics, Vol.11, 1-37.

Cerveny, V., M.M. Popov and I. Psencik (1982). Computation of wave field in inhomogeneous media -Gaussian beam approach-, Geophys. J. Royal astr. Soc., Vol.70, 109-128.

Cerveny, V. (1985). Ray synthetic seismograms for complex two-dimensional and three-dimensional structure, J. Geophys., Vol.58, 2-26.

Dobrin, M.B. (1976). Introduction to geophysical prospecting, third edition, McGraw-Hill.

Dziewonski, A., S. Bloch and M. Landisman (1969). A technique dor the analysis of

transient seismic signals, Bull. Seism. Soc. Am., Vol.59, No.1, 427-444.

Fuchs, K. and G. Mueller (1971). Computation of synthetic seismograms with the Reflectivity method and comparison with observations, Geophys. J. Royal astr. Soc., Vol.23, 417-433.

Fukuda, O., T. Kakimi, H. Kawachi, S. Takagi and S. Tanaka (1976). On the borehole for observation of water level and quality in Kawasaki, Geological news, Vol.259, 1-14 (in Japanese).

Hanks, T.C. (1975). Strong ground motion of the San Fernand, California, earthquake: Ground displacements, Bull. Seism. Soc. Am., Vol.65, No.1, 193-225.

Hanks, T.C. (1976). Observation and estimation of long-period strong ground motion in Los Angles basin, Earthq. Eng. and Struc. Dyn., Vol.4, 473-488.

Harkrider, D.G. (1964). Surface waves in multilayered elastic media 1. Rayleigh and love waves from buried sources in a multilayered elastic half-space, Bull. Seism. Soc. Am., Vol.54, No.2, 627-679.

Harkrider, D.G. (1970). Surface waves in multilayered elastic media. Part II. Higher mode specta and spectral ratios from point sources in plane layered earth models, Bull. Seism. Soc. Am., Vol.60, No.6, 1937-1987.

Hatayama, T. (1964). A synthetic investigation of the geophysical methods in Kanto plain, Butsuri-Tanko (Geophysical Exploration), Vol.17, No.2, 2-23.

Haskell, N.A. (1953). The dispersion of surface waves in multilayered media, Bull. Seism. Soc. Am., Vol.43, 17-34.

Hong, T.L. and D. V. Helmberger (1978). Glorified optics and wave propagation in non-planar structure, Bull. Seism. Soc. Am., Vol.68, No.5, 1313-1330.

Horike, M. (1985). Inversion of phase velocity of long-period microtremors to the S-wave-velocity structure down to the basement in urbanized area, J. Phys. Earth, Vol.33, 59-96.

Horike, M. (1987). Extension of the Aki and Larner method to absorbing media with plural

curved interfaces and several characteristics of a seismic response on a sedimentary basin, Zisin (J. Seism. Soc. Japan), Ser.2, 40, 247-259 (in Japanese).

Horike, M. (1988). Seismic response on a three-dimensional sedimentary basin with irregular interface, Abst. of spring meeting of Seism. Soc. Japan, 251 (in Japanese).

Hoshiba, M, M. Horike, T. Idei and T. Iwata (1988). Effects of surface geology on seismic motions -Analysis and simulation of seismic motions in a sedimentary basin-, Zisin (J. Seism. Soc. Japan), Ser.2, 41, 195-202 (in Japanese).

Hydrographic Department, Maritime Safety Agency (1987). Free-air gravity anomalies at Sea in the vicinity of southern Kanto district, Report of the Coordinating Committee for earthquake Prediction, Vol.37, 170-171 (in Japanese).

Inoue, R., Y. Fujino, K. Matsubara and M. Hakuno (1982). Estimation of relatively long-period ground motions by a fualt dislocation theory, Proc. of the Japan Soc. of Civil Eng., No.317, 47-60 (in Japanese).

Ishii, M (1962). Basement of the Kwanto plain, Jour. Japan Assoc. Petro. Techn., Vol.27, No.6, 615-640 (in Japanese).

Ishii H. and R. M. Ellis (1970). Multiple reflection of plane SH waves by a dipping layer, Bull. Seis. Soc. Am., vol.60, 15-28.

Irikura, K. (1976). Amplification characteristics of earthquake motions at the ground with dipping layers, Annuals. Disast. Prev. Res. Inst., Vol.19B, 39-57 (in Japanese).

Irikura, K. and S. Kasuga (1980). Effects og ground structures with laterally sttep variations on seismic motions, Proc. 8th World Conf. Earthq. Eng., Vol.3, 479-483.

Kagami, H., S. Okada, K. Shiono, M. Oner, M. Dravinski and A.K. Mal (1986). Observation of 1- to 5-second microtremors and their application to earthquake engineering. Part.III: A two-dimensional study of site effects in the San Fernando valley, Bull. Seism. Soc. Am., Vol.76, No.6, 1801-1812.

Kakimi, T. (1973). Neotectonic map Tokyo, Geological Survey of Japan.

Kamiyama, S. (1979). Nonstationary characteristics and wave interpretation of strong earth-

quake ground motions, Proc. of the Japan Soc. of Civil Eng., No.284, 35-48 (in Japanese).

Kanai, K. (1983). Engineering Seismology, Univ. of Tokyo Press.

Kaneda, Y., N. Nishide, Y. Sasaki, S. Asano, T. Yoshii, Y. Ichinose, M. Saka (1979). Explosion seismic observation of reflected waves from the Mohorovicic discontinuity and crustal structure in western Kanto district, J. Phys. Earth, Vol.27, 511-526.

Kasahara, K., H. Suzuki, H. Takahashi (1976a). On a survey of basement in the western district of Tokyo 1, Abst. of spring meeting of Seism. Soc. Japan, 54 (in Japanese).

Kasahara, K., H. Suzuki, H. Takahashi (1976b). On a survey of basement in the western district of Tokyo 2, Abst. of autumn meeting of Seism. Soc. Japan, 139 (in Japanese).

Kasuga, S. and K. Irikura (1982). Lateral variations of ground motions on surface layers with a horizontal discontinuity, Proc. of 6th Japan Earthq. Eng. Sym., 65-72.

Katayama, T. and I. Shino (1984). An engineering study of long period strong motion using displacement seismograph records, Proc. 8th World Conf. on Earthq. Eng., Part.2, 289-296.

Kato, S. (1984). Multi-channel seismic reflection survey in Tokyo Bay, Report of Hydrographic Researches, No.19, 1-57.

Kelly K.R., R.W. Ward, S. Treitel and R.M. Alford (1976). Synthetic seismograms: A finite difference approach, Geophys., Vol.41, N0.1, 2-27.

Kikuchi, Y. (1962). Subsurface microbiostratigraphy of the Hodogaya area, Yokohama city, J. Japanese Assoc. Petroleum Technologists, Vol.27, No.5, 18-23.

Kinoshita, S. (1985). Propagation of total reflected plane SH pulses in a dipping layer, Zisin (J. Seism. Soc. Japan), Ser.2, 38, 597-608 (in Japanese).

Kitsunezaki, C., N. Goto and Y. Iwasaki (1971). Underground structure of the southern part of the Kyoto basin obtained from seismic exploration and some related problems of earthquake engineering, Annuals. Disast. Prev. Res. Inst. Vol.14A, 203-215 (in Japanese).

Kohketsu, K. (1987a). 2-D reflectivity method and synthetic seismograms for irregular layered structure-1. SH-wave generation, Geophys. J. R. astr. Soc., vol.89, 821-838.

Kohketsu, K. (1987b). Synthetic seismograms in realistic media: A wave-theoretical approach, Bull. Earthq. Res. Inst., Vol.62, 201-245.

Kohler, W.M. and G.S. Fuis (1986). Travel-time, time-term, and basement depth maps for the Imperial valley region, California, from explosions, Bull. Seism. Soc. Am., Vol.76, No.5, 1289-1303.

Korn, M. and H. Stoeckl (1982). Reflection and transmission of Love channel waves at coal seam discontinuities computed with a finite difference method, J. Geophys., Vol.50, 171-176.

Kudo, K. (1978). The contribution of Love waves to strong ground motion, Proc. 2nd Intern. Conf. on Microzonation, Vol.2, 765-776.

Kudo, K. (1980). A study on the contribution of surface waves to strong ground motions, Proc. 7th World Conf. earthq. Eng., Vol.2, 499-506.

Kudo, K., E. Shima and Y. Sawada (1984). Comparative observation of ground motions at different soil condition from moderately large earthquakes, Proc. 8th World Conf. Earthq. Eng., Vol.2, 769-776.

Liu, H.L. and T. Heaton (1984). Array analysis of the ground velocities and accelerations from the 1971 San Fernando, California, Earthquake., Bull. Seism. Soc. Am., Vol.74, No.5, 1951-1968, 1984.

Lysmer, J. and L.A. Drake (1972). A finite element method for seismology. In method in Computational Physics, Vol.11, ed. B.A. Bolt, Academic Press, New York, 181-216.

Maczo, P., P.-Y. Bard and I. Psencik (1987). Seismic response of two-dimensional absorbing structures by the ray method, J. Geophys, Vol.62, 38-49.

Masaki, M.(1985). Investigation of earthquake ground motion for the prevention of earthquake disaster in urban area, Dr-thesis, Tokyo Institute of Technology (in Japanese).

Mooney, W.D. and Luetgert, J.H. (1982). A seismic refraction study of the Santa Clara val-

ley and southern Santa Cruz mountains, west-central California, Bull. Seism. Soc. Am., Vol.72, No.3, 901-909.

Mikumo, T. (1966). A study on crustal structure in Japan by the use of seismic and gravity data, Bull. Earthq. Res. Inst., Vol.44, 965-1007.

Nowack R. and K. Aki (1984). The two-dimensional Gaussian beam synthetic method: Testing and application, J. Geophy. Res., Vol.89, No.B9, 7797-7819.

Ohsawa, Y., ed. (1972). A report on characteristics of underground structure and strong ground motion obtained during the Okachi-Oki earthquake of 1968.

Ohta, Y. and N. Goto (1976). Estimation of S-wave velocity in terms of characteristics indices of soil, Butsuri-Tanko (Geophysical exploration), Vo.29, N0.4, 31-41 (in Japanese).

Otha, Y., N. Goto, K. Shiono, H. Takahashi, F. Yamamizu and S. Kurihara (1977). Shear wave velocities in deep soil deposits -Measurement in a borehole to the depth of 3500 meters and its significance, Zisin (J. Seism. Soc. Japan), Ser.2, 30, 415-433 (in Japanese).

Otha, Y., N. Goto, K. Shiono, H. Takahashi, F. Yamamizu and S. Kurihara (1978a). Shear wave velocities in deep soil deposits. Part II -Measurement in a borehole of Shimofusa observatory to the depth of 2300 meters, Zisin (J. Seism. Soc. Japan), Ser.2, 31, 299-308 (in Japanese).

Ohta, Y., H. Kagami, N. Goto and K. Kudo (1978b). Observation of 1- to 5-second microtremors and their application to earthquake engineering. Part.I: Comparison with long-period accelerations at the Tokachi-oki earthquake of 1968, Bull. Seism. Soc. Am., Vol.68, No.3, 767-779.

Okada, H. (1971). A seismic refraction survey in Hachinohe City, Aomori Prefecture, Geophys. Bull. Hokkaido Univ., Vol.26, 147-166 (in Japanese).

Okada, S. and H. Kagami (1978). A point by point evaluation of amplification characteristics in Japan on 1-10 sec seismic motions in relation to deep soil deposits, Trans. of

Architectural Institute of Japan, Vol.267, 29-38.

Omote, S. (1978). Analysis of JMA strong motion records obtained in Kushu area during Central Ohita Earthquake of 1975, in Research report of study on earthquake disaster of large structures and their prevention (in Japanese).

Ohbo, N., I. Onda, Y. Sato and T. Katayama (1986). Wave propagation in a stteped structure based on a numerical experimental approach, J. Phys. Earth, Vol.34, 475-485.

Ohtsuki, A. and K. Harumi (1983). Effect of topography and subsurface inhomogeneities on seismic SV waves, Earhtq. Eng. and Struct. Dyn., Vol.11, 441-462.

Ohtsuki, A., H. Yamahara and K. Harumi (1984). Effect of topography and subsurface inhomogeneities on seismic Rayleigh waves, Earhtq. Eng. and Struct. Dyn., Vol.12, 37-58.

Ohtsuki, A. and J, Yamahara (1984b). Effect of lateral inhomogeneities on seismic waves, II. Observations and analyses, Earhtq. Eng. and Struct. Dyn., Vol.12, 795-816.

Reshef, M., D. Kosloff, M. Edwards and C. Hsiung (1988). Three-dimensional elastic modeling by the Fourier method, Geophysics, Vol.53, No.9, 1184-1193.

Reynolds, A.C. (1978). Boundary condition for the numerical solution of wave propagation problems, Geophy., Vol.43, No.6, 1099-1110.

Sanchez-Sesma, F.J. and S. A. Velazquez (1987). On the seismic response of a dipping layer, Wave motion, Vol.9, 387-391.

Sanchez-Sesma, F.J. (1988). On the seismic response of alluvial valleys, Proc. of the IASPEI/IAEE joint working group on effects of surface geology on seismic motion, Second workshop, 4/1-4/20.

Scheidegger, A.E. and P.L. Willmore (1957). The use of a least square method for the interpretation od data from seismic surveys, Gephys. Vol.12, No.1, 9-22.

Seo, K. (1978). Earthquake motions modulated by deep soil structure of Tokyo, Proc. 5th Japan Earthq. Eng. Sym., 281-288.

Seo, K. and H. Kobayashi (1980). On the rather long-period earthquake ground motions

due to deep ground structure of Tokyo area., Proc. 7th World Conf. on Earthq. Eng., Part.1, 9-16.

Seo, K. (1981). The influences of deep ground structure on earthquake ground motions, Dr thesis, Tokyo Institute of Technology (in Japanese).

Seo, K., S. Midorikawa, Y. Mitani and S. Shu-Geun (1982). Deep subsurface ground structure of the south-western Kanto district, Proc. 6th Japan. Earthq. Eng. Sym., 49-56.

Shima, E. (1970). Seismic surface waves detected by the strong motion acceleration seismograph., Proc. 3rd Japan Earhq. Eng. Sym., 277-284 (in Japanese).

Shima, E., M. Yanagisawa, K. Kudo, T. Yoshii, Y. Ichinose, K. Seo, K. Yamazaki, N. Ohbo, Y. Yamamoto, Y. Oguchi and M. Nagano (1976a). On the base rock of Tokyo, Bull. Earthq. Res. Inst., Vol.51, 1-11 (in Japanese).

Shima, E., M. Yanagisawa, K. Kudo, K. Seo and K. Yamazaki (1976b). On the base rock of Tokyo 2, Bull. Earthq. Res. Inst., Vol.51, 45-61 (in Japanese).

Shima, E, M. Yanagisawa, S. Zama and K. Seo (1976c). Basement structure in the southern part of Tokyo, Abst. of autumn meeting of Seism. Soc. Japan., 140 (in Japanese).

Shima, E., M. Yanagisawa, K. Kudo, T. Yoshii, K. Seo and K. Kuroha (1978a). On the base rock of Tokyo. 3, Bull. Earthq. Res. Inst., Vol.53, 305-318 (in Japanese).

Shima, E., M. Yanagisawa, K. Kudo, T. Yoshii, K. Seo, N. Ohbo, T. Hoshino, M. Nagano (1978b). On the base rock of Tokyo. 4, Bull. Earthq. Res. Inst., Vol.53, 1245-1255 (in Japanese).

Shima, E., M. Yanagisawa, K. Kudo, K. Seo (1981). On the base rock of Tokyo, Bull. Earthq. Res. Inst., Vol.56, 265-276 (in Japanese).

Shima, E. (1980). On the deep underground structure of Tokyo Metropolitan area, Proc. 7th World Conf. on Earthq. Eng., Vol.1, 205-208.

Sino, I and T. Katayama (1985). Evaluation of validity of digitization of records from the JMA strong motion seismometer, Proc. 18th Sym. EArthq. Eng., Japan Soc. Civil Eng., 69-72 (in Japanese).

Smith, W.D. (1975). The application of finite element analysis to body wave propagation problems, Geophys. J. Royal satr. Soc., Vol.42, 747-768.

Sutton, G.H. and P.W. Pomeroy (1963). Analog analysis of seismograms recorded on magnetic tape, Joun. Geophys. Res., Vol.68, 2791-2815.

Swanger, H.J. and D.M. Boore (1978). Simulation of strong-motion displacements using surface-wave modal superposition, Bull. Seism. Soc. Am., Vol.68, No.4, 907-922.

Tada (1976). On the subcrustal structure beneath the Kanto plain, Zisin (J. Seism. Soc. Japan), Ser.2, Vo.29, 47-53 (in Japanese).

Tada (1982). Structure of the basement and gravity anomaly in the Kanto plain (1) -Depth distribution of the basement-, Zisin (J. Seism. Soc. Japan), Ser.2, Vo.35, 605-617 (in Japanese).

Tada (1983). Structure of the basement and gravity anomaly in the Kanto plain (2) -A geophysical study of active fault-, Zisin (J. Seism. Soc. Japan), Ser.2, Vo.36, 359-372 (in Japanese).

Tajime, K. (1981). Geophysical survey of subsurface structure in terms of elastic waves, Maki Shoten, Tokyo (in Japanese).

Takeo, M and N. Mikami (1987). Inversion of strong motion seismograms for the source process of the Naganoken-Seibu earthquake of 1984, Tectonophysics, Vol.144, 271-285.

Tanaka, T., S. Yoshizawa and Y. Osawa (1979). Characteristics of strong earthquake ground motion in the period range from 1 to 15 seconds. Analysis of the low-magnification seismograph records, Bull. Earthq. Res. Inst., Vol.54, 629-655 (in Japanese).

The Research Group for Active Faults (1980). Active faults in Japan, -sheet maps and inventories, p146-148 (in Japanese).

Toriumi, I. (1975). Earthquake characteristics in plain, Proc. 4th Japan Earthq. Eng. Sym., 129-136 (in Japanese).

Toriumi, I., S. Ohba. and N. Murai (1982). Propagation of earthquake wave in Osaka

plain., Proc. 6th Japan Earthq. Eng. Sym., 465-472 (in Japanese).

Toriumi, I (1988). Estimation of velocity structure by the 1st Kitakoh explosion experiments, Abst. of autumn meeeeting of Seis. Soc. of Japan., No.2, 67.

Trorey, A.W. (1970). A simple theory for seismic diffraction, Geophysics, Vol.35, No.5, 762-784.

Trifunac, M.D. and A.G. Brady (1975). A study on the duration of strong earthquake ground motion, Bull. Seism. Soc. Am., Vol.65, No.3, 581-626.

Tsuboi, T. (1979). Gravity, 2nd edition, Iwanami Shoten, Tokyo (in Japanese).

Vidale, J.E. and D.V. Helmberger (1988). Elastic finite-difference modeling of the 1971 San Fernado earthquake, Bull. Seism. Soc. Am, Vol.78, No.1, 122-141.

Yajima, Y. (1981). Petrological characteristics and geological structure of the pre-Tertiary basement of the Kanto plain.

Yamada, Y., S. Noda, A. Okaichi (1988). Evaluation of long-period component of strong-motion seismograms obtained from shaking table test., Jour. Structural Eng. Vol.34A, 923-935 (in Japanese).

Yamamizu, F., H. Takahashi, N. Goto and Y. Ohta (1981), Shear wave velocities in deep soil deposits. Part 3, Zisin (J. Seism. Soc. Japan), Ser.2, vol.34, 465-479 (in Japanese).

Yamamizu, F. (1983). Deep underground structure in Tokyo metropolitan area, Abst. of autumn meeting of Seism. Soc. Japan, 193 (in Japanese).

Yoshii, T. and S. Asano (1972). Time-term analysis of explosion seismic data, J. Phys. Earth, Vol.20, 47-57.

Yoshii, T. (1979). Crustal structure in Japan, Univ. of Tokyo Press (in Japanese).

Yuan, Y., S. Yoshizawa and Y. Osawa (1986). Strong ground motion simulation of the 1976 Ninghe, China earthquake, Bull. Earthq. Res. Inst., Vol.61, 97-127.

Zama, S. (1981a). Behavior of the elastic waves propagating through the irregular structures. I. Effects on cliff by earthquake ground motions, Bull. Earthq. Res. Inst., Vol.56, 741-752 (in Japanese).

Zama, S. (1981b). Behavior of the elastic waves propagating through the irregular structures. II. Damage at Asaba-cho in the lower reaches of the Ohta river in Shizuoka Prefecture due to the 1944 Tonankai earthquake, Bull. Earthq. Res. Inst., Vol.56, 753-760 (in Japanese).

Zama, S. (1981c). Behavior of the elastic waves propagating through the irregular structures. III. Love waves propagating through the nonhorizontal structures, Bull. Earthq. Res. Inst., Vol.56, 761-777 (in Japanese).